DEVELOPMENT OF CHITOSAN BASED COMPOSITE MATRICES FOR BONE TISSUE ENGINEERING

A THESIS SUBMITTED

FOR THE AWARD OF THE DEGREE

OF

Doctor of Philosophy

IN

BIOTECHNOLOGY AND MEDICAL ENGINEERING

BY

NADEEM SIDDIQUI M.A

(ROLL NO. 510BM102)

UNDER THE GUIDANCE OF

Prof. (Mrs.) Krishna Pramanik

NATIONAL INSTITUTE OF TECHNOLOGY
ROURKELA - 769008, INDIA

2014

National Institute of Technology, Rourkela

CERTIFICATE

This to certify that the thesis entitled "**Development of Chitosan Based Composite Matrices For Bone Tissue Engineering"** being submitted by **Mr. Nadeem Siddiqui** for the award of the degree of Doctor of Philosophy in Biotechnology & Medical Engineering of NIT Rourkela, is a record of bonafide research work carried out by him under my supervision and guidance. Mr. Nadeem Siddiqui has worked for four years on the above problem in the Department of Biotechnology & Medical Engineering, National Institute of Technology, Rourkela and his work has reached the standard for fulfilling the requirements and the regulation relating to the degree. The contents of this thesis, in full or part, have not been submitted to any other University or Institution for the award of any degree or diploma.

(Dr. Krishna Pramanik)
Professor& Head
Dept. of Biotechnology & Medical Engineering,
NIT Rourkela

Place: Rourkela

Date:

Dedicated To

MY FATHER

ACKNOWLEDGEMENTS

*First and foremost I praise and acknowledge **Allah**, the most beneficent and the most merciful. At this moment of accomplishment, it is easy to recognize that many people have helped me to achieve such an important stage of my life. Herein I express my deep gratitude to all of you who supported me throughout these years.*

I would like to express my sincere gratitude to my supervisor, Dr. (Mrs.) K. Pramanik, for her relentless encouragement, constructive guidance and words of motivation throughout the duration of my research study and moreover for the inspiration she provided to ensure the completion of this work. Her expertise, availability to discuss ideas and willingness to give of her knowledge were instrumental. For this, I will be eternally grateful.

I gratefully thank Doctoral Research Committee (DSC) members, Prof. S.Paul and Prof. Amit Biswas from the Department of Biotechnology and Medical Engineering, Prof. S.K.Pratihar from the Department of Ceramic Engineering, and Prof. M.Kundu from the Department of Chemical Engineering for their constructive comments to improve the quality of this thesis. I also acknowledge the help provided by Dr. Esmael Jabbari, and his research group, Department of Chemical Engineering, University of South Carolina, USA for his provision of a three month time to me in his lab.

Collective and individual acknowledgments are also owed to research group members; I belong to Varshini Vishwanath, Akalabya Bissoyi, Partha Sarthi Majhi, Bhisham Narayan Singh, Parinita Agrawal, Pallavi Pushp, Saheley Saha, Sai Satish, Jeevan, Tarangini, Amit Kumar, Iqbal Hussain, Amjad Ali, Sarfaraz Alam, Suktika Chandra and Vinay Kumar whose presence somehow perpetually refreshed, helpful, and memorable. Many thanks go in particular to Prof. Sirsendu Ray, Prof. B.P.Nayak, Prof. Mukesh Gupta, Prof. Indranil Banerjee, and Prof. Devendra Varma for giving me such a pleasant time since I knew them in NIT Rourkela.

Finally I would like to convey my heartiest thanks to my loving mom, brothers and sister for their support and love during my stay in Rourkela.

Nadeem Siddiqui

ABSTRACT

The thesis work deals with the development of chitosan (CS) based composite scaffold matrices with improved material and osteogenic differentiation property for bone tissue engineering. Pure CS and CS/ β-TCP composite scaffolds reinforced with micro and nano sized β-TCP with different CS:β-TCP ratios were successfully prepared by freeze gelation method and characterized for morphological, structural, mechanical, swelling, wettability and degradation. Pure CS and composite scaffolds possess interconnected open pore microstructure with desired pore size and porosity. The compressive strength of CS scaffold was remarkably increased by the incorporation of micro and nano sized β-TCP. However, the highest compressive strength of 2.67±0.21 MPa was achieved with CS/nano β-TCP composite scaffold at optimal CS:β-TCP ratio of 60:40. The scaffold also exhibited favourable biodegradation and improved bioactivity. The biocompatibility of the scaffold is confirmed by *in-vitro* cell culture study using human mesenchymal stem cells (hMSCs) seeded on the scaffold. Conjugation with fibrin is shown to be beneficial for improving cellular affinity of the scaffold which is evident by the enhanced cell attachment (FE-SEM), metabolic activity (MTT assay), proliferation (DNA quantification) and osteogenic differentiation (ALP), bio-mineralization, total calcium content and expression of osteogenic specific genes (semi quantitative RT-PCR) of seeded hMSCs. CS/nano β-TCP scaffold was cross-linked with genipin (GN) and sodium tri poly phosphate (TPP) with the aim of controlling rapid degradation rate of CS scaffold and improving mechanical strength. Thus the developed GN cross-linked CS/nano β-TCP composite scaffold has shown favourable degradation (8%) and higher compressive strength (2.78±0.11) than the scaffold cross-linked with TPP. CS/nano β-TCP/GN scaffold was further coated with fibrin thereby a significant improvement of cellular responses such as cell attachment, proliferation, metabolic activity and osteogenic differentiation was achieved. The enhanced osteogenic differentiation ability of the fibrin coated scaffold was further evident by Semi Quantitative RT-PCR study that has revealed up regulation in the expression of osteogenic specific genes like collagen 1 (COL1), osteocalcein (OC), bone sialo protein (BSP), osteonectin (ON), β-actin and ALP. *In-vivo* biocompatibility of the CS/nano β-TCP/GN/F composite scaffold was confirmed by animal testing using mice model. All together, the study has demonstrated that the developed CS composite scaffolds in particular CS/nano β-TCP/GN/F can be used as potential artificial ECM (extra cellular matrix) for various non-load bearing bone tissue engineering applications.

Key words: Chitosan, bio-ceramic, beta-tricalcium phosphate, scaffold, compressive strength, genipin, tripolyphosphate, fibrin, hMSCs, bone tissue engineering, osteogenesis

TABLE OF CONTENTS

CHAPTER 5: RESULTS & DISCUSSIONS

List of Figures

LIST OF TABLES

LIST OF ABBREVIATIONS

ALP	Alkaline Phosphatase
ANOVA	Analysis of Variance
β-GP	Beta Glycero Phosphate
β-TCP	Beta Tri Calcium Phosphate
BSP	Bone Sialo Protein
CAD	Computer Aided Design
CD	Cluster of Differentiation
3D	Three Dimensional
COL 1	Collagen 1
CS	Chitosan
DEX	Dexamethasone
DMEM	Dulbecco's modified Eagle's medium
DMMB	1, 9-dimethylmethylene blue
DTBP	Dimethyl 3,3-dithio-propionimidate
ECM	Extracellular Matrix
EDC	1-ethyl-3-(3-[dimethylamino] propyl) carbodiimide)
EDTA	Ethylene diamine tetra acetate
EtOH	Ethanol
F	Fibrin
FACS	Fluorescence Assisted Cell Sorting
FBS	Fetal Bovine Serum
FDA	Food and Drug administration
FITC	Fluorescein Isothiocyanate
FTIR	Fourier Transform Infra Red
GAG	Glycosaminoglycan
GN	Genipin
H&E	Hematoxylin & Eosin
HAp	Hydroxy apatite
HEPES	4-(2-hydroxyethyl)-1-piperazineethanesulfonic acid
ICR	Imprinting Control Region (Mice strain)

hMSCs	Human Mesenchymal Stem Cells
MTT	3-[4,5-dimethyltriazol-2-y1]-2,5-diphenyl tretrazolium
Mg	Magnesium
MEM	4-Morpholino Ethane sulfonic acid
NaHCO3	Sodium bi carbonate
Na2SO4	Sodium Sulphate
NHS	N-hydroxysuccinimide
OC	Osteocalcin
ON	Osteonectin
PI	Propidium Iodide
PBS	Phosphate Buffer Saline
R&D	Research & Development
RGD	Arginine-Glycine-Aspartic acid
RP	Rapid Prototyping
RT	Room Temperature
RT-PCR	Reverse Transcription Polymerase Chain Reaction
TIPS	Thermally Induced Phase Separation
TPP	Tri Poly Phosphate
SF	Silk fibroin
UCB	Umbilical Cord Blood
XRD	X-ray Diffraction

Chapter 1

General Introduction

1.1 Background and significance of study

Bone tissue defects and diseases due to the consequence of trauma, injury, infections and degenerative bone loss are of major concern in the field of human health [1]. Every year more than 1 million cases of bone injuries is reported to occur in USA alone and an alarming increase in number of bone injuries is expected to continue around the globe, which leads to high demand for bone substitutes [2]. The current clinical option for repairing bone defects and diseases is bone grafting which is classified as autografts and allografts [3]. Failure rates in these techniques are attributed to several reasons like disease transfer, immune rejection and donor crisis [4-5]. This has prompted a lot of research interest among the scientific community for an alternative solution [6]. In this context, bone tissue engineering has emerged as an alternative strategy to repair and/or replace diseased and/or damaged bone tissue through the development of a biologically active substitute so called tissue engineered scaffold that offers complete recovery of original state and bone tissue function [7]. The development of three dimensional porous scaffold matrices from a variety of biocompatible polymers with a desired set of properties such as optimum degradation rate, bio-resorbable, non immunogenic, interconnected pores with optimum porosity, high mechanical strength and biocompatibility is a key challenge for the success of bone tissue engineering. Furthermore, scaffold must facilitate bone formation by stimulating cell adhesion, proliferation and regulating osteogenic differentiation of host cells [2, 8-9]. The component of natural bone matrix is the combination of organic, inorganic materials and a variety of proteins, the main type of which is collagen and apatite as biological mineral [8]. To meet these requirements, a lot of research interest has been generated in recent years to explore potential biopolymers and their composites to develop a suitable scaffold material for bone tissue regeneration.

Chitosan, a natural biopolymer is considered as an ideal biomaterial due to its excellent biocompatibility, abundant availability, intrinsic antibacterial property and biodegradability [9-10]. The ability of CS to bind with growth factors makes it a competent candidate for scaffold material [11]. Chitosan can be easily molded into different forms such as porous 3D structures [12], gels [13], thin films [14], membranes [15] and fibers [16] which are favourable for bone cell growth. However, CS has several drawbacks which limit its use as scaffold material particularly for bone tissue engineering. The major limitations are lack of sufficient mechanical strength, cell binding ability, rapid degradation and deficient of bioactive cell signalling molecules which are vital for bone tissue regeneration [12, 18-19]. Besides material and biological properties, fabrication of 3D porous scaffold is another important aspect that needs to be considered. In this context, freeze-gelation is one of the scaffold fabrication techniques which is very simple, time and energy saving [17]. Hence the present research focuses on the development of CS based 3D composite matrices by freeze-gelation method to mimic the unique hierarchical architecture of bone matrix by addressing the above three major issues that limit the use of CS in bone tissue engineering.

1.2 Tissue regeneration strategies

Tissue Engineering (TE) applies biological, chemical, and engineering principles towards the repair, regeneration or restoration of living tissues using biomaterials, cells, and growth factors such as basic fibroblast growth factor (bFGF), vascular endothelial growth factor (VEGF) and platelet derived growth factor (PDGF) alone or in combination [18]. Usage of tissue engineering triad is considered as an excellent strategy for existing bone tissue related defects by using stem cells and bioactive molecules onto scaffold matrix [19]. TE approaches were classified based on triad components, either used individually or in combination [20] as

(i) cell based therapies, (ii) inducing tissue regeneration by soluble bioactive factors and (iii) employing artificial extracellular matrix system namely scaffold.

1.3 Applications of tissue engineering

Tissue engineering aims at repairing damaged or diseased tissues and organs by offering long term cure with low cost. A new era has already begun in the field of medicine with the aim of solving bone tissue related defects by using the advancement of tissue engineering strategies [21]. The important applications of tissue engineering include cartilage [24-26], bone [11, 22-24] skin [27-30], cardiovascular [20, 25], ligament [32-34], tendon [26-27], neural [37-39], liver [40-42] and musculo-skeletal [43-45] related diseases.

1.4 Tissue engineered scaffold

A scaffold is a temporary matrix which aids in the proliferation of cells until they attain the ability to support themselves. Scaffolds hence degrade after a certain period of time permitting the formation of new tissue.

1.4.1 Properties of scaffold

Structural property

Pore size: Scaffold should have interconnected network of pores and desired pore size for proper diffusion of nutrients and exchange of metabolic wastes thus facilitates the cells to grow, proliferate and differentiate into specific lineage [28-29]. The pore size varies depending on specific tissue engineering applications such as bone tissue (50-300 μm), cartilage tissue regeneration (150-300 μm) [8, 30-31].

Porosity: Scaffold should have optimum porosity to facilitate nutrient diffusion and allow cell migration. It should not be highly porous which ultimately decreases the mechanical strength of the scaffold [32-33].

Mechanical property:

Scaffold must possess mechanical strength that matches with the target tissue to avoid shear stress at the site of implantation [34-35]. The scaffold should be finely tuned for lineage specific differentiation [36].

Biodegradability:

The scaffold must be biodegradable. The rate of degradation should match with the rate of new tissue formation without release of any toxic by products. Furthermore, scaffold should not solubilise rapidly during tissue regeneration process [14, 37].

Bioactivity:

Scaffold should form and deposit apatite crystals in both *in-vitro* and *in-vivo* environments [38-39].

Surface property

Hydrophilicity: Hydrophilicity is the ability of getting wet by a biomaterial which plays a crucial role in governing cell responses especially cell attachment, cell growth and proliferation. Reports suggest higher hydrophilic surfaces of scaffold matrices are responsible for improved cellular attachment where as relatively hydrophobic surfaces are essential for improved protein adsorption [36, 40].

Biocompatibility:

Scaffold material and its degraded products should not be toxic and non-immunogenic in both *in-vitro* as well as *in-vivo* conditions [21].

Tissue inductive property:

The scaffold should promote cell attachment, spreading, migration, proliferation and differentiation of particular phenotypic tissue as needed [21]. For example, scaffold must have osteoinductive and osteoconductive property essential for bone tissue engineering. Osteoinduction is the ability to attract the osteoprogenitor cells to the bone healing site in order to undergo differentiation [32]. Unfortunately lack of such osteoinduction property is found in majority of the natural polymers [11]. Therefore it is preferable to choose a scaffold system with innate osteoinductive properties for better performance at the healing site.

1.4.2 Biomaterials for scaffold development

In order to achieve desired cell growth and proliferation, the artificial extracellular matrix (ECM) i.e. scaffold is a prerequisite for any tissue engineering application including bone tissue regeneration [41]. Scaffolds should provide required structural support to the host bone cells and facilitate cell adhesion, spreading, proliferation and finally osteogenic differentiation [21]. Designing of a temporary scaffold matrix with a desired set of properties such as optimum degradation rate, bio-resorbable, non immunogenic, interconnected pores and optimum porosity, high mechanical strength and biocompatibility is one of the most challenging tasks in the area of bone tissue engineering [5]. In this context, biopolymers are considered as ideal biomaterial for scaffold development and they are classified as natural and synthetic polymers.

1.4.2.1 Natural polymers

Natural polymers are obtained from natural sources such as animal (chitosan-crustacean shells) or vegetal (cellulose-plants) and have been reported to create a better environment for cell growth, spreading and proliferation [42]. Scaffolds from natural polymers have been extensively studied in the last decade. Collagen [43], chitosan [44], gelatin [45] and silk fibroin [46] are found to be important polymers for various tissue engineering applications. The degradation products from these natural polymers do not offer any apparent immune reactions. Further, Majority of these polymers are hydrophilic which makes them suitable for cell culture studies [2]. However, in most of the cases, single polymer does not possess all the desired characteristics of tissue engineered scaffold. Natural polymers lack shape retention ability due to excess swelling and poor mechanical strength that restrict their use in bone tissue engineering applications [47].

1.4.2.2 Synthetic polymers

Synthetic polymers have increased applications as they are well defined with reproducible mechanical and physical properties such as tensile strength, elastic modulus and degradation rate [48]. Typical biodegradable synthetic polymers for biomedical use are hydrophobic polyesters such as poly lactic acid (PLA) [49], poly lactic glycolic acid (PLGA) [50], poly glycolic-co-lactic acid (PGLA), poly3 hydroxy butyrate (PHB), poly 3 hydroxy valerate (PHV), poly ortho esters, poly α-hydroxyl acids, polycaprolactone (PCL) and poly urethane (PU) [51]. The major drawback of these synthetic polymers is their degradation products which are toxic and thus harmful to the cells. For example, PLGA and PGLA release lactic acid and glycolic acid which enter tri carboxylic acid cycle thus creating imbalance in cell

metabolism [32]. Further, these degradation products have been reported to cause inflammation at the site of implantation [19].

1.4.2.3 Ceramics

Ceramics such as hydroxyapatite (HAp) [52], tri-calcium phosphate (TCP) [50, 53], biphasic calcium phosphate (BCP) [21] and wollastonite [54] have been studied to develop composite scaffolds for bone tissue regeneration. The composite scaffolds are characterized by high mechanical strength and enhanced osteogenic property. In bone tissue engineering, they exhibit chemical and structural similarity to the mineral phase of native bone and enhance osteoblast differentiation and proliferation [70-71]. The application of ceramics is common in dental [40], maxillofacial and orthopaedic surgery for filling and coating implant surface of host bone [55]. However, their brittleness and difficulty in remodelling limit their clinical application of scaffold based bone tissue regeneration. Though bio-ceramics are equally strong in their mechanical behaviour, they are deficient in supporting cell growth [52]. It is therefore interesting to note that the combination of biopolymer and bio-ceramic (polymer-ceramic composites) can provide suitable platforms with enhanced cell supportive property and mechanical strength [72-74] for bone tissue regeneration.

1.4.2.4 Composites

Composite materials can be defined as a material composed of two or more distinct phases such as metallic, ceramic and polymeric, which are separated by an interface [56]. By taking advantage of this combining concept, many researchers have given efforts in developing composite materials for tissue engineering to enhance mechanical properties and cellular function. Generally, polymers are known to be flexible and exhibit lack of mechanical strength and stiffness [57]. However, polymers are simple to mold and can easily form

complex structures, while ceramics are stiff and brittle [9]. Composites aim to combine the desired properties of both materials to enhance tissue reconstruction. For example, a natural polymer chitosan is a known for its excellent biocompatibility but lacks sufficient mechanical strength in order to use in bone tissue regeneration [47]. Similarly, a robust biopolymer, silk fibroin, though mechanically stable, lacks hydrophilic property. Considering these, polymer composite or polymer blend biomaterials, have been developed to combine the desired characteristics of both polymer and/or bio-ceramic to overcome the drawbacks of individual polymer or ceramic [29]. Fabrication of such composite scaffolds is one of the promising efforts towards successful bone tissue regeneration [58].

1.4.3 Scaffold fabrication techniques

The search for an ideal biomaterial has been under progress since the conception of tissue engineering. Much significant development has been witnessed in recent years which include an assortment of scaffold fabrication techniques and various polymers. The potential for scaffolding techniques are still in their burgeoning stage and need to be established further to achieve excellence. Each method is unique in terms of its principle and working conditions. Depending upon the requirement and application, fabrication techniques differ. Various methods currently in use for scaffold fabrication include electrospinning, phase separation, solvent casting, particulate leaching, gas foaming, rapid prototyping etc [58-59] which are described below.

1.4.3.1 Salt leaching

Salt leaching developed by Mikos et al. in the year of 1994 [60], is relatively simple method used to develop porous scaffolds**.** This process involves the addition of soluble salt particles as porogen in polymer solution and casting into suitable molds [61-62]. After evaporation of

the solvent, the salt particles are removed by leaching thereby porous scaffolds are formed. The major drawbacks of this method are poor interconnectivity, lower mechanical strength, difficulty in controlling porosity and usage of high toxic solvent [63]. However, by controlling the size of the salt particle, it is possible to tailor the properties of the resultant porous structure [64-65].

1.4.3.2 Gas foaming

Gas foaming is a unique method to produce porous matrices. This method can produce porous materials without the interference of any solvent [66]. Carbon dioxide is the most commonly used gaseous agent for the formation of porous foam. Polymer disks at their solid state are subjected to CO_2 environment where gas bubbles are allowed to form in the polymer system, thereby creating porous sponges. The disadvantages of this method include need of specialized equipment to handle high pressure CO_2 and the process is limited to very few polymers [61].

1.4.3.3 Thermally induced phase separation (TIPS)

Thermally induced phase separation is defined as the separation of solid-liquid or liquid-liquid phases which can be triggered by thermal changes [59]. In this method the temperature of the polymer solution is lowered to bring about phase separation thereby forming polymer-rich and polymer-lean phases. Once the phase-separated system is stabilized, the solvent-rich phase is removed by sublimation using vacuum leaving behind the polymer as foam [67]. Polymer-solvent phase separation can be divided into liquid-liquid and solid-liquid phase separation. Phase separation, which avoids harsh chemical or thermal environments, has been utilized to incorporate small bioactive molecules into scaffolds [68]. The advantage of this method is that the scaffolds often have good mechanical property compared to salt leaching

technique [69]. The optimal pore size and morphology can be achieved by a suitable choice of processing conditions such as quenching temperature, concentration, molecular weight of polymer, solvent/non-solvent composition and additives [70]. Though the process is simple and cost effective, the major limitation lies with precise control over pore size of developed scaffolds [59].

Liquid– liquid phase separation

Phase separation occurs in a liquid-liquid solution by decreasing temperature to an upper critical solution temperature. The addition of a non-solvent to the polymer solution may induce liquid-liquid phase separation thus forming polymer rich and polymer lean phases [71]. The scaffolds prepared by this method offer open pore structure after the removal of excessive solvent.

Solid-liquid phase separation

Solid-liquid phase separation occurs when the temperature is lowered to freeze a polymer solution and the solvent in the system forms crystals and polymer is separated from the solvent crystallization front [72]. This process takes place by a nucleation and growth mechanism. Interconnected pores are generated after the removal of solvent crystals by sublimation or solvent exchange [73]. Thus porous structures can be formed by freezing polymer solution, followed by solvent removal by either freeze drying or freeze-gelation [74], which are described below.

(i) Freeze-drying: Freeze-drying works on the principle of thermally induced phase separation. During this process, the phase-separated mixture is maintained at low temperatures and subjected to a high vacuum to sublime the solvent [75]. Pores are generated by the removal of ice crystals of solvent formed within the polymer solution. These solvent

crystals serve as porogen whose size can be easily controlled by adjusting freezing temperature and concentration of the polymer solution [72]. The main drawbacks of freeze drying include scaffolds with low mechanical strength, smaller pore size and difficulty in complete removal of the residual solvent [76].

(ii) Freeze-gelation: Freeze-gelation is a unique method of scaffold fabrication, which involves the principle of thermally induced phase separation. Problems encountered with the freeze drying process are destruction of pores in scaffold and formation of surface skin which are overcome by freeze-gelation method [77]. The main advantage of freeze-gelation process is its simplicity. The frozen polymer solution is immersed in a gelation environment at a temperature lower than the freezing point of polymer solution [78]. In this technique, since the polymer matrix becomes gel before the drying stage, the porous structure is retained without freeze-drying. The formation of ice crystals within the solution occurs at 273 K, but gelation does not occur until the temperature reaches a few degrees below freezing (~270 K). After freezing, the gel is warmed to melt the ice crystals and then dried. This causes a relatively high degree of continuous porosity with pores duplicating the morphology and dimension of the ice crystals formed during the freezing process [15]. This method overcomes the limitations of freeze drying and sol-gel processing. It permits the formation of low-cost, crack-free, essentially zero-shrinkage scaffolds [79]. Freeze-gelation has been used in wide areas of tissue engineering applications by using natural, synthetic polymers and their composites such as CS [78], silk [17], CS/β-TCP [10], CS/PGA [68] and CS/alginate/carboxy methyl cellulose [74].

1.4.3.4 Electrospinning

Electrospinning is a method to generate nanofibers from various biomaterials. Electrospinning is a widely used technique that utilizes electric field to facilitate the formation of polymer deposits over a suitable collector [50, 100-102]. The polymer solution is induced using a strong electric potential due to which it acquires an imbalanced charge. After a critical voltage is attained, surface tension of the polymer solution is overcome by the charge imbalance leading to an electrically charged jet. This jet is focussed towards a target which is grounded. After solvent evaporation, nanofibers are deposited over the collector. Process parameters that make the formation of ideal nanofibers include concentration of the polymer solution, applied voltage, tip to collector distance etc [43]. Different natural and synthetic polymers were used to fabricate nanofibers for various applications such as wound healing [103-107], bone [108-110], skin [80-81], cartilage regeneration [82] and drug delivery applications [83-84]. The main disadvantages of electrospinning include high energy requirement and high cost. Low pore size of the developed scaffolds further limit the cellular infiltration inside the fibers [34].

1.4.3.5 Rapid prototyping

Rapid prototyping (RP) also known as solid free-form fabrication (SFF) is one of the most appropriate methods to fabricate complex porous 3D structures [85]. It works on the principle of building 3D models using layer by layer methodology [86]. RP (SFF) refers to a group of techniques that will manufacture scaffolds based on computer aided design (CAD) data. Various rapid prototyping methods are stereo-lithography, fused deposition modelling, selective laser sintering and 3D printing [87]. RP was used to make bone grafts with complex geometry and interconnected networks to mimic micro environment of natural bone [88]. Furthermore, this method overcomes the disadvantages of conventional fabrication techniques

such as freeze drying and salt leaching by developing scaffolds with complex geometries. The major limitations of this method are the use of expensive machinery and difficulty in operating the instrument [89].

1.5 Stem cells for tissue engineering

Stem cells are one of the constituents of tissue engineering triad and play a major role in success of an implant. Multilineage differentiation property of mesenchymal stem cells (MSCs) makes them potential cell source for tissue regeneration applications [90]. The various sources of MSCs include placenta, umbilical cord blood (UCB), blood, adipose tissue and bone marrow. Ease of handling and considering it as cheaper hospital waste product, UCB is considered as one of the promising sources for the isolation of MSCs [91-92]. Stem cells and their usage for curing tissue related defects are expected to continue as a foremost area of development for successful tissue engineering applications.

1.5.1 Embryonic stem cells

Embryonic stem cells (ESC) originate from the inner cell mass of blastocyst from which embryo derives. These cells are isolated and cultured in media from the past 2 decades and able to differentiate to all somatic cell types. The unique properties of embryonic stem cells include their self renewal property and capacity to differentiate via precursor cells. ESC has the differentiation ability to adipocytes [93], chondrocytes [94], neuron [95], hepatocytes [96] and osteocytes [97-98]. However, immunological incompatibility and uncontrolled proliferation which leads to teratomas and teratocarcinomas are the limitation of using ESC. Further, the major issue with the usage of ESCs is ethical conflicts between the researchers and patients continue to exist [99]

1.5.2 Adult stem cells

An adult stem cell belongs to the category of undifferentiated cells found amid differentiated cells in tissues or organs. Adult stem cells are considered as the most potential cell source for tissue engineering. These cells can be found in bone marrow [100], periosteum [101], muscle [102-103], fat [93] and skin [45]. Presence of osteogenic precursors in bone marrow makes it a special choice for bone tissue engineering applications. The prime role of ASC is to maintain and repair the tissue in which it is found. Furthermore, on *in-vivo* implantation, these cells exhibit immunosuppressive ability which makes them a suitable candidate for allogenic transplantation [104].

1.5.3 Mesenchymal stem cells (MSCs)

Mesenchymal stem cells (MSCs) also known as somatic cells are undifferentiated and present in any tissue or organ. These cells are of mesodermal origin and develop into various connective tissue types like blood, muscle, bone, cartilage, tendon, and ligament. These cells have the capacity of self renewal and can differentiate into specialized cell types. MSCs can be easily isolated, cultured and expanded under *in-vitro* conditions. MSCs, under culture conditions possess morphology similar to fibroblasts and exhibit good affinity to the tissue culture substrate; So, MSCs are good choice for tissue engineering applications including cell based therapies. There are several reports on the *in-vitro* culture of MSCs and their differentiation into dermal, musculo-skeletal [105], adipogenic [106], bone [107] , cartilage [108], tendon [109], and ligament [110] tissue.

1.6 Role of signalling molecules in tissue regeneration

Signalling molecules also known as growth factors which control a variety of cellular responses through specific binding of transmembrane receptors on target cells [111]. The method of binding results into translation of a specific protein kinases which further activates cascade of both intra and extracellular events [112]. The various growth factors which reside in the ECM of bone are transforming growth factor-β (β-TGF), insulin-like growth factor (IGF), platelet-derived growth factor (PDGF), fibroblast growth factor (FGF) and bone morphogenic protein (BMP). The specific role of these growth factors is given in **Table 1.1**.

Table 1.1: ***Growth factors and their specific function***

S. N.	Growth factor	Forms	Role/function
1	TGF-β1	TGF-β1 TGF-β2 TGF-β3	Haematopoiesis, formation of skin, mammary glands, wound healing, stimulates collagen, ALP, osteonectin, synthesis and angiogenesis [113]. Decreases osteocalcin synthesis [114].
2	IGF	IGF-I IGF-II	Osteoclast formation[115].
3	PDGF	PDGF-AA PDGF-BB PDGF-AB	Increases collagen and non collagenous protein production and helps in fracture healing [116].
4	FGF	FGF	Shows dose dependent action; elicit or inhibits bone repair [19].
5	BMP/OP	BMP-2 BMP-7	Healing in long and non union bones [117-118].

1.7 Bone

Bone is a form of mineralized tissue which is highly vascularised and ultimately provides a skeletal support to the body, including protection of various internal organs [32, 59]. So any major defects in its structure affects entire body functionality and thus lifestyle too [21]. Bone regeneration has many intricate factors which include mimicking the microenvironment of

natural bone. Though it has intrinsic ability to regenerate to certain extent, larger defects make healing improper and thus may start damaging themselves in the long run [119].

1.7.1 Structure and composition of bone

Bone comprises of a variety of cells with specific functions and an extra cellular matrix (ECM). Collagen I is the major component of bone which occupies 95% of bone ECM. Proteoglycans and non-collagenous proteins contribute only 5% [120]. Glycosaminoglycan [GAG] is an example of proteoglycans which is found in bone and cartilage. Bone can form and deposit calcium phosphate salts in the matrix which provides rigidity and strength to bone [98]. The composition of bone is given in **Table 1.2.**

Table 1.2: ***Composition of bone***

S.NO	Component	Percent (wt %)
1	Hydroxy apatite	69
2	Organic matrix (i) Collagen [Organic matter] (ii) Other organic matter	22 90-96% of organic matrix 4-10% of organic matrix
3	Water	9

1.7.2 Types of bone

Bones are classified into two categories namely cortical (hard) and cancellous/trabecular bone (spongy). The typical cortical bone is the outer layers of most of the bones and occupies various long bones with 80-90% mineralization [121]. It provides mechanical strength to the entire skeleton. Cancellous bone consist of 15-20% minerals and occupies the interior of bones [122]. The cancellous bone is full of vasculature and hence metabolic actions are taken

care by it. The mineral containing fibers are arranged into lamellar sheets which are arranged in concentric rings forming an osteon [123].

1.7.3 Types of bone cells

There are three types of cells that contribute to bone formation such as osteoblasts: bone-forming cells, osteoclasts: resorb or break down bone and osteocytes: mature bone cells. The various types of bone cells and their functions are represented in **Table 1.3**.

Table 1.3: ***Types of bone cells and their function***

CELL TYPE	MORPHOLOGY	FUNCTION
Osteoblasts	Cuboidal in shape; located at the bone surface with their precursors	Synthesis and regulation of bone ECM deposition
Osteocytes	Stellate shaped	Calcification of osteoid matrix
Osteoclasts	Multinucleated cells	Bone resorption

1.7.4 Mechanism of bone healing

The native architecture of damaged bone is restored by regeneration of normal cell population rather by repair of injured area as it occurs in other connective tissues [124]. The healing mechanism can be classified as immediate bleeding and blood clotting, which provides the basic platform for inflammation [125]. The neo bone produced thus replaces the blood clot with soft callus (fibrous tissue and cartilage) which is later on replaced by hard callus. Finally the tissues become compact and thus remodelling occurs [126].

1.8 Chitosan as ideal polymer for tissue regeneration

Chitosan, obtained by partial deacetylation of chitin, is a polysaccharide which is available abundantly in nature after cellulose [9]. The basic unit of CS is 2-amino-2-deoxy-D-glucose with β→1-4 glucosidic linkages. CS is insoluble in water but soluble in dilute aqueous

solutions. The most commonly used organic solvents are acetic acid and formic acid. The unique properties of CS make it an excellent biomaterial in many fields of tissue engineering. Low cost, wound healing, minimal immunogenicity [3], antimicrobial activity [127], biocompatibility and ability to adsorb proteins grab the attention of researchers towards CS in various tissue engineering applications [44, 128]. Positive charge of CS in aqueous acidic conditions attracts negatively charged plasma proteins which lead to thrombus formation and blood coagulation during the process of wound healing [11, 38]. Ability of CS to bind with sialic acid in phospholipids restricts the metabolism of microorganisms which is responsible for its antimicrobial activity [129]. One of the most promising features of CS include its flexibility to mold into different forms (porous 3D scaffolds, fibers, thin films) to be used in tissue engineering applications with different pore size [130]. Most importantly, chitosan, possess relatively better mechanical strength when compared to other natural polymers [11]. However, CS lacks some specific aspects that are important in tissue engineering. For example, poor mechanical strength of CS scaffolds makes it unsuitable particularly for bone tissue engineering applications [56]. CS is deficient in bioactive signal molecules which help in cell attachment, spreading, growth, differentiation and proliferation [131]. Nevertheless, incorporation of bio-ceramic particles and signalling molecules into it surpasses the mentioned limitations.

1.9 Future prospects of tissue engineering

Tissue engineering is an offset of regenerative medicine that can cater to the need of millions of patients worldwide suffering from various tissue diseases. Though tissue engineering is promising as an exciting industry with a potential market, it is still facing numerous challenges like the establishment of a quality control program that can ensure the safety of the ultimate tissue engineered bone or other implant [32, 121]. Recently, efforts to address these issues are on track and this technology is expected to have a major boom in cell based remedies. The FDA has already initiated some regulatory efforts and guidelines related to certain tissue engineered bone implants. In the forthcoming years, these guidelines are expected to be standardized that will ensure the safety of these marketed implants [33]. Thus, this promising wing of future medicine will enable to enlighten lives of needful patients and prevail as an alternative to traditional bone and other grafting methodologies.

1.10 Thesis Outline

The whole thesis work has been organized in six chapters as follows: **Chapter 1-** includes general introduction and significance of the research work. **Chapter 2-** presents literature review including concepts and fundamental understanding of recent advancement in chitosan based tissue engineering and possible improvement in potency of current implantable chitosan biopolymers in bone tissue repair. It has also been discussed, the need and possible ways to improve the material and bio-relevant properties of CS scaffold to make it more effective as bone tissue engineering scaffold materials. **Chapter 3-** presents scope and objective of the study. **Chapter 4-** presents materials and methods adopted for the preparation of CS and CS based composite scaffolds and their physical, chemical and biological characterisation. **Chapter 5-** describes the results and discussion of experimental work which is sub-divided into the following parts: **Part I** reports the development of CS/β-TCP composite scaffolds and their characterization including the investigation on the effects of micro and nano β-TCP on various scaffold properties and their comparison. **Part II** deals with the development of fibrin conjugated CS/nano β-TCP composite scaffolds and their characterization. **Part III** describes the development and characterization of genipin (GN) and tripolyphosphate (TPP) cross-linked CS/nano β-TCP composite scaffolds. **Part IV** presents the further improvement of the cell supportive property of GN cross-linked CS/nano β-TCP composite scaffolds by fibrin coating. **Chapter 6** includes a brief summary and conclusion of the thesis work along with suggested future study.

Chapter 2

Literature Review

2.1 Current status of bone tissue diseases and defects

Bone defects and diseases because of the consequence of trauma, injury and infections are of major concern in the field of health sector [2]. It is estimated that more than 50% of all osteoporotic hip fractures will occur in Asia alone by the year 2050 [132]. In India, the number of osteoporosis patients alone has been reported in the order of 26 million till 2003 and expected to increase to 46 million by 2023 [133]. Surgical reconstruction, transplantation (auto and allografts), drug therapy, artificial prostheses and medical devices which are current clinical treatment options for various tissue related disorders including bone tissue [134]. These treatment options have disadvantages such as severe pain, risk of infections, hematoma, immune rejection, donor site morbidity, transmission of viral (HIV, hepatitis-B) and prion proteins [135]. In this context, in recent years bone tissue engineering has emerged as an appropriate strategy to repair and/or replace damaged and/or diseased bone tissue defects.

2.2 Challenges and prospects of bone tissue engineering

Bone tissue engineering uses a temporary porous structure known as scaffold. The design and development of 3D scaffold matrix from a variety of biocompatible polymers with desired tailor properties is the key challenge for the success of tissue engineered bone grafts. Scaffolds provide suitable platform for the seeded cells and fill the defect and helps in forming a new tissue [136].

2.3 Ideal biomaterials for bone tissue engineering

The ideal biomaterial for bone tissue engineering should have specific characteristics such as providing a momentary mechanical support to the affected area, should possess porous interconnecting architecture for allowing vascularization and bone in-growth. Further, the biomaterial should be biocompatible with appropriate surface chemistry in order to permit cell adhesion and provide sufficient integration with host bone tissue [137]. Furthermore, a biomaterial should encourage migration of bone cell into the scaffold, should help in promoting osteogenic differentiation, osseointegration and degrade in a controlled manner to facilitate load transfer to developing bone [138].

2.3.1 Polymer/polymer blend and polymer/ceramic composites

It is evident that a single biomaterial does not possess all the desired properties and thus there is need for the development of a polymer blend and/or composite material with an appropriate composition from a variety of biopolymers and other biomaterial [30]. Various research groups have attempted to combine natural polymers with some other natural or synthetic polymers for achieving better results in terms of compressive modulus, surface property such as wettability and biocompatibility [139-140]. Natural or biological polymers namely chitosan, silk fibroin, alginate, fibrin, agarose, gelatin, hyaluronan etc possess superior biocompatibility and are thus utilized in various tissue engineering applications. Synthetic polymers containing aliphatic polyesters are easily degradable within the biological and the degradation products are adsorbed in the metabolic pathway. However, these synthetic materials are chemically and biologically inert and thus require optimum surface modification with ECM mimicking molecules such as RGD and also osteoconductive moieties like bio-ceramics. Micro and nano sized bio ceramics incorporated in natural biopolymers are considered as a promising option in developing scaffolds with desired mechanical property for bone tissue regeneration [141]. Polymer ceramic composites consist of two or more components where ceramic particles are distributed homogenously in polymer matrix [9]. In this regard, few researchers adopted biomimetic approaches to enhance the mechanical properties of polymeric scaffolds. In such studies, researchers used Collagen type I [142], type III and glycosaminoglycans (GAGs) as an organic phase and nano Hydroxyapatite (nHAp) as inorganic phase [18].

2.4 Surface modification

Surface properties of a biomaterial determine its efficacy in cellular binding. Scaffold material can be improved by modifying their surfaces chemically or physically, and a variety of such surface modified scaffolds have been used for investigating cellular behaviour [63]. Modification of biomaterials and understanding of cell behaviour have made it clinically possible to replace or reconstruct damaged host cells and tissues [51]. As far as there is advancement in biomaterial research, new biomaterials and novelty in their usage will

continue to emerge. CS has been used with surface of various prosthetic materials used for bone tissue engineering applications. Availability of free NH_2 and OH groups makes CS more special and ease in modification with wide range of applications [11]. Titanium (Ti) surfaces were coated with CS by using silane glutaraldehyde chemistry and an enhanced cellular responses of osteoblast like cells have been observed [143]. CS also has been modified for improving its physico-chemical, biological and degradation properties by cross linking and grafting with cell adhesive peptides by using carbodimide chemistry [19, 97, 170].

2.5 Role of chitosan scaffold matrices in tissue regeneration

Pore size and porosity, biodegradability, mechanical strength and immunogenicity and porosity are the important characteristics of an ideal scaffold for various tissue engineering applications. Chitosan, a linear polysaccharide consisting of repeating units of D-glucosamine and N-acetyl-D-glucosamine linked by β-1,4 glycosidic bonds obtained from deacetylation of chitin present in shells of crustaceans and molluscs [12]. Tissue engineering approaches for bone repair with different forms of CS namely films [14], membranes [15, 144], fibers [145], 3D matrices [38] and sponges [146] has been reported. CS has better mechanical and biological properties as compared to other natural polymers. However, CS has limitations like low mechanical strength [10], rapid biodegradability [16] and low bioactivity etc., in order to use as scaffold material for bone tissue regeneration.

2.5.1 Chitosan based composite scaffolds in tissue regeneration

Published reports have shown enhanced mechanical and biocompatible properties of ceramic reinforced chitosan based composite scaffolds along with the decelerated degradation rate [147]. Calcium phosphate ceramics (CPC) are widely used as fillers to overcome the mechanical inferiority of polymeric scaffolds [148]. CPC interacts with the body fluids to form apatite on its surfaces that offers bone healing due to osteoconduction [149]. The uniform surface morphology of CPC is a vital factor which promotes cell proliferation and differentiation. Hydroxyapatite (HAp), beta-tricalcium phosphate (β-TCP), octa calcium phosphates (OCP) and biphasic calcium phosphates (BCP) are the major constituents which fall under calcium phosphate ceramics [150]. These biomaterials can be manufactured in

various forms such as blocks, powders and coatings [151]. Published reports on β-TCP confirm its excellent biocompatibility, osteoconductivity and favours cell growth, proliferation and differentiation of MSCs [4, 152]. Optimal resorption, high bone bonding ability and degradation similar to natural bone makes β-TCP a suitable scaffold candidate for bone tissue regeneration than HAp [55]. Furthermore, HAp degrades slowly and thus remains for a long time once implanted in critical size bone defect [53]. With rapid advances in nanotechnology, nano-structured biomaterials gained high importance due to their high surface area and excellent bioactivity. Nano-sized bio-ceramics are the most promising because of their structural similarity to inorganic phase (HAp) of the bone [153]. Enhanced cell migration, proliferation and differentiation of seeded cells has been reported by incorporating nano sized ceramic particles like HAp and bi-phasic calcium phosphate (BCP) [120, 154]. Thein et al. reported the reinforcement of nano HAp particles into CS matrix not only increased the mechanical strength but also decreased degradation rate by 10%. Furthermore, MC3T3 cell proliferation in the composite scaffolds was increased by 1.5 times when compared to pure CS scaffold [38]. Incorporation of β-TCP in CS-gelatin composite system has produced scaffolds with higher mechanical property and better biocompatibility. The maximum compressive strength obtained was 0.8 MPa with an average pore diameter of 337μm [53]. In another study, introduction of β-TCP in poly (*L*- lactic acid)/chitosan/gelatin scaffold matrix has enhanced the osteogenic differentiation potential of bone marrow mesenchymal stem cells was increased in the above mentioned composite scaffold due to osteo-inductive nature of β-TCP [4] Stiffness of polymeric matrices has also been increased by various physical and chemical cross linking agents such as Ultra Violet rays [155], glutaraldehyde (GLT) [127], carbodimide [156], genipin (GN) [145] and tripolyphosphate (TPP) [16]. Furthermore, cross-linking has been reported to have a direct influence on degradation rate of polymeric matrices. Lee et al. developed glutaraldehyde cross-linked gelatin/chitosan porous 3D scaffold with tunable compressive moduli and surface roughness for bone tissue regeneration [45]. Reis et al. has improvised physico-chemical properties of chitosan based scaffold by cross-linking with genipin by freeze drying. The pore size of genipin cross-linked composite scaffolds has been increased which shows direct effect on cell

growth, proliferation and differentiation for cartilage tissue engineering [28]. Dhara et al. reported a significant increase in MG63 cellular responses, osteoblastic differentiation and compressive strength (~3MPa) on chitosan-TPP sodium tripolyphosphate (TPP) cross-linked 3D nanofibrous scaffolds [16]. Though composites overcome mechanical limitations, still challenge exists in designing a scaffold which mimics the host tissue [49]. Furthermore, among the biomaterials used for producing 3D scaffolds, chitosan seems to be an attractive option [11]. However, the major drawback of chitosan is lack of cell binding molecules like RGD (Arginine-Glycine-Aspartic acid) to attract more number of cells on its surface [157]. Surface modification of chitosan scaffolds with RGD peptide has been reported to improve cell adhesive property of seeded MSCs. In this context, efforts have been given by Tsai et al. to immobilize RGD peptide on CS based 3D porous scaffold to further improve the biocompatibility of CS. They reported an increase in cell attachment and cell number of seeded rat osteosarcoma cells [155]. Sheikh et al. has reported the role of fibrin in improving cell binding ability of polymers [158]. He et al. reported that having numerous cell binding sites on fibrin makes it a special in overcoming the cell seeding defects and thus promoting excellent tissue growth [159]. Gray et al. has proved the importance of fibrin in various tissue engineering applications [160]. Yilgor et al. incorporated BMP-2 and BMP-7 signalling molecules into chitosan/poly lactic acid-co-glycolic acid (PLGA) composite scaffold and noticed increased levels of cell number and thus ALP activity which confirms the osteogenic lineage commitment of rat bone marrow mesenchymal stem cells [117]. Yamada et al. and Tholpady et al. investigated the effect of fibrin by culturing MSCs on 3D scaffold and reported an increased cell adhesion, proliferation and thus better osteogenic differentiation ability [131, 161]. **Table 2.1** depicts the various CS based composite scaffolds with improved properties reported so far.

Table 2.1: ***Chitosan based composite scaffolds with enhanced properties***

Composite	**Out come**	**Reference**
CS/nano Hap	Increased mechanical strength, superior cell attachment, high proliferation of MC3T3 cells	Han et al [101].
CS/ALRGDN-peptide	Promoted biocompatibility	Huang et al [51]
CS/Gelatin/β-TCP	Increased osteoblast attachment and proliferation	Mohammadi et al [4]
CS/Alginate/Carboxy methyl cellulose	Increased compressive modulus	Yuan et al [74].
CS/RGD/ UV cross-linking	Increased proliferation [GAG and DNA]	Tsai et al. [158]
CS/HAp nanofibers	Increased interconnected architecture of scaffold	Frohbergh et al [145]
CS/SF	Controlled bio-degradation rate	Bharadwaj et al [17]
CS/nHAp	Increased mechanical strength	Thein-Han et al [38]
CS/Bioactive glass	Increased mechanical strength, cell attachment	Fu, Q et al [121].
CS/PLGA .	Increased stiffness of scaffold, Biocompatibility	Jiang et al [29]
CS/PLA	Increased compressive strength Neutralize the acidity of PLA degradation products	Van de Witte et al [69]
CS/gelatin/TCP/Glutraldehyde	Increased cell spreading	Yin et al [53]
CS/Bioglass	Increased mechanical property and decreased inflammatory actions of bio glass.	Chen et al [162].
CS/BMP	Increased porous morphology, cell viability and controlled release of FGF	Luca et al [163].
CS/wollastonite	Increased mechanical strength and bioactivity	Li Zhao et al [54].
CS/HAp/collagen I	Controlled pore size and biodegradation	Pallela et al [44]

CS/alginate	Increased ligament and tendon growth	Majima et al [164]
CS/PLAGA/Fibrin	Increased mechanical strength, Osteoblast cell proliferation	Mol et al [20]
CS/Fibroin	Enhanced stiffness and biocompatibility	She et al [70].
CS/Ca_3P0_4	Increase in cell attachment, proliferation and phenotypic expression of osteoblastic markers	Lin et al [165].

Beside material properties, another challenging aspect that needs to be focussed is the fabrication of scaffolds using a simple and cost effective method. Freeze-gelation is one of the scaffold developmental techniques which is very simple, time and energy saving [17]. The amount of residual solvent and formation of surface skin is limited which helps in better growth of cells cultured on these freeze-gellled scaffolds [76]. Furthermore, the scaffolds developed by this method possess an interconnected porous network with better mechanical properties [77]. Earlier research suggests the usage of this method to develop 3D scaffolds from various biopolymers like collagen [166], carboxy methyl cellulose [74], poly (d,l-lactic-co-glycolic acid) [76], chitosan [78], pectin [79] and silk fibroin [17]. CS can be easily modified in combination with other materials to achieve required mechanical and surface properties of scaffold [167]. Chitosan has been utilized as promising biomaterial with a wide range of processability and applications as illustrated in **Figure 2.1 and Table 2.2**

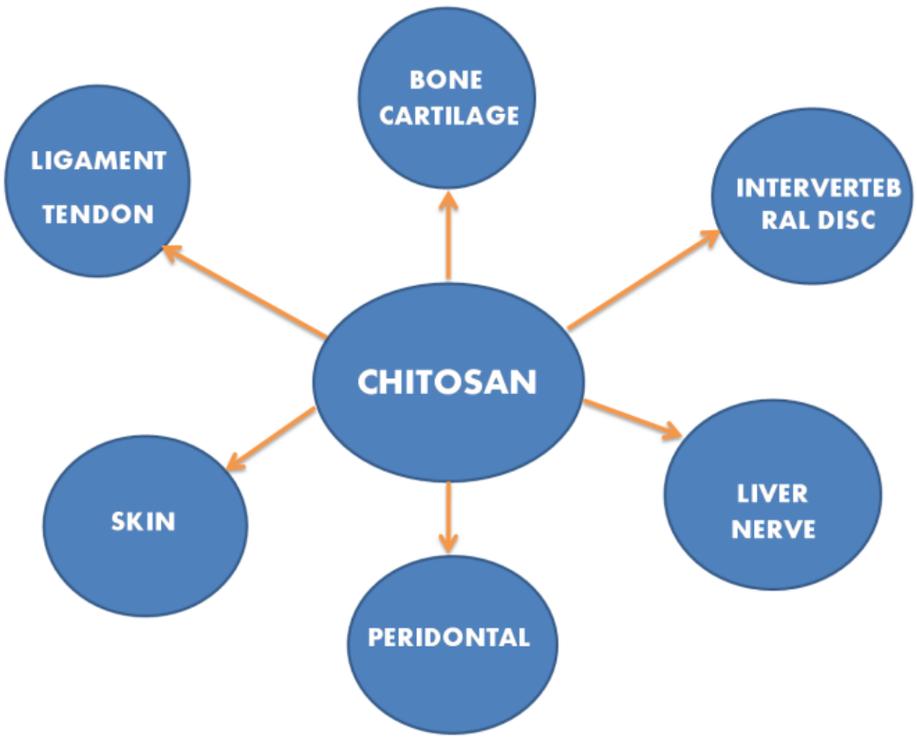

Figure 2.1: ***Chitosan for different tissue engineering applications***

CS scaffolds in various forms such as 3D porous, fibrous, films etc developed for tissue engineering application is listed in **Table 2.2**

Table 2.2: ***Various forms of CS in tissue engineering applications***

Chitosan	**Fabrication method**	**TE application**	**References**
3D scaffolds	Freeze drying	Tendon tissue engineering Skin tissue engineering	Majima et al [164] Bagnaninchi et al [168] Adekogbe et al [169]
	Freeze-gelation	Bone tissue engineering	Hsieh et al [78]
	Salt leaching	Ligament tissue engineering	Funakoshi et al [170]
Fibers	Electrospinning	Wound dressings	Zhou et al [171]. Tuzlakoglu et al[172] .
		Bone tissue engineering	Frohbergh et al [145]
		Cartilage tissue engineering	Subramanian et al [127]
Films	Salt leaching	Connective tissue Bone repair	Yoon et al [61] Wang et al [173]
	Lyophilization	Wound dressing/skin repair	Zhou et al [157] Zhou et al [171]
Hydrogel	Sol–gel transition	Cartilage tissue Engineering Bone tissue engineering	Drury et al [174] Luca et al [163]
Sponges	Freeze drying	Wound dressings Bone tissue engineering Cartilage tissue engineering	Denkbas et al [175] Seol et al[176] Silva et al [146]

2.6 Applications of CS in tissue engineering

2.6.1 Skin/wound healing

Research groups Zhou et al. and Lee et al. have reported the *in-vitro* dermal fibroblasts spreading and proliferation on 3D CS/gelatin scaffold and CS/PVA nanofibrous membranes [45, 171]. Bharadwaj et al. reported excellent cell viability of human keratinocytes on 3D CS/silk fibroin freeze-gelled composite scaffolds [17]. In another study, Denkbas et al. developed norflaxin loaded CS sponges for enhanced skin wound healing effects [175]. The enhanced tensile strength of CS nanofibers containing HAp particles was reported by Frohbergh et al [145]. Furthermore, wound healing ability of composite nanofibers was found to increase as compared to pure CS nanofibers. Adekogbe et al. developed dimethyl 3,3-dithio-propionimidate (DTBP) dihydrochloride cross-linked 3D chitosan scaffolds for skin tissue engineering by freeze drying [169]. The cross-linking with DTBP has remarkably increased the tensile strength from 20 ± 6 KPa to 160 ± 12 KPa which is suitable for skin tissue engineering applications.

2.6.2 Cartilage

Application of CS based 3D scaffolds for cartilage tissue engineering was reported by Silva et al [146] and Krampera et al [177] by freeze drying. Subramanian et.al reported the effect of cross-linking on stiffness of CS matrix and chondrocyte viability and proliferation [127]. Tortelli et al cultured human mesenchymal stem cells (MSCs) on 3D chitosan scaffolds and allowed them to differentiate into chondrocytes. They reported an enhanced expression of collagen type II and GAG [97]. CS sponges were prepared by Nettles et al using freeze drying and noticeable differences were reported in chondrocyte proliferation and differentiation in 28 days of incubation in chondrogenic media [167]. Malafaya et al developed an innovative route for processing CS particles into agglomerated 3D scaffolds for osteochondral defects by using adipose tissue derived stem cells [178]. Cytotoxicity studies reported the biocompatible nature of CS agglomerates. In a similar study conducted by Li et al. reported that the CS/alginate scaffolds has shown excellent adhesion, proliferation and enhanced differentiation of HTB-94 cells to chondrocytes in 3 weeks of incubation time [30].

2.6.3 Bone

Tissue engineering strategy to repair damaged bone tissue with different morphologies using chitosan based scaffolds in various forms have been reported by Hsieh et al [78], Tuzlakoglu et al [172], Zhou et al [171], Luca et al [163], Seol et al [176], Li et al [40]. Initial effort was dealt with CS hydrogels by Yamamoto et al [13] and Drury et al [174]. CS membranes were successfully prepared by Liao et al [179] and Orrego et al [15] for bone regeneration. However, in the last decade, due to technological advances, many methods have been reported to develop 3D porous CS based scaffolds and seeded with MSCs for the repair of bone defects. Laurencein et al and Reis et al reported the usage of CS in bone tissue engineering applications. CS/PLAGA composite scaffolds were prepared with enhanced compressive moduli for bone tissue engineering. Osteoblasts like cells were seeded on composite scaffolds and found the enhanced cellular responses in terms of cell number, proliferation and differentiation over composite scaffolds as compared to pure CS scaffolds [29, 172]. CS was processed into films [14] and electrospun to form fibrous scaffolds [34] or a 3-D porous scaffold by freeze-gelation [17] and freeze drying [180]. Introduction of RGD peptide sequence and growth factors such as BMP-2 and VEGF was reported to enhance surface properties for cellular activities [188, 204]. CS scaffolds were UV cross-linked to immobilize RGD cell signalling peptide for improving cell binding affinity of CS scaffolds. MC3T3 cells were seeded to evaluate the biocompatibility of these scaffolds. They observed the enhanced adherent cells on RGD immobilized CS scaffolds. Furthermore, enhanced mineralized matrix is also observed as compared to scaffolds without RGD [155]. Injectable BMP-2 loaded CS hydrogels have been reported to induce osteogenesis *in-vitro* and *in-vivo* bone formation [181]. CS based composites have been reported to outperform *in-vivo* bone growth than commercially available synthetic polymers. Reports demonstrate the successful differentiation of MSCs into osteogenic lineages grown over CS/nano-hydroxyapatite. CS/PCL composite 3D scaffolds which were observed to promote osteogenesis at both non-load bearing [182] and load-bearing [157] sites implanted in small animal (nude mice) models. Angiogenic activity associated with the external implant surface was clearly observed. Further, lymphocyte proliferation assays and low antibody responses indicated a

very low immune rejection of CS-PCL composite scaffolds [183]. Li et al. reported the biocompatible nature of CS/alginate scaffold system by culturing MG63 osteoblast-like cells. Furthermore, an enhanced cell proliferation, matrix deposition and higher levels of osteogenic gene expression were reported [30]. Interconnectivity between pores of these scaffolds has increased neo vascularisation as revealed by *in-vivo* tests in mice for 12 weeks and thus useful for both bone and cartilage load bearing defects. CS/Poly-L-lysine films were developed by Zhenhaun et al which supported the growth, proliferation and differentiation of MC3T3-E1 osteoblast like cells. RT-PCR analysis proved the increased expression of osteoblast related specific genes osteocalcin (OC) on composite films as compared to pure CS films [184].

2.6.4 Ligament/tendon

The flexibility of chitosan into controllable physical forms makes it promising for ligament and tendon tissue engineering. CS fibers resemble the collagen fibers present in ligaments and tendons. Ceramic reinforced chitosan nano fibers possess better mechanical properties and larger surface area for cell attachment and ECM secretion. CS fibers has been investigated for proliferation and differentiation of MSCs towards ligament tissue, expression of ligament-specific markers (collagen type I, collagen type III) and cellular response for mechanical stimulus [189, 194]. HAp coated chitosan nanofibers have been reported to restore the mechanical strength without influencing *in vitro* cytotoxic effects and *in vivo* inflammatory response for ligament tissue engineering [185]. RGD coated CS matrix showed enhanced ECM production and increased expression of Collagen type I as compared to unmodified CS fibers [164].

2.6.5 Other tissues

Studies of Jiankang et al. have reported that CS and other synthetic polymer conjugates support the attachment and proliferation of hepatocytes [186]. Feng et al reported that cells cultured on nanofibrous galactosylated CS are able to detoxify ammonia by increasing urea synthesis [96]. CS has also been demonstrated to support the growth and proliferation of schwann cells for nerve tissue engineering [95]. Masuko et al. have developed Arginine, Glycine-Aspartic acid-Serine-Glycine-Glyicine-Cystine (RGDSGGC) peptide conjugated CS

scaffolds and reported an increase in chondrocyte and fibroblast adhesion, proliferation on RGDSGGC conjugated CS scaffolds due to RGD cell recognition peptide as compared to pure CS scaffolds [187]. Shao et al. have shown elevated levels of collagen I, II, aggrecanin annulus fibrosus (AF) cells seeded on CS alginate hybrid scaffolds thus proved the potentiality of CS in intervertebral disc tissue engineering applications [188]. Akman et al evaluated the role of CS in periodontal tissue engineering by fabricating bFGF loaded CS/HAp composite scaffold. Peridontal ligament cells and cementoblasts were seeded and found that they were spreading and proliferating on scaffold surface which were revealed by confocal microscopy and cell viability assays [181]. Zhao et al. explored the usage of CS in liver tissue engineering by developing CS/TiO_2 composite scaffolds. Hepatic immortal cell lines (HL-7702) were found to restore their long term viability along with albumin secretion and synthesis of urea which indicated the potentiality of CS/TiO2 scaffolds for liver tissue engineering [189].

Chapter 3

Scope and objective

In recent years, bone tissue engineering has been emerged as the most promising technique for the treatment of bone tissue defects and diseases through the development of a biologically active 3D artificial extracellular matrix so called tissue engineered scaffold. The design and fabrication of such 3D porous scaffolds with a desired set of properties is a key challenge. Among the various biopolymers explored for tissue engineering applications, chitosan is considered as one of the potential candidates owing to its biocompatibility, biodegradability and wound healing properties [57]. However, chitosan lacks desired mechanical strength, bioactivity, degradation and cell binding ability which limits its use in bone tissue engineering. Therefore, the present research focuses on the development of a novel chitosan based composite porous scaffold for bone tissue engineering application by solving the various limitations associated with chitosan.

The specific objectives of this research work are:

i. To develop chitosan-bio-ceramic composite scaffolds with improved bioactivity and mechanical property
ii. To improve the cell supportive property of the developed composite scaffolds by conjugation with bioactive molecule
iii. To develop cross-linked composite scaffolds with controlled biodegradation property
iv. To study physico-chemical and mechanical properties of the scaffolds
v. To assess biocompatibility and osteogenic potentiality of the developed composite scaffolds

The scope of the research work is enumerated as follows-

1. *Preparation of Chitosan/bio-ceramic based composite scaffolds*

Chitosan is an attractive biopolymer for tissue engineering applications. However, chitosan lacks in sufficient mechanical strength and bioactivity that limit its use particularly in bone tissue engineering. In this phase of research work, efforts will be given to develop composite scaffolds with improved mechanical and bioactive property by incorporating β-TCP into CS. It is further evident that the use of particles at nano size is better than micro one. Therefore, the effect of nano and micro sized β-TCP on the properties of the developed CS composite scaffolds will be evaluated to achieve potential tissue engineered scaffold.

2. Characterization of scaffolds

It is utmost important to assess surface, mechanical and biological properties of the scaffold to confirm their suitability for bone tissue regeneration. Morphological, structural, pore size, hydrophilicity, porosity, compressive strength, biodegradability, swelling behaviour and bioactivity of the developed scaffolds will be characterized. The cell supportive property in terms of cell attachment, cell proliferation, metabolic activity and osteogenic differentiation potential will be evaluated.

3. Development of fibrin conjugated Chitosan/β-TCP composite scaffolds

It is evident from literature that CS lacks in cell signalling molecules representing its lower cell supportive property. Hence, the cell binding affinity of the developed CS/β-TCP composite scaffold will be improved by surface modification with fibrin as bioactive molecule. The developed fibrin conjugated composite scaffold will be characterised as mentioned above.

4. Development of cross-linked Chitosan/β-TCP scaffolds

The rapid degradation of chitosan is another important factor that needs to be addressed to match between the degradation and the rate of new tissue formation. Though an improved degradation is expected by the addition of bio-ceramic, still challenge will remain for further improvement of this property to achieve desirable degradation level. In this context, the fast degradation of the developed scaffolds will be reduced by cross-linking with suitable cross linking agent. The modified scaffold will be characterised for its physico-chemical, mechanical and biological properties.

5. Development of fibrin coated cross-linked Chitosan/β-TCP composite scaffolds

To make the developed cross-linked chitosan/β-TCP composite scaffold more effective towards bone tissue regeneration, the cell supportive property will be improved by surface coating with fibrin. The developed scaffolds will be evaluated for their *in-vitro* biocompatibility in terms of cell attachment, spreading, proliferation and differentiation etc and *in-vivo* animal testing.

Chapter 4

Materials and Methods

4. 1 Materials

4.1.1 Preparation of scaffold

Chitosan of medium molecular weight-190kD and degree of deacetylation 90% was purchased from Marine chemicals, India. Micro and nano sized β-tricalcium phosphate [$Ca_3(PO_4)_2$ with >98%, β-phase, fibrinogen, prothrombin *N*,*N*-(3-dimethylaminopropyl)-*N*′-ethyl carbodimide (EDC), *N* hydroxysuccinimide (NHS), 2-(*N* morpholino) ethanesulfonic acid (MES), lysozyme, genipin, NaCl, KCl, $CaCl_2$, $MgCl_2$, K_2HPO_4, $NaHCO_3$, Na_2SO_4 and sodium tripolyphosphate (TPP) were procured from Sigma Aldrich (USA). Sodium hydroxide (NaOH), di sodium hydrogen phosphate (Na_2HPO_4), glycine, ethanol (C_2H_5OH) and acetic acid were obtained from Merck India Ltd.

4.1.2 Cell culture study

Dulbecco's modified eagle medium (DMEM) from Gibco (BRL, USA) and (Hyclone FBS, USA), penicillin-streptomycin solution, fetal bovine serum (Hi-FBS), Dulbecco's phosphate buffered saline (DPBS), Collagenase type I and 0.25% Trypsin/EDTA solutions were obtained from Gibco (BRL, USA). Para formaldehyde and MSCs qualified Fetal bovine serum (FBS) were purchased from (Hyclone FBS, USA). Quant-it Pico Green dsDNA reagent kit and TRIzol were procured from Invitrogen, USA. Ascorbic acid, β-glycero-phosphate, Triton X, Calcein-AM, Ethediumhomodimer, Quanti chrome calcium and ALP assay kits were purchased from Bioassay Systems, USA. Phalloidin-Alexa Fluor 488 conjugate, Hoescht dyes were purchased from Invitrogen, USA. MTT assay reagent, Commassie blue G-250 are from Hi-Media labs, India. Growth factors EGF and bFGF, BD FACS lysis buffer, CD 34-FITC, CD 29-FITC, CD44-FITC, CD45- FITC, CD73- FITC, CD90- FITC, CD105- FITC and HLA-DR- FITC were purchased from Becton Dickenson, San Jose, CA. Dexamethasone (DEX), staurosporine, α-MEM, L-glutamine, L-ascorbate, β-glycerophosphate (βGP), protease XIV, bovine serum albumin (BSA), Alizarin red S**,** propidium iodide, Osmium tetroxide, tris-buffer, Mg acetate and 1, 9-dimethylmethylene blue (DMMB) were from Sigma-Aldrich (St Louis, MO, USA). Primers used for PCR were purchased from Sigma Aldrich and cDNA synthesis kit from Fermentas. All the tissue culture plastic wares were purchased from BD falcon and RNase was purchased from MP Biomedicals, USA.

4.2 Characterization of β-TCP powder

4.2.1 Morphology: FE-SEM was used to observe the morphology of both sized β-TCP

4.2.2 Average particle size crystallite size: Average particle size was measured by DLS (Dynamic Light Scattering) method

4.2.3 Specific surface area: BET was used to calculate the surface area of both micro and nano sized β-TCP.

4.2.4 Crystallite size: Crystallite size of β-TCP particles was calculated by "Tiny tools" (online tool) using the following equation. $D_p = 0.94\lambda / \beta_{1/2} \cos\theta$. D_p = crystallite size, β = line broadening in radius, θ is the Bragg angle and wavelength (λ=1.54056 A^0). Peak length and peak position are obtained from X'pert high score.

4.3 Preparation of scaffolds

4.3.1 Preparation of CS scaffolds

Chitosan scaffolds were prepared by following the procedure reported elsewhere [17]. Briefly, CS was dissolved in aqueous acetic acid (0.1M) solution to form 2.5 wt% of polymer solution. The prepared polymer solution was poured into petridishes and kept at -20°C for 6 hr. The frozen petri dishes containing chitosan solution was immersed in a gelation medium consisting of pre cooled (-20ºC) NaOH: EtOH of 70:30(v/v) solutions. The petridishes were frozen at -20°C for 6 hr. The petridishes were removed from the gelation medium and dried in a vaccum drier [Labtech, Daihan LabtechCo.Ltd] for 6-8 hrs at 40°C. Finally the scaffold was rinsed thoroughly with phosphate buffer saline (PBS) and deionised water thrice followed by drying. The scaffolds were cut into specific dimensions and made ready for different characterization techniques.

4.3.2 Preparation of CS/β-TCP composite scaffolds

Beta tri calcium phosphate powder in micro and nano size (0.1, 0.2, 0.3, 0.4, and 0.5 wt %) was dispersed in deionised water for 5 min hr by ultrasonication. The dispersed particles were added to the chitosan solution drop by drop and allowed to stir overnight until homogeneity is achieved [38]. After this, exactly same method of the preparation of CS scaffold was followed. The obtained composite scaffolds were cut into specific dimensions and made ready for different characterization techniques. The schematic representation of the preparation of CS/β-TCP composite scaffolds is depicted in **Figure 4.1.**

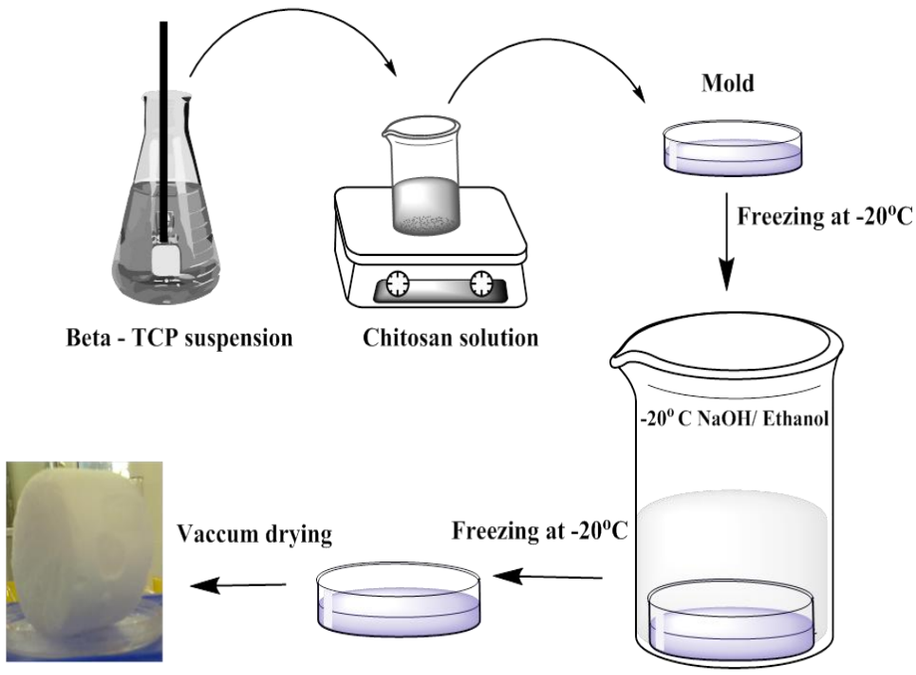

Figure 4.1: ***Schematic representation for the preparation of CS/β-TCP scaffolds by freeze-gelation method***

4.3.3 Development of fibrin conjugated CS/nano β-TCP composite scaffolds

Fibrin was conjugated to CS/nano β-TCP composite scaffolds by following the protocol reported earlier [190]. Briefly, CS/nano β-TCP composite freeze-gellled scaffolds were cross-linked with *N*,*N*-(3-dimethylaminopropyl)-*N′*-ethyl-carbodimide(EDC),*N* hydroxysuccinimide (NHS) solution at 105°C for 24 hrs. After washing with double-distilled water for 3 times (10 min each), the scaffolds were dried to obtain EDC/NHS-treated CS/nano β-TCP composite

scaffolds. The scaffolds were then sterilized in 75% ethanol overnight followed by a PBS wash. 50 μL of fibrinogen (80 mg/ml) and thrombin (600 U/ml) solutions were spread on the surface of the CS/nano β-TCP scaffolds and kept for incubation at 37°C for 30 min till fibrin forms on the surface of CS/nano β-TCP composite scaffolds.

4.3.4 Development of cross-linked CS/nano β-TCP composite scaffolds

Different concentrations of genipin (GN) and sodium tripolyphosphate (TPP) in the range of 0.01-0.20 % (w/v) were added to CS/nano β-TCP composite solutions. The mixture was then stirred for 2 hrs and poured into petri-dishes according to the protocol followed earlier [78]. Cross-linked CS/nano β-TCP composite scaffolds were obtained by following the same protocol used for CS and CS/β-TCP composite scaffolds. The scaffolds were immersed in a standard glycine solution to remove the traces of unreacted cross-linking agents. Finally scaffolds were neutralized by 0.1 M Na_2HPO_4 rinsed with deionised water, dried and preserved for further experiments [191].

4.3.5 Development of fibrin coated GN cross-linked CS/nano β-TCP composite scaffolds

Genipin cross-linked CS/nano β-TCP composite scaffolds were coated with fibrin by following the protocol reported elsewhere [192]. Briefly, 1 ml of fibrinogen solution (2 wt%) was added in a test tube containing genipin cross-linked CS/nano β-TCP composite scaffolds and dried in a dessicator by applying vacuum. 1 ml of thrombin solution was added to the above dried sample in a test tube and incubated by using vacuum drier at 37° C for 12 hrs till fibrin forms on the scaffold.

4.4 Characterization of scaffolds

4.4.1 Rheological behaviour

The viscosity of pure CS and CS/β-TCP composite solutions was analyzed by rotational cone (diameter = 30 mm; angle = 5.4°) and plate viscometer [Bohlin Visco-88, Malvern, UK]. A constant gap of 0.15 mm was maintained between cone and the plate throughout the study. The variable shear rate applied was in the range of 20 to 100 sec^{-1} in 16 min. All the samples

were analysed at room temperature. The data has been analyzed with Bohlin visco-8 software using cross model [193].

4.4.2 Morphological study

Scanning Electron Microscopy (SEM) was performed using a JEOL-JSM 6480 LV to observe the morphology of developed pure CS and CS based composite scaffolds. The traces of moisture present in the scaffolds were removed by drying in a vacuum drier for 2 hrs at 40°C. Platinum coating was done prior to imaging. A minimum of 25 pores were considered for calculating the pore size of the developed scaffolds by using Image J (USA) software.

4.4.3 Porosity measurement

The porosity of developed scaffolds was measured by Mercury intrusion porosimeter [Poremaster-33, Quantachrome, USA].The bulk density of samples was calculated by equation, $B.D = D/W - S$, where D = dry weight, S = suspended Weight, W = soaked Weight. The percentage porosity was calculated from intrusion data. For all types of scaffolds, experiments were carried out in triplicates. The porosity was measured using Washburn equation: $D = (1/P)4\gamma(\cos\varphi)$ which is based on the relationship between the applied pressure and the pore diameter into which mercury intrudes. The various parameters of the equation are: D is the pore diameter, γ is surface tension of mercury, φ is the contact angle between mercury and the pore wall P is the applied pressure [128].

4.4.4 Phase analysis

Phase analysis of developed CS and CS based composite scaffolds was performed by X-ray Diffractometer [PANalytical, X'pertPhilips,USA] using Cu-Kα radiation (λ= 0.1542 A°) in a step-scan mode in the 2θ range of 10-80° with a scanning speed of 2° per min [194]. The operating conditions were 30 kV and 30 mA.

4.4.5 Functional analysis

Fourier transform infrared spectroscopy (FTIR) was performed to evaluate the structural property and functional groups of the developed CS and CS based composite scaffolds by using an Infra red Microscope [Shimadzu AIM-8800, Japan]. Hydraulic press was used to

pelletize the scaffold samples by mixing them with dry KBr powder. The mixture was pressed into transparent disks and used for IR analysis. The machine was operated in transmittance mode by using the range 500 to 4000cm^{-1} with a resolution of 8cm^{-1} [30].

4.4.6 Contact angle measurement

The contact angle of the developed pure CS and CS based composite scaffolds (films) was measured by a contact angle meter K100MK3 tensiometer (KrussGmbH, Hamburg, Germany). Films of width (15mm), height (10mm) and thickness (1mm) were used for analysis. Water was used as the solvent for accomplishing the measurements. All the samples were analyzed at room temperature in triplicates [184].

4.4.7 Mechanical strength

Compressive tests of the prepared CS and CS based composite scaffolds were carried out by Universal testing machine (H10 KS Tinius Olsen USA). Cylindrical samples with a diameter of 10 mm and thickness of 15 mm were used for analysis. Compression test was performed with a crosshead speed of 1 mm/min with a load cell of 1000N. Each scaffold sample was tested in triplicate. Compressive strength was calculated by using the formula $S = F_{\max} / A$, where F_{max} represents the force applied and A is the cross sectional area of the sample [191]. Similarly, compressive strength of (cross-linked scaffolds) in wet condition is also measured by following the procedure reported elsewhere [16]. Briefly, the scaffolds were immersed in PBS for 30 min and similar process was repeated as mentioned above.

4.4.8 Swelling behaviour

Swelling behavior of the developed CS and CS based composite scaffolds was evaluated using deionised water at room temperature until they reach equilibrium at different time intervals (1 h, 3 hrs, 5 hrs, 7 hrs, 24 hrs and 42 hrs). The weight of the scaffold samples before immersion in water is DRY_{wt} and after immersion at particular time point is denoted as WET_{wt}. The following formula (Mathtype 5.0) was used to determine % swelling of scaffold [16].

$$\% \, Swelling = (WET_{wt} - DRY_{wt}) / DRY_{wt} \times 100 \qquad \text{..... (1)}$$

4.4.9 *In-vitro* biodegradation study

In-vitro biodegradation study of the developed CS and CS based composite scaffolds was performed by soaking them in PBS containing 500 µg ml^{-1} of lysozyme. The initial dry weight of the scaffold samples were weighed and noted as W_I. The soaking time of the samples was 1,7,14 and 28 days. The samples were removed at regular time intervals and freeze dried before calculating the final weight, $W_{F.}$ The remaining weight % (W_R) was calculated according to the formula given below. All the experiments were performed in triplicates [38].

$$\%\ \ Weight\ \ remaining = 100 - [(W_o - W_t)/W_o \times 100] \quad \text{..... (2)}$$

4.4.10 Bioactivity

SBF was prepared according to the previous reports by adding NaCl (7.995 g), KCl (0.224 g), $CaCl_2 \cdot 2H_2O$ (0.368 g), $MgCl_2 \cdot 6H_2O$ (0.305 g), K_2HPO4 (0.174 g), $NaHCO_3$ (0.349 g), and $Na_2SO_4 \cdot 10H_2O$ (0.161 g) to 1 L of distilled water in the same order as mentioned [195]. The final pH of the solution was maintained at 7.4 by the addition of Tris/HCl. In order to assess the bioactivity of developed scaffolds *in-vitro*, the samples were incubated in the prepared SBF. 1.5 g of the sample was placed in SBF (20 ml) and incubated at 37°C for 1, 7, 14, 21 days. After each time point of soaking, scaffolds were taken out from SBF, rinsed with distilled water and the moisture was removed with tissue paper. Finally the samples were vacuum dried at room temperature to remove the traces of moisture present in them. SEM was used to observe the crystals formed on the scaffold surface. Morphology and elemental analysis of the scaffolds were done using SEM and EDX facilities [191].

4.5 *In-vitro* cell study

4.5.1 Isolation and culture of MSCs

Umbilical Cord Blood was collected from the Ispat General Hospital, Rourkela, India with prior consent of the patient. Mononuclear cells (MNCs) were isolated in our stem cell lab by Ficoll Hypaque technique described in literature [196]. The isolated MNCs were cultured in Dulbecco's Modified Eagle Medium adjunct with 10% fetal bovine serum, 1% non-essential amino acid, 1% 200mM L-glutamine, 2% 1M HEPES [4-(2-hydroxyethyl)-1-piperazineethanesulfonic acid)] buffer**,** 0.150 gms/liter L-ascorbic acid, 100U/ml penicillin

and 0.1 mg/ml streptomycin [expansion medium]. The cell culture conditions were 37 ^{0}C, 5% CO_2 with 80% relative humidity. Based on the unique adherent property, MSCs were separated from non-adherent cells in culture flasks and non adherent cells were discarded. The adherent cells consisting of MSCs were washed thoroughly with D-PBS/EDTA and supplemented with freshly prepared expansion medium. The cells were cultured upto 4th passage by changing the media twice in a week.

4.5.2 Characterization of MSCs

Fluorescence activated cell sorting (FACS ARIA III; BD Biosciences) was used to sort the MSCs from the cultured MNCs. CD90 FITC-, CD73- FITC, CD105- FITC, CD44-FITC, CD45 FITC, HLA-DR FITC and CD34 FITC (BD Pharmingen, San Jose, CA make) were used for sorting. CD44, CD90, CD73 and CD105 were used as positive markers. Further culturing of sorted MSCs was done in DMEM by changing media twice in a week. Fibroblast like morphology of cultured cells indicates the presence of mesenchymal stem cells.

4.5.3 Cell seeding and culture

Scaffolds (10x10x1.5 mm) were sterilized prior to cell seeding by soaking in 70% ethanol and 10 U/ml penicillin solution for 2 hrs followed by sterile PBS wash. Cells from 4th passage were seeded on sterilized scaffolds with a seeding density of 5×10^6 cells/ml by static method [197]. The cell seeded scaffolds were incubated in culture medium with a media change for every 3 days.

4.5.4 Cell morphology and cell attachment

Human mesenchymal stem cell (hMSCs) seeded CS and CS based composite scaffolds were cross-linked with 4% paraformaldehyde in phosphate buffered saline (PBS). 2% (v/v) gluteraldehyde was used for fixing the cells and the samples were rinsed with wash buffer. Osmium tetroxide (1%) was added to the samples and kept aside for 30 min. Then the samples were rinsed with wash buffer for five times and dehydrated with series of ethanol gradations (50, 70, 80, 95 and 100%) for 10 min each [128]. Finally the samples were air dried at 37°C and sputter coated with gold, platinum for 30 sec prior to imaging.

(Quorumtech, Q150RES, Czech Republic). Images were taken by SEM [JEOL-JSM 6480 LV], SEM [Tescan Vega-3, SBU-USA] and Field Emission Scanning Electron Microscopy (FE-SEM) [Nova SEM-Czech Republic] in high vacuum at 30 kV.

4.5.5 Metabolic activity

4.5.5.1 MTT assay

The metabolic activity of hMSCs cultured on CS and CS based composite scaffolds was evaluated quantitatively by MTT [3-(4, 5-dimethylthiazol-2-yl)-diphenyltetrazolium bromide] assay [198]. Fresh media was supplemented to the cells consisting of 100µl MTT solution (diluted in 1:10 PBS). Then the cells were incubated at 37°C for 4 hrs 0.5 ml DMSO was added and centrifuged at 1000 rpm for 5 min. The optical density (O.D) of intense pink colored formazan derivative was measured using a spectrophotometric plate reader (2030 multi label reader Victor X3, Perklin Elmer, USA) at 595 nm.

4.5.6 Cell proliferation study

4.5.6.1 Fluorescence Microscopy

CS and CS based composite scaffolds with a dimension of 1cm×0.5cm×1mm were used for fluorescent imaging. Cell (hMSCs) seeded scaffolds were cultured for predetermined time periods, collected on a clean microscopic slide and finally mounted with glycerol: PBS (1:1 ratio). Fluorescent microscope [Carl Zeiss E_{600}, Wavelength= 450 nm] was used for imaging using a green filter at wavelength 490 nm [199].

4.5.6.2 Alamar blue assay

Proliferation of hMSCs on the developed scaffolds was checked by Alamar blue dye reduction assay at specific time intervals of 3, 5 and 7 days of culture. The colour change of alamar blue dye can be attributed to the reduction of dye by mitochondrial enzymes. 100 µL of Alamar blue was added to the scaffolds in 1 ml of the media and incubated for 5 h at 37ºC. The absorbance was measured at 570 nm using a multi plate reader and proliferation was calculated according to manufacturer's protocol [200].

4.5.6.3 DNA quantification assay

Proliferation of hMSCs on CS and CS based composite scaffolds was also studied by DNA quantification assay. Cell scaffold constructs from each predetermined time period of culture (3, 7, 14 and 21 days) were collected and washed with serum free DMEM to remove the traces of serum components. Finally the constructs were washed with PBS and cells were lysed using 0.4 mL of Lysis buffer containing 10 mM tris and 2% triton for 1 hr. Quant-it PicoGreen reagent was used according to the manufacturer's protocol. Briefly, 100 µL of Quant-it PicoGreen reagent was added to 100 µL of sonicated cell lysate and incubated at room temperature for 10 min. The fluorescence was measured with a spectrofluorometric plate reader (LS 55, Perklin Elmer, USA) at excitation and emission wave lengths of 528 nm and 485 nm respectively. The readings were correlated with the number of cells using a calibration curve constructed with hMSCs of known concentration [201].

4.5.7 Cell distribution and cytoskeletal organization

Cell distribution and cytoskeletal organisation on cell seeded scaffolds were analyzed by confocal laser scanning microscopy using Hoescht and Alexa Floor 488 Phalloidin according to the protocol followed elsewhere [202]. Briefly, cell scaffold constructs after 14 days of culture were fixed with 4% paraformaldehyde for 1 min followed by Hoescht nuclear staining for 1 min. Prior to stain F–actin, the cell seeded scaffold constructs were fixed with 3.7% paraformaldehyde for 10 min followed by permeabilization with Triton-X for 5 min and then blocked with PBS containing 1% Bovine Serum Albumin for 30 min. Finally, the constructs were stained with Phalloidin conjugated to Alexa Floor and the samples were examined by confocal laser scanning microscope (CLSM Leica SP8 inverted microscope, Germany equipped with HeNe 633 nm laser) at excitation wavelength of 488 nm and 633 nm. Images were collected in z-stack mode with optical sectioning at 0.2 µm and converted to 3D images in Leica LAS AF lite software to visualise distribution of cells inside the scaffold.

4.5.8 Osteogenic differentiation potential

4.5.8.1 Alkaline Phosphatase assay (ALP)

Alkaline phosphatase (ALP) activity of hMSCs grown on CS and CS based composite scaffolds was performed to assess the osteogenic differentiation ability by using Quanti Chrom Alkaline Phosphatase Assay Kit according to manufacturer's protocol. In brief, the scaffolds cultured in osteogenic differentiation medium for 3, 7, 14 and 28 days were collected and washed with PBS. The cells were treated with 1% Triton X-100 for 60 min and centrifuged at 10,000 rpm at 4˚C for 15 min.190 µL of working solution having 10 mM p-nitro phenyl phosphate and 5mM magnesium acetate was added to the 10 µL cell lysate and incubated for 4 min at 37°C. The absorbance was measured at 405 nm with a micro plate reader at time zero and after 4 min. ALPase activity was calculated according to the equation given below and the measured ALPase activity was normalized to DNA content [201].

$$[(A_{t=4} - A_{t=0}) / (A_{calibrator} - A_{ddH_2O}) \times 808] \quad \text{..... (3)}$$

4.5.8.2 Measurement of total calcium content

Total calcium content of hMSCs cultured on CS and CS based composite scaffolds was measured by QuantiChrom Calcium Assay according to manufacturers' protocol. Briefly, 0.2 ml of 2M HCl was added to 0.2 ml aliquot of sonicated cell lysate to dissolve the calcium content of mineralized matrix. 5 µL of cell lysate was added to 200 µL of working solution and incubated for 3 min at 27ºC. The absorbance was measured at 612 nm with a micro plate reader. The measured absorbance was correlated to equivalent amounts of Ca^{+2} using a standard calibration curve of $CaCl_2$ solution of known concentration ranging from zero to 200 µg/mL [201]. The scaffold without cells was used as control. The calculated Ca content of control (time zero) was deducted from the amount of total Ca content obtained at predetermined time points.

4.5.8.3 *In-vitro* biomineralization (Alizarin red assay)

Alizarin red assay was used to quantify the mineralization of hMSCs on the CS based composite scaffolds. hMSCs seeded scaffolds were washed with PBS and fixed with 4% paraformaldehyde for 20 min. The scaffolds were then washed thoroughly with distilled

water. 400 µL of Alizarin red stain (40 mM pH 4.1) was added and the samples were incubated at room temperature for 10 min. Images were taken using optical microscope. In order to determine the mineralization, alizarin red stains were removed from the scaffolds by treating with 500 µL of cetylpyridinium chloride for 1 hr. 300 µL of the extract was collected and O.D was measured at 540 nm using 2030 multi label reader Victor X3, Perklin Elmer, USA [203]. The scaffold without cells was used as control.

4.5.8.4 Estimation of GAG (Glycosamino glycan)

The amount of intracellular GAG secreted by the MSCs cultured on developed scaffolds was evaluated by GAG assay using 1, 9-dimethylmethylene blue (DMMB) in a microplate reader. The intracellular GAG was removed from the cells by digestion with papain solution (125 µg/mL of papain, 5 mM L-cystein, 100 mM Na_2HPO_4, 5 mM EDTA) at pH 6.8, 60°C for 16 hrs and analyzed using a microplate reader. Then, the absorbance of the GAG-DMMB complexes was measured at 525 nm [204].

4.5.8.5 Expression of osteogenic specific genes

Semi-quantitative RT-PCR was performed to assess the expression of osteoblast related markers at mRNA level for cells cultured for 28 days. Primer sequences used for the study are shown in **Table 4.1**. For RT-PCR analysis, the total cellular RNA from osteoblasts (differentiated from hMSCs) was extracted by TRIzol. Synthesis of cDNA was carried out using first strand cDNA synthesis kit following the manufacturer's protocol. The synthesized cDNA was used as a template for the semi-quantitative RT-PCR following the procedure followed elsewhere [205]. The β-actin gene was used as a housekeeping gene for normalizing mRNA level of ALP, OC, ON, BSP and Col-1 gene. The PCR reaction mixture consists of 1X PCR buffer, 50 mM $mgCl_2$, 10 mM dNTPs, 0.2 µM of each primer, 1U Taq polymerase and autoclaved water. PCR chain reactions were performed at 94°C for 2 min, 35 cycles at 96°C for 30s, 55–63°C for 45s, and 72°C for 45s and 72°C for 10 min. Finally, the amplified DNA fragments (PCR products) were subjected to electrophoresis on 1.5% agarose gel and the band intensity was analysed using Image J software for evaluating the relative expression of selected genes (BioRad, USA).

Table 4.1: ***RT-PCR Primers used for expression of osteogenic specific genes***

Gene	Direction	Primer sequence
β-actin	Forward Reverse	5^1- TCTACAATGAGCTGCGTGTG-3^1 5^1- CAACTAAGTCATAGTCCGCC-3^1
Bone Sialo protein (BSP)	Forward Reverse	5^1- CTTACCGAGCTTATGAGGATGAATA-3^1 5^1- ATTGGGAAGCAGAAAGATTAGATG-3^1
Osteonectin (ON)	Forward Reverse	5^1- CAC TGG CGC TGC AACAAG A-3^1 5^1- CAT TCC GGA GCT CAGCAG AAT-3^1
Alkaline phosphatase (ALP)	Forward Reverse	5^1- GGG GGT GGC CGG AAATAC AT-3^1 5^1- GGG GGC CAG ACC AAAGAT AG-3^1
Osteocalcin (OC)	Forward Reverse	5^1- CCC AGG CGC TAC CTGTAT CAA-3^1 5^1- GGT CAG CCA ACT CGTCAC AGTC-3^1
Collagen I (Col I)	Forward Reverse	5^1- GGCAATAGCAGGTTCACGTACA -3^1 5^1- CGATAACAGTCTTGCCCCACTT-3^1

4.6 *In-vivo* biocompatibility test in animal model

The developed scaffolds have been transplanted under the skin of 4 to 6 weeks old mice as per procedure described previously with a slight modification [206]. In brief, intra-peritoneal injection of avertin (Tri-bromoethanol, 0.25 mg/g of body weight; 2-methyl-2-butanol, 0.16 mL/g) was given to anesthetize the mice and the skin was sterilized with 70% (v/v) ethanol. Approximately ~1 cm linear incision was made on the back in the cervical region of NMRI-nude mice and scaffolds have been implanted subcutaneously. Scaffolds of dimension 5 x 5 cm^2 have been transplanted into the surgically-created subcutaneous pouch and the incision was closed using nylon suture. The mice were monitored routinely for the skin and systemic diseases, if any. After one month, they were sacrificed by cervical dislocation and the scaffolds were explanted. Histological analysis was done with the skin around the site of transplantation [207]. The skin samples were fixed with 10% (v/v) neutral buffered formalin and dehydrated in ascending grades of 40%, 60%, 80%, 95% and 100% ethanol and then embedded in paraffin wax. 5 µm thick slices of specimens were made by microtome sectioning and examined histologically after hematoxylin and eosin staining [13, 208]. All the experiments were performed under the aseptic condition in compliance with the guidelines for care and use of animals in research and teaching, published by the Federation of Animal Science Societies (3rd Edition, 2000), and were approved by the Institutional Biosafety and Ethical Committee, University of Konkuk, South Korea. Efforts were given to ameliorate the suffering of animals.

4.7 Statistical analysis

Statistical differences were evaluated by the Tukey-Kramer test after one way analysis of variance at $p < 0.05$ by using online version of graphpad quick calc software. The statistical analysis data was expressed as mean ± standard deviation with $n = 3$.

Chapter 5

Results and discussion

PART-I

Preparation and Characterization of Freeze-gelled CS and CS/β-TCP Composite Scaffolds

From literature it is evident that chitosan (CS) is a potential scaffold material for tissue engineering applications because of its high biocompatibility, biodegradability, intrinsic anti bacterial property**,** renewability and bio-functionality [57]. However, CS lacks sufficient mechanical strength and bioactivity that limits its application in bone tissue engineering. Recent research, therefore, focuses on the improvement of mechanical strength and bioactivity of CS by adding bio-ceramics. Among bioactive ceramic materials, hydroxy apatite (HAp) [11, 20, 54, 149], and beta tricalcium phosphate (β-TCP) [12, 73, 228] are attractive scaffold materials for bone tissue repair and regeneration due to their compatibility to natural bone tissue and excellent osteogenic property [209]. However, the limitation of HAp is that it is not degradable in physiological conditions and resides within the regenerated bone tissue [55]. The use of β-TCP is advantageous with respect to its biodegradability [50] and its osteoconductive as well as osteoinductive property instead of mainly osteoconductive property of HAp [210]. Development of 3D porous scaffolds that can resemble natural extra cellular matrix by suitable fabrication technique is another important aspect for tissue engineering applications [63]. These methods offer scaffolds with adequate pore size and porosity. In this context, freeze-gelation which works on the principle of phase separation offers a simple, low cost, easy to scale up, time and energy saving method for the fabrication of 3D porous scaffold that can mimic unique hierarchical architecture of bone matrix. [74, 76, 78]. Keeping the above aspects in view, in this phase of thesis, efforts have been given to develop CS/β-TCP composite scaffolds by incorporating β-TCP as a bioactive material by freeze-gelation method. The effect of micro and nano size β-TCP on CS scaffold properties was investigated to achieve optimal mechanical strength of freeze-gelled scaffolds. The potentiality of the scaffold for bone tissue regeneration was evaluated by various physico-chemical, mechanical and biological characterizations. Result and discussion of this research work is described in this chapter.

5.1.1. Characterization of β-TCP powder

The commercially available β-TCP powder was characterised by standard methods and the results are presented here-

The morphological features were observed by FE-SEM images as shown in figure 5.1.

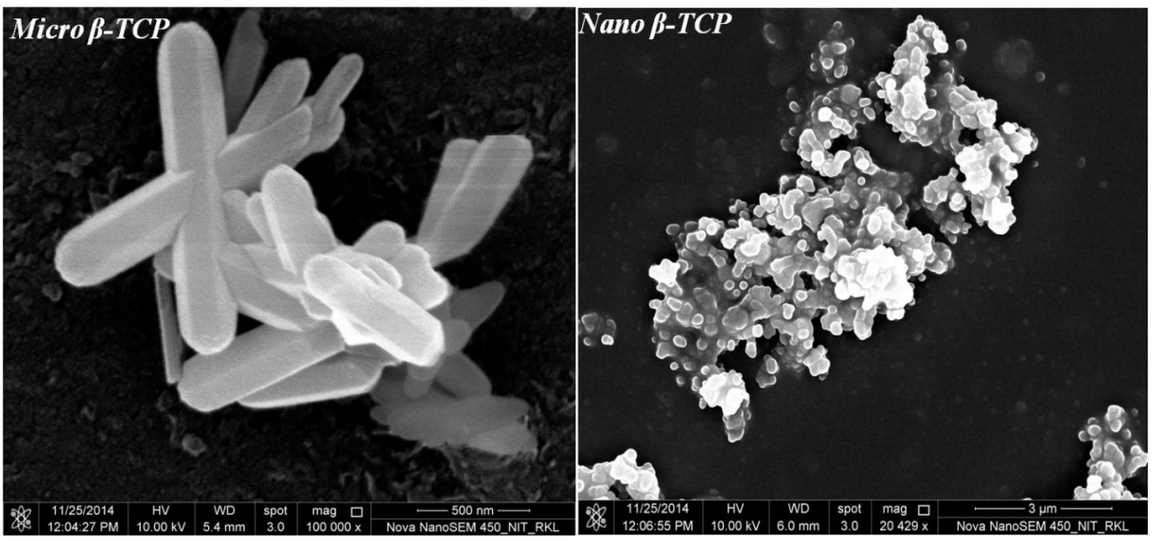

Figure 5.1: FE-SEM images of micro and nano β-TCP

The average particle size of β-TCP was measured by DLS method. The particle sizes are 811nm and 82nm for micro β-TCP and nano β-TCP respectively.

The average surface area of micro β-TCP and nano β-TCP was calculated by BET and the corresponding values are 1.24 m^2 /gm and 6.67 m^2 /gm.

The crystallite size measured from XRD data are 142 nm and 13.9 nm of micro and nano β-TCP particles respectively.

5.1.2 Rheological behaviour of CS and CS/β-TCP composite solutions

The flow behaviour of a polymer solution has been reported to depend on the composition and stability of the composite suspensions [211]. Viscosity was therefore analyzed for both polymer (CS) and polymer-ceramic solutions (CS/β-TCP) under varied shear stress. All the solutions have shown non-Newtonian behaviour with shear thinning property. **Figure 5.2** depicts the shear thinning ability of pure and composite [CS/micro β-TCP (80:20), CS/nano β-TCP (80:20)] solutions. CS solution has shown lower viscosity (1.21 Pa s) in comparison to the composite solutions with varied micron (1.31-1.99 Pa s) and nano sized β-TCP content (1.25-1.36 Pa s). It is further observed that the increase in β-TCP content increases the

viscosity of CS/β-TCP composite solution in a linear fashion**.** The viscosity of all other solutions with different β-TCP ratios is shown in **Table 5.1.** As indicated, the decrease of particle size decreases the viscosity of suspension as reported earlier [250]. The homogeneity of composite solution is observed to be decreased as TCP concentration increases. As a result, the layers in the composite solutions begun to show restricted movement cumulating in increased viscosity. This alteration in viscosity has an impact on pore size of developed scaffolds as reported earlier [53].

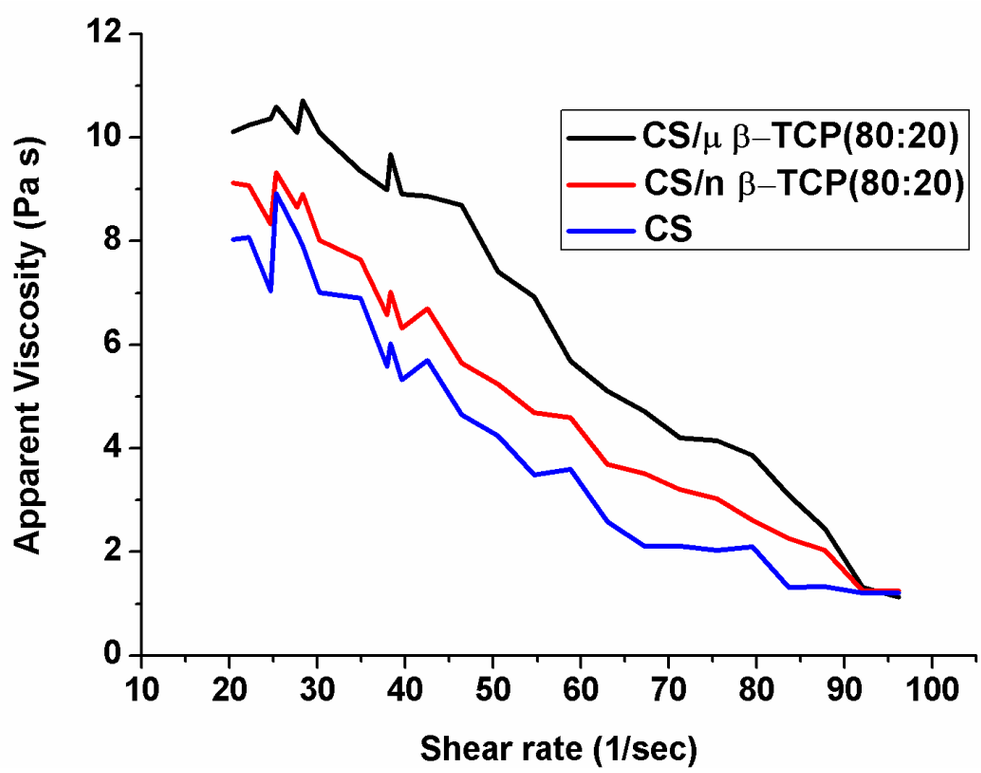

Figure 5.2: ***Rheological behaviour of CS, CS/micro β-TCP (80:20) and CS/nano β-TCP (80:20) composite solutions. All the solutions show non Newtonian behaviour with shear thinning property. CS/micro β-TCP and CS/nano β-TCP scaffolds are represented as CS/μ β-TCP and CS/n β-TCP in the figure respectively. [Data with other ratio of CS and β-TCP are not shown]***

Table 5.1: ***Viscosity of CS, composite scaffolds with varied content of β-TCP***

S.No	Sample	Viscosity (Pa s)
1	CS	1.214
2	CS/μ β-TCP (90:10)	1.317
3	CS/μ β-TCP (80:20)	1.609
4	CS/μ β-TCP (70:30)	1.722
5	CS/μ β-TCP(60:40)	1.860
6	CS/μ β-TCP(50:50)	1.991
7	CS/n β-TCP (90:10)	1.256
8	CS/n β-TCP (80:20)	1.277
9	CS/n β-TCP (70:30)	1.313
10	CS/n β-TCP (60:40)	1.342
11	CS/n β-TCP (50:50)	1.368

5.1.3 Preparation of scaffolds

3D porous chitosan and its composite scaffolds with varying amount of micro and nano size β-TCP were prepared by freeze-gelation method. The scaffolds are shown in **Figure 5.3**. The scaffolds are designated as CS (pure chitosan), CS/micro β-TCP (composite scaffold with micro size β-TCP) and CS/n β-TCP (composite scaffold with nano size β-TCP).

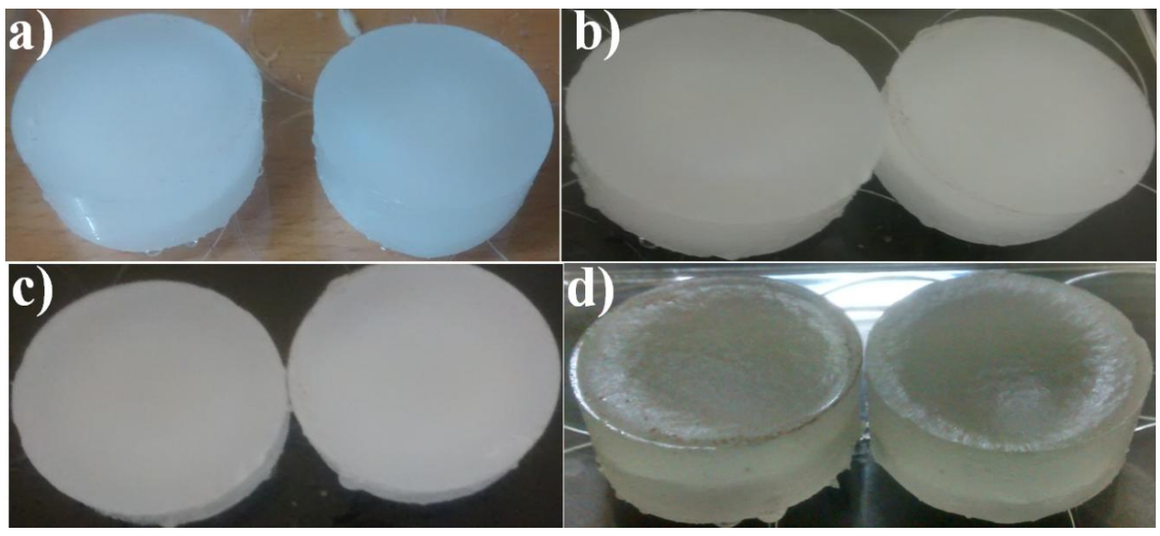

Figure 5.3 ***Developed pure CS scaffolds (a), CS/nano β-TCP composite scaffolds (b, c) and CS/micro β-TCP freeze-gelled composite scaffolds (d)***

5.1.4 Morphology and pore size

Adequate pore size and interconnectivity of pores in scaffolds are vital factors for the diffusion of oxygen and nutrients to the cells and foster transfer of metabolic wastes [102]. SEM images were taken to visualize these features. As observed, pure CS scaffold shows porous and excellent interconnected network of open pore microstructures **[Figure 5.4-(a)]** with a pore size range of 61-171 μm. Similar morphology and pore structure are also achieved with composite scaffolds. However, the pore diameter of CS scaffolds is found to decrease with increase in β-TCP content. This may be attributed to a slight increase in viscosity of composite solutions with increase in β-TCP content, which leads to restricted movement of ice crystal during freezing as reported earlier [54]. The ice crystal mobility responsible for pore diameter is reduced in high viscous solutions and hence a decrease in pore size of composite scaffolds is observed as compared to pure CS scaffolds. Similar observation of decrease in pore size was reported earlier when β-TCP was incorporated in various weight ratios into CS/gelatin 3D composite matrices developed for bone tissue regeneration **[53].** The other reason may be due to the loss of structural integrity of scaffolds at higher content of β-TCP resulting in irregularity in the pores and thus decrease in pore size [54]. Similar findings related to decrease in pore size of CS scaffolds reported earlier by incorporating bio-ceramics such as HAp, β-TCP and wollastonite [54, 68-69]. As observed, β-TCP is found to be more or less uniformly distributed over the scaffold surface and on the pore walls. **Figure 5.4** illustrates that there is no significant difference observed between pore size of nano β-TCP and pure CS scaffolds. On the contrary, scaffolds with varied micro β-TCP composite scaffolds show smaller pore size in comparison to pure CS scaffolds as shown in **Figure 5.4 (b - f).** The pore size range obtained with varied micro β-TCP content is 45-165 μm. However, after a certain limit of micro β-TCP content (>30% wt), the distribution of β-TCP is found to be non uniform due to the formation of agglomerates along the periphery of the pores as shown in **Figure 5.4 (A-b) and Figure 5.4 (B)** Whereas with CS/nano β-TCP composite scaffolds, the pores are found to be regular **[Figure 5.4 (A - c) and Figure 5.4 (C)]** and β-TCP is uniformly distributed over the entire scaffold surface and in the pore walls. The pore size range obtained with CS/nano β-TCP scaffold is 51-168 μm. The pore size range of

developed scaffolds with varied ratios of micro and nano β-TCP were measured and depicted in **Table 5.2.** Published reports suggest that the pore size of scaffolds should be in the range of 50-300 μm for bone tissue engineering applications and results obtained matches with the reported pore size range [134]. Thus the developed freeze-gelled CS and CS/β-TCP composite scaffolds have the required morphological necessity in terms of pore size and interconnecting pore networks for proper cell growth and proliferation of osteoblasts.

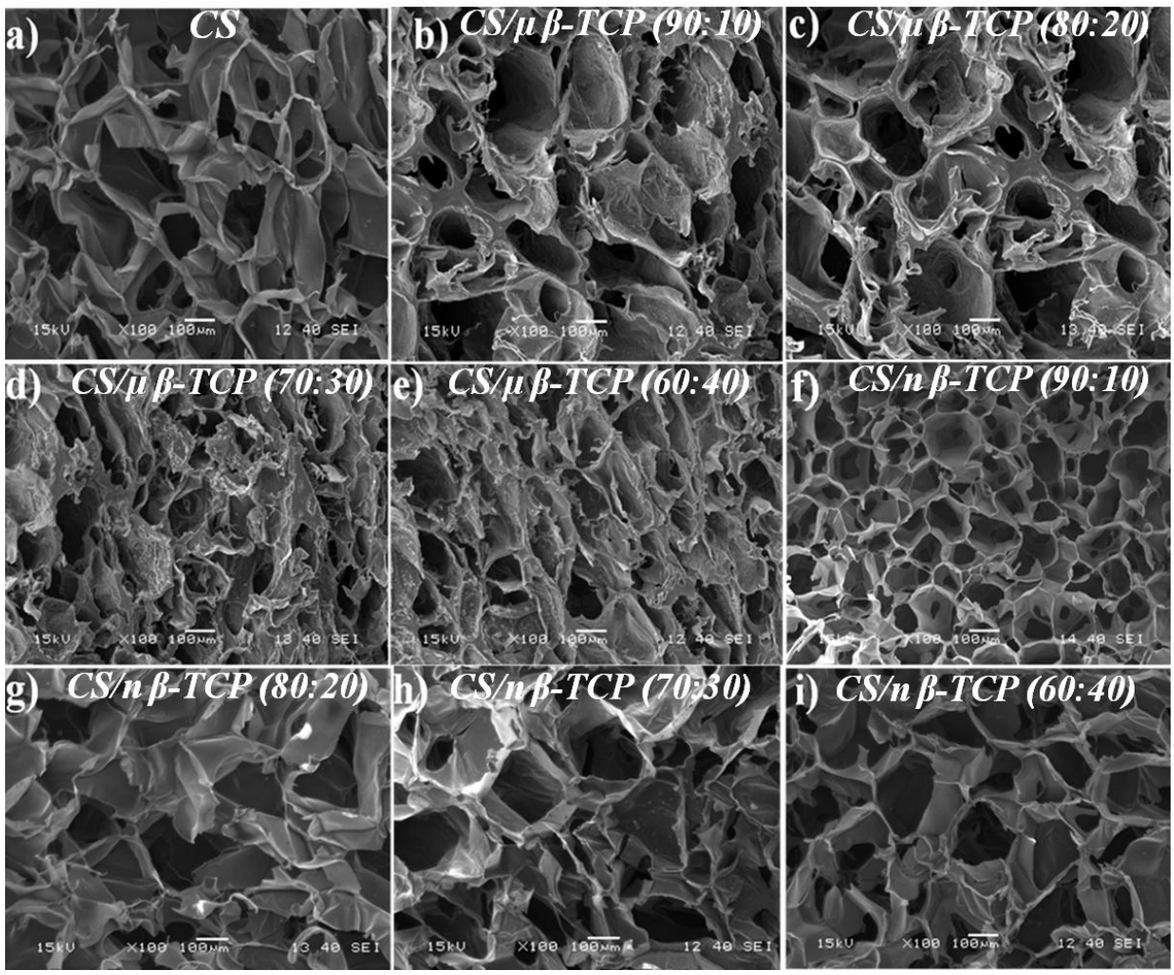

Figure 5.4: ***SEM images of the prepared freeze-gelled scaffolds. Open porous microstructure with interconnectivity is evident in pure CS and CS/β-TCP composite scaffolds. Decrease in pore size of composite scaffolds with increase in β-TCP content is noticed***

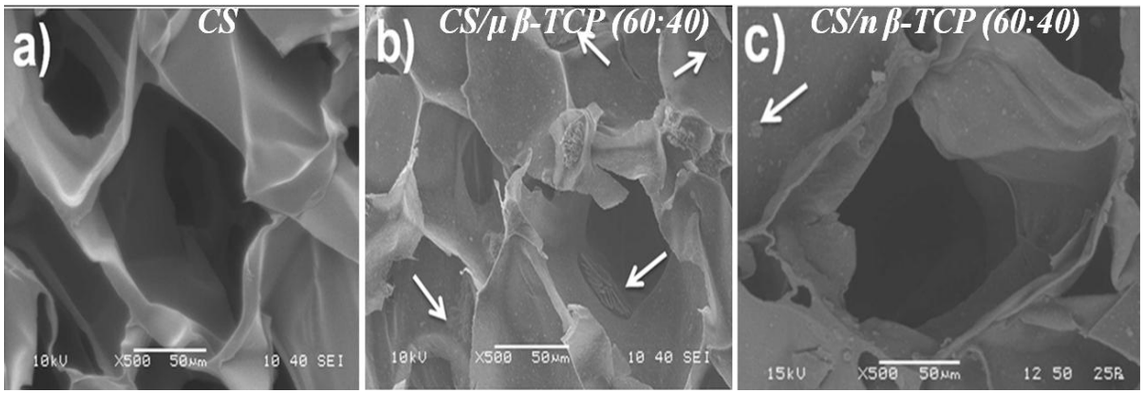

Figure 5.4 (A): ***SEM images of scaffolds at higher magnification. Pure CS scaffold (a); agglomerates of micro β-TCP are represented with white colour arrow marks (b); uniform distribution of nano β-TCP is represented with white colour arrow marks in (c)***

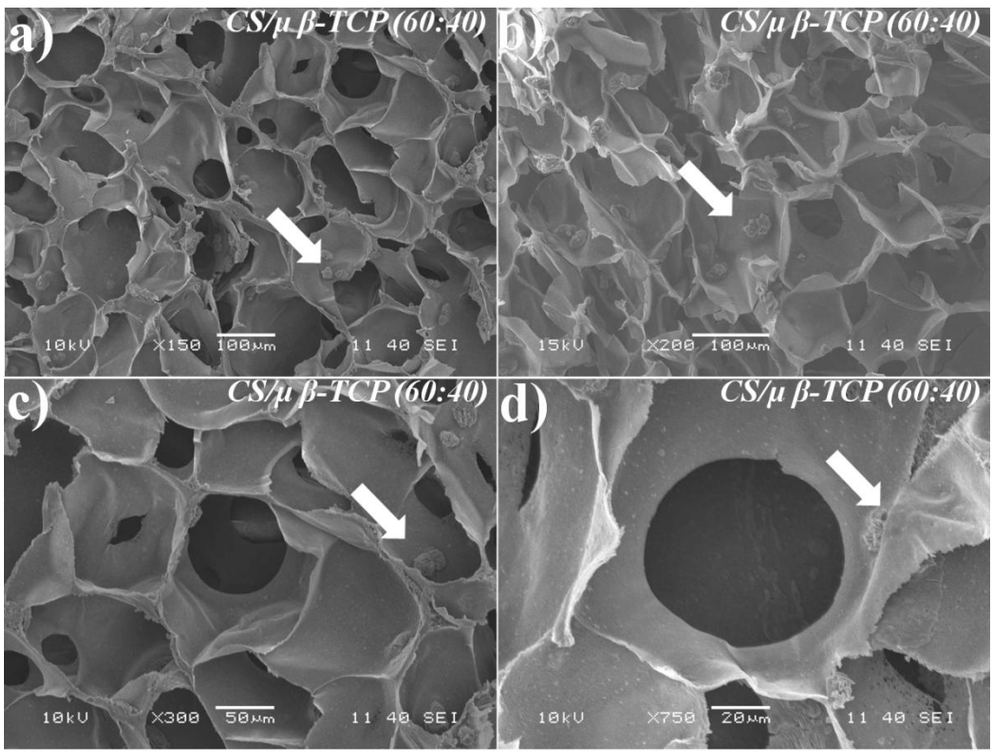

Figure 5.4 (B): ***SEM images of CS/β-TCP scaffolds at higher magnification. Agglomerates of micro β-TCP are represented with white colour arrow marks***

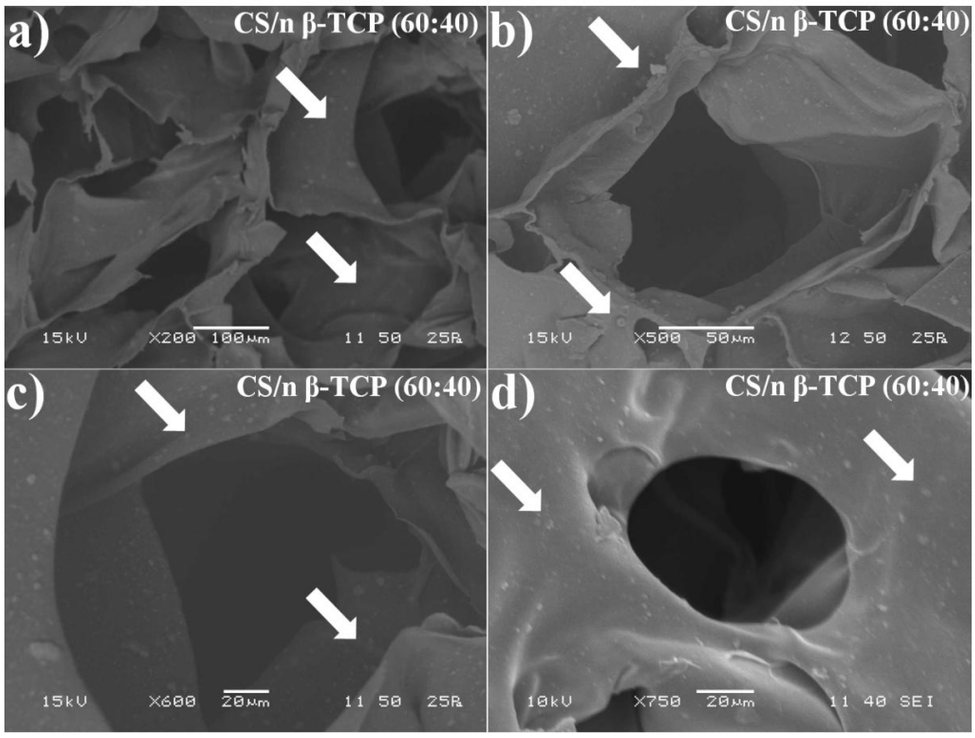

Figure 5.4 (C): ***SEM images of CS/β-TCP scaffolds at higher magnification. Uniform distribution of nano β-TCP is represented with white colour arrow marks***

5.1.5 Porosity

The porosity of scaffold is an important factor that decides not only the transport of nutrients required for cell growth but also cell infiltration and migration [5, 117]. **Table 5.2** shows the % porosity of the developed scaffolds. As indicated, the porosity of CS scaffold (86 ± 3.21) is decreased with increase in both nano and micro β-TCP content. The corresponding % porosity of CS/micro β-TCP and CS/nano β-TCP composite scaffolds are 80.7 ± 2.33 to 74.2 ± 5.2 and 84.6 ± 2.65 to 78.3 ± 2.9 respectively. Furthermore, the decrease in porosity is slightly higher in case of scaffolds with micro β-TCP than scaffolds loaded with nano β-TCP. The overall trend of porosity is CS>nano β-TCP>micro β-TCP. However, the porosity of the composite scaffolds is still high enough for bone tissue engineering applications. This phenomenon of decrease in porosity may be attributed to the gradual increase in the density of β-TCP in CS matrix as reported earlier [54]. The porosity result has followed the same trend as pore size and the result obtained in our study is in good agreement with the results reported earlier when wollastonite and HAp were used for the development of composite CS scaffolds [54, 119].

5.1.6 Phase analysis

X-ray diffraction pattern was used to analyze the phase changes, if any occured in CS based composite scaffolds. A broad dome shaped curve is shown with pure CS scaffold representing its amorphous nature as shown in **Figure 5.5** [38], whereas in composite scaffolds, the CS peak is completely dominated by the incorporation of ceramic which is attributed to high crystalline nature of β-TCP [36]. The broad, dome-shaped and low-intensity peaks at 2θ = 9.16° and 20.6° correspond to pure CS and that of β-TCP are at 2θ = 31.7°, 32.1° and 39.7° confirming the presence of β-TCP in the composite scaffold. Furthermore, the effect of nano β-TCP is higher in dominating the CS peaks at 2θ = 20.6° as compared to micro β-TCP. Diffractograms of composite scaffolds with varied ratios of micro and nano β-TCP are shown in **Figure 5.6 (C-A and B).** As indicated, no significant change in peak intensity of β-TCP is observed with varied size of β-TCP. Further, the crystallite size of β-TCP particles in micro and nano size in composite scaffold were calculated using XRD peaks of Figure 5.5 (B). The corresponding values are 30.8nm and 10.82nm respectively. Thus it is established that the increase in crystallinity of CS/β-TCP composite scaffold is due to β-TCP as indicated from **Figure 5.5 and 5.6.**

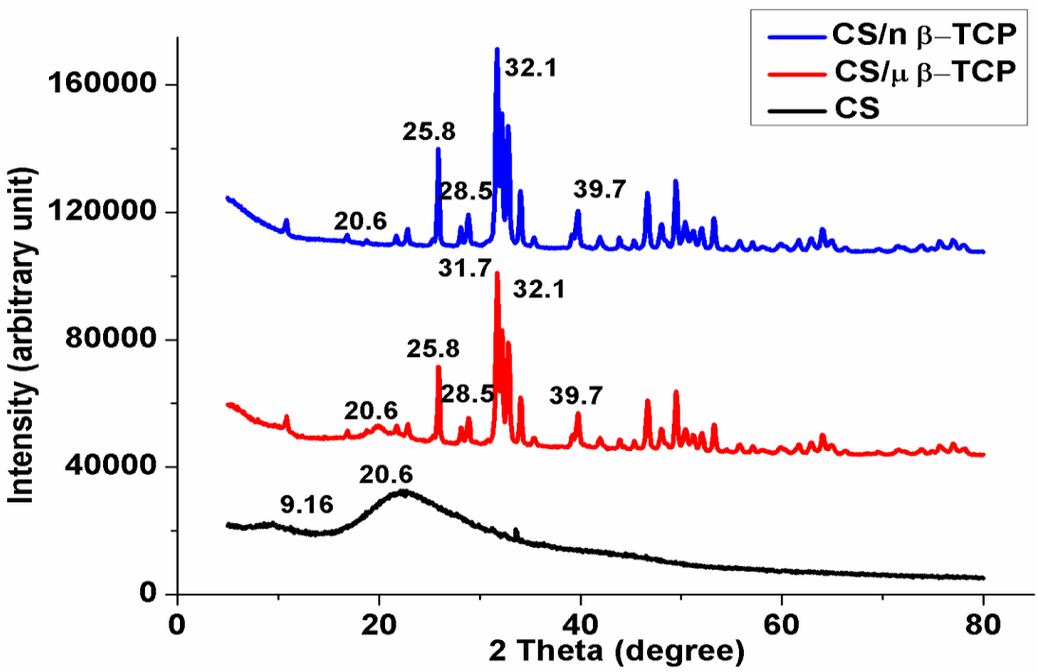

Figure 5.5 (A): ***XRD pattern of pure CS, CS/micro β-TCP (90:10) and CS/nano β-TCP (90:10) composite scaffolds. Peaks at 2θ=9.16° and 20.6° denotes CS where as twin peaks at 2θ=31.7° and 32.1° denote β-TCP. CS peak at 2θ= 20.6° is dominated by the incorporation of β-TCP***

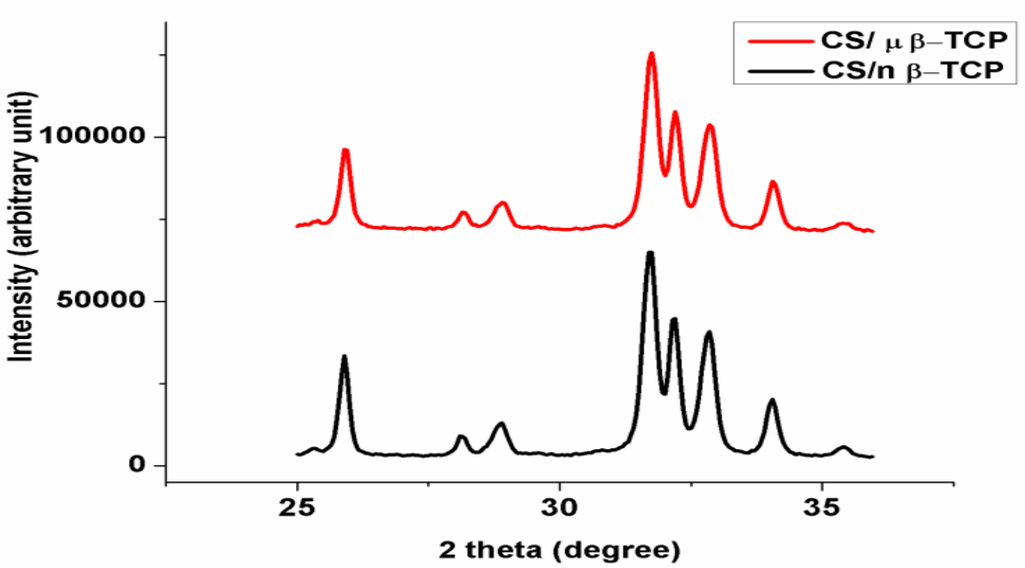

Figure 5.5 (B): ***XRD pattern of CS/micro β-TCP and CS/nano β-TCP (90:10) composite scaffolds. Crystallite size of micro and nano β-TCP is 30.8nm and 10.82nm respectively***

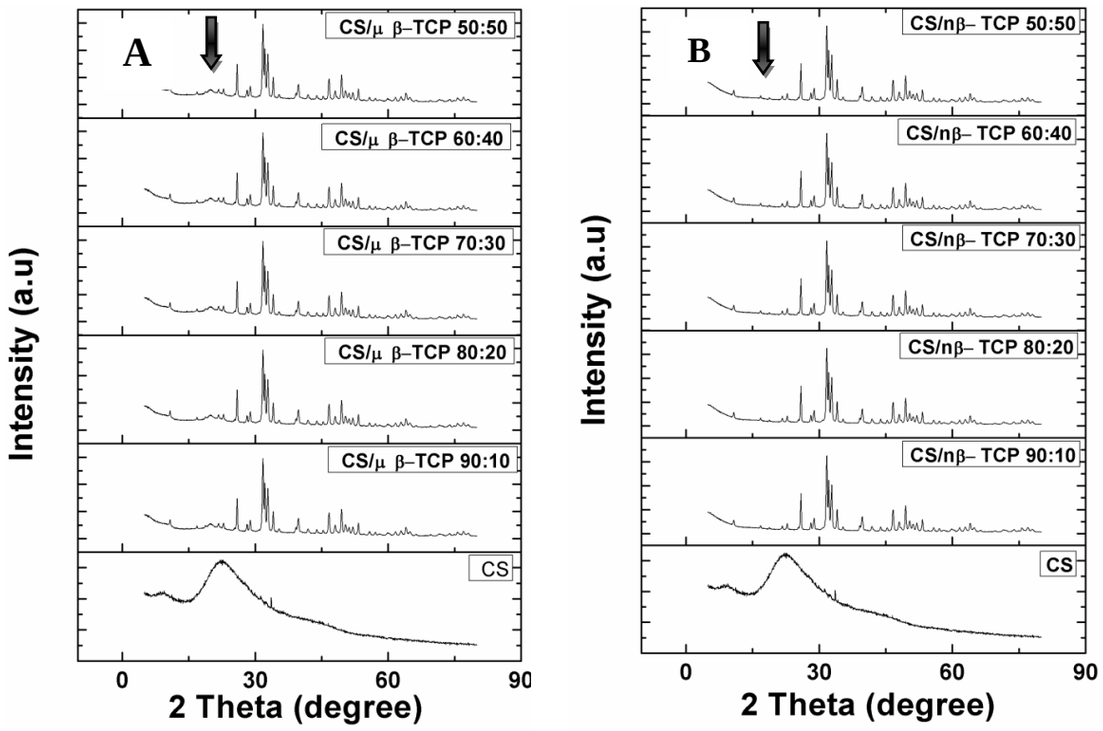

Figure 5.6 (C): ***XRD patterns of freeze-gelled composite scaffolds consisting of varying ratios of chitosan and β-TCP. Extent of decrease in amorphous nature of CS with respect to size of β-TCP is well represented. Nano sized β-TCP has completely dominated the amorphous nature of CS indicating higher crystallinity to composite scaffolds as compared to scaffolds with micro β-TCP as denoted with black colour arrow marks. The XRD peaks of composite scaffolds are compared with XRD peaks of pure CS peaks***

5.1.7 Functional analysis

An infrared spectrum represents the characteristics of a material with absorption bands. Thus infrared spectroscopy can provide a positive identification of every different constituent present in the composite matrices [154]. FT-IR analysis of CS and CS/β-TCP composite scaffolds was therefore, done to evaluate the interaction between the individual components present in the scaffolds. The bands generated as a result of chemical interactions is shown in **Figure 5.7**. Pure CS scaffold shows bands around 897 and 1154 cm^{-1} of assigned saccharide structure and the characteristic bands of N–H bending (amide-I) of CS is observed at 1560 cm^{-1} [70]. The typical band range of tetrahedral anions is 790–1190 cm^{-1}. Our analysis has demonstrated PO_4^{-3} bands at 1040, 1122, 610, and 551 cm^{-1} fall within the reported range [211]. Reports suggest the shifting and formation of new bands due to the interaction of ceramic material with the polymer functional groups [38]. The bands ranging from 1560-1587 cm^{-1} N-H bending has been shifted to 1556-1573 cm^{-1} which may correspond to the interaction of β-TCP with CS. The bands around 1000-1300 cm^{-1} are due to the interaction of phosphate with oxygen and nitrogen of CS [130]. IR pattern of composite scaffolds with varying content of β-TCP are not shown as no significant variation between the obtained peaks is observed.

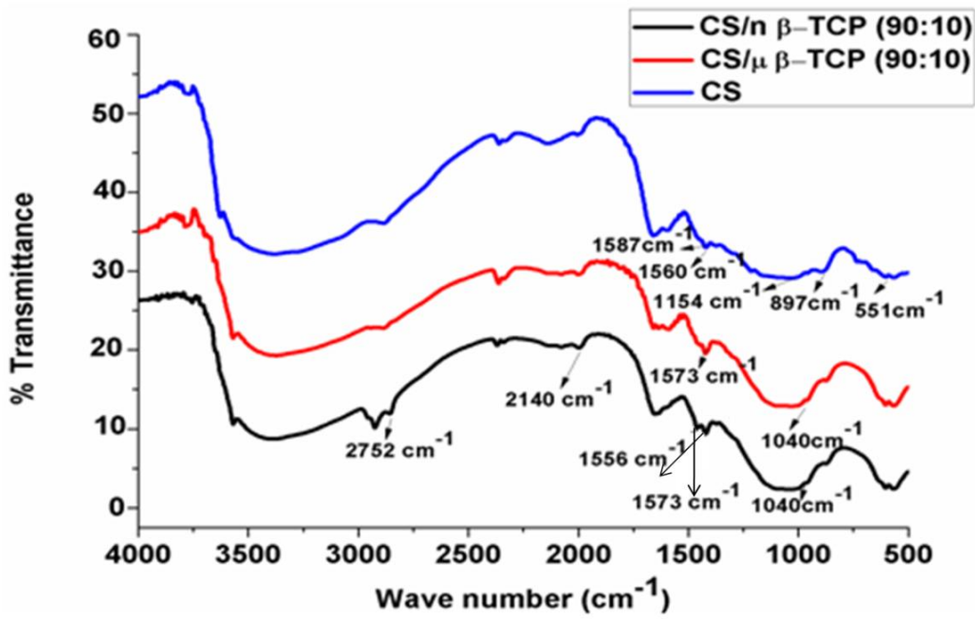

Figure 5.7: ***FT-IR spectra of CS and composite scaffolds. Bands ranging from 1560-1587 cm^{-1} corresponds to N-H bending has been shifted to 1556-1573 cm^{-1} due to the interaction of P=O with CS***

5.1.8 Compressive strength

The scaffolds must possess enough strength to withstand the force exerted by the neo tissue formed under *in-vivo* handling of implanted scaffold [212]. The stress strain curve and the corresponding compressive strength of the developed porous CS and CS/β-TCP composite scaffolds are shown in **Figure 5.8 (a) and (b)** respectively. It is clear from **Figure 5.8 (b)** that, the compressive strength (0.19 ± 0.05) of CS scaffold is remarkably increased with the addition of both types and content of β-TCP. The increase in compressive strength is due to reinforcing effect of bio-ceramic. The enhanced mechanical strength of polymeric scaffolds by the incorporation of bio-ceramic has also been reported earlier[162]. Further, the compressive strength of CS/micro β-TCP composite scaffolds is increased with increase in β-TCP content which is due to the good dispersion of the ceramic material into the CS polymer matrix that helped the stress to spread over a larger area of the composite scaffold surface. However, a decline in compressive strength is observed when the β-TCP content was over 30%. This decrease in compressive strength at higher β-TCP content is due to the agglomeration of β-TCP observed in CS matrix **(Figure 5.5)** that led the stress to be concentrated at the interface of the polymer-ceramics. When the particle size is in nano range, the reinforcement effect is found to be better in achieving higher compressive strength [213]. A linear relationship of compressive strength is observed with CS composites loaded with nano β-TCP (upto 40 wt%) and a slight decrease in compressive strength is observed with further increase in β-TCP content. This may be due to the decreased ability of scaffold to further reinforce the ceramic material into CS polymer matrix. More precisely, the compressive strength of scaffolds with nano β-TCP has been increased steadily upto 40% [CS/nano β-TCP 60:40-2.67 ± 0.21 MPa] and then a slight decrease in strength is observed [CS/nano β-TCP 50:50-2.55 ± 0.15 MPa] which represents the desired compressive strength of typical cancellous bone 2-10 MPa [214]. The compressive strength of all the developed scaffolds with varying micro and nano β-TCP content is depicted in **Table 5.2.** The high surface-to-volume ratio of nano size particle results in improved mechanical properties of bio-ceramics as reported earlier with β-TCP, wollstonite, HAp and bioglass [4, 69, 149, 187]. A similar increase in compressive strength of CS gel and 3-D CS scaffolds has also been

reported and the strength was increased to 0.8 and 1.8 MPa respectively by incorporating β-TCP [10, 53].

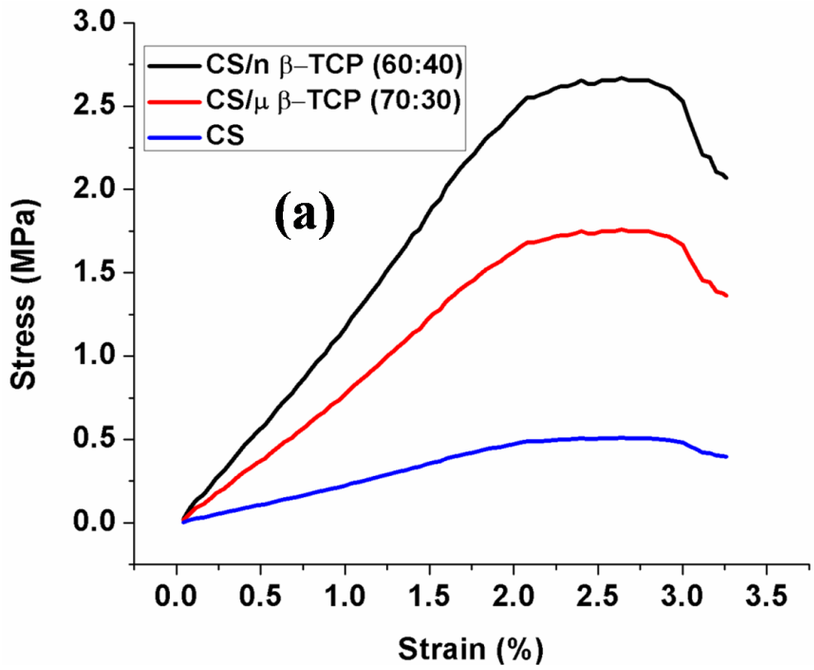

Figure 5.8 (a): ***Stress-Strain plot of CS and CS/β-TCP composite scaffolds***

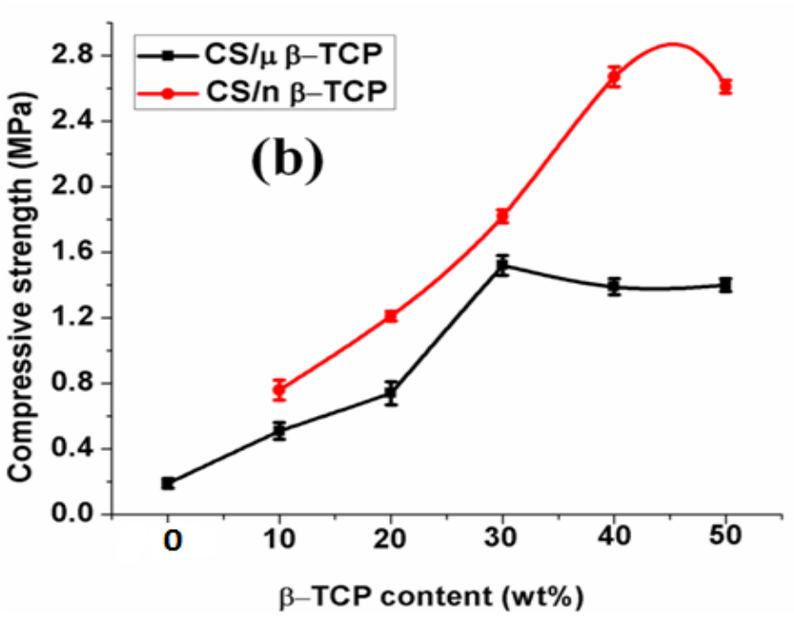

Figure 5.8 (b): ***Compressive strength of CS and CS/β-TCP composite scaffolds with different weight ratios of CS and β-TCP. Compressive strength of CS/ micro β-TCP composite scaffold increases with increase in β-TCP content upto 70:30 CS/ β-TCP ratio beyond which a decline trend is observed due to the agglomeration of β-TCP in the polymer matrix. Increase of nano β-TCP content has improved compressive strength of composite scaffold upto 40%***

5.1.9 Swelling behaviour

The swelling behaviour is one of the key factors of a scaffold determining its ability to qualify for *in-vitro* cell culture study. Swelling enables the cells to utilize the internal region of scaffolds upto maximum possible extent [234-235]. The trend obtained with swelling behaviour of CS and CS/β-TCP composite scaffolds is represented in **Figure 5.9.** The % swelling of all the developed scaffolds with varying β-TCP content is shown in **Table 5.2.** Among the developed scaffolds, pure CS scaffold shows a higher swelling percentage (~326%) than any of the CS/β-TCP composite scaffolds. The swelling ratio is observed to be decreased with increase in ceramic content. The decrease in % swelling of composite scaffolds is caused by the incorporation of β-TCP in the polymer matrix which ultimately leads to a decrease in diffusion of water as reported earlier when HAp was used as filler in CS [54]. The composite scaffolds with nano β-TCP shows higher swelling rate (~190 to 275%) as compared to scaffolds loaded with micro β-TCP (~155 to 212%) which may be due to the difference in distribution ability of micro and nano sized filler [38]. The other reason for the difference in swelling behaviour of composite scaffolds is may be attributed to gradation in pore size and porosity [38].

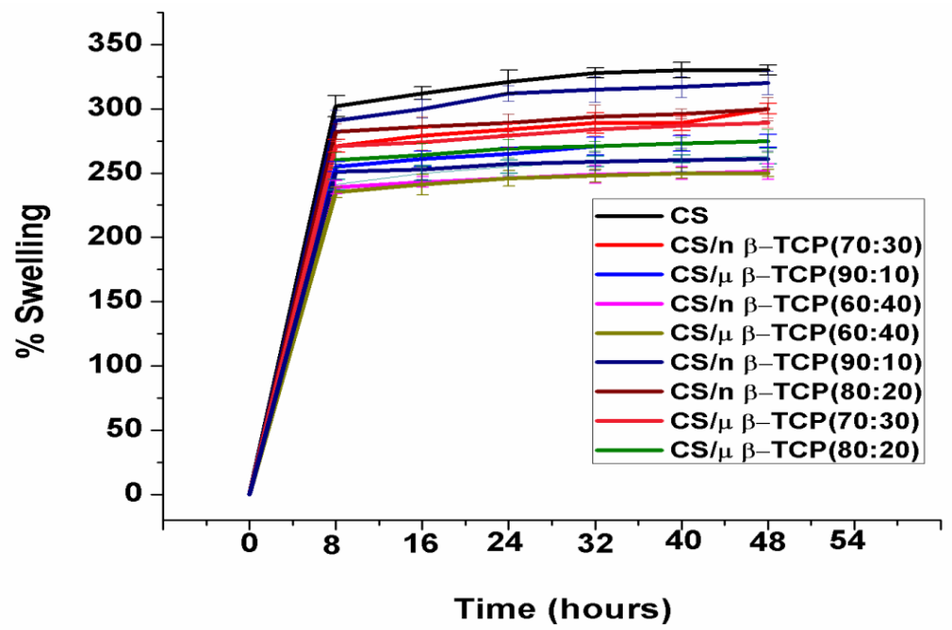

Figure 5.9: ***Swelling behaviour of CS and CS/β-TCP composite scaffolds. Pure CS scaffold shows a higher swelling than composite scaffolds. The swelling ratio decreases with increase in ceramic content that implies that the ceramic content has a direct influence on the diffusion of water into the scaffold matrix***

5.1.10 Measured contact angle

The water contact angle is determined to assess the hydrophilicity characteristics of the scaffold surface which is important for various cellular responses as reported earlier [215]. Therefore, the contact angle of the best composite scaffolds selected based on high mechanical strength was measured and compared with pure CS scaffold. There is no significant change in contact angle is observed between pure CS scaffold (51.2 ± 0.8°) and CS/nano β-TCP (60:40) [51.9 ± 1.1°] which represents their similar hydrophilic characteristics. However, a slightly lower hydrophilicity characteristic is shown by CS/micro β-TCP (70:30) [53.1 ± 0.5°] scaffold which may be attributed to micron size of the ceramic particle which restricted the flow of water through the scaffold architecture. Thus it has been demonstrated the superior surface property of CS composite reinforced with nano β-TCP is favourable for bone tissue engineering application than the composite made with micro sized β-TCP.

5.1.11 *In-vitro* biodegradation study

The degradation of scaffolds is one of the major goal of tissue engineering research because of the self repairing ability of various tissues are different implying that scaffold should have corresponding degradation rates to facilitate new tissue synthesis [216]. So, adequate control over the rate of degradation plays a major role to be on par with the growth rate of neo tissue formed [74]. Therefore, biodegradation of the prepared CS and various CS/β-TCP composite scaffolds was studied in phosphate buffer saline containing Lysozyme for four weeks and compared with control. Biodegradation data is shown in **Figure 5.10.** The degradation rate of CS scaffold (31% of its initial weight) is observed to decrease with increase in micro and nano β-TCP content. Further, as β-TCP content increases, a decelerated degradation rate is observed upto 30 and 40 wt% of micro and nano β-TCP loading, beyond which a slight increase in degradation rate is found. Scaffolds with varied ratios of micro and nano sized β-TCP have degraded to 25-30% and 16-24% of their initial weights respectively. However, the best result is achieved with CS/micro β-TCP (70:30) and CS/nano β-TCP (60:40) scaffolds as they degraded to 25% and 16% respectively. The difference in degradation rate is probably

due to the higher mechanical stability of nano β-TCP scaffolds as they are uniformly distributed throughout the matrix, resisting PBS seepage into the scaffold architecture. Similar trend in decreased degradation has been observed when nano HAp was incorporated in CS matrix as reported earlier [38]. The result further reveals that the addition of nano sized β-TCP decelerated the rate of degradation of CS higher than scaffolds with micro β-TCP. Thus it has been demonstrated that the degradation rate of CS can be controlled by β-TCP content and use of nano β-TCP is more advantageous than micro size β-TCP as potential bio-ceramic.

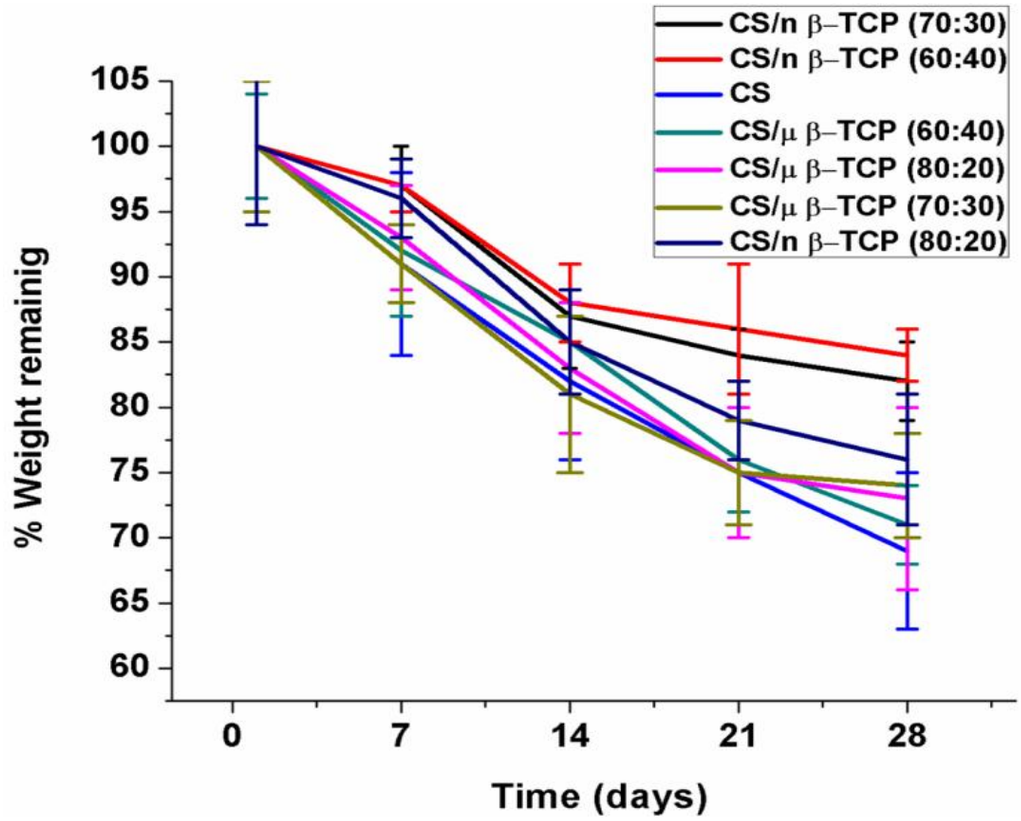

Figure 5.10: ***Observed degradation behaviour of CS and CS/β-TCP composite scaffolds by soaking in PBS for four weeks. The degradation rate of CS scaffold is decreased with increase in β-TCP content upto 30 and 40 wt% of micro and nano β-TCP loading, beyond which a slight increase in degradation rate is observed. Further, nano β-TCP is superior in controlling degradation rate of CS than micro size β-TCP***

Table 5.2: ***Pore size, porosity, compressive strength and % wt loss of pure CS and CS composite scaffolds with different size and ratios of β-TCP.***

Scaffold Type	Pore size range (μm)	% Porosity	Compressive Strength (MPa)	% Mass loss [28 days]
CS	61-171	86.9 ± 3.21	0.19 ± 0.05	31
CS/μ β-TCP (90:10)	55-165	80.7 ± 2.33	0.51 ± 0.09	29
CS/μ β-TCP (80:20)	53-161	79.3 ± 4.96	0.74 ± 0.08	27
CS/μ β-TCP (70:30)	51 -158	77.1 ± 3.21	1.52 ± 0.09	25
CS/μ β-TCP (60:40)	49-151	75.7 ± 6.1	1.39 ± 0.11	29
CS/μ β-TCP (50:50)	45-147	74.2 ± 5.2	1.12 ± 0.14	30
CS/n β-TCP (90:10)	59-168	84.6 ± 2.65	0.76 ± 0.17	24
CS/n β -TCP (80:20)	57-166	82.8 ± 3.43	1.21 ± 0.13	21
CS/n β-TCP (70:30)	55-165	81.2 ± 2.87	1.82 ± 0.19	18
CS/n β-TCP (60:40)	55-162	80.1 ± 3.6	2.67 ± 0.21	16
CS/n β-TCP (50:50)	51-158	78.3 ± 2.9	2.55 ± 0.15	17

5.1.12 Bioactivity

Deposition of apatite crystals over the surface of a material assesses its osteogenic behaviour, which is one of the key aspects in the development of neo bone tissue [71, 227]. The developed composite scaffolds such as CS/micro β-TCP (70:30) and CS/nano β-TCP (60:40) were selected for this study because of their higher mechanical strength and favourable degradation rate. The pure CS scaffold was used as control. The result of bioactivity is shown in **Figure 5.11 (a-f).** The initiation of the formation of apatite layer on the surface of scaffolds was observed after 7 days of treatment (the image of 7^{th} day study is not shown in the figure as the apatite deposition was not much noticeable). The amount of apatite formed is gradually increased with time with varying degree of deposition on the different scaffolds as shown in SEM images **(Figure 5.12)**. The entire surface area of all the scaffolds is found to be covered with Ca and P minerals after 21days. Similar observation of apatite deposition over the entire surface of wollastonite loaded on CS scaffolds during 14-21 days of study has been reported earlier [54]. In the present study, the higher amount of apatite formation obtained with

CS/nano β-TCP may be due to the uniform distribution of nano sized bio-ceramic on the scaffold matrix that leads to an increased nucleation sites in CS. The other reason may be the higher density of nano sized β-TCP particles on the scaffold matrix which is responsible for higher amount of apatite formation on CS/nano β-TCP composite scaffold. The formation of white coloured globular entities on scaffold surface is confirmed by EDX and the chemical constituents are found to be Ca and P. Furthermore, XRD analysis revealed sharp characteristic peaks of formed globular structures at 2θ = 25.2º and 31.8º confirming the formation of hydroxy apatite (HAp). Thus it has been demonstrated that the bioactivity of CS scaffold can be enhanced by the incorporation of β-TCP. Furthermore, the use of nano size β-TCP is advantageous than microsize particle achieving higher bioactivity.

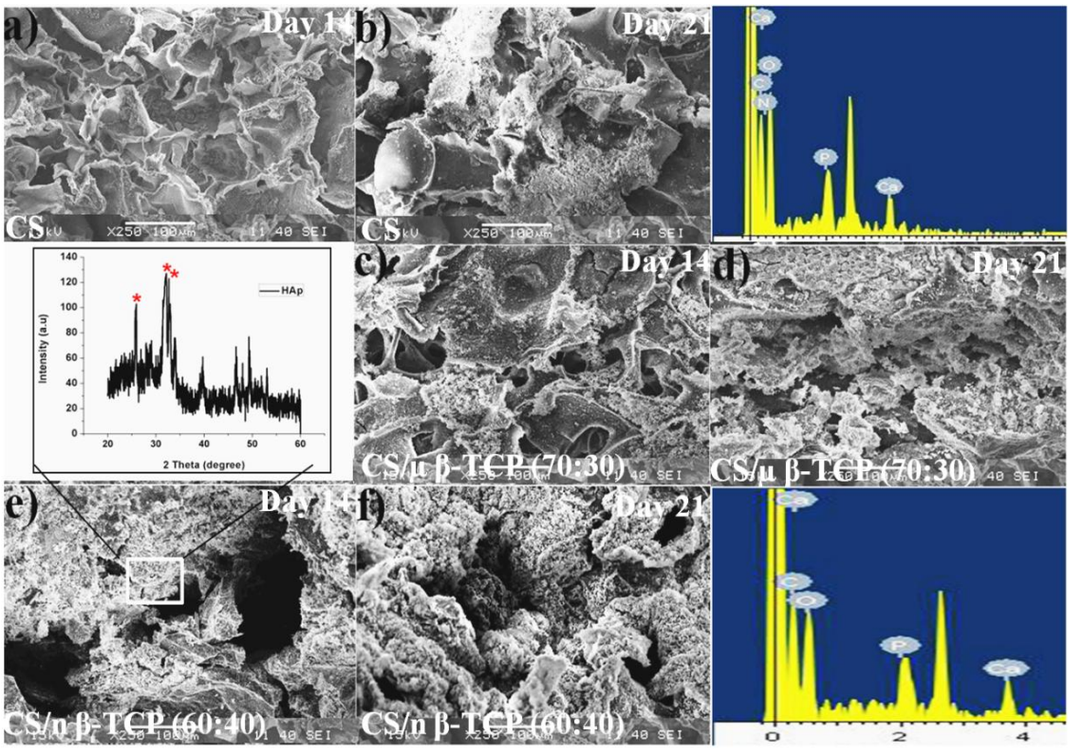

Figure 5.11: ***Apatite crystal formation on CS (control), CS/micro β-TCP (a & b) and CS/n β-TCP (b)] scaffolds upto 21days of treatment in SBF. EDX analysis shows the components of globular structures formed on the surface of developed scaffolds. Deposition of Ca and P indicates the constituents of HAp. Furthermore, the prominent peaks at 2θ=25.7º and 31.8º in XRD diagram confirm the formation of globular structures of HAp on the scaffold surface. Overall, the bioactivity of CS scaffold is shown to be remarkably enhanced by the incorporation of nano β-TCP***

5.1.13 *In-vitro* cell study

Among the various CS composite scaffolds prepared using micro and nano size β-TCP, CS/nano β-TCP (60:40) was found to be best followed by CS/micro β-TCP (70:30) in terms of various physico-chemical, degradation and mechanical properties. Therefore, these two composite scaffolds were selected for cell culture study and CS scaffold was used as control.

5.1.13.1 Morphology of hMSCs

Human mononuclear cells (hMNCs) were isolated from Umbilical Cord Blood by Ficoll Hypaque technique and cultured in Dulbecco's Modified Eagle Medium supplemented with fetal bovine serum (FBS), penicillin and streptomycin. Cultured cells upto 4^{th} passage were used for cell culture study to assess the cell supportive property of the developed composite scaffold matrices. Morphological characterization of MSCs were assessed by phase contrast microscopy and illustrated in **Figure 5.12.** As seen in figure, cells are spherical during initial days of culture and have shown fibroblast like morphology at later time periods representing the cultured cells are mesenchymal stem cells. Further, the cultured cells attain confluence at 14^{th} day as depicted in **Figure 5.12 (f).**

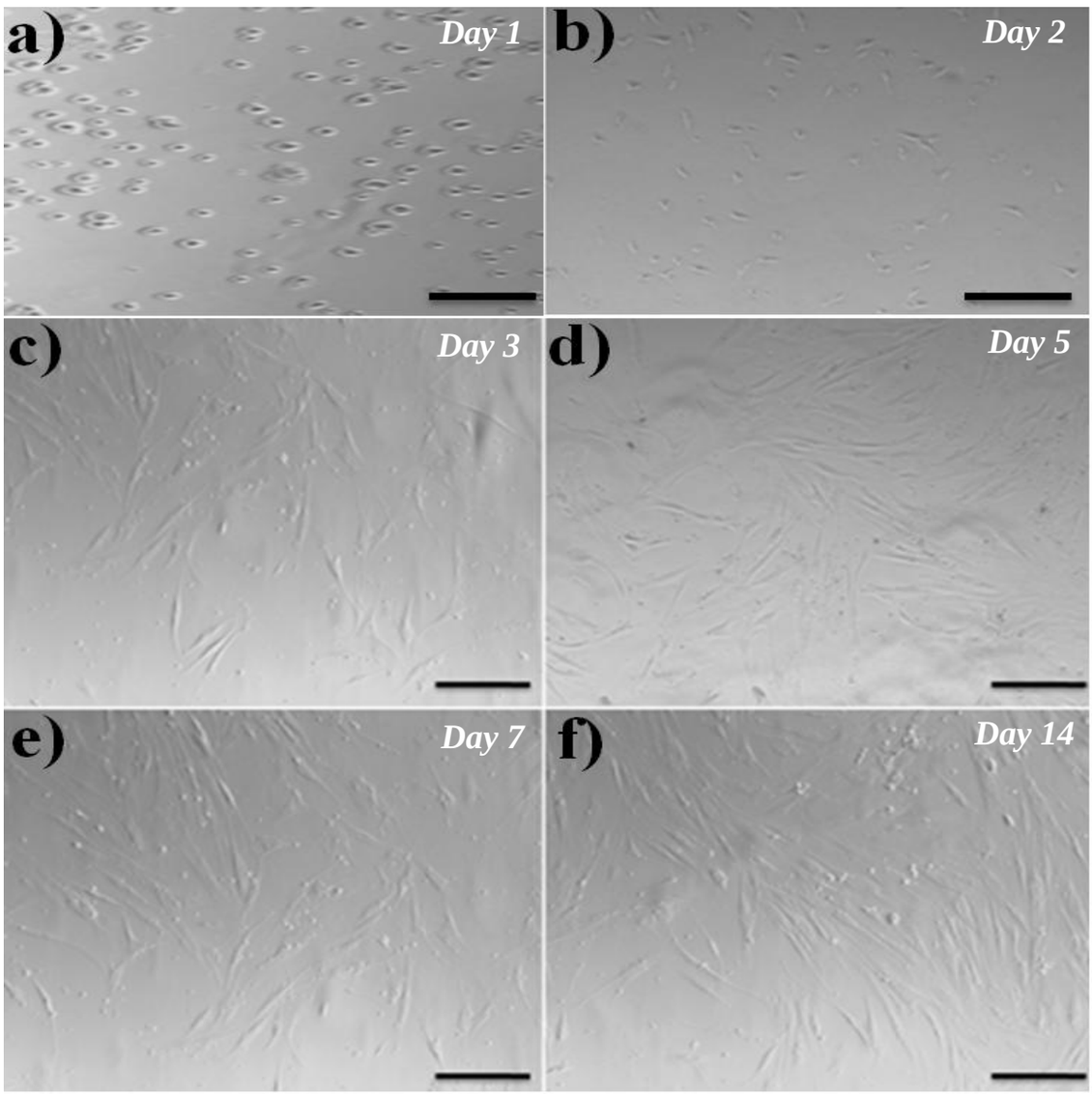

Figure 5.12: ***Morphological changes of hMSCs during 14 days of culture period observed under phase contrast microscope at magnification 50X and scale bar 100µm. Initially the cells are found to be spherical in shape and slowly changed to fibroblast like morphology***

5.1.13.2 Immunophenotypic characterization of hMSCs

Besides morphology, immunophenotypic characterization of hMSCs was assessed by flow cytometry analysis and the results are shown in **Figure 5.13.** The positive expression of CD90 (99.01%), CD73 (96.5%) and CD105 (95.5%) and negative expression of CD34 (1.0%), CD45 (0.5%), and HLA-DR (1.2%) signify that the cells are MSCs**.**

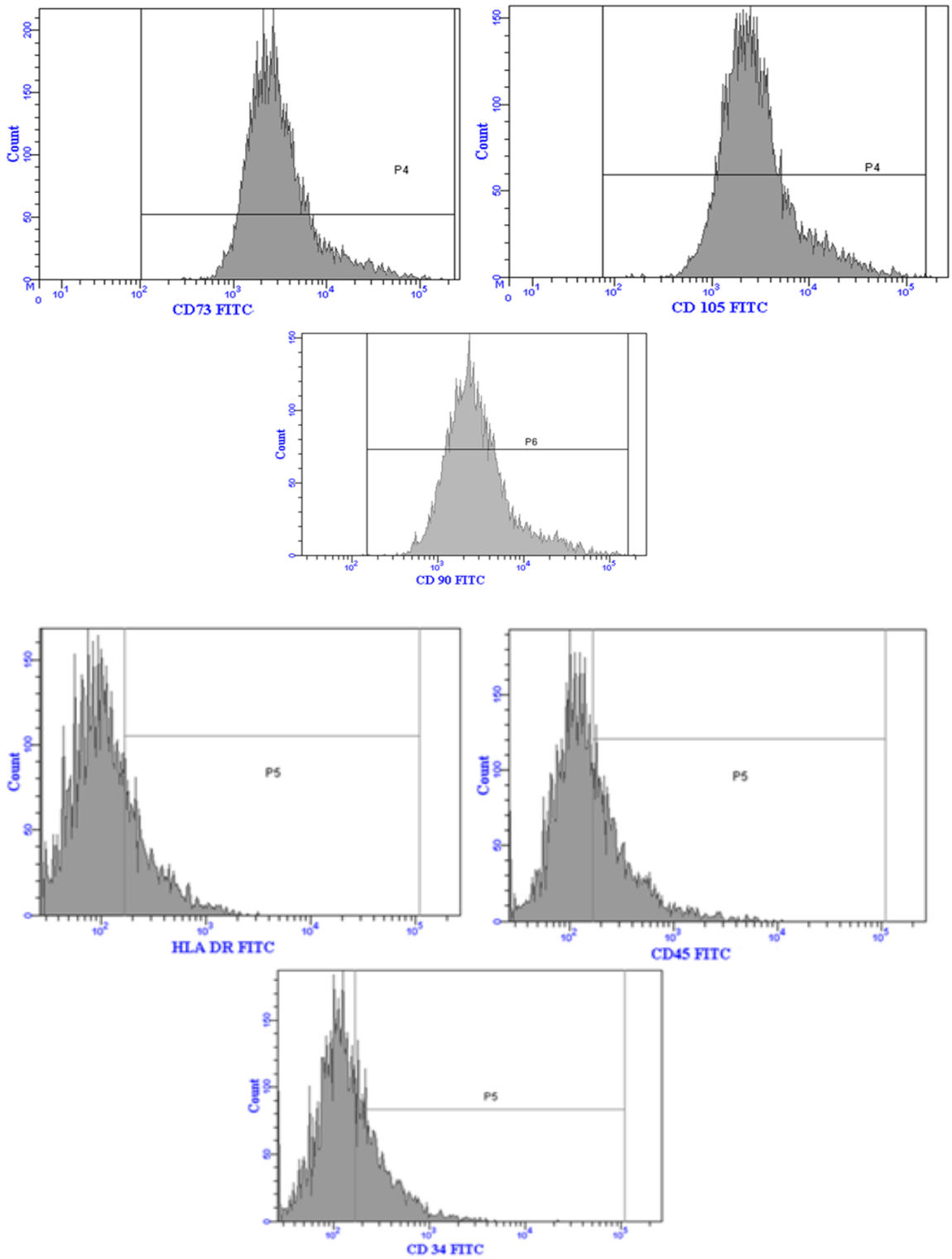

Figure 5.13: ***Flowcytometric analysis of cultured hMSCs. The positive expression of CD90 (99.01%), CD73 (96.5%) and negative expression of CD105 (95.5%) CD34 (1.0%), CD45 (0.5%), and HLA-DR (1.2%) confirm that the cells are MSCs***

5.1.13.3 Cell morphology and cell attachment

Cell morphology and cell attachment are the indicators of the affinity of seeded cells to the scaffold and hence are important aspect in forming a cell scaffold construct [30]. The attachment and morphological change of MSCs seeded on the various scaffolds are observed by SEM micrographs **(Figure 5.14)** during the 7 days of culture period. As indicated, on day 3, the cells are shown to be spherical on pure chitosan, whereas MSCs started to elongate on CS/micro β-TCP scaffold. However, the cells are observed to attach and well spread on CS/nano β-TCP composite scaffold. Moreover, the number of cells is found to be relatively higher over CS/nano β-TCP scaffolds as observed on day 7 with spindle like morphology in comparison to CS and CS/micro β-TCP scaffolds. This confirms the higher compatibility of the scaffolds to the cells thus providing a suitable environment for attachment, spreading and proliferation of hMSCs.

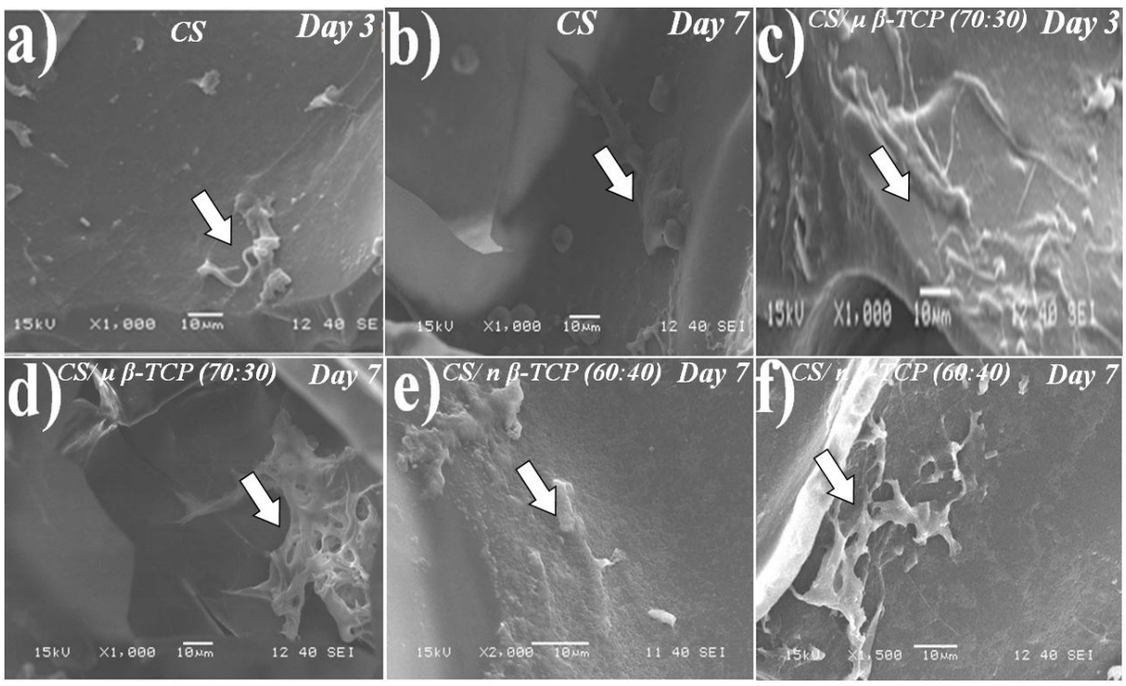

Figure 5.14: ***SEM images of hMSCs seeded on CS (a, b) as control, CS/micro β-TCP (c, d) and CS/nano β-TCP (e, f) composite scaffolds representing the morphology, attachment and spreading of hMSCs on 3rd (a, c, e), and 7th day (b, d, f) of culture. White arrow marks represent significant morphological changes of seeded hMSCs. Change in cell morphology from spherical to elongate is observed with increase in culture time. However, better cell attachment and proliferation are depicted on CS/nano β-TCP scaffold***

5.1.13.4 Metabolic activity by MTT assay

Cell viability depends on scaffold architecture especially pore size, porosity and their interconnectivity [8]. Metabolic activity signifies the potentiality of cells to progress in the cell cycle [217]. The metabolic activity was also compared with the metabolic activity of hMSCs on pure CS scaffold as control. **Figure 5.15** shows the relative cellular metabolic activity measured by MTT assay of hMSCs grown over the developed scaffolds during 3, 5 and 7 days of culture. The number of cells is found to increase with culture time on all types of scaffolds with a varying rate of proliferation. However, the highest cellular metabolic activity is shown by CS/nano β-TCP composite matrix followed by CS/micro β-TCP and control. The corresponding O.D values are 0.614 ± 0.016 with CS/nano β-TCP, 0.52 ± 0.012 - CS/micro β-TCP and 0.4 ± 0.018 - CS**.** The maximum compatibility for cells seeded on CS/nano β-TCP scaffold confirming its superiority over CS and CS/micro β-TCP scaffolds and this may be due to its increase in surface area and surface roughness of the scaffold which favour adherence of cells to a greater extent [218]. Further, it is reported that, nano crystalline calcium phosphate scaffolds enhance cell proliferation by releasing Ca and phosphate ions in the culture medium and similar result of enhanced metabolic activity of seeded cells on CS scaffolds reinforced with nano hydroxyapatite has also been reported earlier [18].

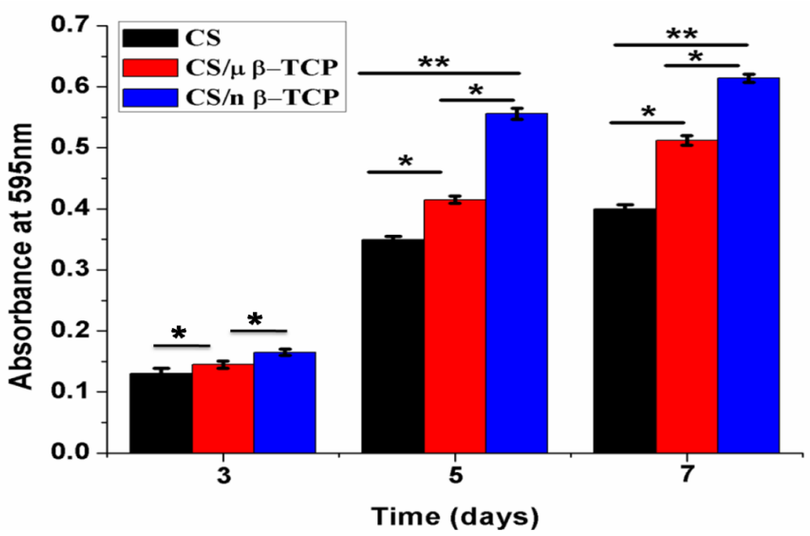

Figure 5.15: ***Metabolic activity of hMSCs on CS (control), CS/micro ß-TCP and CS/nano ß-TCP scaffold after 3, 5 and 7 days of culture. Each point represents the mean ± SD (n= 3), * and ** shows significant differences between groups at p> 0.05 and p<0.05 respectively. The metabolic activity increases with culture time and the higher metabolic activity is shown by CS/nano ß-TCP scaffold***

5.1.13.5 hMSCs proliferation study

The proliferation of MSCs seeded on CS/micro β-TCP and CS/nano β-TCP scaffolds was evaluated both qualitatively and quantitatively by fluorescence microscopy study and Alamar blue and DNA quantification assay respectively.

(i) Fluorescence microscopy

As mentioned, proliferation activity of hMSCs on scaffolds assessed qualitatively by the analysis of fluorescence microscopy images is shown in **Figure 5.16 (a-f)**. The number of cells is observed to increase with respect to culture time on both the scaffolds with varying degree of proliferation. However, number of cells on CS/nano β-TCP scaffold is higher representing higher metabolic activity of hMSCs as compared to pure CS and CS/micro β-TCP scaffolds. The increased cell proliferation on composite scaffold may be attributed to release of Ca and P ions in the culture medium by β-TCP which favoured the increased metabolic activity of seeded cells [50].

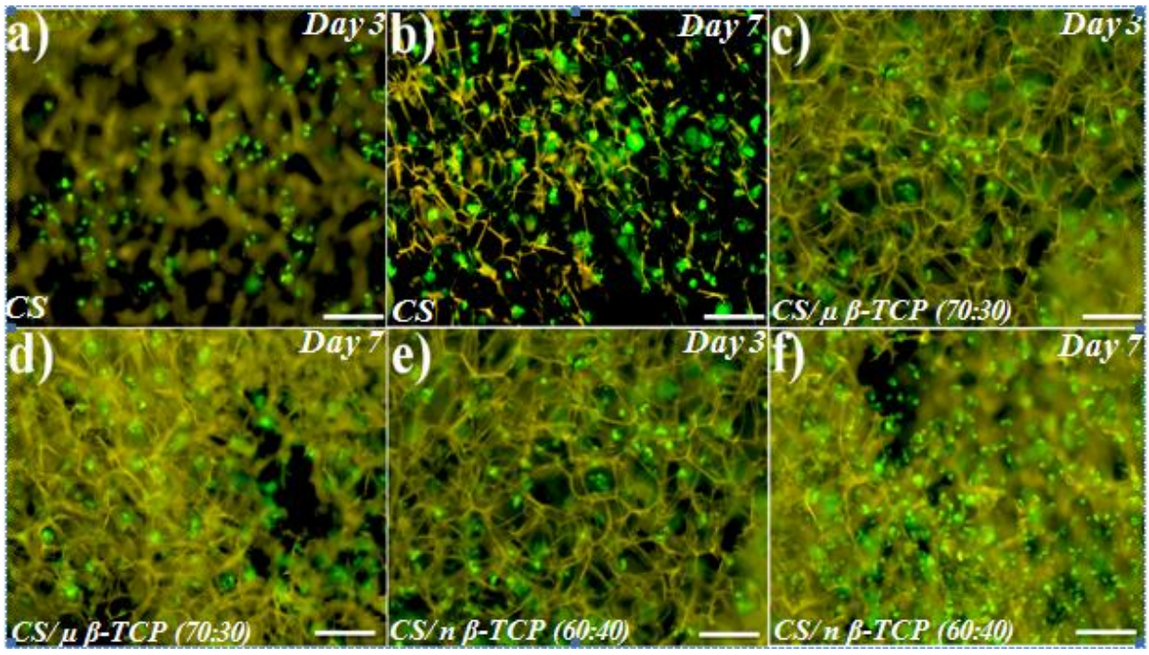

Figure 5.16: ***Cell distribution is visualized under fluorescent microscopy using FDA dye. Images were taken after 3rd (a, c, e) and 7th (b, d, f) days of MSCs culture on CS (a,b), CS/micro β-TCP (c, d) and CS/nano β-TCP (e, f) composite scaffolds. A significant increase in cell number is observed with time representing an increased proliferation rate. The highest metabolic activity is, however, achieved with CS/nano β-TCP composite scaffolds. Scale bar corresponds to 200 µm***

(ii) Alamar blue assay

Cell proliferation on scaffolds indicates their compatibility and represents appropriate behaviour towards hosting the seeded cells [184]. The proliferation of MSCs cultured on CS (control), and composite scaffolds upto 7 days of culture was evaluated by alamar blue assay, the result of which is shown in **Figure 5.17.** Alamar blue dye undergoes oxido-reduction reactions due to the action of mitochondrial enzymes present in the living cells and changes its colour according to the metabolic activity of the cells [17]. The greater reduction in the alamar blue dye indicates higher proliferation of hMSCs. Higher percentage reduction o dye with increase in culture time is observed with all the scaffolds. However, results of pure CS, CS/micro β-TCP and CS/nano β-TCP composite scaffolds showed a significant difference at $p < 0.05$. The higher percentage of alamar reduction than control observed with composite scaffolds is due to the presence of Ca ions in β-TCP which triggers the proliferation of seeded cells as compared to control. Furthermore, among the developed scaffolds, the highest reduction of dye is achieved with CS/nano β-TCP composite matrix. This higher proliferation on CS/nano β-TCP scaffold may be attributed to the uniform distribution of nano β-TCP and no agglomerate formation in CS matrix which in turn allows uniform nutrient permeation through the scaffold architecture [120]. Our results are in good agreement with the previously published reports with keratinocyte proliferation observed on Silk Fibron/CS composite scaffolds [17, 152]**.** Thus, this study proves that, the particle size of bio-ceramic has a direct impact on scaffold biocompatibility and cell proliferation as reported earlier when CS scaffolds are incorporated with nano sized bioglass and HAp achieving enhanced biocompatibility of CS matrix seeded with osteoblast like cell line MG 63 and MC3T3-E1 respectively [54, 234].

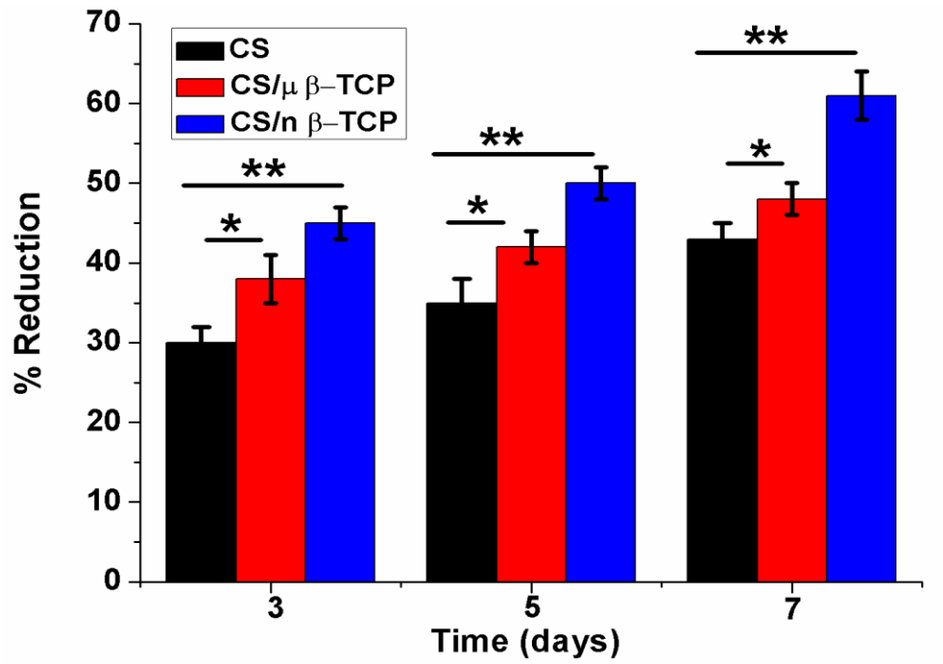

Figure 5.17*: Proliferation of hMSCs on CS (control), CS/micro β-TCP and CS/nano β-TCP scaffolds on 3, 5 and 7 days of culture. Each point represents the mean ± SD (n= 3) * and ** shows significant differences between groups at p > 0.05 and p < 0.05 respectively*

(iii) DNA quantification

The proliferation of MSCs on the developed scaffolds was evaluated by DNA quantification assay. **Figure 5.18** shows an increase in DNA content of MSCs with time as observed in all the developed scaffolds with varying degree of DNA content. The corresponding DNA contents of hMSCs cultured on control (CS), and CS/micro β-TCP composite scaffolds on 3 to 21 days of culture are 75±11 ng/ml to 204±19 ng/ml, 89±9 ng/ml to 254±16 ng/ml and respectively. However, among the scaffolds developed under study, CS/nano β-TCP composite scaffold has shown the highest DNA content representing highest proliferation rate of MSCs. The DNA content of hMSCs cultured on CS/nano β-TCP composite scaffolds on 3 to 21 days is 91±13 ng/ml to 289±22 ng/ml. Thus CS/nano β-TCP composite scaffold is proved to be superior over other CS scaffolds.

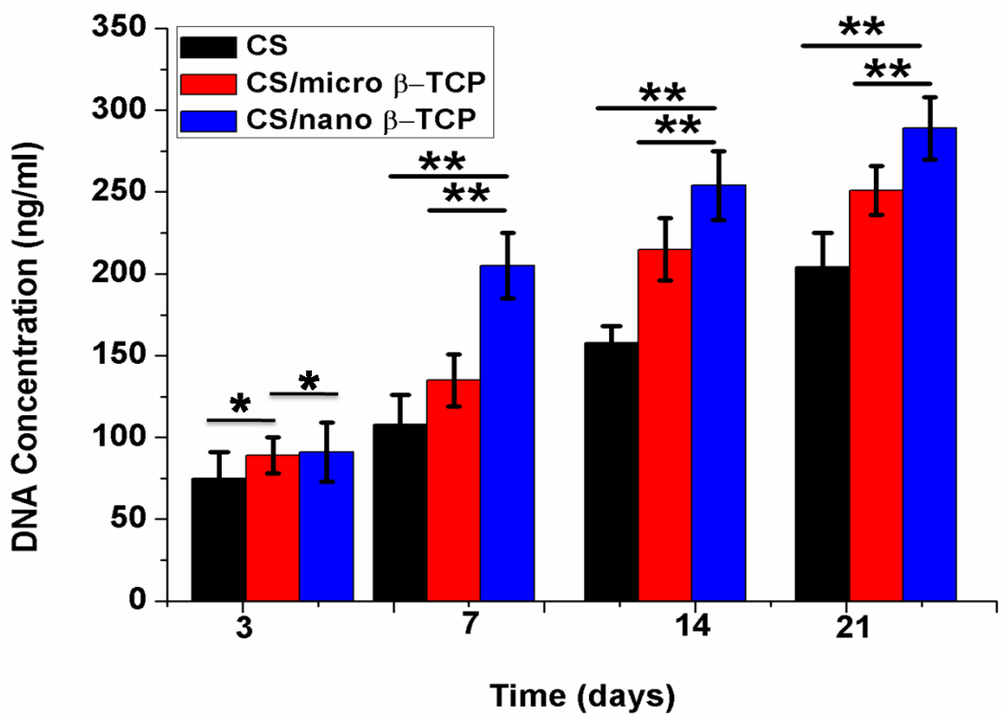

Figure 5.18: ***Cell proliferation represented in terms of DNA quantification on CS, CS/micro β-TCP, CS/nano β-TCP composite scaffolds observed during 21 days of culture. An increased trend in DNA content is observed on all the scaffolds with varying degree of DNA content. However, CS/nano β-TCP scaffold shows higher DNA content compared to other scaffolds. Each point represents the mean ± SD (n=3) * and ** represents p>0.05 and p < 0.05 respectively***

Therefore, qualitative and quantitative assessment of hMSCs proliferation demonstrates the biocompatibility of developed freeze-gelled scaffolds.

5.1.13.6 Cytoskeletal organization

Confocal laser microscopy was done to visualize the cell spreading, proliferation, development of F-actin and to understand the cell scaffold interactions [219]. **Figure 5.19** shows the distribution and morphology of MSCs cultured on CS/micro β-TCP and CS/nano β-TCP scaffolds on 7th day. Profuse cell growth is found on CS/nano β-TCP scaffolds compared to CS/micro β-TCP scaffolds. It is also observed from the figures that, more number of cells covered the scaffold surface on CS/nano β-TCP scaffolds with extensive developed actin indicating the enhanced spreading, proliferation. Furthermore, establishment of cell-cell interactions were also observed on CS/nano β-TCP composite scaffolds.

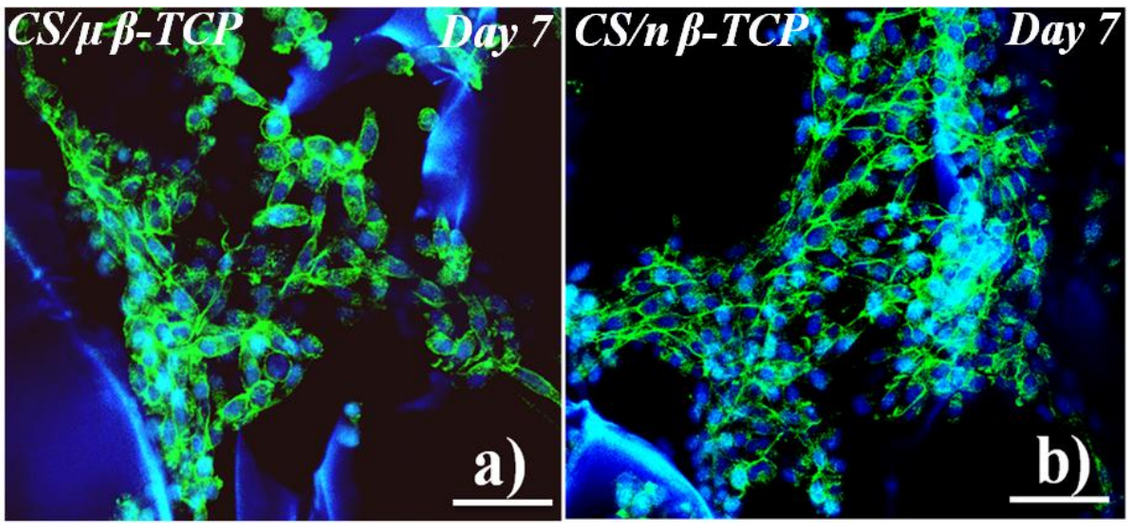

Figure 5.19: ***Cell distribution is visualized under confocal microscopy on CS/micro β-TCP and CS/nano β-TCP scaffolds. Few cells are spherical in shape as observed on CS/micro β-TCP where as the cells are uniformly spread on CS/nano β-TCP scaffolds which confirms the superior biocompatibility of CS/nano β-TCP scaffolds. Nuclei of the cells stained with Hoechst 33342 (blue) and actin filaments with phalloidin (green). Bar indicates 200μm.***

5.1.13.7 Osteogenic differentiation potential

The osteogenic differentiation of MSCs over the scaffolds was evaluated by ALP activity and total calcium content which are described below.

(i) ALP assay

ALP activity is a critical tool for the assessment of cellular differentiation. The organic phosphate esters in the bone matrix are cleaved by ALP enzyme which enables the supply of free phosphate ions to the zones of mineral nucleation. ALP is an early marker which represents the differentiation and mineralization of the osteoblast phenotype [220]. ALP assay of hMSCs seeded scaffolds was done to evaluate the osteogenic potential of the scaffolds as shown in **Figure 5.20.** During initial days of incubation, an increase in ALP activity is evident upto 14 days since ALP is an early osteogenic marker. A decrease in ALP activity is noticed after 14 days of culture. Further, hMSCs cultured on CS/nano β-TCP expresses higher ALP activity than on control (CS) and CS/micro β-TCP composite scaffold. A rapid increase in ALP expression is observed with all scaffolds from day 7 to day 14 ($p < 0.05$) with a variation in ALP activity. The ALPase activity of hMSCs cultured on control (CS) and CS/micro β-

TCP composite scaffolds at 7 to 21 days is 1.1 ± 0.3 IU/µg to 2.81 ± 0.11 IU/µg and 1.75 ± 0.29 IU/µg, to 3.25 ± 0.17 IU/µg respectively. ALPase activity of hMSCs cultured on CS/nano β-TCP composite scaffolds at 7 to 21 days is 2.96 ± 0.29 IU/µg, to 5.11 ± 0.17 IU/µg. Thus enhanced ALP activity is noticed on CS/nano β-TCP composite scaffolds due to osteoinductive property of nano β-TCP which helped the differentiation of seeded hMSCs into osteoblasts to a greater extent than micro β-TCP [36].

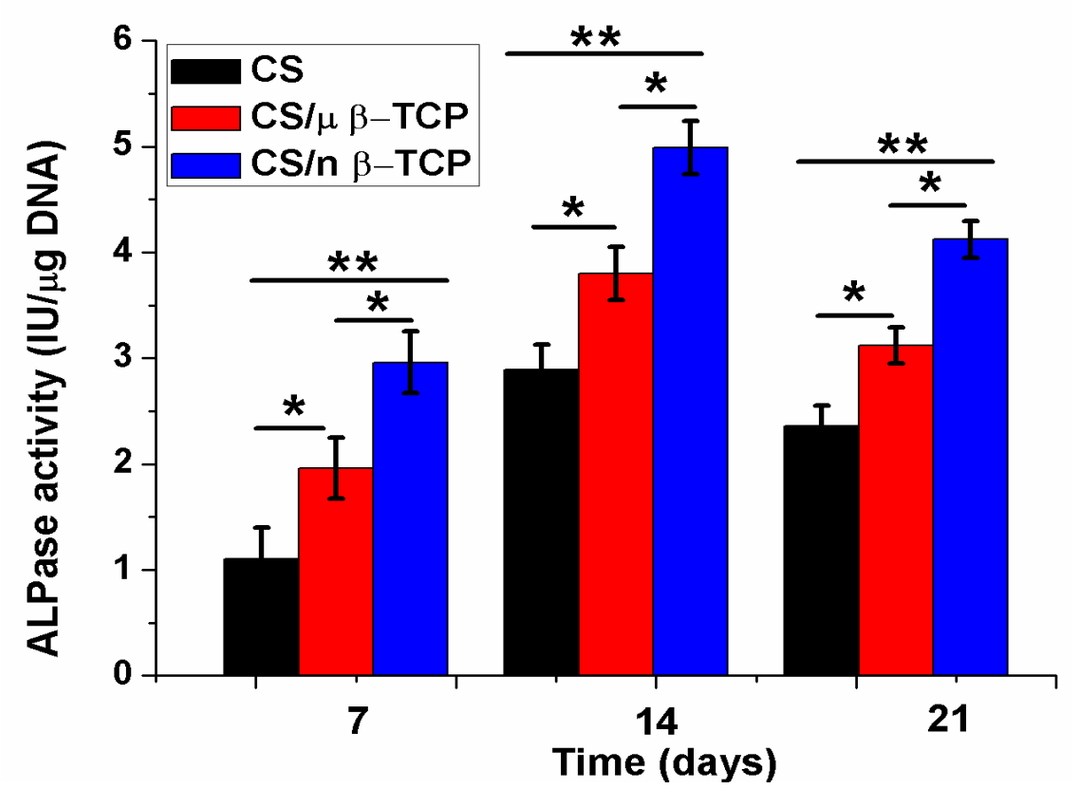

Figure 5.20: ***Alkaline Phosphatase activity of CS, CS/micro β-TCP and CS/nano β-TCP composite scaffolds after 7, 14 and 21 days of cell seeding. Each point represents the mean ± SD (n= 3) * and ** shows significant differences between groups at p >0.05 and p < 0.05 respectively***

(ii) Total calcium content

The total calcium content is the determination of the total mineral level present in the MSCs differentiated to osteogenic lineage [221]. **Figure 5.21** shows the measured calcium content of hMSCs seeded scaffolds upto 21days of culture. An increase in calcium content is observed with increase with time representing an increased degree of mineralization on both CS/micro β-TCP and CS/nano β TCP scaffolds. However, hMSCs seeded on CS/nano β-TCP scaffold

possessed higher ($p < 0.05$) calcium content (224-821 mg/mg DNA) than on pure CS (101-512 mg/mg DNA) and CS/micro β-TCP composite scaffold (132-712 mg/mg DNA) as observed on day 21 of incubation. Higher mineralization activity of MSCs represents the superior osteogenic potential of CS/nano β-TCP scaffold in comparison to CS/micro β-TCP scaffold [201].

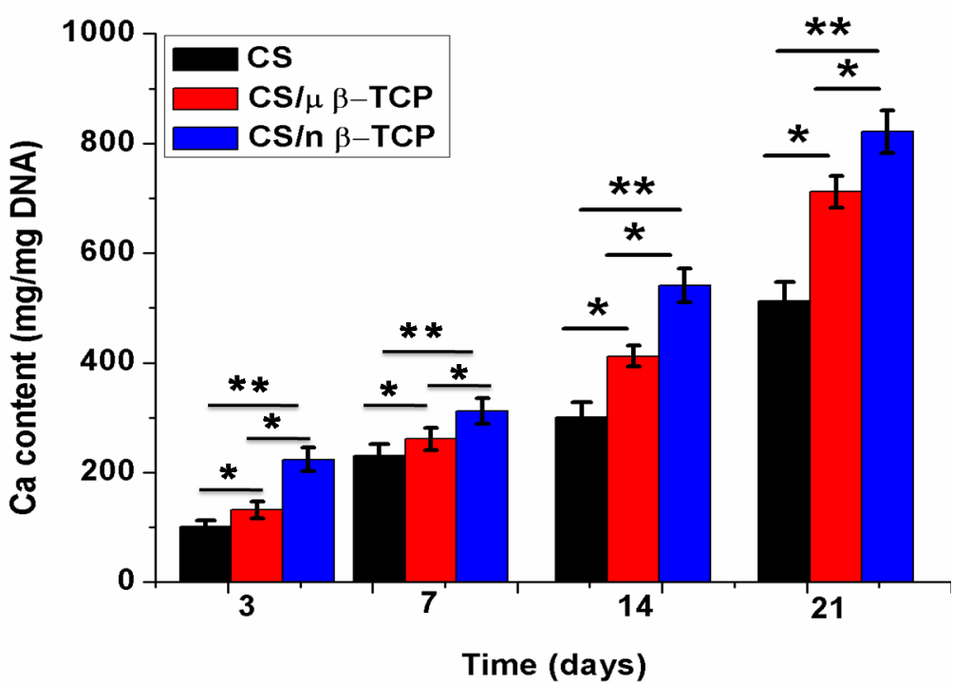

Figure 5.21: ***Total calcium content of CS, CS/micro β-TCP and CS/nano β-TCP composite scaffolds. Each point represents the mean ± SD (n= 3) * and ** denotes significant differences between groups at p > 0.05 and p < 0.05 respectively***

PART-II

Development of Fibrin Conjugated CS/nano β-TCP Composite Scaffolds

In the previous section, the limitation of low compressive strength and bioactivity of chitosan was addressed through the fabrication of CS/β-TCP composite scaffolds by reinforcing β-TCP with varying particle size. Among the various composite scaffolds, CS/nano β-TCP was found to be the most potential possessing high compressive strength, enhanced bioactivity and cell supportive property. It is further evident that CS lacks desired cell signalling molecules which are essential for cell attachment, growth, proliferation and differentiation and hence CS have less cellular affinity. The deficiency of cell affinity of CS scaffolds can be overcome by the incorporation of bioactive protein molecules [156]. In this context, Arginine-Glycine-Aspartic acid (RGD), a cell-binding peptide is most commonly used to enhance the cellular affinity of scaffold by improving its surface property [155]. Fibrin a biocompatible and biodegradable insoluble protein is reported to be a promising bioactive molecule for improving cell attachment, cell proliferation and extra cellular matrix formation in wound healing [158], due to the presence of numerous cell binding domains (RGD) in fibrin [20]. It is further reported that fibrin and its degradation products induce angiogenesis [222]. Fibrin plays important role in orthopaedic surgery to enhance osteogenesis and also act as angiogenic factor to increase cell retention thereby promotes early osteogenic differentiation of bone cells [161].

Keeping the above aspect of fibrin in view, efforts have been given in this phase of research to investigate the effect of fibrin conjugation on the cell binding affinity of CS/nano β-TCP composite scaffold with the intention to achieve better cell attachment, proliferation and osteogenic differentiation of MSCs. A results and discussion on this study is described in this chapter.

5.2.1 Morphology and pore size

SEM images as depicted in **Figure 5.22 (A)** reveal an open and interconnected porous network of the fibrin conjugated CS/nano β-TCP composite scaffolds. There is no significant difference in pore size range of CS/nano β-TCP due to fibrin conjugation. The pore size range of CS/nano β-TCP/F scaffold is 49-151 μm and is beneficial by allowing the diffusion of water soluble substances to the cells through the porous architecture of composite scaffolds [223]. The microstructure of developed fibrin conjugated scaffolds can play dual role by providing suitable porous platform to the cells and offers micro-channels for the efficient transport of nutrients from the media to the cultured cells. The micro channels formed on the scaffold surface is represented in **Figure 5.22 (B).** Furthermore, the microstructure of fibrin conjugated scaffolds has become rough in nature which might have one of the reasons in enhanced cellular responses on fibrin conjugated scaffolds. A slight decrease (~15) in the pore size of CS/nano β-TCP/F composite scaffolds is observed which may be due to cross linking by EDS-NHS. The phenomenon of decrease in pore size has also been reported earlier when CS/collagen 3D matrices was cross-linked with carbodimide [224]. The obtained pore size range is adequate for hosting the seeded cells, cell adhesion to the inner surface and diffusion of nutrients through the scaffold.

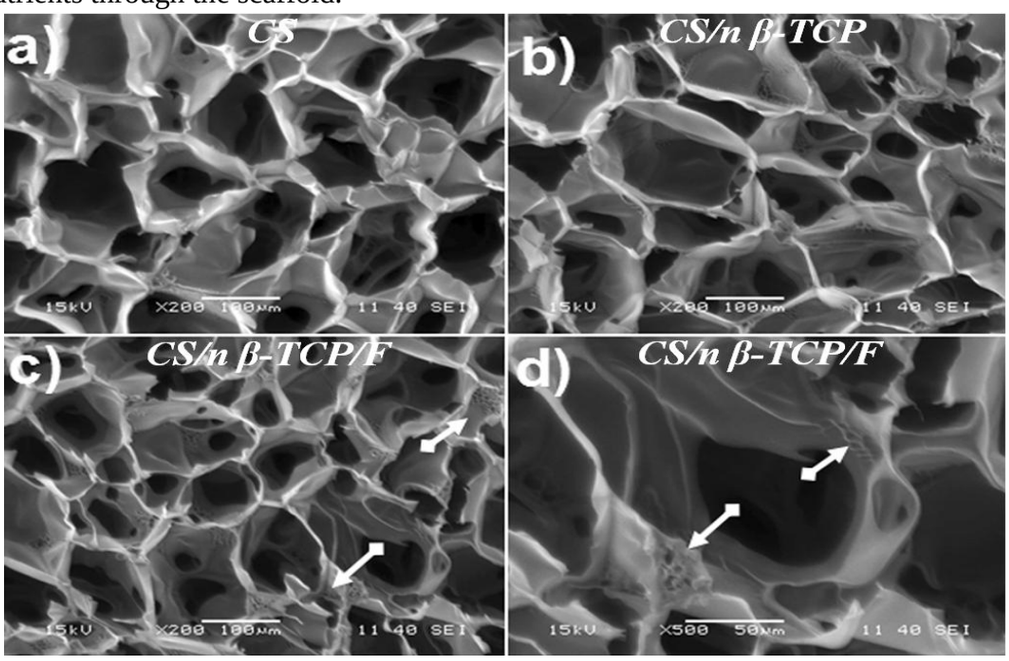

Figure 5.22 (A): ***Morphology of pure CS; fibrin conjugated and non conjugated CS/nano β-TCP composite at different magnifications. Fibrillar network like structure inside the pore walls of fibrin conjugated scaffolds is shown in white colored arrow marks (c, d)***

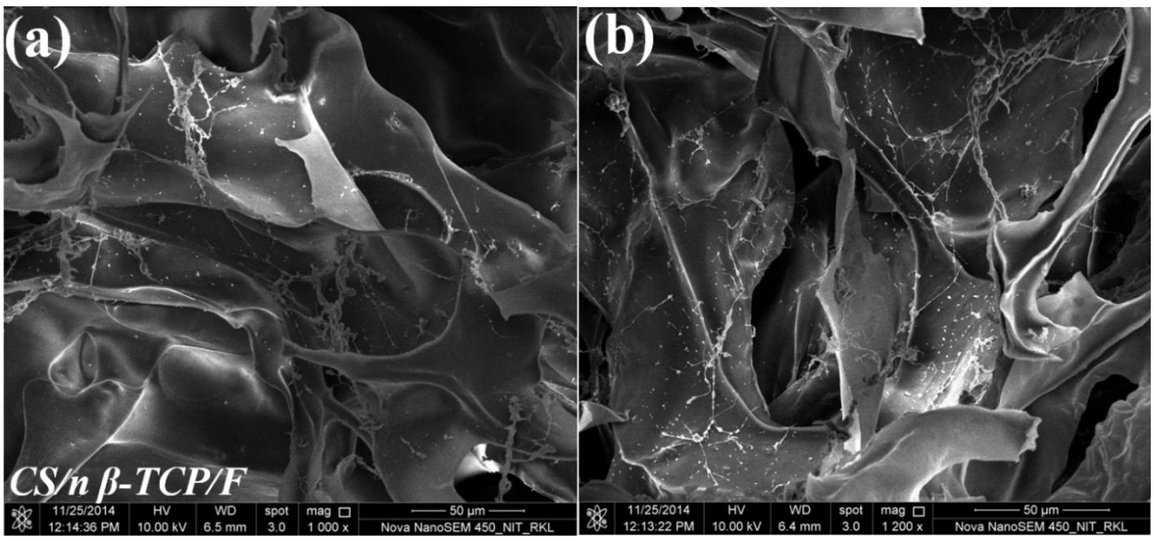

Figure 5.22 (B): ***FE-SEM images depicting the fibrillar structures of fibrin formed on the surface of composite scaffolds***

5.2.2 Porosity

The porosity of the fibroin conjugated composite matrix was measured to assess any change has occurred in porosity due to conjugation of fibrin. A slight increase in porosity is obtained with the fibrin conjugated composite scaffold compared to non conjugated one and corresponding % porosity measured as 81.4 ± 4.1 and 80.1 ± 3.60. This slight increase in porosity may be as a result of reduced pore size caused by EDC-NHS cross-linking [78, 225]. Both conjugated and non conjugated scaffolds have shown decreased % porosities as compared to pure CS scaffold (86%) which may be due to the incorporation of β-TCP and EDC cross-linking. Similar trend of decrease in porosity was observed in study reported by Lein et.al where the porosity of gelatin scaffolds was increased due to cross-linking with genipin [226].

5.2.3 Phase analysis

Figure 5.23 shows X-ray diffraction patterns of pure CS, fibrin conjugated and non conjugated CS/nano β-TCP composite scaffolds. Fibrin being non crystalline in nature, it will not change the phase of the composite system with which it gets conjugated. So, the XRD pattern of composite scaffolds remains unaltered even after fibrin conjugation as shown in figure. Sharp peaks at 2θ = 31.7 and 32.1 confirm the presence of β-TCP in CS/nano β-TCP/F scaffolds similar to XRD pattern observed with CS/nano β-TCP [211]. As indicated in **Figure**

5.23, the intensity of peaks corresponding to CS is decreased due to the incorporation of nano β-TCP. Amorphous nature of CS is diminished in composite scaffolds. However, the decrease in the intensity of CS peak is higher in fibrin conjugated scaffolds attributed to cross-linking. Rafat et.al observed the similar increase in intensity of collagen/CS hydrogels when cross-linked using carbodimide [224].

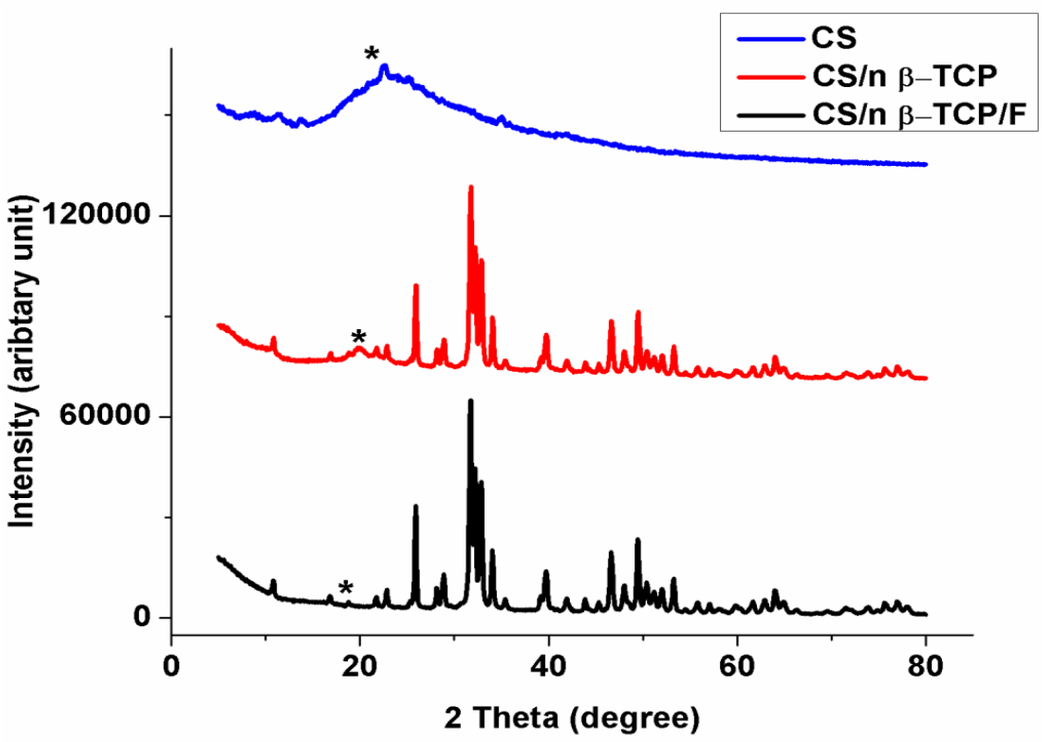

Figure 5.23: ***XRD pattern of CS, CS/nano β-TCP and CS/nano β-TCP/F composite scaffolds. Pure CS has shown prominent peak at 2θ=9.16° & 20.6°; sharp peaks at 2θ = 31.7 and 32.1° indicates the presence of β-TCP in the composite. * represents the decrease in intensity of CS peak at 2θ=20.6 °***

5.2.4 Functional analysis

Figure 5.25 illustrates the FTIR spectra generated with CS/nano β-TCP composite scaffolds with and without conjugation to assess any change in functional characteristics of the scaffold due to fibrin conjugation. **Figure 5.24** illustrates the bands observed in the IR spectra for CS/nano β-TCP and CS/nano β-TCP/F scaffolds. Bands at 1040, 1122, 610, and 551 cm^{-1} correspond to PO_4^{-3} of β-TCP [53]. It has been reported that shifting as well as generation of new peaks occur due to chemical interactions between individual components of composite scaffolds [227]. Nature of bonding between fibrin and chitosan caused by the cross-linking of

EDC, where carboxylic group of EDC bonded with amide groups of fibrin. The amide II and amide III absorption bands at 1550 and 1240 cm^{-1} belong to fibrin protein have been shifted to 1577 cm^{-1} and 1251 cm^{-1}. New bands at 751 cm^{-1} and 3540 cm^{-1} is seen in both scaffolds which may be due to the interactions between PO_4^{-3} with C=O of fibrin and N-H of CS respectively. These observations clearly indicate the interaction between $–NH_2$ of fibrin with $–CH_2$ of chitosan and PO_4^{-3} of β-TCP.

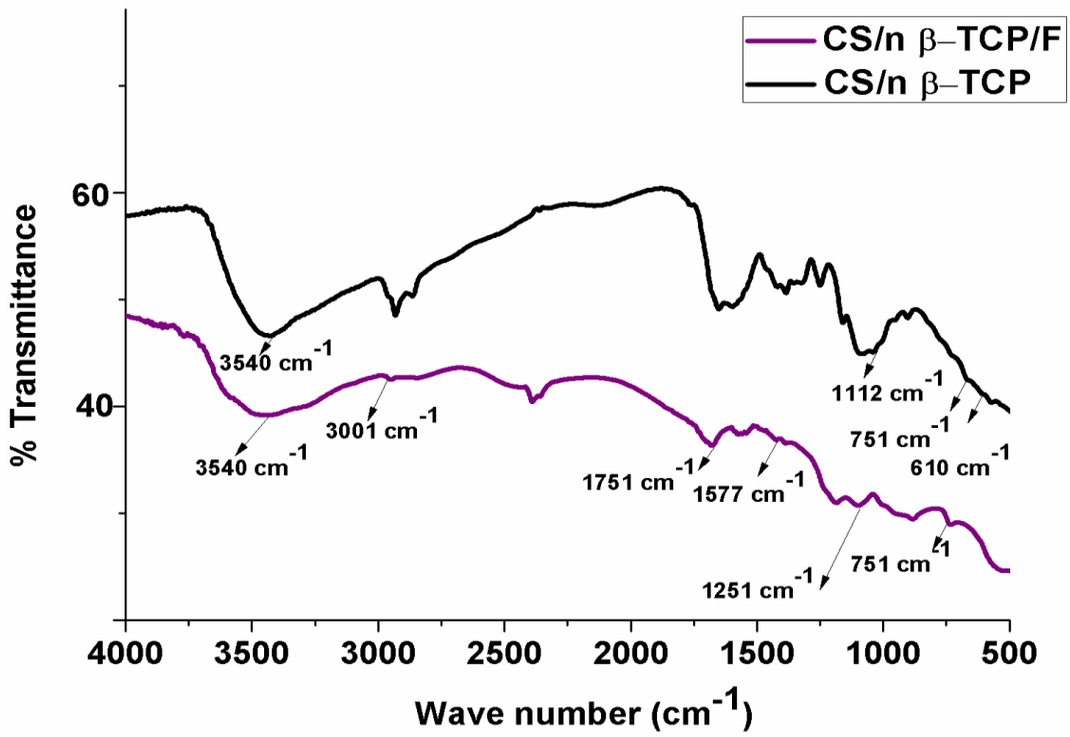

Figure 5.24: ***FT-IR pattern of CS/nano β-TCP and CS/nano β-TCP/F composite scaffolds***

5.2.5 Compressive strength

Figure 5.25 depicts compressive strength of the developed fibrin cross-linked CS/nano β-TCP composite scaffold. There is no significant increase in compressive strength is observed due to fibrin conjugation. The similar compressive strength of conjugated and non-conjugated scaffold may be attributed to the non-homogenous crosslinking between EDC and chitosan that leads to propagation of crack within the scaffold. The mechanism of cross-linking between EDC with chitosan involves the reaction between amino and carboxylic groups. The cross linking reaction between amino groups of CS may not be homogenous and unevenly spread in the scaffold as reported elsewhere [78]. Some degree of uncross- linked CS is present in the scaffold which is well evident from the very less change in elastic modulus

(0.1MPa) calculated from stress strain plot. The developed crack due to non-uniform crosslinking might have propagated through the weakest link in the conjugated scaffold and therefore no significant change in compressive strength is obtained due to fibrin conjugation. Both conjugated (2.71 ± 0.14 MPa) and non-conjugated (2.67 ± 0.21 MPa) scaffolds possess higher compressive strength as compared to pure CS scaffold (0.19 MPa). The result is in good agreement with the published reports where the use of varied concentrations of EDC-NHS has no effect on mechanical properties of freeze-gellled CS scaffolds [78].

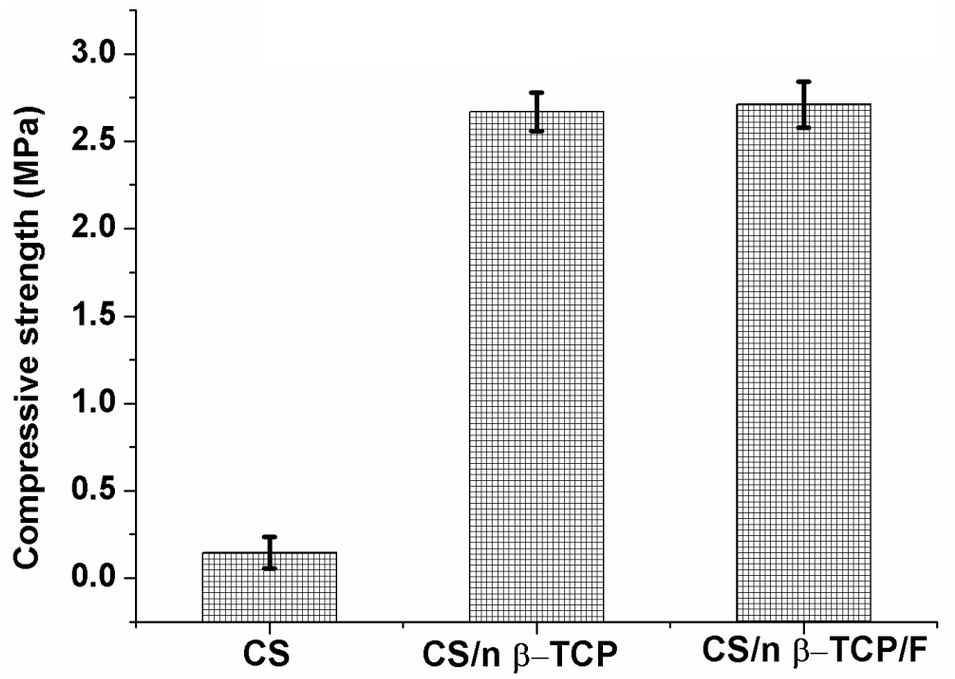

Figure 5.25: ***Compressive strength of CS, CS/nano β-TCP and CS/nano β-TCP/F composite scaffolds***

5.2.6 Measured contact angle

From the assay result, a slight increase in measured contact angle is observed in case of CS/nano β-TCP conjugated with fibrin (53.1 ± 0.5°) representing a slightly lower hydrophilicity. No significant change is noticed between the contact angle of pure CS (51.2 ± 0.8°) and CS/nano β-TCP composite scaffold (51.9 ± 1.1°). The slight increase in contact angle observed with fibrin conjugated scaffold may be explained as fibrin is a water insoluble protein (hydrophobic). Though fibrin conjugation has resulted a slight decrease in the hydrophilicity of CS composite scaffold, the presence of numerous cell binding domains like RGD peptides is expected to manifold its cell adhesive property as reported earlier [228].

Most of the important protein- protein interactions occur between hydrophobic residues of proteins and thus increase of contact angle in a certain limit also might have favoured the enhanced protein-protein interactions resulting in improved cellular responses on fibrin conjugated scaffolds [51].

5.2.7 Swelling behaviour

Figure 5.26 shows the swelling of behavior of scaffolds during 48 hours of time. As observed in figure, during initial period (5-6 hrs) of the experiment, a rapid increase in swelling is prominent beyond which the scaffolds show a saturated swelling without any further change in % swelling. CS scaffold have shown the highest swelling (312% of its initial weight) than the other types of scaffolds. CS/β-TCP composite showed higher swelling (276% of initial weight) compared to the scaffolds with fibrin (243%). The decrease in swelling of fibrin conjugated scaffold may be attributed to the hydrophobic nature of fibrin which resisted the flow of water into the scaffold resulting in decreased swelling [229].

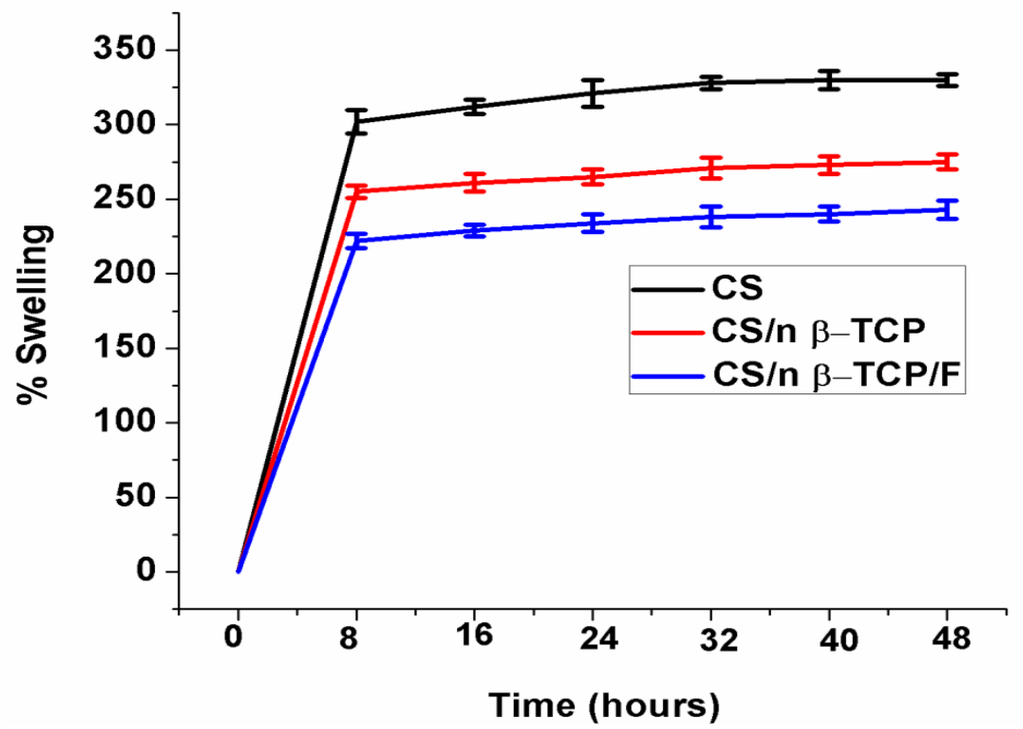

Figure 5.26: ***Swelling behaviour of CS, CS/nano β-TCP and CS/nano β-TC/F composite scaffolds. CS/nano β-TCP scaffold shows a higher swelling than CS/nano β-TCP/F scaffold***

5.2.8 *In-vitro* biodegradation study

The scaffolds should preserve its structural and mechanical stability until the seeded cells secrete sufficient amount of ECM for their sustenance [56]. In this context, degradation behaviour of the scaffold plays a vital role in the formation of neo tissue at the site of implant [135]**.** The *in-vitro* degradation pattern of the prepared fibrin conjugated scaffold (CS/nano β-TCP/F) is shown in **Figure 5.27** and the degradation behaviour is also compared with the pure CS and CS/nano β-TCP composite scaffolds. The degradation pattern shows a favourable impact of fibrin conjugation achieving a slight decrease in degradation of conjugated scaffold (15%) than the non-conjugated one (16%). The reduced degradation in fibrin conjugated CS/nano β-TCP composite scaffold may be due to increase in intra and inter molecular hydrogen bonds that resulted in the increased compactness of scaffold matrix [230]. Both conjugated and non conjugated scaffolds have shown a decelerated degradation when compared to pure CS scaffold-31% ($p < 0.05$). Previous reports suggest that optimal degradation of scaffolds eases the longevity of scaffold implantation at tissue damaged site [231]. Dimethyl 3,3-dithio-propionimidate [DTBP] cross-linked CS scaffolds well maintained their structural integrity and degraded to 10% during 21 days of degradation [169]. Thus the prepared cross-linked CS/nano β-TCP/F composite scaffold is expected to provide adequate support to the growing cells for a certain longer period of time, which may be of a greater importance in *in-vivo* handling as the scaffolds will degrade in pace with neo tissue formation.

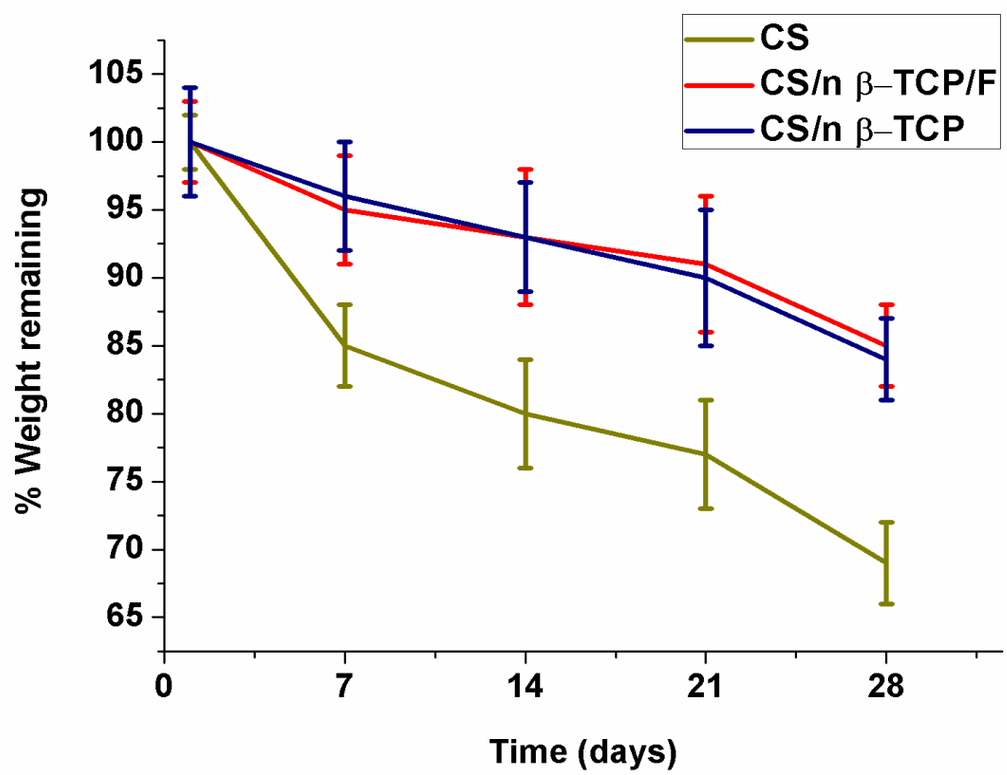

Figure 5.27: ***In-vitro degradation pattern of CS/nano β-TCP/F composite scaffold in PBS for 28 days treatment compared with pure CS and CS/nano β-TCP composite scaffolds. Significant difference in degradation noticed in pure CS and fibrin conjugated scaffolds where as slight difference in degradation rate is seen between CS/nano β-TCP and fibrin conjugated CS/nano β-TCP composite scaffolds***

5.2.9 Cell morphology and cell attachment

Cell attachment and morphology of MSCs seeded on the scaffolds are visualized by FE-SEM images **(Figure 5.28 a-f).** On close observation, MSCs are found to attach and spread on the scaffold surface during the culture period. On day 1, cells are found to be spherical in shape with distinct appearance **[Figure 5.28 (a&b)].** The cells are well spread throughout the scaffold and colony formation is observed on day 7 and 14 as shown in **Figure 5.28 (c-f).** Furthermore, cells are found to attach on the surface and in the pores of scaffolds by filopodia like structures. The surface of CS/nano β-TCP scaffolds appear relatively smoother representing the less number of cells attached and proliferated. Whereas, the entire surface is covered with more number of cells attached and proliferated on CS/nano β-TCP/F scaffolds as compared to non conjugated scaffolds representing superior cytocompatibility of CS/nano β-

TCP/F scaffolds. The presence of numerous cell binding domains (RGD) favoured the enhanced attachment and spreading of seeded hMSCs on CS/nano β-TCP/F scaffolds.

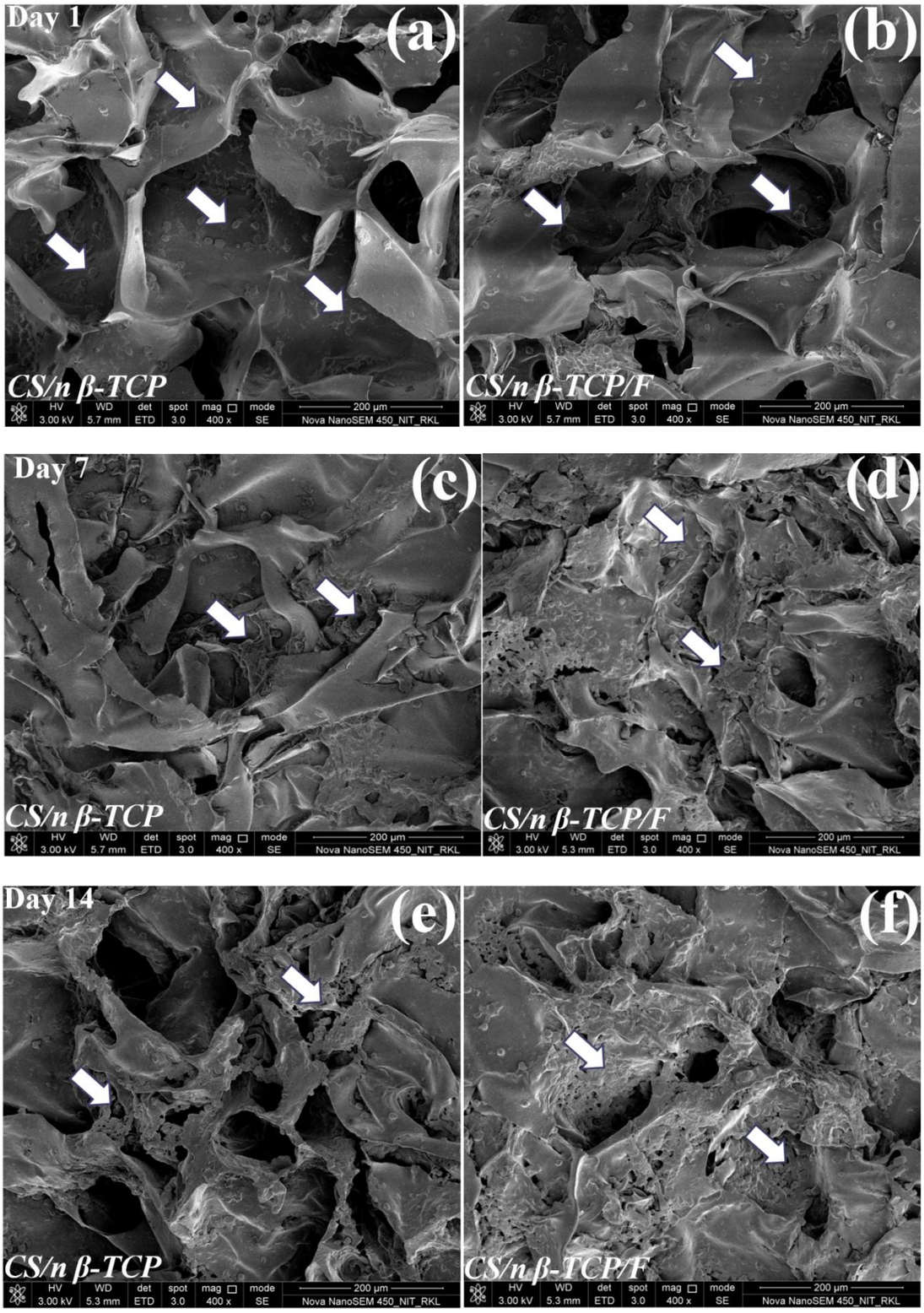

Figure 5.28*: FE-SEM images showing morphological changes an attachment of hMSCs on CS/nano β-TCP (a, c, e) and CS/nano β-TCP/F composite scaffolds (b, d, and f) during 14 day culture period. Images depict the morphological changes of hMSCs. Spherical shape (a, b) on day 1, colonization (c, d) on day 7 and well spreading sheet like structures (e, f) on day 14*

5.2.10 Metabolic activity by MTT assay

The cellular viability in terms of metabolic activity of the MSCs seeded on the prepared scaffold was further evaluated quantitatively by MTT assay as shown in **Figure 5.29.** As indicated, an increase in O.D (optical density) with culture period is observed. The higher O.D value representing higher metabolic activity is obtained with CS/nano β-TCP/F (0.915 ± 0.12) scaffolds as compared to control [CS (0.4 ± 0.018)] and CS/nano β-TCP (0.614 ± 0.016) after 7 days of culture. The increase in metabolic activity achieved with CS/nano β-TCP can be attributed to the presence of RGD sequences in fibrin which provides suitable cell recognition sites to attract more number of cells on the scaffold surface [232]. Thus, the fibrin conjugated scaffolds proved their superior biocompatibility over CS/nano β-TCP and CS scaffolds by MTT assay.

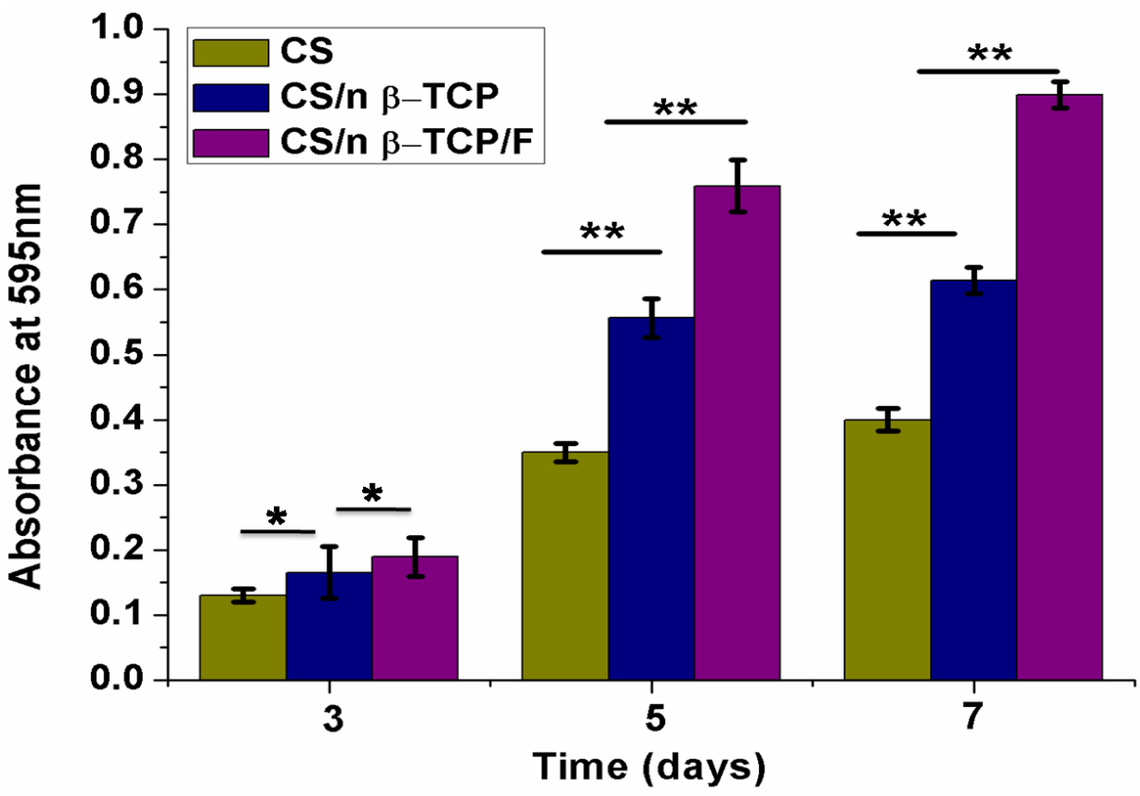

Figure 5.29: ***MTT assay of hMSCs seeded on fibrin conjugated and non conjugated composite scaffolds on 3, 5 and 7 days of culture. Each point represents the mean ± SD (n=3) * and ** shows significant differences between groups at p >0.05 and p < 0.05. After 7 days of incubation higher cell viability is achieved with CS/nano β-TCP/F composite scaffolds compared to pure CS as well as CS/nano β-TCP composite scaffolds***

5.2.11 hMSCs proliferation

(i) Fluorescence microscopy

The proliferation of MSCs on the developed scaffolds was qualitatively assessed by the analysis of fluorescence microscopic images **(Figure 5.30)** during the 14 days of culture period. **Figure 5.30** represents 7th (a, c, e) and 14th day (b, d, f), images of the relative cellular proliferation of MSCs grown over CS/nano β-TCP and CS/nano β-TCP/F composite scaffolds. Further, the number of cells on fibrin conjugated scaffold is observed to be higher as compared to non conjugated and pure CS scaffolds.

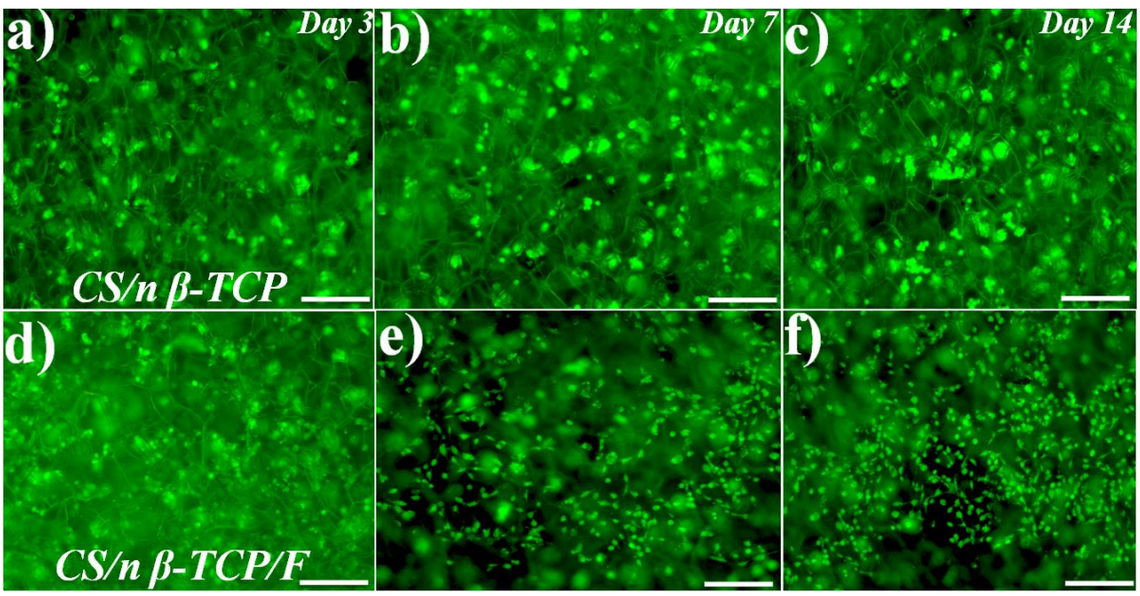

Figure 5.30*: Fluorescence images of hMSCs cultured on CS/nano β-TCP (a,b,c) and CS/nano β-TCP/F (d, e, f) scaffolds showing cell proliferation on day 3 (a, d); day 7 (b, e) and day 14 (c, f). Dense distribution of hMSCs is clearly seen on fibrin coated scaffolds compared to non fibrin coated scaffolds. Scale bar indicates 200µm*

(ii) DNA quantification assay: The proliferation of MSCs on the developed scaffolds was evaluated by DNA quantification assay. **Figure 5.31** shows an increase in DNA content with time in all the developed scaffolds with a varying degree of DNA content. Among the scaffolds used under study, CS/nano β-TCP scaffolds conjugated with fibrin has shown highest DNA content representing an enhanced proliferation rate. The increase in proliferation rate achieved with CS/nano β-TCP/F is attributed to the presence of cell recognition binding sites or specific peptides like RGD on the surface of scaffold matrices enhance cell polymer

interactions as reported earlier [40]. The corresponding DNA content of hMSCs cultured on CS/nano β-TCP/F composite scaffold for 3 to 21 days is 109 ± 12 ng/ml to 501 ± 24 followed by DNA content obtained with non conjugated composite matrix and pure CS scaffold. Thus the fibrin conjugated scaffolds is proved to mimic the native environment in a better way that results in the higher proliferation of hMSCs than other CS scaffolds.

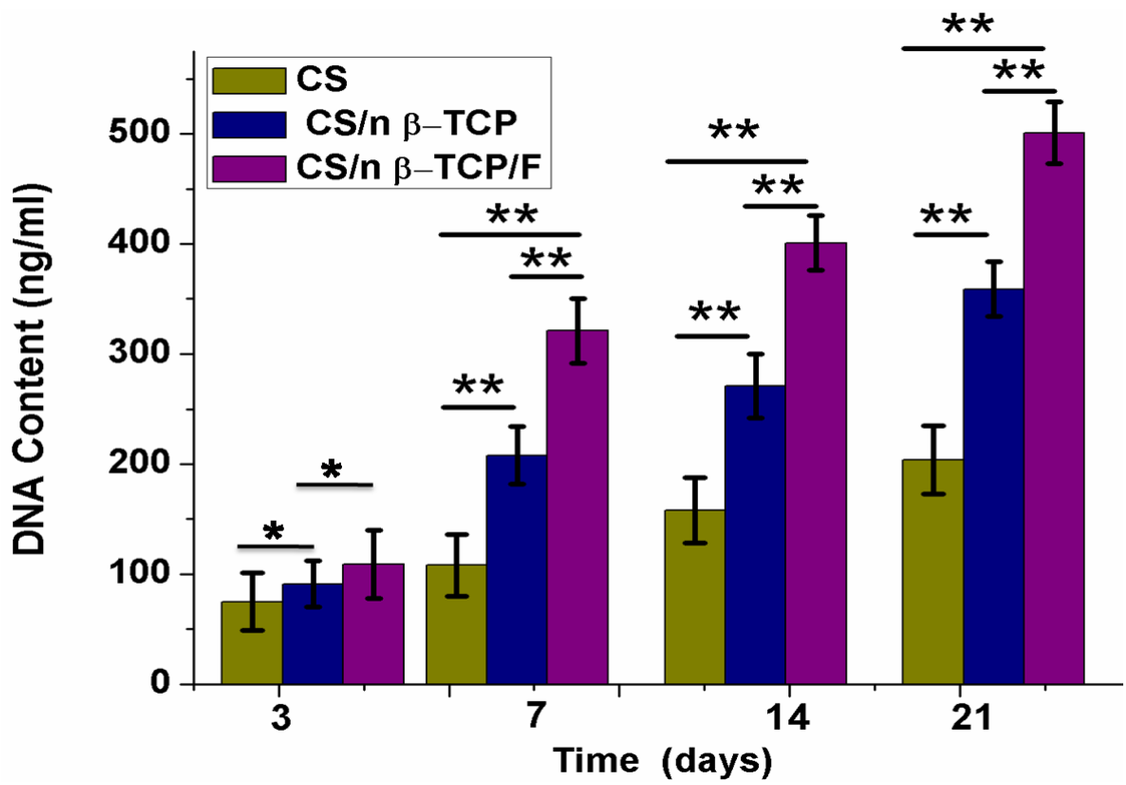

Figure 5.31: ***Cell proliferation represented in terms of DNA quantification on CS, CS/nano β-TCP and CS/nano β-TCP/F composite scaffolds upto 21 days of culture. An increased DNA content pattern is seen with all scaffolds with varying degree of DNA content. Fibrin conjugated scaffold has shown highest proliferation at any time point. Each point represents the mean ± SD (n=3) * and ** represents p>0.05 and p < 0.05respectively***

5.2.12 Cytoskeletal organization

It is important to know the cell distribution in the inner sections of 3D scaffold for understanding the cell penetration which ultimately helps in tissue regeneration [233]. The cell infiltration and uniform distribution of hMSCs within the scaffold architecture was observed under confocal microscope. FITC conjugated Phalloidin and Hoescht dye was used to stain actin filaments and nuclei of cultured cells respectively. 3 dimensional confocal laser scanning microscopic (CLSM) images depict the cell penetration in 3D scaffold matrix upto a

depth of ~ 40 µm and 50 µm on CS/nano β-TCP and CS/nano β-TCP/F composite scaffolds respectively as shown in **Figure 5.32 (b-d).** On 14th day of culture, number of viable cells observed is more on fibrin conjugated scaffolds than non fibrin conjugated scaffolds. **[Figure 5.32 (c)]** A similar observation in uniform distribution and enhanced infiltration of cells is reported earlier when alginate/micro β-TCP composite systems coated with fibrinogen [234].

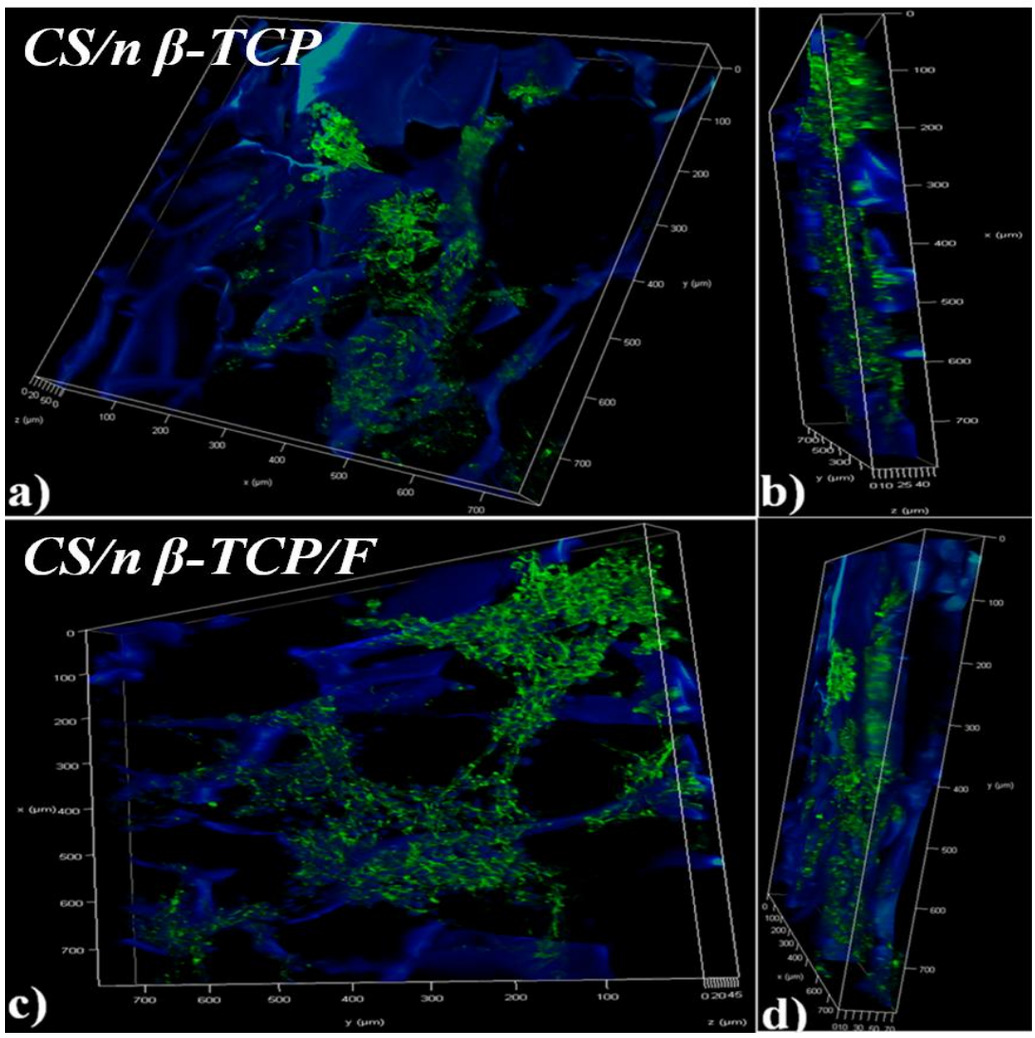

Figure 5.32*: 3D laser scanning confocal images (Z stacks) of hMSC morphology after 14 days of culture on CS/nano β-TCP (a, b) and CS/nano β-TCP/F composite scaffolds (c, d). Nuclei of the cells are stained with Hoechst 33342 (blue) and actin filaments with phalloidin (green). (b) and (d) represent z-stacks rotated in 3D space to depict cell infiltration into the porous architecture of CS/nano β-TCP and CS/nano β-TCP/F composite scaffolds respectively*

5.2.13 Osteogenic differentiation potential

(i) Alkaline phosphatase assay

The osteogenic potential of hMSCs seeded scaffolds was evaluated by alkaline phosphatase assay as illustrated in **Figure 5.33. A**LP activity is found to increase steadily upto 14 days of culture. As observed, the slight decrease in ALPase activity after 14th day of incubation indicates that cells have overcome the initial stage of osteogenic differentiation. Among the developed scaffolds, MSCs cultured on CS/nano β-TCP/F scaffold expresses higher ALP activity ($P < 0.05$) than cells grow on control (CS) and CS/nano β-TCP composite scaffold. A rapid increase in ALP expression is observed with all scaffolds from day 7 to day 14 ($p< 0.05$) with a variation in ALPase activity. However, higher ALP activity is achieved with fibrin conjugated scaffold. The corresponding value is 3.87 ± 0.32 IU/µg and 6.61 ± 0.11 IU/µg. Thus enhanced ALP activity is noticed on fibrin conjugated scaffolds which is due to osteoinductive property of fibrin and similar result was observed with fibrin coated PCL/HA composite system as reported earlier by Kang et al [235].

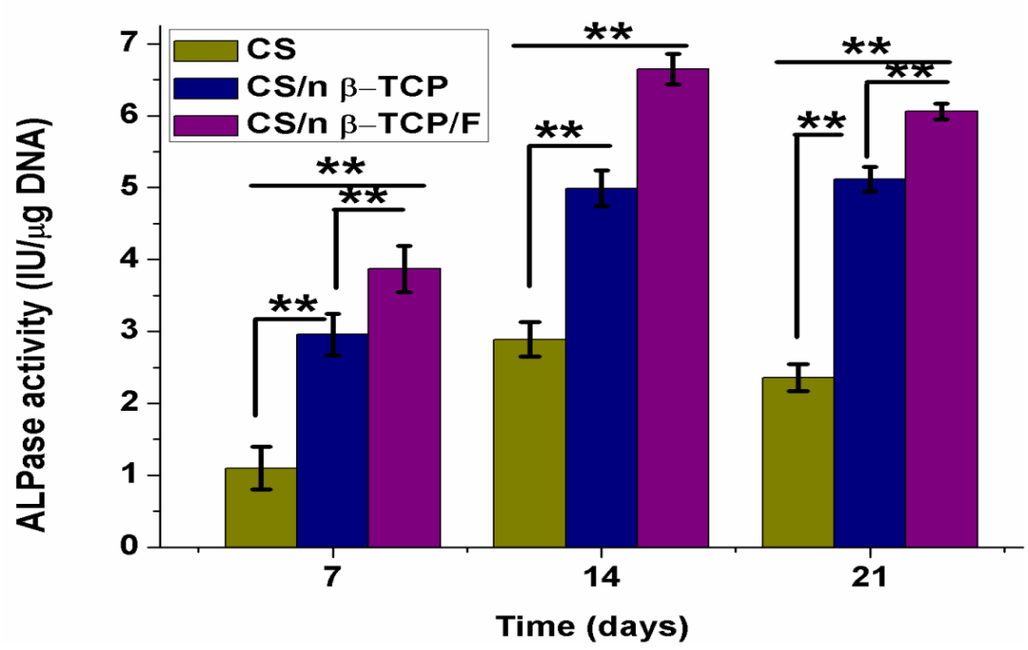

Figure 5.33: ***Alkaline Phosphatase activity of pure CS, fibrin conjugated and non conjugated CS/nano β-TCP composite matrices during after 21 days of culture. ALP activity increased upto 14 days of culture and then a slight decrease in ALP activity is observed. Fibrin conjugated scaffold shows highest ALP activity. Each point represents the mean ± SD (n= 3) ** shows significant differences between groups at p < 0.05***

(ii) *In-vitro* biomineralization

Mineralization is a phenomenon in which calcium phosphate deposits on the surface of scaffolds and represent one of the evidences for cells to differentiate in to osteoblastic lineage [236]. Alizarin red assay was performed to assess the extent of matrix mineralization by MSCs differentiated on CS/nano β-TCP (with and without cells) and CS/n β-TCP/F composite scaffolds during 21days of incubation. As observed from **Figure 5.34,** CS/nano β-TCP/F scaffold has shown enhanced mineralization throughout incubation time indicating greater osteogenic differentiation of hMSCs as compared to CS/nano β-TCP (with and without cells) composite scaffolds. Furthermore, mineralization of scaffolds is quantified by measuring the OD of the dye extracted from the stained nodules and the trend is shown in **Figure 5.35.** Increase in OD value with respect to time is seen on both the scaffolds which indicate the differentiation of hMSCs on scaffolds under study. However, on day 21 significant difference is observed in the measured optical density (O.D value) of fibrin conjugated scaffolds with other scaffolds. Alizarin staining results are in good accordance with the previous reports where RGD conjugated CS has shown greater mineralization compared to the unmodified CS scaffolds [40].

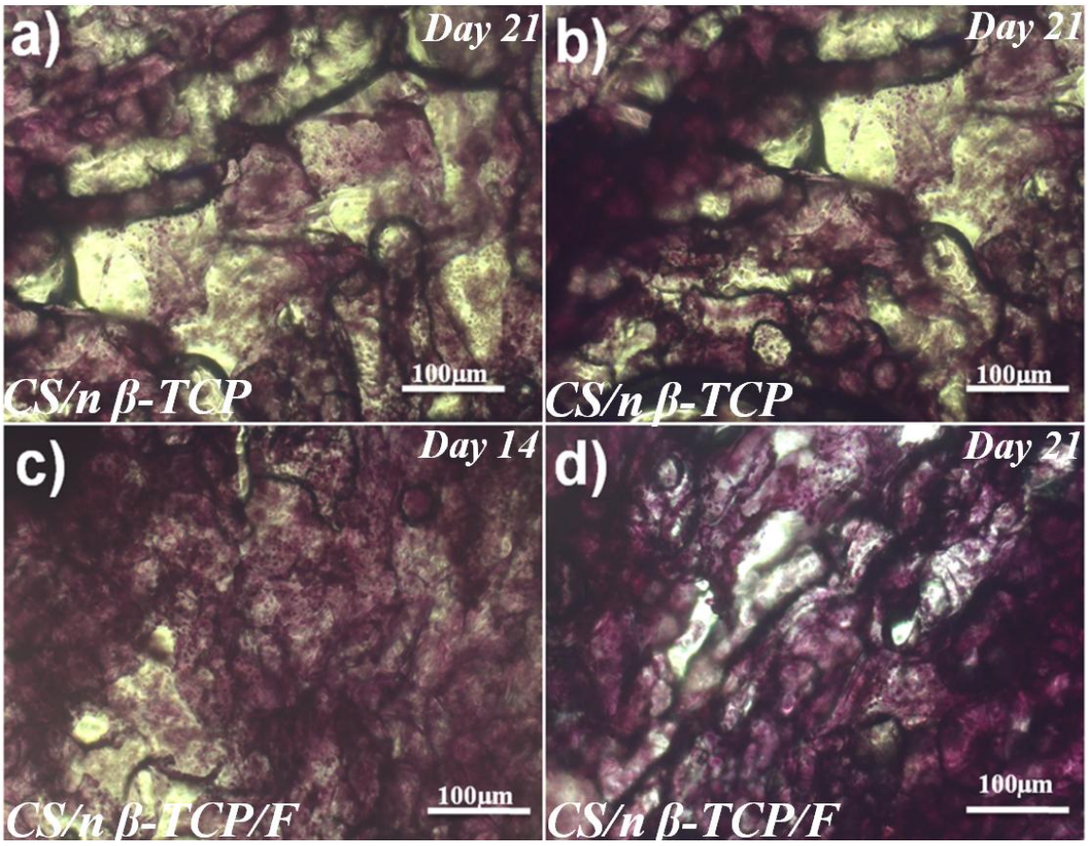

Figure 5.34: ***Optical microscopy images for CS/nano β-TCP (without cells: a), CS/nano β-TCP (with cells: b) and CS/nano β-TCP/F (c, d) composite scaffolds. Intense red stains are observed on CS/nano β-TCP/F scaffolds on both 14 and 21 days (c, d) as compared to non conjugated scaffolds indicating enhanced mineralization on fibrin conjugated scaffolds***

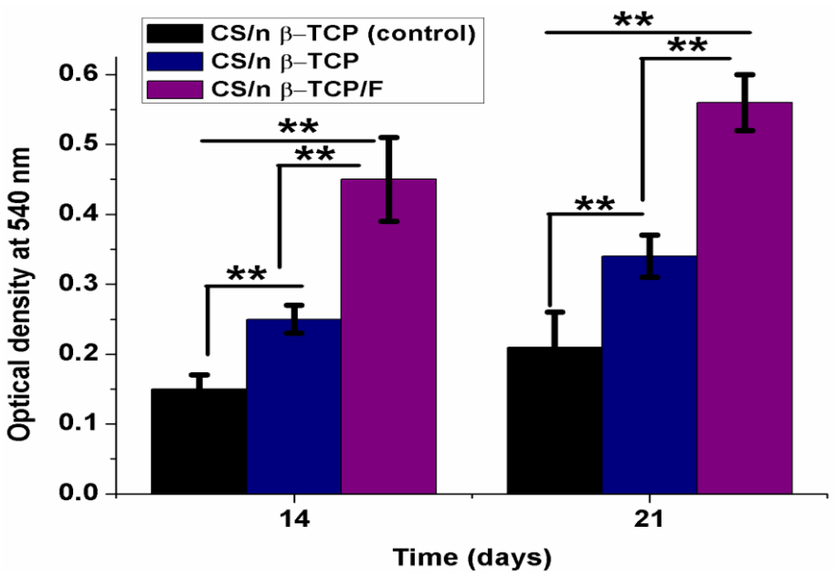

Figure 5.35: ***Quantitative representation of mineral deposition on CS/nano β-TCP and CS/nano β-TCP/F composite scaffolds upto 21 days of incubation, ** represents p < 0.05***

(iii) Expression of osteogenic specific genes

Semi quantitative RT-PCR was performed to assess the expression of osteoblast related genes at mRNA level for MSCs cultured for three weeks. The mRNA expression of genes such as ON, ALP and OC are observed to be significantly higher in hMSCs cultured on CS/nano β-TCP/F composite scaffold than non conjugated one as shown in **Figure 5.36.** The reason behind the increase in gene expression may be attributed to the synergic effect between β-TCP and fibrin which helped in increased differentiation of seeded cells [4]. The obtained band intensities were further quantified to examine the increased level of gene expression. **Figure 5.37** depicts the relative expression levels of the genes associated with osteogenic differentiation. Collagen type I and BSP are abundantly available proteins in bone ECM and deposited in the matrix during the maturation of osteoblasts as reported earlier [151]. Up-regulation of collagen type I and BSP genes on non fibrin conjugated scaffolds may be due to positive effect created by β-TCP as reported earlier with osteogenic differentiation of adipose derived stem cells cultured on akermanite and β-TCP ceramics [237]. A statistical difference ($p<0.05$) was observed in the expression levels of specific genes on both CS/nano β-TCP and CS/nano β-TCP/F scaffolds. Similar increase in expression of osteoblast specific genes was observed with rabbit mesenchymal stem cells when seeded in fibrin coated β-TCP 3D scaffolds as reported earlier [194, 234].

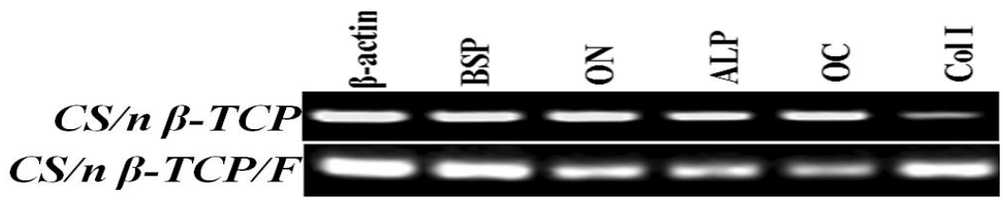

Figure 5.36: ***Images of amplified cDNA products using specific osteogenic primers (BSP, ON, ALP, OC and Col-I) for hMSCs cultured on CS/n β-TCP and CS/n β-TCP/F freeze-gelled composite scaffolds in osteogenic media for 21 days***

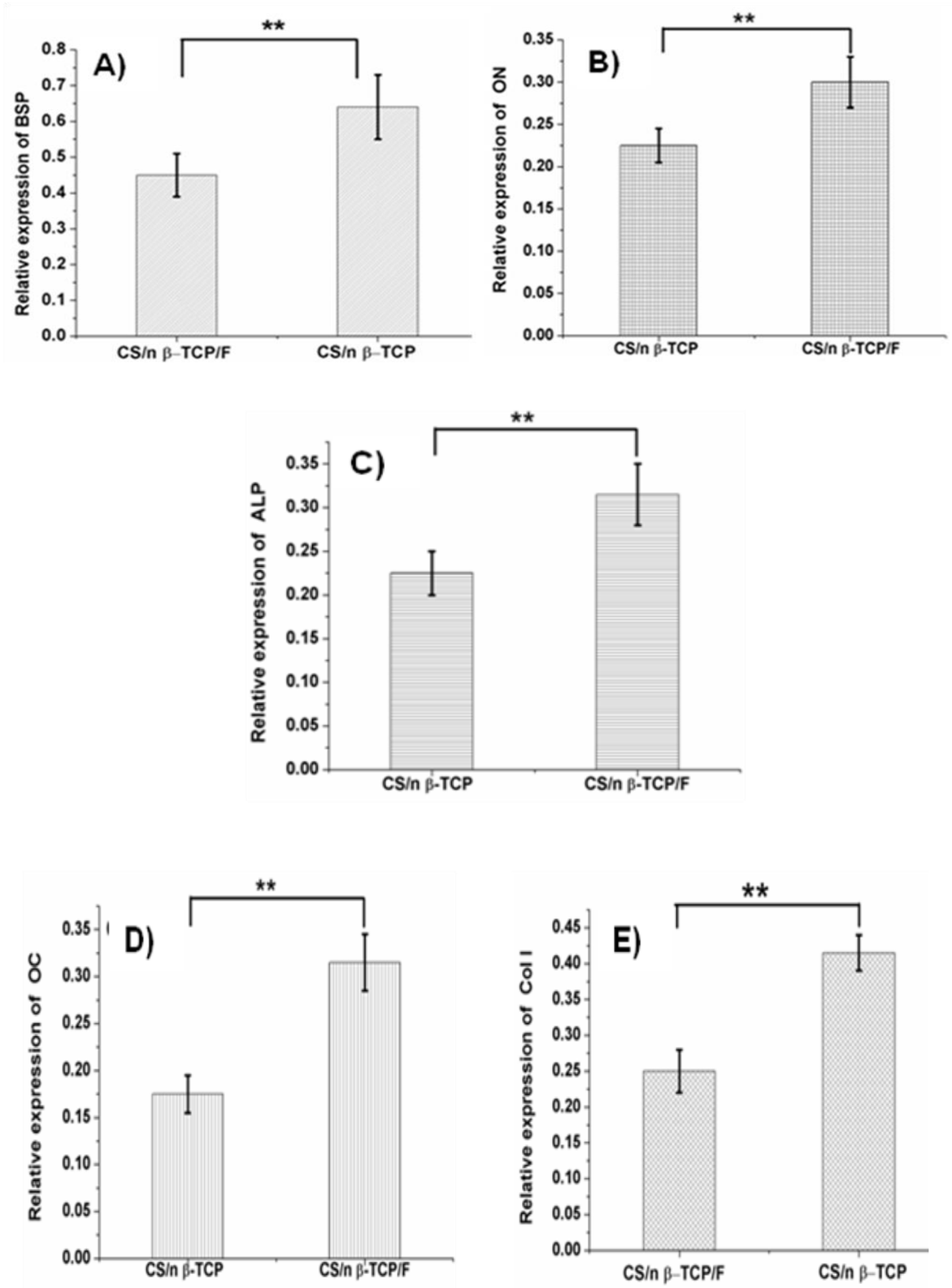

Figure 5.37: ***Relative Expression of BSP (a), ON (b), ALP (c), OC (d) and Col I(e) on mRNA of MSCs cultured on CS/nano β-TCP and CS/nano β-TCP/F composite scaffolds for 28 days of incubation. Expression levels are normalized to β actin expression. ** Represents a statistical difference at p < 0.05***

PART-III

Development of Cross-linked CS/nano β-TCP Composite Scaffolds

In the last two phases of research work, attempt has been made to improve the mechanical strength, bioactivity and cell binding affinity of the CS scaffolds by the incorporation of β-TCP as bioactive ceramic material and cross-linking with fibrin. The rapid degradation of chitosan is another important aspect that needs to be addressed to achieve controlled degradation rate compatible with the rate of neo tissue formation [57]. To overcome such limitation, in last decade several approaches have been adopted by different researchers by incorporating bio-ceramics and cross-linking agents [21]. In the previous section, though a slight improvement in degradation rate (slow degradation) is achieved by incorporating nano β-TCP, there is still need of controlling this degradation rate to a desirable level. This may be achieved by cross-linking scaffold with a suitable cross-linker. Glutaraldehyde is widely used as a cross-linking agent to reduce degradation of biopolymers, but the by-products of its degradation are shown to be harmful to cells [179]. As an alternative, the inorganic tripolyphosphate (TPP) has been used to cross-link collagen and reduce its degradation rate without harmful side effects [142]. Furthermore, the presence of phosphate moiety may be effective in promoting the growth of osteogenic cells [16]. Genipin (GN) a natural compound extracted from Gardenia fruits has been used as a cross-linking agent for synthesis of elastic gels in wound healing without causing any undesirable effects [130, 179]. Both these cross-linkers are water soluble which are reported to be beneficial to crosslink polymeric matrices and proved to decelerate degradation rate as well as enhance mechanical properties of various polymeric matrices without any toxic or undesirable side effects [179, 238].

The main aim of this part of thesis work was to prepare cross-linked composite scaffolds with controlled degradation rate, characterize their physicochemical and mechanical properties and investigate their *in-vitro* biological performance. The result and discussion of these studies are described in this chapter.

5.3.1 Development of GN and TPP cross-linked CS/nano β-TCP composite scaffolds

Different batches of genipin and tripolyphosphate cross-linked freeze-gellled CS/nano β-TCP composite scaffolds were prepared. The different concentrations of cross-linking agents are in the range of 0.01 to 0.2% (w/v). The mechanism of GN cross- linking is put forward based on the published literature [239]. In brief, nucleophilic attack by amino groups of CS on olefenic carbon atom of GN results in dihydropyran ring opening of GN. Another attack of secondary amino group of CS is on newly formed aldehydo groups of GN resulting in formation of cross-linked bridges [146]. TPP is an ionic cross-linker with negative charge which forms ionic linkages with amino groups of CS. Henceforth; it is expected to enhance the amphoteric nature of chitosan which ultimately results in better protein adhesion, followed by increased cellular responses [240-241].

5.3.2 Morphology and pore size

SEM images of CS/nano β-TCP/GN and CS/nano β-TCP/TPP along with CS and CS/nano β-TCP scaffolds for comparison are shown in **Figure 5.38.** All the developed scaffolds displayed interconnected honeycomb like microstructures with desired pore size suitable for bone tissue engineering applications. The concentration of the cross-linking agent is found to have a great influence on the pore size of the scaffold, trend being greater the concentration larger is the pore size. This phenomenon may be due to the fact that the pore structure is observed to be restrained from collapsing and thus results in an increase in pore size (**Table 5.3).** The pore size of developed cross-linked scaffold is higher than the non cross-linked CS and CS/nano β-TCP composite scaffolds. However, the pore size range of GN cross-linked scaffolds is higher (57-199 μm) than TPP cross-linked scaffolds (55-186 μm). Similar results in increase in pore size of CS/collagen matrices were reported by cross-linking with amino acids [166]. It is further observed that the thickness of the pore walls has been increased due to cross-linking which is evident from **Figure 5.38 (c-i).** Thus, cross-linking has slightly increased the pore size of the developed scaffolds which meets the desired requirement for cell culture studies.

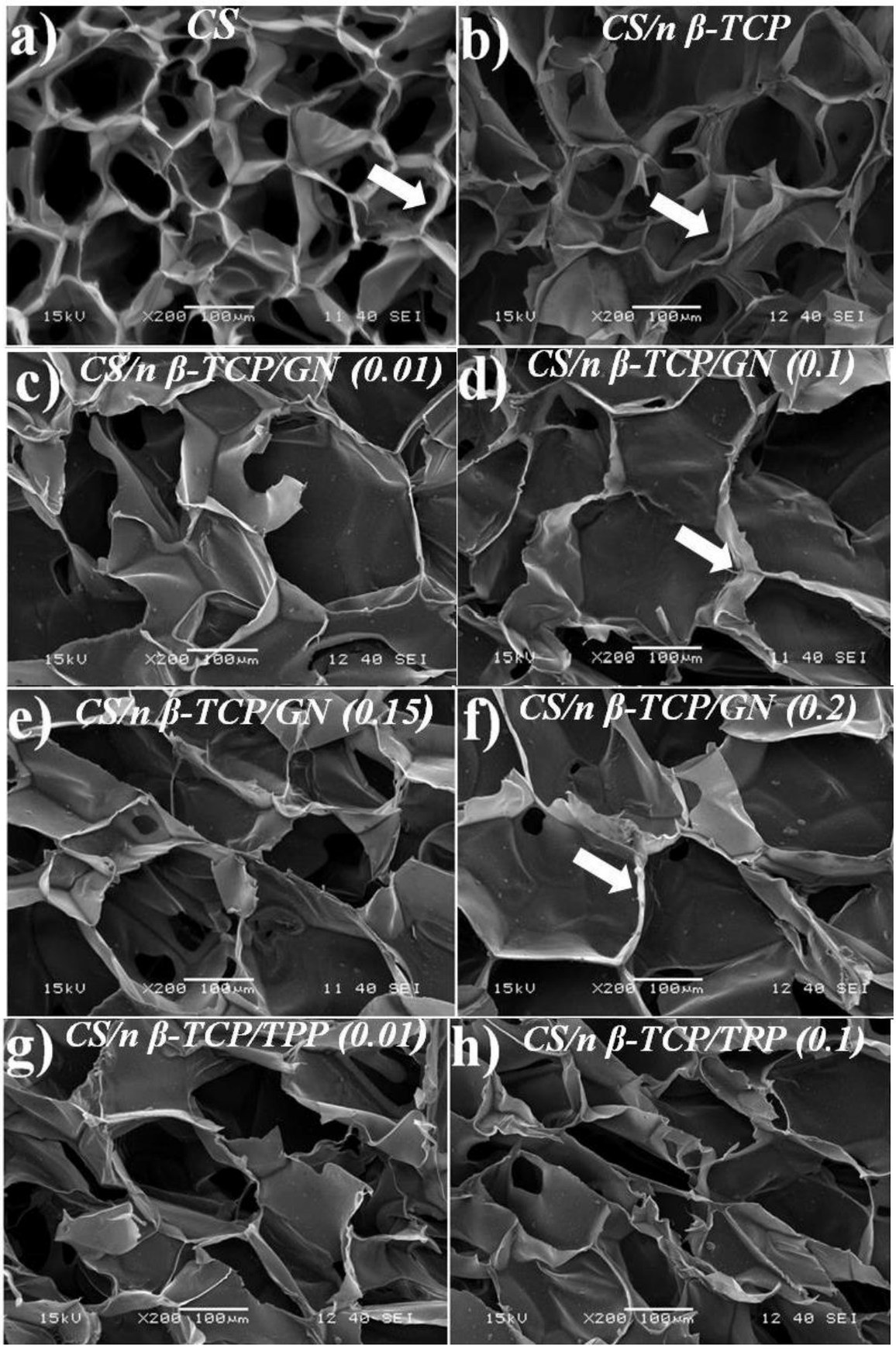

Figure 5.38: ***SEM images of cross-linked and non cross-linked composite and pure CS scaffolds. The developed scaffolds are highly porous and interconnected. Pore size of scaffold increases due to cross-linking and also increase in cross-linking agents. Furthermore, the increase in pore size of GN cross-linked scaffolds is higher than TPP cross-linked scaffolds. White colored arrow marks indicating thin (a-b) and thick (d-i) pore walls of non cross-linked and cross-linked scaffolds respectively***

5.3.3 Porosity

Table 5.3 shows the porosity results of the cross-linked scaffolds and its comparison with non cross-linked CS/β-TCP and pure CS scaffolds. Similar to pore size, the cross linking agents have an impact on porosity of the scaffolds. A decrease in % porosity is observed with cross-linked scaffolds as compared to non cross-linked and pure CS scaffolds. The % porosity of GN cross-linked scaffolds is slightly lower than TPP cross linking. The % porosity of GN and TPP cross-linked scaffolds is in the range of 68 ± 2.1 to 76 ± 2.8 and 71 ± 1.9 to 78 ± 2.9 respectively within the entire range of concentration (0.01- 0.2%).The decrease in porosity observed with increase in concentration is attributed to increase in pore size of cross-linked scaffolds as compared to non cross-linked scaffolds. For a given cross-linker, scaffold porosity decreased with increasing cross-linker concentration **(Table 5.3).** For example, as the TPP concentration was increased from 0.01 to 0.05, 0.10, 0.15 and 0.20, scaffold porosity decreased from 78 ± 2.9 to 76 ± 1.1, 75 ± 2.2, 73 ± 2.1 and 71 ± 1.9 respectively, whereas scaffold porosity decreased from 76 ± 2.8 to 74 ± 1.9, 73 ± 2.1, 70 ± 1.9 and 68 ± 2.1 for the same concentrations of GN. From pore size and porosity results, it is observed that increase in pore size resulted in decrease in % porosity and our results correlates the published data where CS/collagen and CS matrices were cross-linked with glutaraldehyde and genipin respectively [191, 231].

5.3.4 Phase analysis

XRD was performed to assess any phase change occur due to cross-linking of the composite scaffolds and the pattern is shown in **Figure 5.39.** The scaffolds cross-linked with GN (0.1%) and TPP (0.1%) are shown to decrease the intensity of CS peak (amorphous nature) and its disappearance indicates further increase in crystallinity as shown in Figure. The effect of GN concentration on decreasing CS intensity is higher than TPP. XRD patterns of composite scaffolds with varying content of GN and TPP are not shown. Further, shift in the 2θ value of chitosan towards higher angle is evident indicating decrease in amorphous nature of CS.

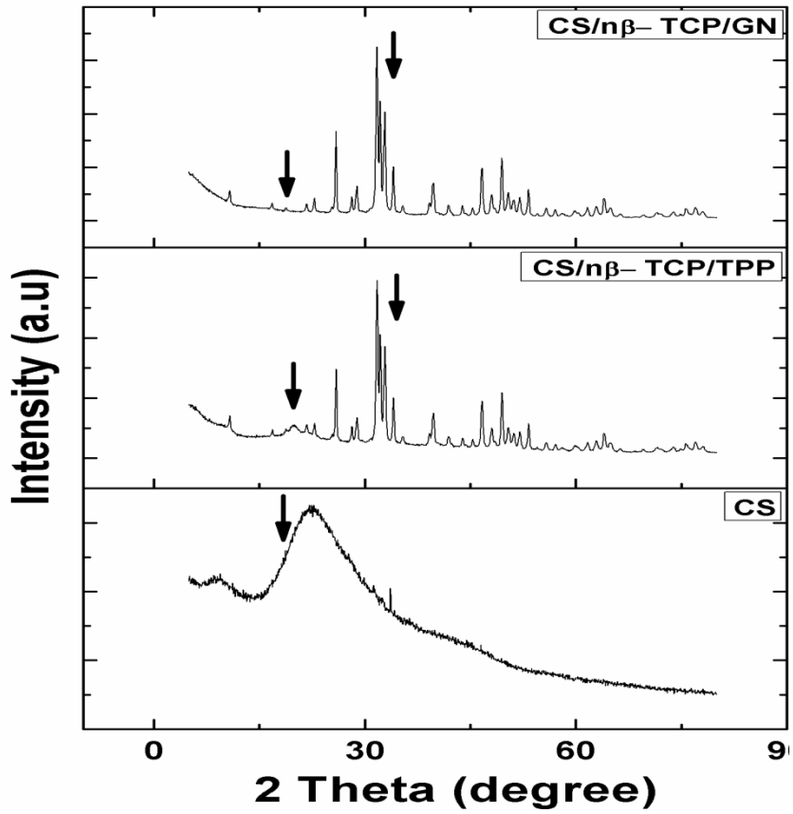

Figure 5.39: ***XRD spectra of CS, CS/nano β-TCP, GN and TPP (0.1 %) cross-linked CS/nano β-TCP freeze-gelled composite scaffolds. Extent of decrease in the peak intensity of CS is greater in GN cross-linked scaffold as compared to TPP cross-linked scaffolds. Decrease in the intensity of CS peak (amorphous nature) and its disappearance indicates further increase in crystallinity of cross-linked scaffolds***

5.3.5 Functional analysis

Figure 5.40 shows FT-IR spectra of cross-linked, non cross-linked CS/β-TCP composite and pure CS scaffolds. In TPP cross-linked scaffolds, band at 1200 cm^{-1} confirms the presence of PO_4 [142], whereas, in case of GN cross-linked composite scaffold, noticeable shifts of band is observed in N-H bending of amide bond in the range 1570 cm^{-1} to 1550 cm^{-1} which may be attributed to the interaction of CS with GN. The absorbance in the range 1000-1300 cm^{-1} bears some additional bands which probably due to the interaction of P=O of TPP with saccharide unit of CS. Roughly similar bands and intensities of cross-linked and non cross-linked scaffolds are indicated by FTIR spectra and CS has presumably retained its molecular structure even after cross linking. [242].

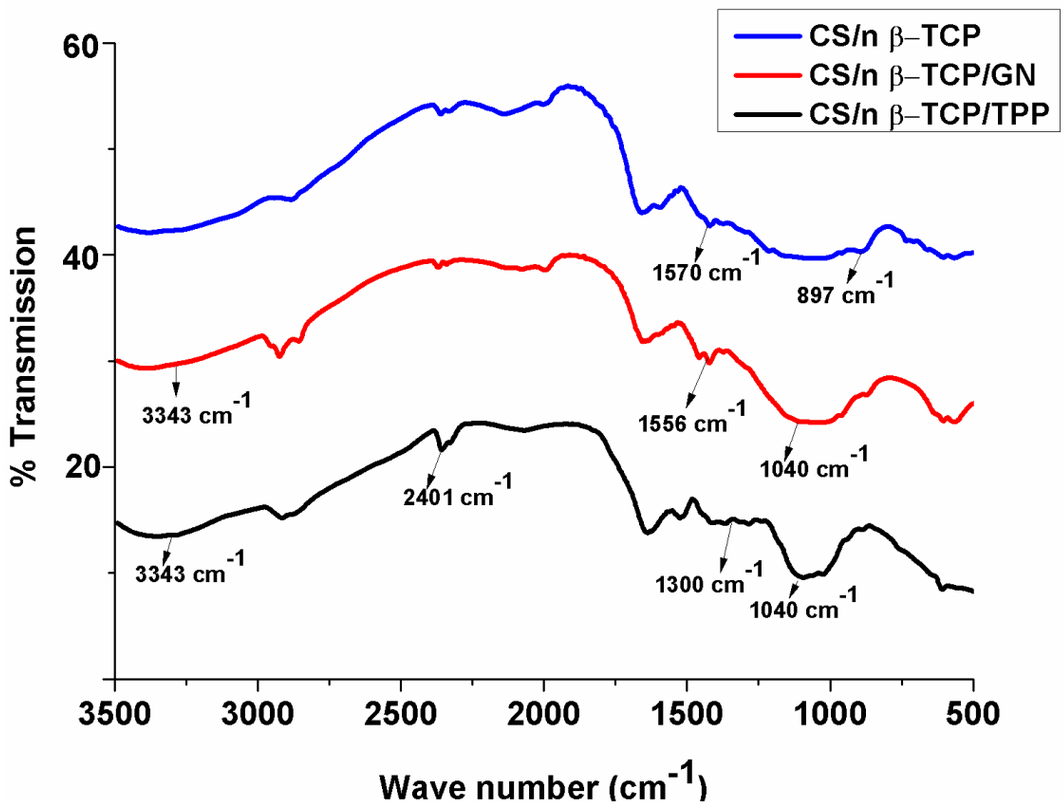

Figure 5.40*: FT-IR pattern of CS/nano β-TCP, GN and TPP (0.1 %) cross-linked CS/nano β-TCP composite scaffolds*

5.3.6 Compressive strength

The compressive strength of all the prepared scaffolds with varied concentrations of GN and TPP along with non-cross-linked scaffold are shown in **Table 5.3.** The obtained stress strain plot is shown in **Figure 5.41 (a).** The compressive strength of CS/β-TCP scaffolds showed a bimodal trend with TPP/GN cross-linking, increasing slightly at low TPP or GN concentrations (0.01-0.1 %) but decreasing significantly at higher TPP or GN concentrations of 0.15 and 0.2 % as shown in **Figure 5.41 (b).** For example, as the TPP concentration increased from 0.01 w/v to 0.05, 0.1, 0.15 and 0.2 w/v, the compressive strength of the scaffolds changed from 2.69 ± 0.17 MPa to 2.71 ± 0.11, 2.72 ± 0.11, 2.59 ± 0.19 and 2.34 ± 0.15 MPa, respectively, for GN cross-linked scaffolds the compressive strength changed from 2.69±0.11 MPa to 2.74 ± 0.13, 2.78 ± 0.14, 2.65 ± 0.17 and 2.49 ± 0.1 MPa **(Table 5.3).** The higher compressive strength achieved with cross-linked scaffolds is due to the bridge forming ability between the free amino groups of CS with the GN/TPP [142, 243]. At higher concentrations of TPP or GN (> 0.1%), cross linking occurs only with the free amino groups

present at the periphery of the polymer matrix, but the inner architecture of scaffold remains unexposed resulting in decreased compressive strength at higher concentrations of cross-linking agents [191]. The other reason behind the decrease in compressive strength may be due to drastic increase in pore size (~10 to 25 µm) of the cross-linked scaffolds when the cross-linker concentration reaches a threshold of 0.1% w/v. The corresponding compressive strength of GN cross-linked scaffold has shown a slightly higher compressive strength (2.78 ± 0.14 MPa) over TPP cross-linked scaffold (2.72 ± 0.11MPa) at a threshold concentration of 0.1%. The compressive strength of GN/TPP cross-linked scaffolds in wet condition were also measured and the compressive strength was drastically reduced in wet condition as shown in Table 5.3 . The decrease in compressive strength may be due to the increase in pore size as reported earlier [49]. Furthermore, the GN cross-linked scaffolds have shown higher compressive strength compared to TPP cross-linked scaffold. The maximum strength achieved with GN and TPP at 0.1% w/v is 0.572 ± 0.07 MPa and 0.438 ± 0.04MPa respectively which belong to the range [255].

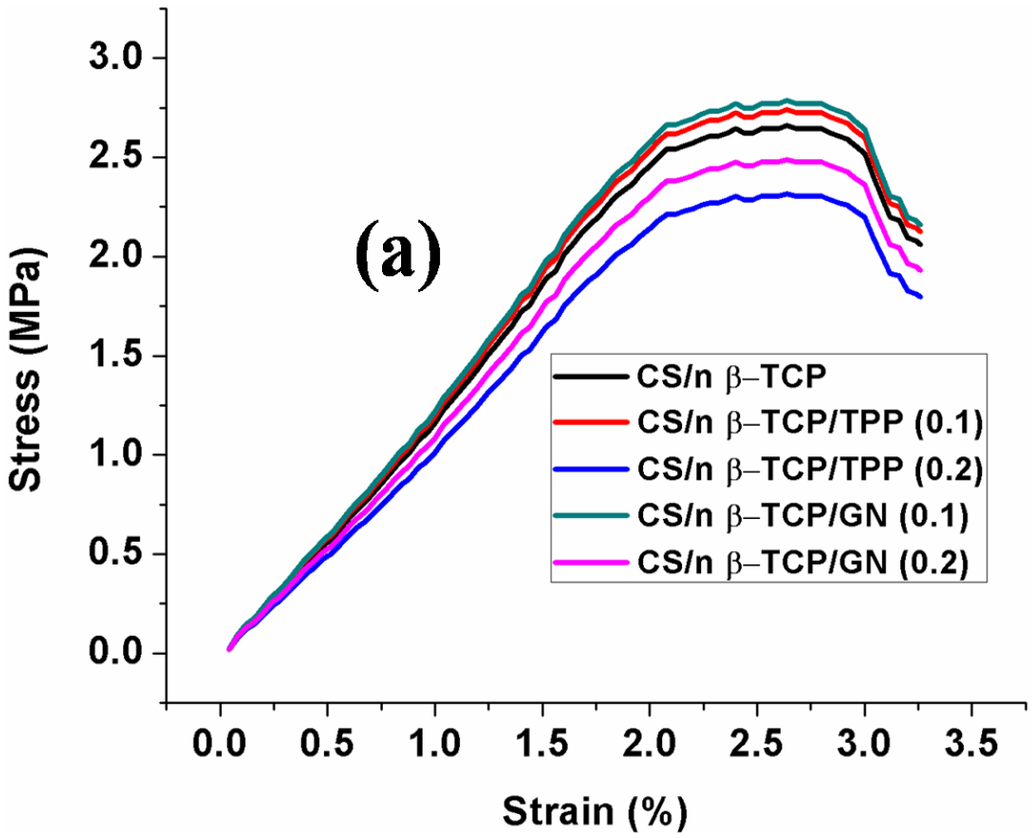

Figure 5.41 (a): ***Stress strain plot of CS/nano β-TCP, CS/nano β-TCP/GN (0.1 % & 0.2 %) and CS/nano β-TCP/TPP (0.1 % & 0.2 %) composite scaffolds***

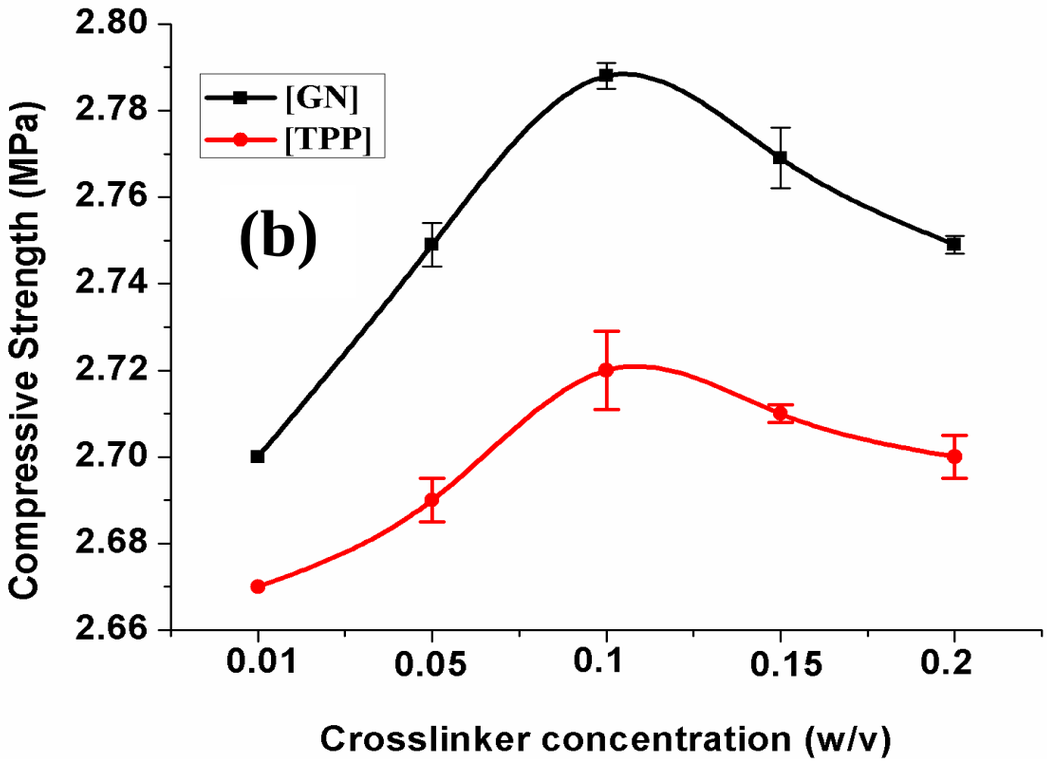

Figure 5.41 (b): ***Compressive strength of GN and TPP cross-linked CS/β-TCP scaffolds as a function of cross-linker concentration. Compressive strength is increased with increase in concentration of cross-linking agent upto 0.1% beyond which, a decline in strength is observed. GN cross-linked scaffolds have shown higher compressive strength than TPP cross-linked scaffolds***

5.3.7 Measured contact angle

Table.5.3 shows the values of measured contact angles for all the prepared scaffolds. The surface hydrophilicity of the scaffolds decreased with TPP or GN cross linking as the water contact angle increased with increasing TPP or GN concentration. As the TPP concentration increased from 0.01 % to 0.05, 0.1, 0.15 and 0.2 %, the water contact angle on CS/nano β-TCP/TPP scaffold surfaces increased from 52.5 ± 0.5° to 53.4 ± 0.9, 54 ± 1.1, 54.6 ± 0.7 and 54.9±0.6° respectively; whereas the contact angle of CS/nano β-TCP/GN scaffold surfaces increased from 54.2 ± 0.4° to 54.7 ± 0.6, 55.1 ± 1, 55.6 ± 0.7 and 56.1 ± 0.5°. The lower wettability of GN cross-linked scaffolds compared to TPP is most likely related to the lower porosity of GN cross-linked scaffolds (**Table 5.3**, lower fraction of water-filled pores on the surface). It has been established that the prepared scaffolds possess adequate hydrophilicity to facilitate hMSCs growth.

Table 5.3: ***A comparative table showing the effect of cross-linking on pore size, porosity, contact angle, compressive strength, swelling and mass loss of developed scaffolds.***

Type Sample	Pore size (µm)	Porosity (%)	Swelling (%)	Contact angle (^{0})	Compressive strength [Dry] (MPa)	Mass loss (%)	Compressive strength [Wet] (MPa)
CS	61-171	86 ± 3.2	325	51.2 ± 0.8	0.19 ± 0.05	31	NA
CS/n β-TCP	55-162	80 ± 3.6	275	51.9 ± 1.1	2.67 ± 0.21	18	0.249±0.02
CS/n β-TCP/TPP (0.01%)	55-168	78 ± 2.9	258	52.5 ± 0.5	2.69 ± 0.17	16	0.257±0.05
CS/n β-TCP/TPP (0.05%)	57-171	76 ± 1.1	246	53.4 ± 0.9	2.71 ± 0.11	15	0.311±0.01
CS/n β-TCP/TPP (0.10%)	60-175	75 ± 2.2	240	54.0 ± 1.1	2.72 ± 0.11	13	0.438±0.04
CS/n β-TCP/TPP (0.15%)	64-179	73 ± 2.1	231	54.6 ± 0.7	2.59 ± 0.19	15	0.214±0.05
CS/n β-TCP/TPP (0.20%)	68-186	71 ± 1.9	222	54.9 ± 0.6	2.34± 0.15	16	0.341±0.03
CS/n β-TCP/GN (0.01%)	57-175	76 ± 2.8	231	54.2 ± 0.4	2.69 ± 0.11	14	0.454±0.06
CS/n β-TCP/GN (0.05%)	59-179	74 ± 1.9	225	54.7± 0.6	2.74 ± 0.13	11	0.492±0.04
CS/n β-TCP/GN (0.10%)	61-183	73 ± 2.1	214	55.1 ± 1.0	2.78 ± 0.14	8	0.572±0.07
CS/n β-TCP/GN (0.15%)	66-189	70 ± 1.9	201	55.6 ± 0.7	2.65± 0.17	10	0.389±0.02
CS/n β-TCP/GN (0.20%)	71-199	68 ± 2.1	189	56.1 ± 0.5	2.49 ± 0.10	12	0.479±0.05

5.3.8 Swelling behaviour

Figure 5.42 shows the swelling of scaffolds with incubation time. All scaffolds reached equilibrium swelling in < 6 hr. CS scaffold without β-TCP and cross-linking showed the highest swelling. For CS/β-TCP scaffolds, TPP or GN cross linking reduced swelling but the swelling of TPP cross-linked scaffolds was significantly higher than those cross-linked with GN. Further, percent swelling inversely varied with cross-linker and decreased with increasing TPP or GN concentration. The decrease in swelling of TPP or GN cross-linked scaffolds is attributed to their lower porosity **(Table 5.2).** Similar results in decrease of swelling is reported earlier by Han et al. and Pati et al. where they have incorporated nano Hap was incorporated into 3D porous chitosan and cross-linked nanofibrous CS matrices with TPP respectively [101, 142].

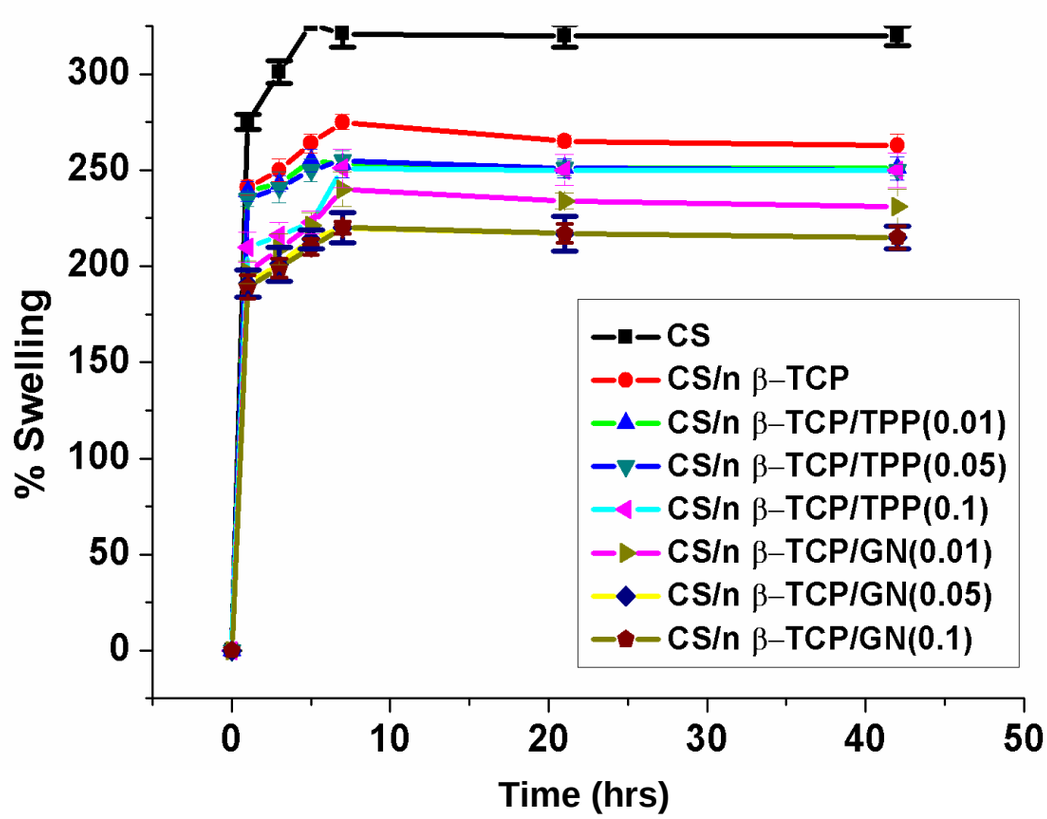

Figure 5.42: ***Swelling behaviour of CS, CS/nano β-TCP, GN and TPP cross-linked CS/nano β-TCP scaffolds for different GN or TPP concentrations with incubation time. Decreased swelling rate with increase in cross-linker concentration is observed in the developed scaffolds. Initially rapid increase in swelling is noticed (1-2hrs) and equilibrium reached in < 6 h for all types of scaffolds. The decrease in swelling of TPP or GN cross-linked scaffolds compared to pure CS and CS/nano β-TCP scaffolds is shown. The swelling of TPP cross-linked scaffolds is significantly higher than GN cross-linked scaffold***

5.3.9 *In-vitro* biodegradation study

The weight loss of the scaffolds with incubation time is shown in Figure 5.41. All scaffolds have degraded to < 20% mass weight after 30 days of incubation. The % weight loss of the scaffolds with varied ratios of TPP and GN are depicted in **Table 5.3.** The weight loss of TPP or GN cross-linked scaffolds is generally less than the non cross-linked CS or CS/β-TCP scaffolds and shows a bimodal trend with TPP or GN concentration. The scaffold weight loss after 30 days of incubation is changed from 14% to 11, 8, 13, 15 and 16% as GN concentration increased from zero to 0.01, 0.05, 0.1, 0.15 and 0.2, respectively. The best result is achieved with CS/nano β-TCP/GN (0.10 %) scaffold which degraded to 8% of its

initial weight, whereas CS/nano β-TCP/TPP (0.10 %) scaffold to 13% and shown in **Figure 5.43.** At a given cross-linker concentration, the weight loss between TPP and GN cross-linked scaffolds is not significantly different. GN cross linking reduced weigh loss of the scaffolds compared to un cross-linked CS/β-TCP scaffolds consistent with previous report by Sarem et al. where various concentrations of genipin were used to control the rate of degradation of gelatin/CS polymer blends [231].

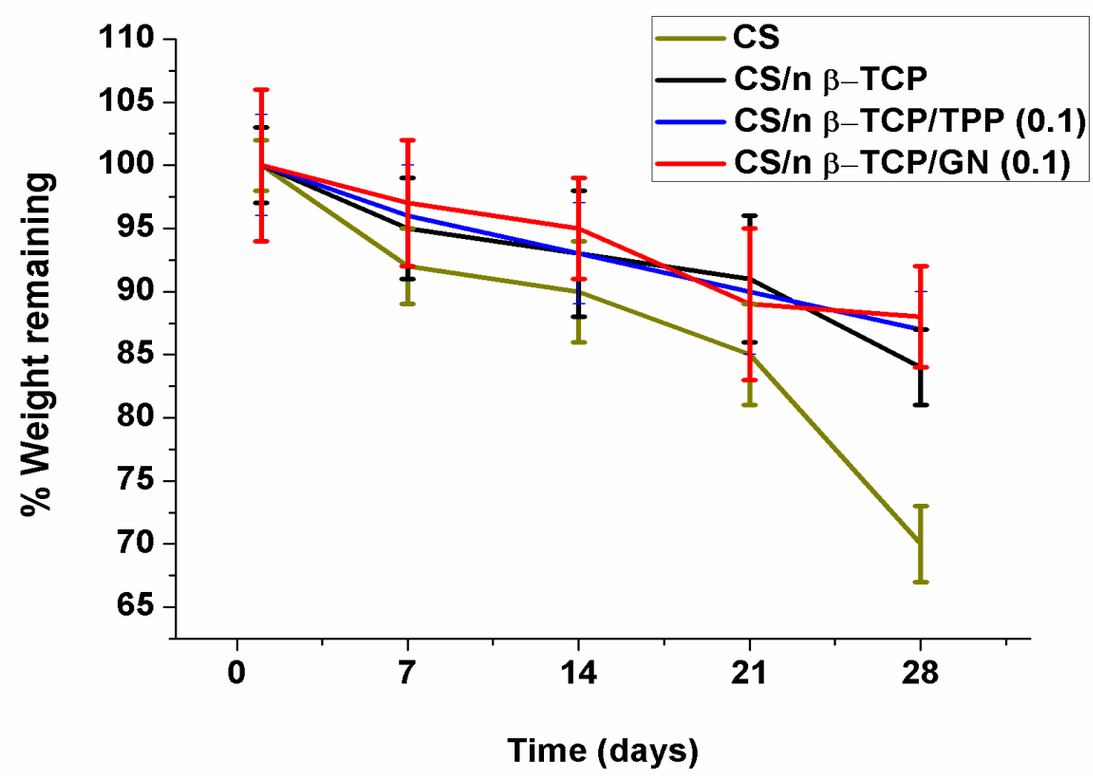

Figure 5.43*: Degradation pattern of CS, CS/nano β-TCP, GN and TPP (0.1 %) cross-linked CS/nano β-TCP composite scaffolds. Reduced degradation with change in type of cross linking agent is observed. The trend observed is CS > CS/nano β-TCP > CS/nano β-TCP/TPP > CS/nano β-TCP/GN*

Based on the above assays, GN and TPP (0.1 %) cross-linked CS/nano β-TCP composite scaffolds were selected for further study because of their superior material property including favorable degradation, higher mechanical strength and structural property.

5.3.10 Cell morphology and cell attachment

In-vitro cell culture studies were performed on GN (0.1 %) and TPP (0.1%) cross-linked CS/nano β-TCP composite scaffolds to evaluate their cell supportive property.

The morphology and attachment of the seeded hMSCs on developed composite scaffolds was observed by SEM. **Figure 5.44 [i-(a-d)]** and **Figure 5.44 [(ii-e-h)]** show the morphology of cells on CS/nano β-TCP/GN and CS/nano β-TCP/TPP scaffolds respectively. After seeding, hMSCs were found to be round in shape on 1st and 3rd days of culture. Later on, cells were found to cover and spread uniformly on the composite scaffold matrices as shown in **Figure 5.44 (a-d)** and **Figure 5.45 (e-f).** A dense cellular mass of seeded hMSCs is observed on these scaffolds with increase in time (7th and 14th day) as shown in **Figure 5.44 (c-d)** and **Figure 5.44 (g-h).** However, the cells were found to be well attached and spread on GN cross-linked scaffolds as compared to TPP cross-linked scaffolds. Furthermore, the deposition of extra cellular matrix found to be profuse on TPP cross-linked scaffolds which may be due to phosphate moiety resulted in enhanced mineral secreting ability of cells as shown in **Figure 5.44 (g-h).** These SEM results prove that GN and TPP cross-linked scaffolds are potential platforms for growth and proliferation of MSCs.

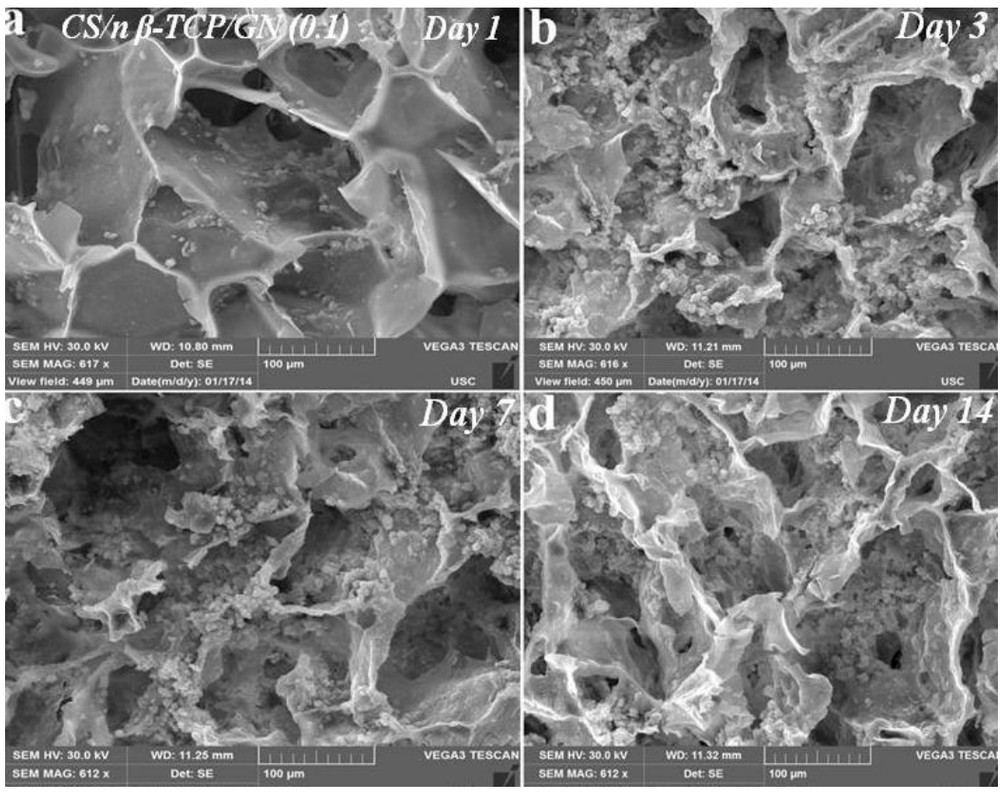

Figure 5.44 (i): ***SEM Micrographs of hMSCs cultured on CS/nano β-TCP/GN scaffolds upto 14 days of incubation. A dense cellular mass of seeded hMSCs is also observed on 7 and 14 days of culture. Profuse ECM secretion by the cultured hMSCs on scaffold surface is evident as represented by arrow marks***

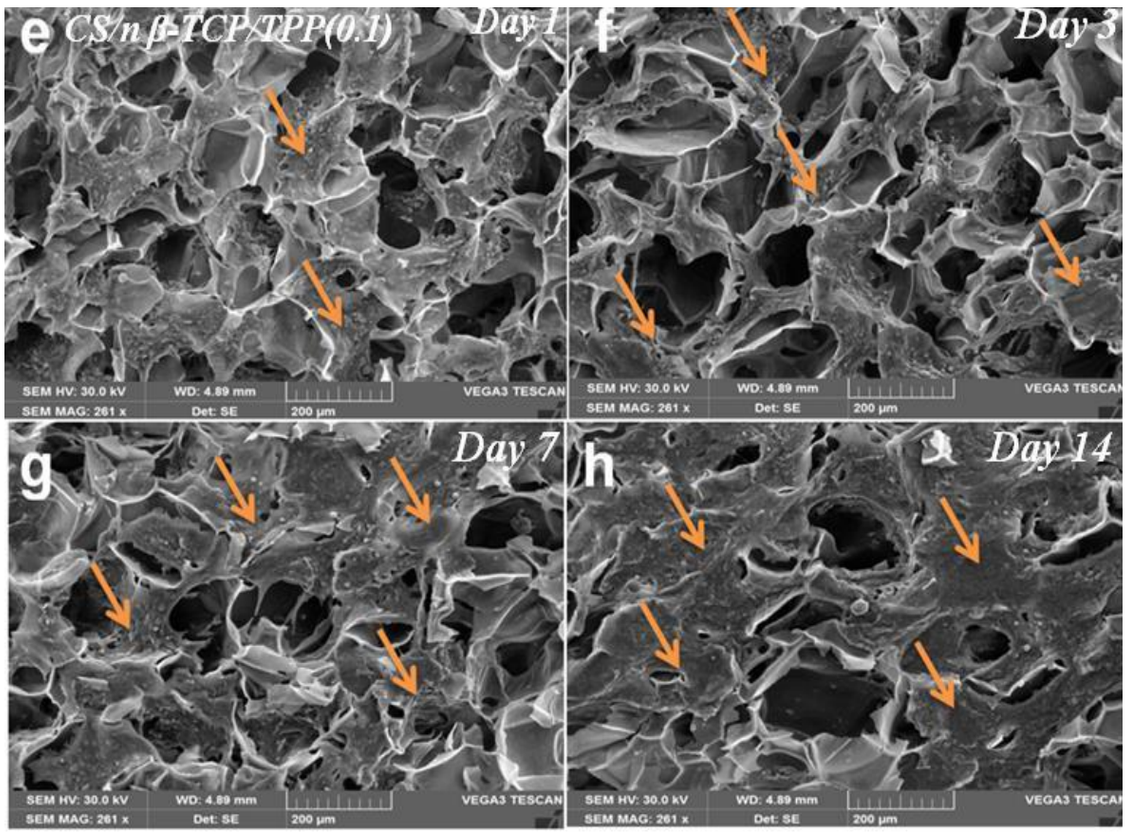

Figure 5.44 (ii): ***SEM Micrographs of hMSCs cultured on CS/nano β-TCP/TPP composite scaffolds upto 14 days of incubation. A dense cellular mass of seeded hMSCs is also observed on 7 and 14 days of culture. Profuse ECM secretion by the cultured hMSCs on scaffold surface is evident as represented by arrow marks***

5.3.11 Metabolic activity by MTT assay

MTT assay was performed to assess metabolic activity of hMSCs cultured on GN and TPP cross-linked CS/nano β-TCP composite scaffolds. CS/nano β-TCP, and pure CS scaffolds for 3, 5, and 7 days and the result is shown in **Figure 5.45.** The obtained results are compared with metabolic activity of cells seeded on CS/nano β-TCP, and pure CS scaffolds. Metabolic activity of hMSCs in all groups increased with time. hMSCs seeded on CS and CS/nano β-TCP/GN scaffold showed lowest and highest metabolic activity, respectively. The higher metabolic activity in terms of absorbance (O.D) value is achieved with CS/nano β-TCP/GN (0.742 ± 0.015) scaffolds as compared to CS (0.4 ± 0.018) CS/nano β-TCP (0.614 ± 0.016) and CS/nano β-TCP/TPP (0.692 ± 0.011) scaffolds after 7 days of culture. Cells were found to be more metabolically active ($p < 0.05$) on GN/TPP cross-linked scaffolds than on pure CS/nano β-TCP scaffold at any point of time. Although GN cross-linked scaffolds had the lower porosity and wettability, but hMSCs seeded on CS/nano β-TCP/GN scaffolds showed highest

metabolic activity in all time points when compared to CS/nano β-TCP and CS/nano β-TCP/TPP which was attributed to the less toxic nature of GN as reported previously [202, 231].

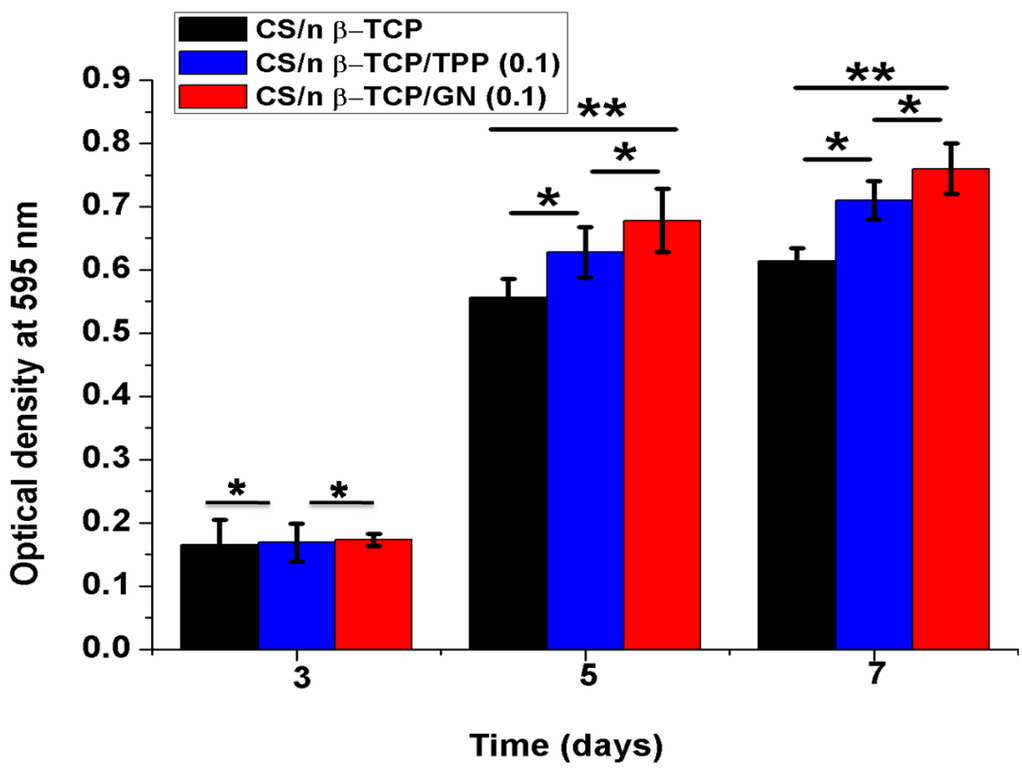

Figure 5.45: ***Metabolic activity of hMSCs cultured on CS/nano β-TCP/GN and CS/nano β-TCP/TPP composite scaffolds upto 7 days of culture. Results are compared with metabolic activity of hMSCs seeded on CS/nano β-TCP composite scaffold which was used as control. hMSCs seeded on CS/nano β-TCP/GN scaffolds showed highest metabolic activity than TPP cross-linked and non cross-linked CS/nano β-TCP composite scaffolds. Each pointrepresents the mean ± SD (n= 3) * and ** shows significant differences between groups at p > 0.05 and p < 0.05 respectively***

5.3.12 Cell Proliferation

(i) Fluorescence microscopy

The fluorescent images were taken to observe the viability of MSCs cultured on the developed scaffolds. Cells are found to increase in number with culture time (as denoted by green fluorescence) from 3rd day [**Figure 5.46 (a, c)]** to 14th day [**Figure 5.46 (b, d)].** The morphology of the cells is spherical in shape till day 3 and found to spread throughout the scaffold matrix at later time points. The cell density of dead cells (as denoted by red fluorescence) is also seen on 3rd day and the number is found to decrease with time. Number

of dead cells is very few on both the scaffolds indicating excellent viability of seeded hMSCs**.** More number of viable cells is seen upto 14th day indicating excellent biocompatibility of developed scaffolds. Furthermore, it is also evident from the figures that, the cell proliferation is higher on GN cross-linked scaffold than TPP cross-linked scaffold

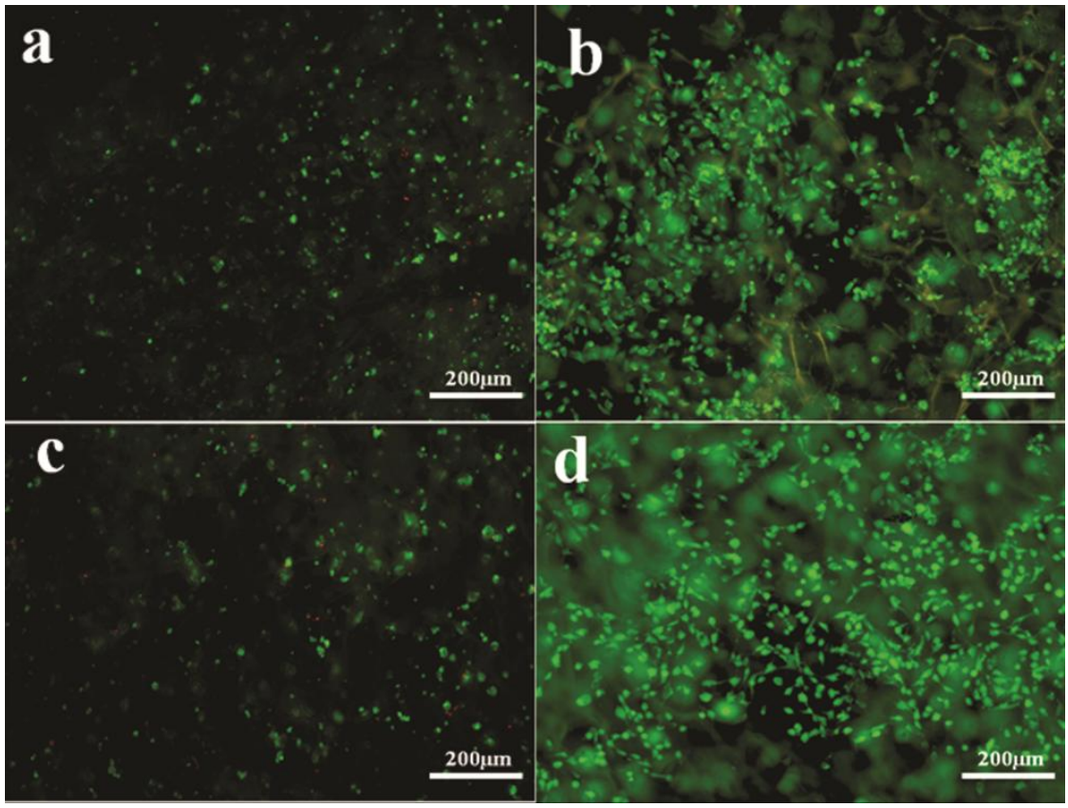

Figure 5.46 ***Fluorescent images of hMSCs on CS/nano β-TCP/GN and CS/nano β-TCP/TPP composite scaffolds upto 14 days of culture. Scaffolds are stained with calcein (green, which transport into cytoplasm of live cells) and ethedium homodimer (red, binds to DNA of dead cells). Number of viable cells is found to increase on both kinds of scaffolds from day 3 to 14. However, more number of viable cells on GN cross-linked CS/nano β-TCP [d] scaffold is seen as compared to TPP cross-linked CS/nano β-TCP [b] scaffold on day 14 indicating increased proliferation on GN cross-linked scaffold***

(ii) DNA quantification assay

The proliferation of hMSCs seeded on the developed scaffolds was further assessed by DNA quantification assay. An increased DNA content is observed with both GN and TPP cross-linked scaffolds with culture time as shown in **Figure 5.47.** However, the DNA content of hMSCs on GN cross-linked scaffold is slightly higher (452 ± 22 ng/ml) as compared to TPP cross-linked scaffold (376 ± 13 ng/ml) upto 21 days of culture which represents the enhanced

proliferation rate on GN cross-linked scaffold, ($p>0.05$). Similar trend in increased DNA content of osteoblasts was observed earlier on TPP cross-linked CS fibrous mats and TCP incorporated PCL 3D porous scaffolds as reported [16, 244].

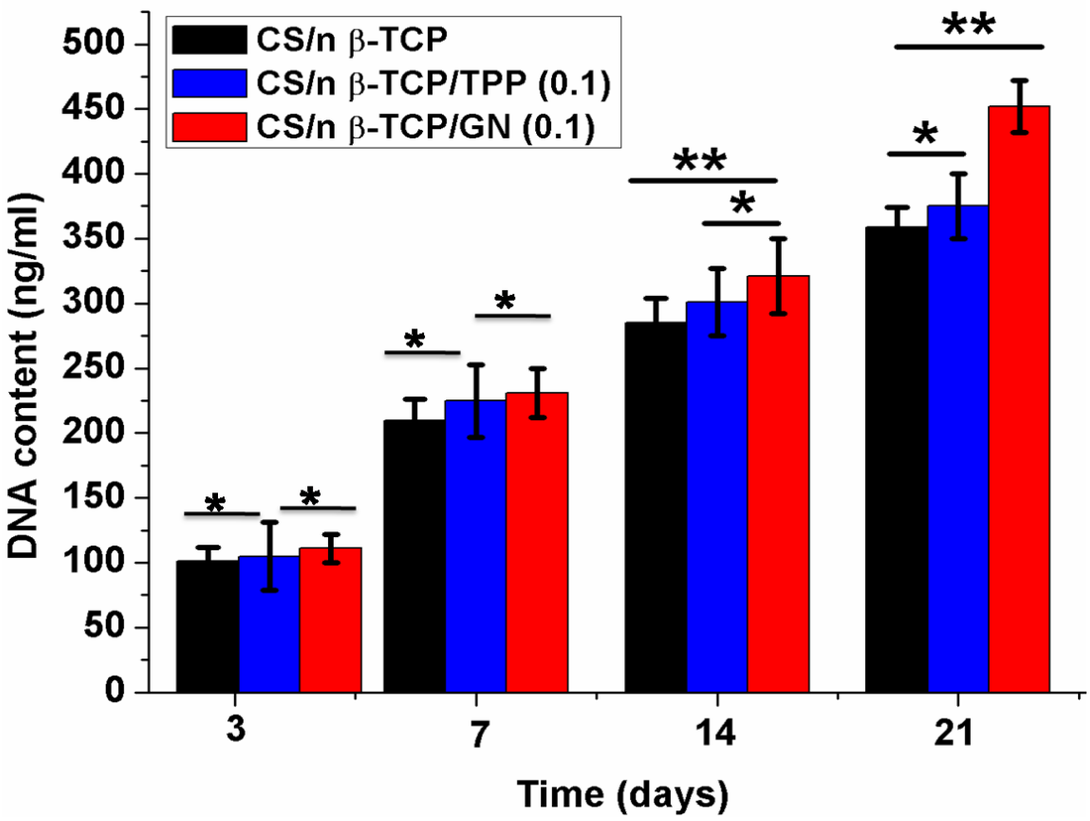

Figure 5.47*: Cell proliferation in terms of DNA quantification on CS/nano β-TCP/GN and CS/nano β-TCP/TPP cross-linked composite scaffolds upto 21 days of incubation. Cell number (DNA content) increases with incubation time. The highest proliferation is observed with GN cross-linked composite scaffolds. Each point represents the mean ± SD (n= 3) * and ** denotes significant differences between DNA content with other scaffolds at $p > 0.05$ and $p < 0.05$*

5.3.13 Cytoskeletal organization

Confocal images of hMSCs cultured on CS/nano β-TCP/GN scaffold upto 14 days were analyzed for cytoskeletal organization as depicted in **Figure 5.48 (i).** On day 7, less intensity of blue color in the figure denotes minimal growth of cytoskeleton **[Figure 5.48 (i-a)].** Whereas, on day 14, images show prominent green color confirming the extensive development of cytoskeleton as a result of increased cell proliferation as shown in **[Figure 5.48 (i-b)].** 3-dimensional confocal laser scanning microscopic images (Z-stacks) depict cell penetration in GN cross-linked composite scaffold matrix upto ~ 50 µm, from the surface of

scaffolds as depicted in **Figure 5.48 (ii).** Similar pattern of cell infiltration and uniform distribution of fibroblasts were observed earlier by Steward et al on fibronectin fibrils [245].

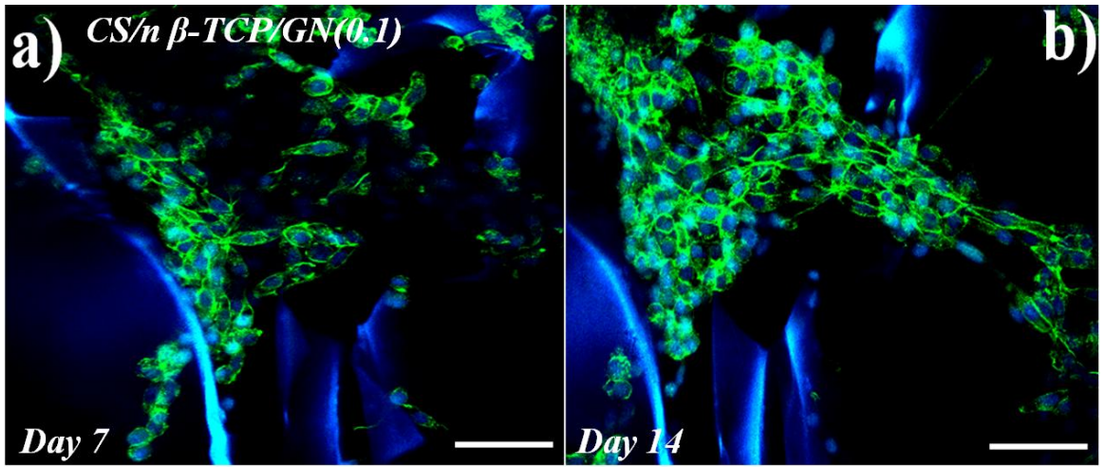

Figure 5.48 (i): ***Confocal laser scanning microscopic images of hMSCs cultured on CS/nano β-TCP/GN composite scaffolds on day 7 and 14. Images depict the development of cytoskeleton with culture time resulting in an extensive cytoskeletal development indicating increased cell proliferation and cell-cell interaction on day 14. Nuclei of the cells stained with Hoechst 33342 (blue) and actin filaments with phalloidin (green). Bar indicates 300µm***

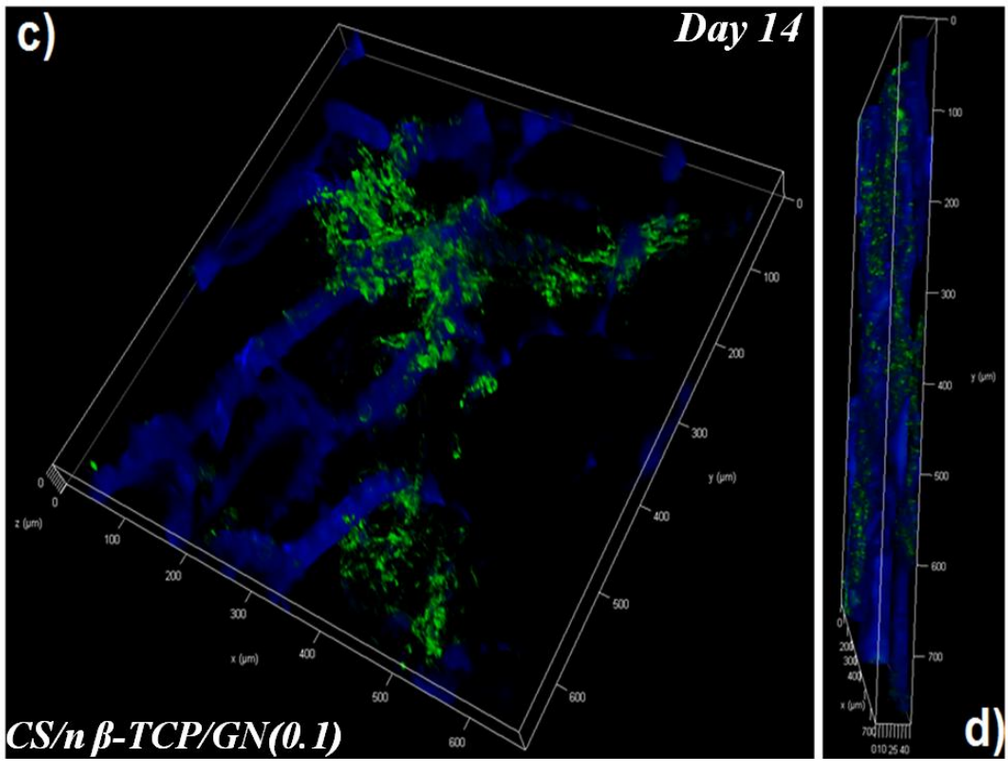

Figure 5.48 (ii): ***3D confocal laser scanning images (Z-stacks) of hMSCs after 14 days of culture on CS/nano β-TCP/GN composite scaffolds (c, d) on day 14. Z-stacks rotated in 3D space (d) to represent internalization of seeded cells in the porous structure of CS/nano β-TCP/GN composite scaffolds. Nuclei of the cells stained with Hoechst 33342 (blue) and actin filaments with phalloidin (green)***

5.3.14 Osteogenic differentiation potential

(i) Alkaline Phosphatase assay

Endogenous alkaline phosphatase activity of hMSCs seeded on CS/nano β-TCP/GN and CS/nano β-TCP/TPP scaffolds were measured by ALP assay. ALP activity of hMSCs seeded on scaffolds is bimodal with respect to incubation time, which increased from day 7 to 14 and decreased from day 14 to 21 (**Figure 5.49),** consistent pattern of ALP activity by MSCs undergoing osteogenesis [221, 246]. **Figure 5.49** demonstrates an enhanced ALP activity ($p < 0.05$) from day 7 to 14 and then a decline in ALP activity is evident for GN and TPP cross-linked scaffolds. The ALPase activity of GN and TPP cross-linked scaffolds at 7^{th} day is 3.51 ± 0.04 and 3.26 ± 0.036 IU/μg where as at 14^{th} day; the activity is 6.09 ± 0.06 and 5.51 ± 0.07 IU/μg respectively. This increase in ALPase activity is thus an evident of osteoblast differentiation. The cells cultured on both types of scaffolds show ALPase activity of 5.01 ± 0.02 and 5.14 ± 0.07 IU/μg respectively on 21^{st} day.

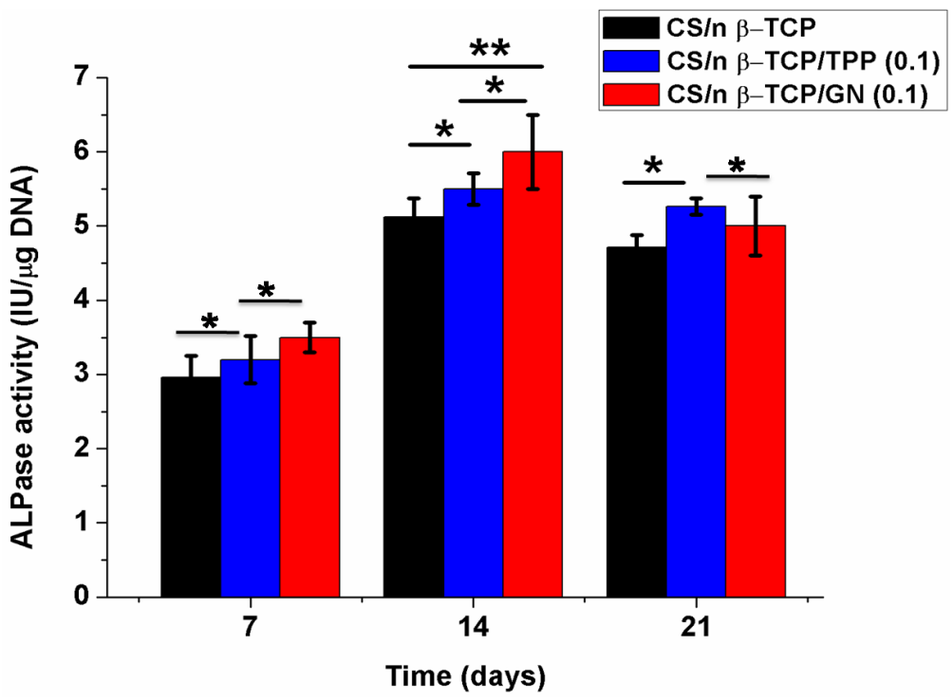

Figure 5.49:*Alkaline Phosphatase activity of CS/nano β-TCP/GN and CS/nano β-TCP/TPP composite scaffolds. Each point represents the mean ± SD (n= 3) * and ** denotes significant differences between groups at p > 0.05 and p < 0.05 respectively. Significant increase in ALP is seen on both scaffolds from day 7 to day 14. Highest ALP activity is evident on GN cross-linked scaffolds*

(ii) Total calcium content

Figure 5.50 depicts the calcium content of hMSCs seeded scaffolds until 21 days of culture. The calcium content is found to be increased in logarithmic pattern with time indicating an increased degree of mineralization with both GN and TPP cross-linked scaffolds. However, GN cross-linked scaffold has expressed higher calcium content (2054 mg/mg DNA) than with TPP cross-linked scaffold (1860 mg/mg DNA) as observed for 21 days of incubation, ($p < 0.05$). Higher mineralization activity of differentiated MSCs represents the superior osteogenic potential of GN cross-linked scaffold compared to TPP cross-linked scaffold. The result is in good agreement with published data where fibers were reinforced into hydrogels [201].

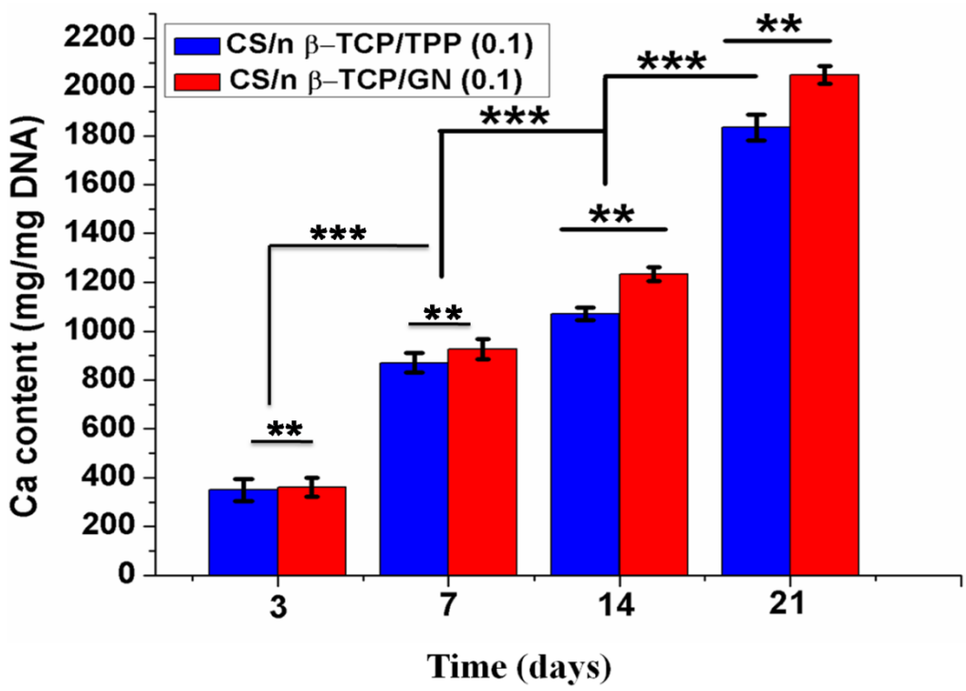

Figure 5.50: ***Total calcium content of CS/nano β-TCP/GN and CS/nano β-TCP/TPP cross-linked CS/β-TCP composite scaffolds. The calcium content increased with culture time. Highest calcium content is obtained with GN cross-linked scaffolds representing its higher mineralization activity depicting superior osteogenic potentiality. Each point represents the mean ± SD (n= 3) ** and *** denotes significant differences between groups at p > 0.05 and p < 0.05 respectively***

PART-IV

Development of Fibrin Coated GN Cross-linked CS/nano β-TCP Composite Scaffolds

It has already been described that the deficiency of cell affinity of CS scaffold can be overcome by the incorporation of bioactive protein molecules like cell binding peptide RGD [151]. Because of the presence of a number of cell binding RGD domains, fibrin has been reported as a promising bioactive molecule that can used as a surface modifier of scaffold thereby improving cell attachment, cell proliferation and extra cellular matrix formation in wound healing [158]. In the second phase of our work, improved cell supportive property of the CS/nano β-TCP composite scaffold has been achieved by fibrin conjugation. Therefore, in this phase of work effort has been given for further improvement of cell affinity of the most potential GN cross-linked CS/nano β-TCP/GN composite scaffold developed under this study by fibrin coating. The result and discussion of this study is described here.

5.4.1 Morphology and pore size

As depicted in SEM micrographs **[Figure 5.51 (A)],** the pore structure of the developed fibrin coated CS/nano β-TCP scaffold matrix is similar to non coated CS/nano β-TCP scaffold without any significant change in pore size. The pore size of fibrin coated scaffolds is measured as 56-179 μm, whereas uncoated scaffolds show 61-183 μm. Furthermore, fibrin coated scaffolds maintained their 3D structure and fibrillar network of fibrin found to deposit around the pores of scaffolds is represented in **Figure 5.51 (B)** with higher magnification. The resultant pore size range is sufficient for nesting the seeded cells and sustaining cell adhesion. Fibrin enables sufficient diffusion of nutrients to the cells due to its fibrillar network present over the scaffold architecture, as reported earlier with fibrin coated PLLA 3D matrices [192]. Thus it is concluded that the coating of fibrin does not show any negative impact on the pore structure and pore size of the composite scaffold.

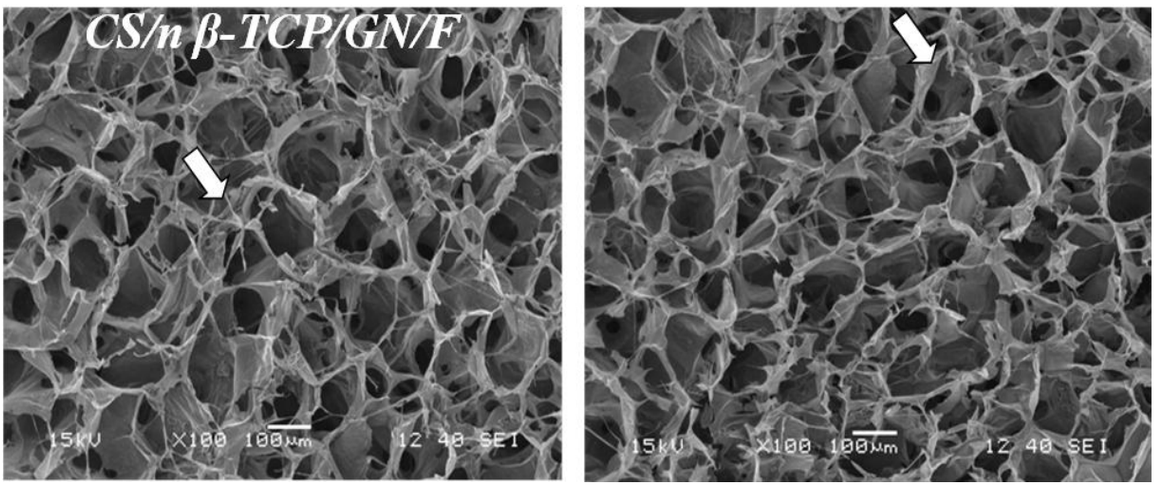

Figure 5.51 (A): ***SEM micrographs of fibrin coated GN cross-linked CS/nano β TCP composite scaffolds. Fibrillar structures of fibrin are represented with white coloured arrow marks. Furthermore, the fibrin coating has added advantage of having fibrillar network facilitating transport of nutrients and metabolic waste***

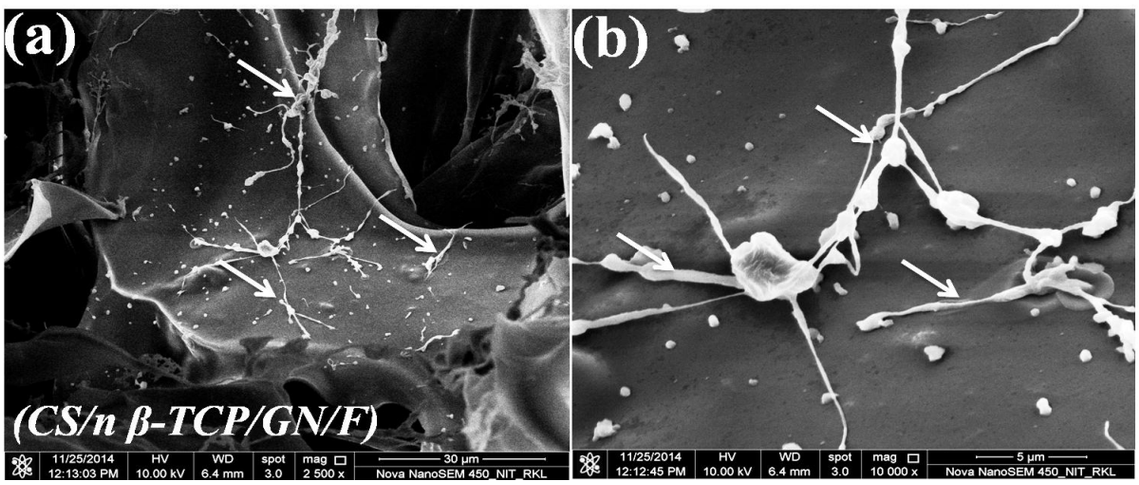

Figure 5.51 (B): ***FE-SEM images of fibrilar structures formed by Fibrin on the scaffold surface are highlighted using high magnification microscopic images***

5.4.2 Porosity

There is no significant change in porosity is observed when CS/nano β- TCP/GN scaffold (73.4 ± 2.1%) was modified with fibrin and the corresponding % porosity measured as 72.0 ± 3.8%. The slight decrease in porosity observed with fibrin coated composite scaffolds may be because of fibrillar network of fibrin on the surface and inside the porous architecture of scaffolds. Similar result of decrease in pore size and porosity has also been reported with fibrin coated gelatin/nano HAp scaffolds loaded with bone morphogenic proteins used for bone tissue regeneration [236].

5.4.3 Functional analysis

Figure 5.52 shows FT-IR spectra of fibrin coated and uncoated CS/nano β-TCP/GN composite scaffolds. Presence of fibrin is confirmed as the FT-IR spectrum shows bands at 1656 and 1533 cm^{-1} attributed to amide I and amide II of fibrin. Band at 926 cm^{-1} shows interactions between COOH group of fibrin and P=O of β-TCP. Furthermore, shift of the OH band at 3348 cm-1 represent the interactions between CS and fibrin. Thus, the formation of new bands and shifting of bands indicate successful fibrin coating on CS/nano β-TCP/GN scaffolds.

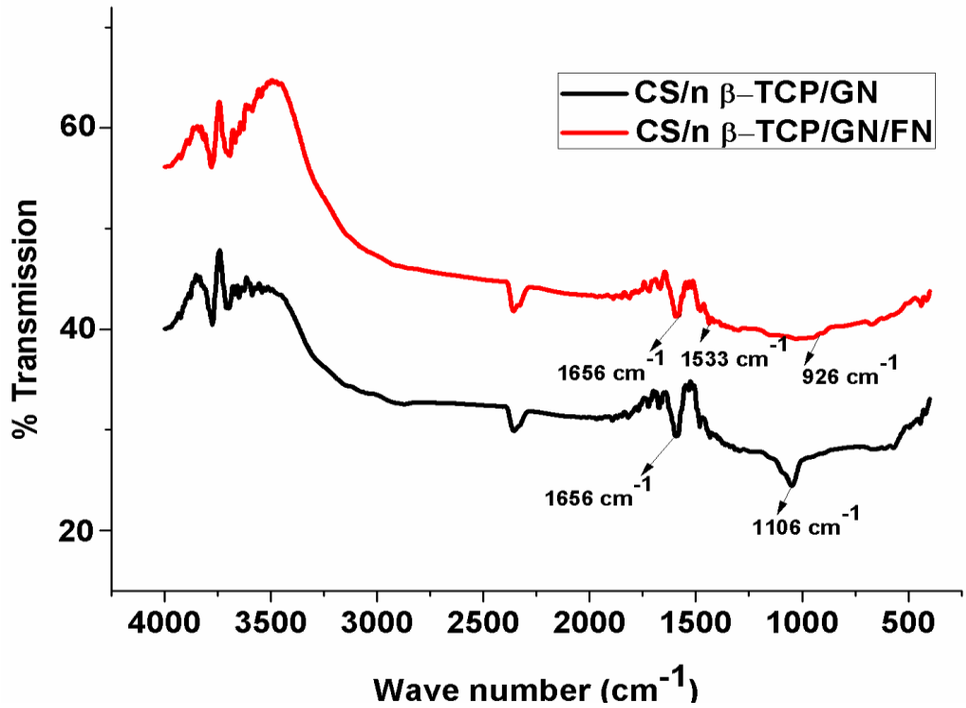

Figure 5.52: ***FT-IR pattern of fibrin coated GN cross-linked CS/nano β TCPcomposite scaffolds. Presence of fibrin is confirmed as the FT-IR spectrum shows bands at 1656 and 1533 cm^{-1} attributed to amide I and amide II of fibrin***

5.4.4 Compressive strength

Figure 5.53 depicts that there is no significant change in the compressive strength with fibrin coated scaffolds indicating that fibrin does not have any negative effect on the compressive strength of CS/nano β-TCP/GN scaffolds. The corresponding compressive strength of uncoated and fibrin coated scaffolds are 2.78±0.14 MPa and 2.8±0.13 Mpa respectively.

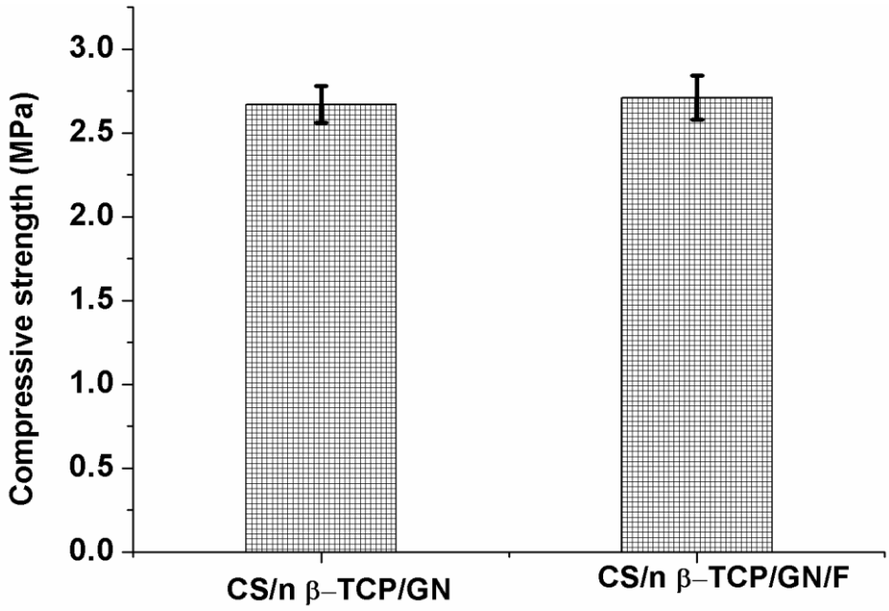

Figure 5.53: ***Effect of fibrin coating on compressive strength of CS/nano β-TCP/GN composite scaffolds. No significant difference is observed in compressive strength of CS/nano β-TCP/GN scaffolds with fibrin coating***

5.4.5 Measured contact angle

The measured contact angles of CS/nano β-TCP/GN/F and CS/nano β-TCP/GN are comparable and the corresponding values of contact angle are 55.4 ± 1.2°and 55.1 ± 1.0° respectively. A slight decrease in hydrophilicity is noticed with fibrin coated scaffolds which may be attributed to water insoluble nature of fibrin [228].

5.4.6 Swelling behaviour

Figure 5.54 shows the swelling of fibrin coated and uncoated scaffolds. Swelling of fibrin coated scaffold is compared to uncoated scaffold. A slight decrease in swelling is observed with fibrin coating on GN cross-linked scaffold. It is a well known fact that the hydrophobic moieties present in the fibrin protein reduce the swelling of GN cross-linked scaffolds. Both the scaffolds showed rapid swelling at initial hours of experiment and reached a state of

equilibrium after > 8 hrs. CS/nano β-TCP/GN composite showed slightly higher rate of swelling (220 % of initial weight) compared to the scaffolds with fibrin coating (203%). The decrease in swelling of fibrin conjugated scaffold may be attributed to the water repelling ability of fibrin which restricted the seepage of water into the porous structure of GN cross linked scaffold [25].

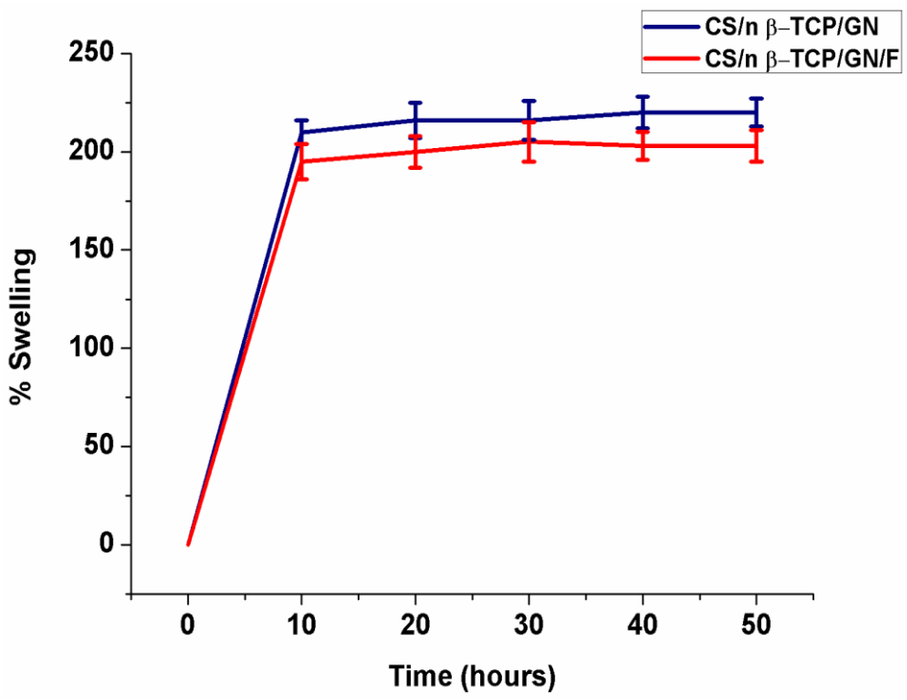

Figure 5.54: ***Swelling behaviour of CS/nano β-TCP/GN/F and CS/nano β-TCP/GN scaffolds decreased swelling rate is observed with fibrin coating. Initially rapid increase in swelling is noticed (1-2hrs) and equilibrium reached in > 6 hrs for all types of scaffolds***

5.4.7 *In-vitro* biodegradation study

The degradation pattern of the developed CS, CS/nano β-TCP/GN/F and CS/nano β-TCP/GN scaffolds are shown in **Figure 5.55**. As observed from figure, no significant difference in degradation is noticed between fibrin coated and uncoated scaffolds. However, pure chitosan scaffolds have degraded to 31% of their initial weight. A slight lower degradation (7%) of fibrin coated GN cross-linked CS/nano β-TCP composite scaffold than uncoated (8%) maybe due to the hydrophobic nature of fibrin.

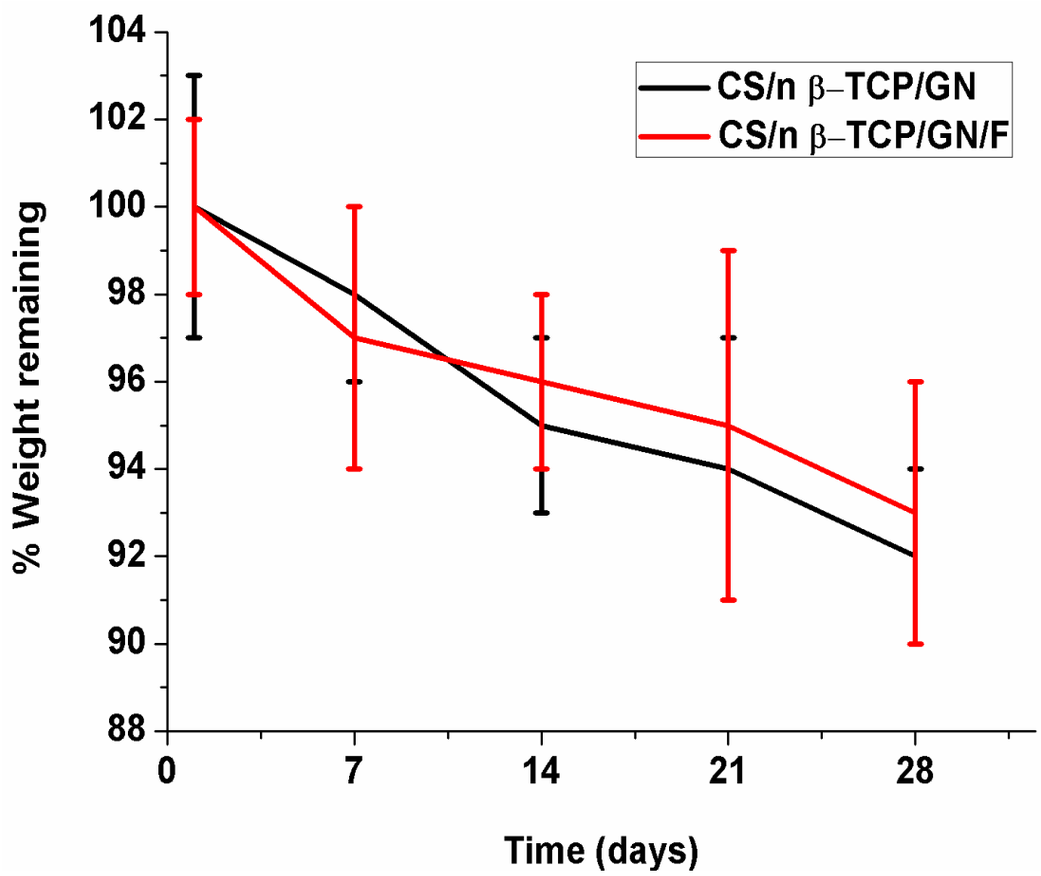

Figure 5.55: ***Biodegradation pattern of CS/nano β-TCP/GN/F composite scaffold in PBS for 28 days and its comparison with CS/nano β-TCP/GN scaffold***

5.4.8 Cell morphology and cell attachment

FE-SEM images **(Figure 5.56)** shows that the seeded MSCs are attached and well spread over the scaffolds. However, the density of cells is found to be higher on CS/nano β-TCP/GN/F scaffold than CS/nano β-TCP/GN scaffolds throughout the 14 days of culture period. Initial spherical shape (**Figure 5.56 a&d**) of MSCs is observed to be changed to spindle like morphology after 7 days of incubation as revealed by FE-SEM images and shown in **Figure 5.56 (c-g).** Excellent cell spreading and cell-material interactions are evident from the filopodia like structures formed as depicted in the higher magnification FE-SEM images **(Figure 5.56-e).** Furthermore, the formation of monolayers of seeded cells on CS/nano β-TCP/GN/F scaffold is also observed indicating the flattened, polygonal morphology and sheet like appearance of seeded hMSCs on 14th day of culture as shown in **Figure 5.56 (B).** All together, the developed fibrin coated scaffold has shown enhanced cell supportive property providing excellent cell attachment and spreading.

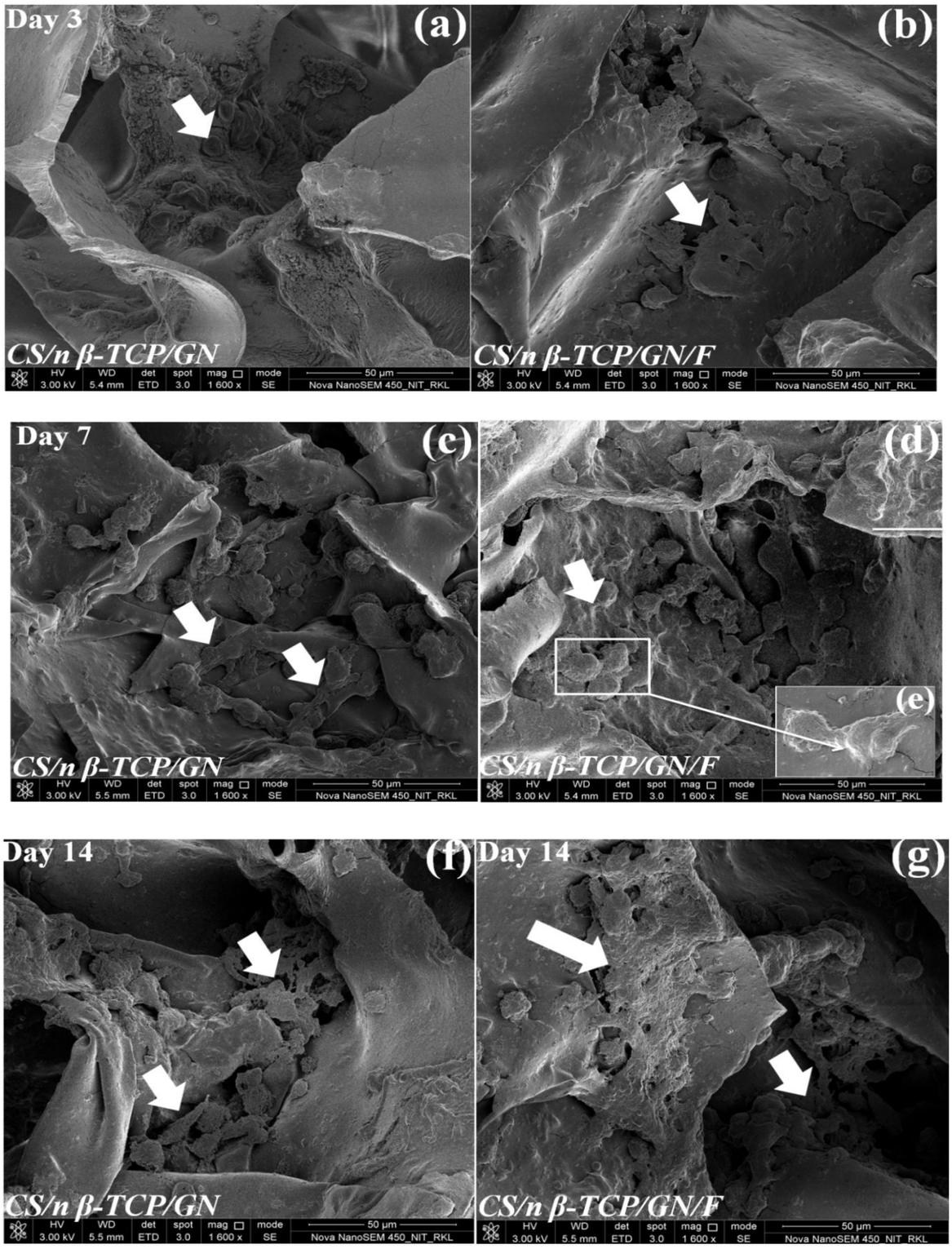

Figure 5.56 (A): ***FE-SEM images showing the morphological changes of hMSCs on CS/nano β-TCP/GN (a-c) and CS/nano β-TCP/GN/F composite scaffolds (d-f) upto 14 days of culture. Cell -cell and cell-material interactions are represented at higher magnification (2000X) in figure 5.57(e-i). Fibrin coated scaffolds have shown more number of cells on both the time points (7^{th} and 14^{th} day). Establishment of cell - cell interactions with the help of filopodia like structures is represented with white coloured arrow marks figure 5.57 (e-i)***

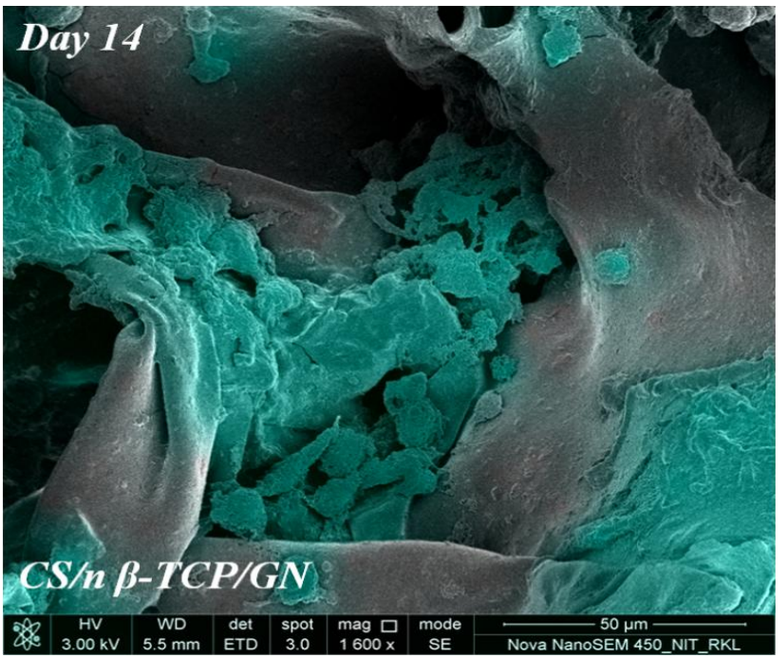

Figure 5.56: (B) ***Cells are highlighted using recolor software***

5.4.9 Metabolic activity by MTT assay

Figure 5.57 shows an increasing trend of optical density indicating increased cell viability with incubation time observed with both fibrin coated and uncoated CS/nano β-TCP/GN scaffolds. However, a significant increase in metabolic activity is achieved with CS/nano β-TCP/GN/F compared to CS/nano β-TCP/GN composite scaffolds with corresponding O.D values of 0.931 ± 0.021 and 0.742 ± 0.015 ($p < 0.05$). This increase in metabolic activity can be attributed to the presence of numerous RGD sites in fibrin which favoured more cells to attach on fibrin coated scaffolds [25]. The fibrin coated composite scaffold has shown to facilitate MSCs to proliferate rapidly in comparison to uncoated composite scaffold. As it is evident from figure, the cell viability is found to be triple from day 3 to day 7. Our results matches with previously published data on the role of fibrin in enhancing cellular responses on collagen matrices [247].

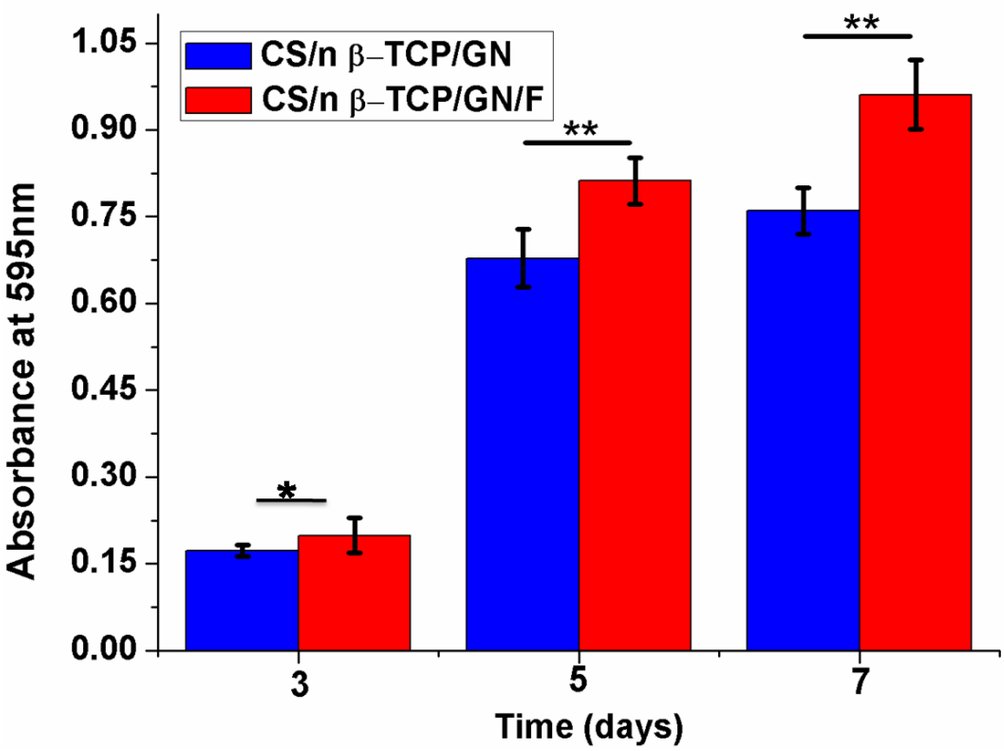

Figure 5.57: ***Metabolic activity of hMSCs seeded on fibrin coated CS/nano β-TCP/GN composite scaffolds upto 7 days of culture. Uncoated CS/nano β-TCP/GN scaffold was used as control. The metabolic activity is found to be tripled from day 3 to day 7 on both types of scaffolds. However, the fibrin coated scaffold has shown highest metabolic activity. Each point represents the mean ± SD (n= 3), * and ** represents significant difference between the two groups at p>0.05 and p< 0.05 respectively***

5.4.10 hMSCs proliferation

(i) Confocal microscopy

Proliferation of hMSCs on fibrin coated and uncoated scaffolds were assessed qualitatively by confocal images as shown in **Figure 5.58.** The number of cells on fibrin coated CS/nano β-TCP/GN scaffold is higher than CS/nano β-TCP/GN scaffold representing its higher metabolic activity of hMSCs. The increased cell proliferation on fibrin coated scaffold may be attributed to the presence of fibrin which enhanced the cellular responses by attracting more number of cells on scaffold surface and the results are matching with the earlier reports on fibrin coated graphene oxide composite scaffolds [228].

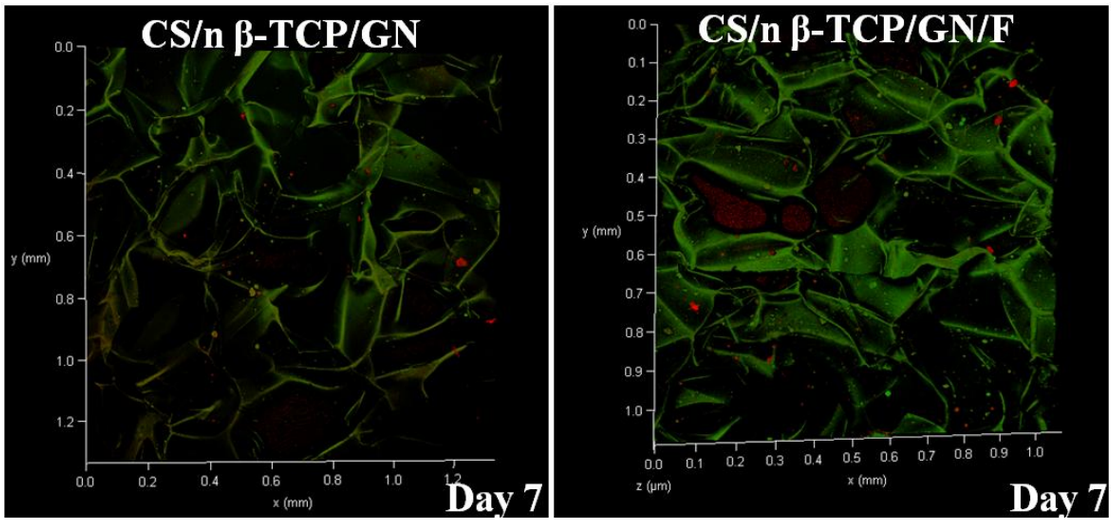

Figure 5.58 ***Confocal laser scanning microscopic images of hMSCs cultured on CS/nano β-TCP/GN and CS/nano β-TCP/GN/F composite scaffolds on day 7. Images depict the increased number of cells on fibrin coated scaffolds compared to uncoated indicating increased cell proliferation. Cells are stained with propidium iodide and fluorescein di acetate***

(ii) hMSCs proliferation by DNA quantification assay

The proliferation of hMSCs on the scaffolds assessed by DNA quantification is shown in **Figure 5.59.** The rate of proliferation in terms of DNA content is found to increase with time and higher rate of proliferation is shown by CS/nano β-TCP/GN/F scaffolds than the scaffolds without fibrin. More precisely, DNA content of hMSCs on fibrin coated scaffolds increased from 119 ± 16 ng/ml to 612 ± 17 ng/ml which is higher than uncoated scaffolds (100 ± 11 ng/ml to 452 ± 22 ng/ml, ($p < 0.05$). Similar result of increased proliferation rate has been reported earlier with fibrin coated graphene oxide scaffolds studied for bone tissue regeneration [228]. Thus, the fibrin coated scaffold possesses superior cell supportive property achieving higher rate of proliferation than the scaffold without fibrin.

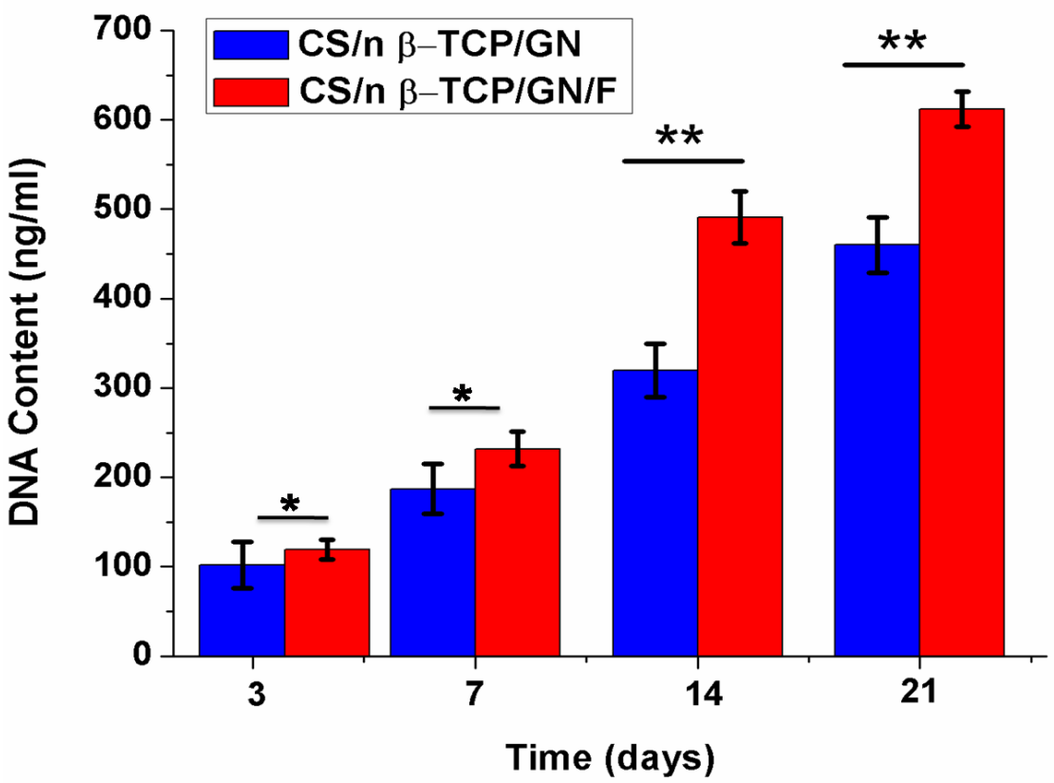

Figure 5.59: ***Effect of fibrin coating on the rate of proliferation of hMSCs seeded on CS/nano β-TCP/GN composite scaffolds. Uncoated CS/nano β-TCP/GN scaffold was used as control. An increase in DNA content with incubation time is observed with both types of scaffolds. The higher proliferation is observed with fibrin coated scaffold. Each point represents the mean ± SD (n= 3) * and ** shows significant differences between groups at p >0.05 and p < 0.05 respectively***

5.4.11 Cytoskeletal organization

Uniform distribution and spreading of hMSCs over the scaffold surface is evident from confocal images as depicted in **Figure 5.60 [(i) a-b].** 3 dimensional confocal laser scanning microscopic images (Z-stacks) shows the cell penetration in CS/nano β-TCP/GN/F composite scaffold matrix upto ~ 70 µm, from the surface of scaffolds. The images of 14th day cultured sample confirm profuse development of cytoskeleton **[Figure 5.60 (ii-a)]** on fibrin coated scaffolds. The development of cytoskeleton is observed to be less on uncoated scaffolds as shown in [**Figure 5.60 (ii-b**)]. Further, a greater population of cells is found on the fibrin coated scaffold when compared to uncoated scaffold. All together, the fibrin coated scaffold is superior to the uncoated composite scaffold in terms of cell supportive property.

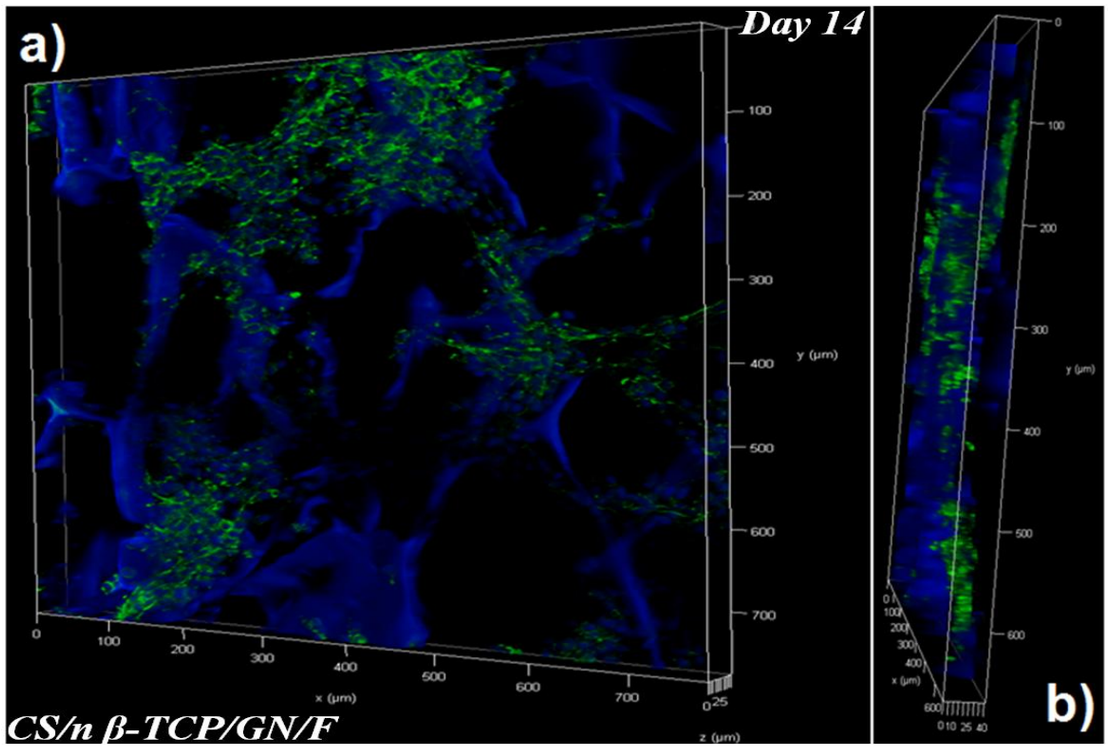

Figure 5.60 (i): ***3D Confocal Laser Scanning Microscopy images of hMSCs after 14 days of culture on CS/nano β-TCP/GN/F composite scaffolds (a,b). Actin filaments (green) and nuclei (blue) were stained Hoechst 33342 and Phalloidin respectively. Cells are found to be well distributed and proliferated over the scaffold with high cell viability. Z-stacks rotated in 3D space (b) to demonstrate penetration and uniform distribution of seeded hMSCs***

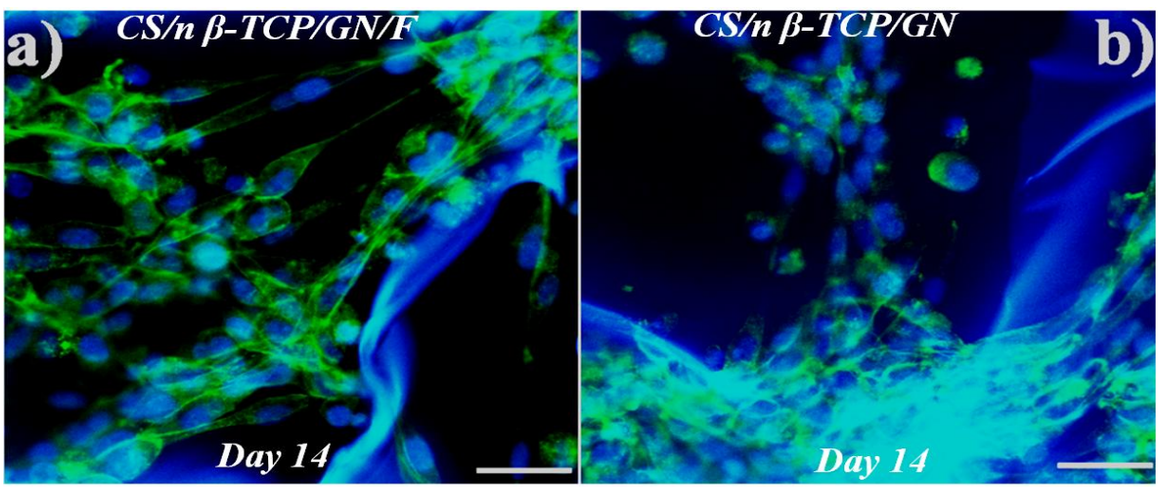

Figure 5.60 (ii)*: Confocal Laser Scanning Microscopy images of CS/nano β-TCP/GN/F scaffolds (a) and CS/nano β-TCP/GN scaffolds (b) after 14 days of culture. Nuclei of the cells stained with Hoechst 33342 (blue) and actin filaments with phalloidin (green). Scale bar indicates 300 µm. Extensive development of cytoskeleton is prominent in CS/nano β-TCP/GN/F when compared to CS/nano β-TCP/GN scaffolds*

5.4.12 Osteogenic differentiation potential

(i) ALP assay

Figure 5.61 shows an increased level of of ALP activity with culture time upto 14days and then a decline trend of ALP is observed. The ALPase activity on fibrin coated scaffolds is measured as 4.25 ± 0.03 IU/µg and 6.61 ± 0.05 IU/µg on 7th and 14th day respectively. However, ALP activity of hMSCs on uncoated scaffold is 3.51 ± 0.04 to 6.09 ± 0.06 on 7 to 14th day which shows statistical significance with fibrin coated scaffolds ($p < 0.05$). As ALP is an early osteogenic marker, the ALPase activity is higher in the initial days of incubation beyond which it found to decrease [201]. The obtained values for fibrin modified and unmodified scaffolds on 21st day are 5.1 ± 0.6 and 5.23 ± 0.13. Similar trend is also observed with BMP-II derived hydrogel matrix as reported earlier [251]. In addition to β-TCP, the presence of fibrin has further enhanced the osteogenic differentiation of seeded hMSCs and the results are consistent with previous reports when RGD was conjugated to CS for improved cellular responses [155].

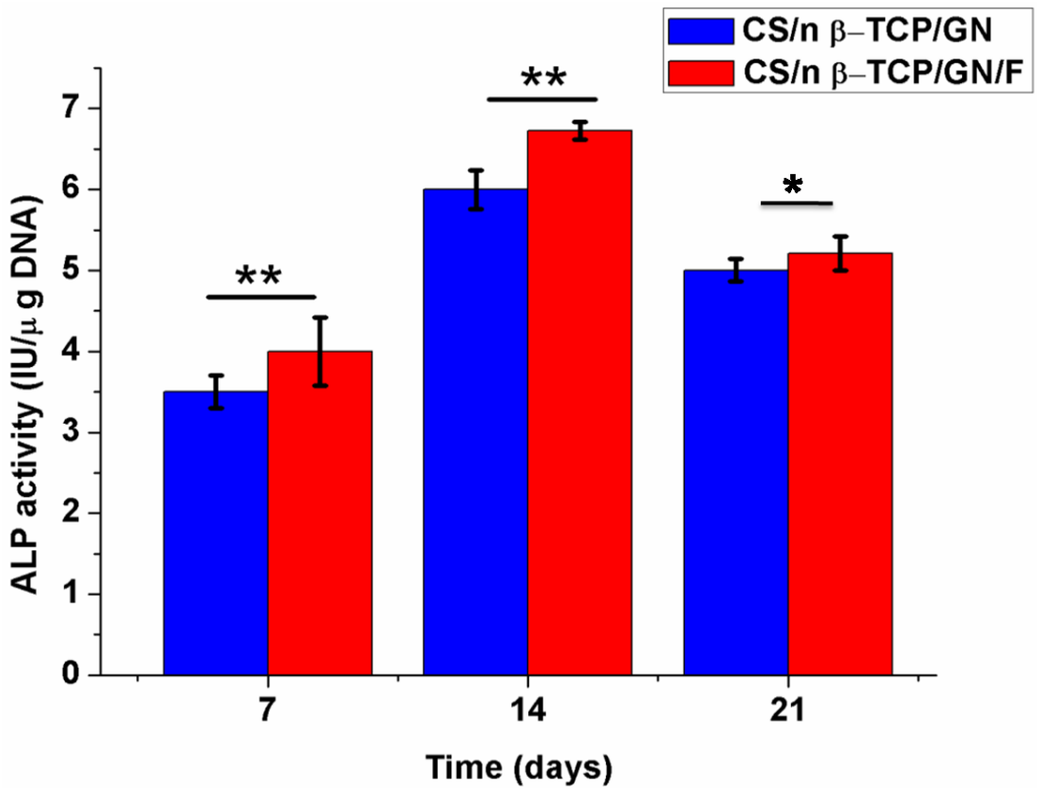

Figure 5.61: ***Alkaline Phosphatase activity of hMSCs seeded on fibrin coated CS/nano β-TCP/GN composite scaffolds upto 21 days of culture. Scaffold without fibrin was used as control. Each point represents the mean ± SD (n= 3) * and ** represents significant differences between the groups at p>0.05 and p < 0.05 respectively***

(ii) Total calcium content

The calcium content of hMSCs seeded scaffolds at different time points is illustrated in **Figure 5.63.** The increase in calcium content is observed to be linear with time representing an increased degree of mineralization as observed with fibrin coated and uncoated scaffolds. The calcium content of hMSCs cultured on CS/nano β-TCP/GN/F scaffolds upto 21 days is 2400 ± 59 mg/mg DNA whereas that of CS/nano β-TCP/GN scaffold is 2054 ± 61 mg/mg DNA. The osteogenic differentiation of hMSCs on the scaffold may be supported by increased number of Ca^{+2} ions generated by TCP dissolution. Superior mineralization activity of MSCs represents the higher osteogenic potential of fibrin coated scaffold when compared to its counterpart. A similar trend in increase of Ca content and cell number were demonstrated in earlier reports where β-TCP was incorporated in fibrin gels [194].

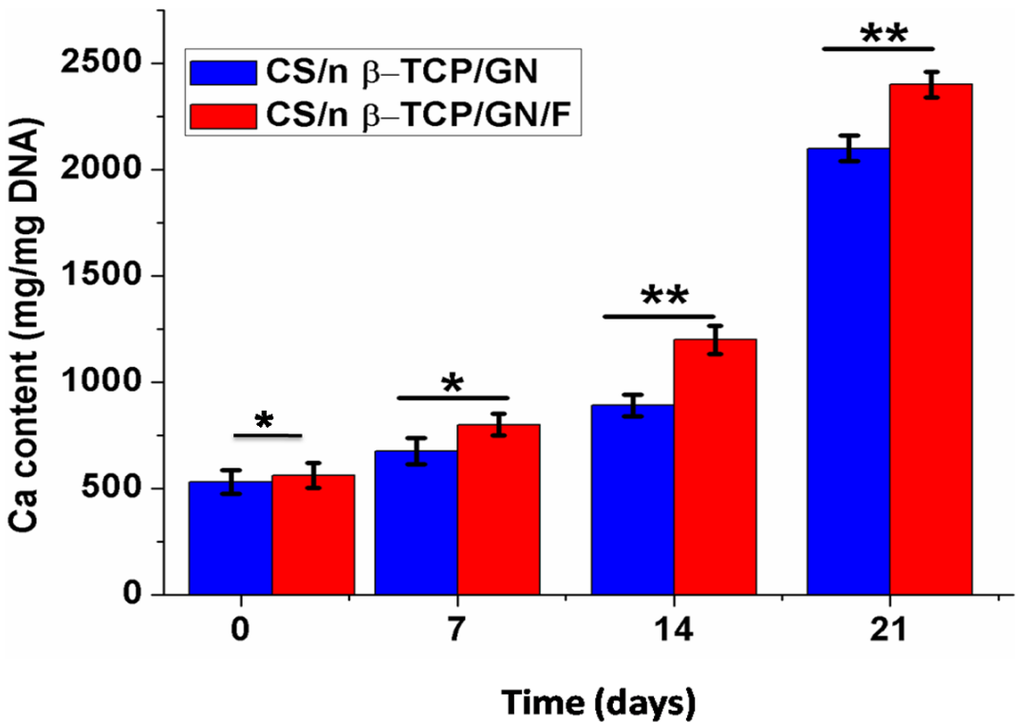

Figure 5.62: ***Total calcium content of CS/nano β-TCP/GN and CS/nano β-TCP/GN/F scaffolds. Calcium content increased linearly with time indicating an increased degree of mineralization. The highest calcium content is observed with fibrin coated composite matrix. Each point represents the mean ± SD (n= 3) * and ** represents p>0.05 and p<0.05 respectively***

(iii) *In-vitro* biomineralization study

The Alizarin red assay result reveals the ability of fibrin modified scaffolds to support mineralization of hMSCs. The optical microscopic images **[Figure 5.63 (i)]** of Alizarin Red stained cell seeded CS/nano β-TCP/GN and CS/nano β-TCP/GN/F composite scaffolds depict an increased mineralization from day 14 to 21. However, a variation in stain intensity (stained nodules) is noticed in the form of prominent red stains on 14^{th} and 21^{st} day images with fibrin coated scaffolds as compared to uncoated scaffolds. Mineralization was further quantified by spectrophotometric measurement of the dye extracted from the obtained stained nodules which is shown in **Figure 5.63 (ii).** Greater absorbance values are obtained from the nodules collected from fibrin coated scaffolds indicating the enhanced ability of mineralization by fibrin coated scaffolds. Significant difference is observed on day 14 and 21 between the samples ($p < 0.05$) as more number of cells differentiated to osteoblasts on fibrin coated scaffolds as compared to other two types of scaffolds. These results are in good agreement with previous reports when RGD conjugated CS showed greater mineralization compared to unmodified CS scaffolds [155-156].

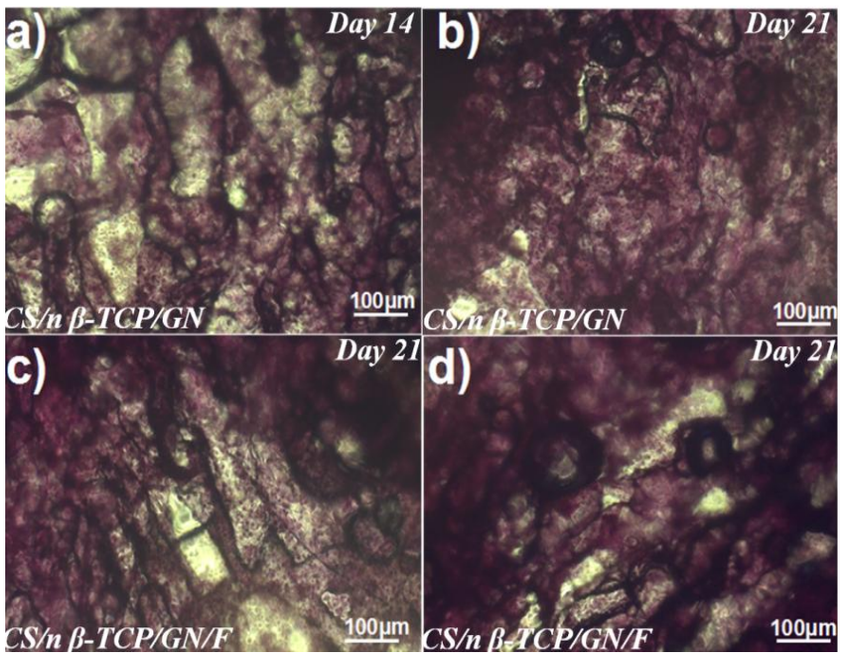

Figure 5.63 (i) ***Alizarin red staining images of CS/nano β-TCP/GN (a, b) and CS/nano β-TCP/GN/F scaffolds (c, d). Number of red stains observed are more prominent with CS/nano β-TCP/GN/F scaffold on both 14 and 21 day images (c, d) as compared to 14^{th} and 21^{st} day images of CS/nano β-TCP/GN (a, b) scaffolds. Intense red stains are observed on CS/nano β-TCP/GN/F scaffolds on both 14 and 21 days suggesting elevated levels of mineralization***

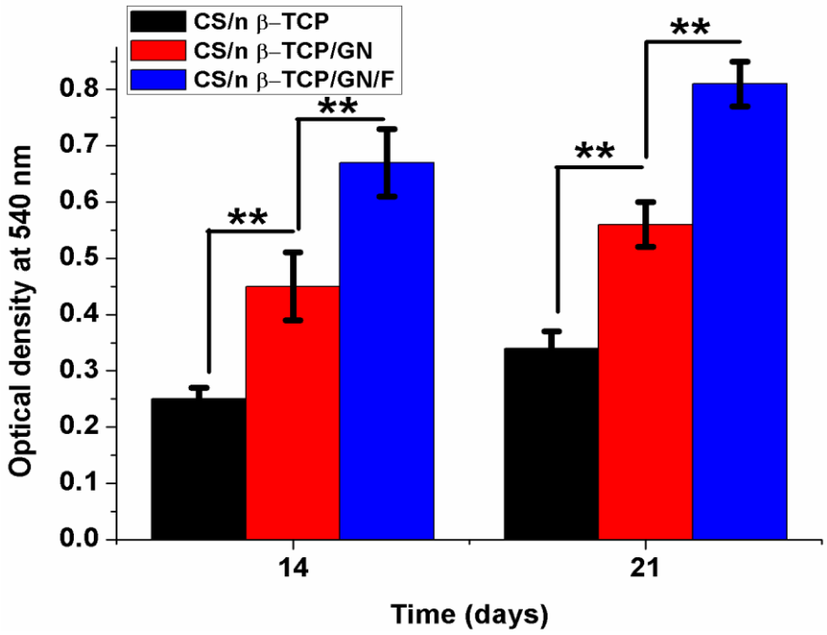

Figure 5.63 (ii): ***Quantitative analysis of mineralization by measuring absorbance of extracted alizarin red dye at 540nm using plate reader. ** denotes differences between groups at p < 0.05***

(iv) Estimation of GAG

GAGs are a trivial component of organic bone ECM and its production is an indication of differentiation towards a specific lineage [248]. **Figure 5.64** shows the GAG content in both fibrin coated and uncoated scaffolds. The difference in GAG secretion between CS/nano β-TCP and CS/nano β-TCP/GN is statistically insignificant. Whereas the amount of GAG secreted is significantly higher with fibrin coated scaffolds when compared to other two scaffolds ($p < 0.05$). GAGs are known to bind and accumulate various proteins including growth factors and cytokines. Further, they are famous for improving and stabilizing the presentation of proteins to their specific receptors thus preventing them from proteolytic degradation. GAG of 28 μg/mg scaffold in MSCs seeded scaffolds containing osteo-differentiation media was higher than that of controls even after 28 days, confirming the superior osteogenic potential of fibrin coated scaffold.

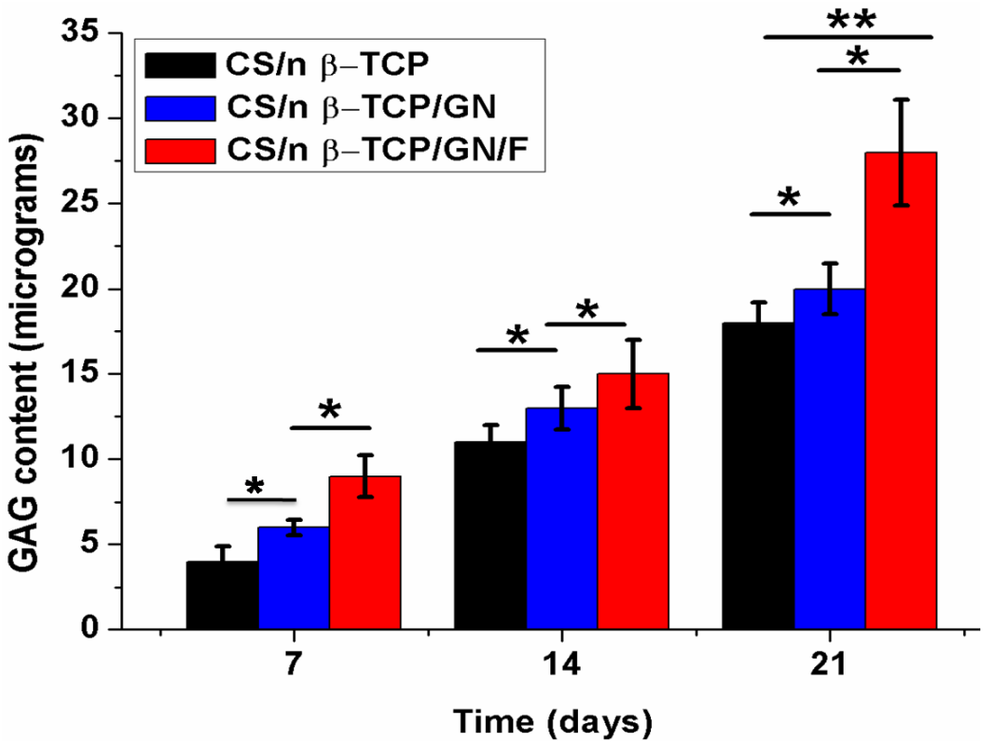

Figure 5.64: ***Biochemical analysis of intracellular GAG by hMSCs cultured in the osteogenic media for 21 days of incubation. * and ** denotes differences between groups at p > 0.05 and p < 0.05***

(v) Expression of osteogenic specific genes

Semi quantitative RT-PCR was performed for analyzing the osteogenic cellular differentiation potential of seeded MSCs on CS/nano β-TCP/GN and CS/nano β-TCP/GN/F scaffolds and the corresponding gene expression bands obtained are shown in **Figure 5.65 (i).** Furthermore, the bands were semi quantified with band intensity and normalized to β-actin to validate the relative expression of osteogenic specific genes as shown in **Figure 5.65 (ii).** As indicated CS/nano β-TCP/GN/F scaffolds exhibits higher levels of osteogenic specific genes when compared to CS/nano β-TCP/GN scaffolds. The expression levels of all the genes selected in the study is higher ($p < 0.05$) on fibrin coated scaffolds as compared to uncoated scaffolds. All the genes are observed to be up regulated on fibrin coated scaffold which is attributed to synergic effects of fibrin and osteoinductive nature of β-TCP [201]. The reason for down regulation of osteogenic specific genes on CS/nano β-TCP/GN scaffolds may be attributed to insufficient cell adhesion sites which resulted in poor cell cycle progression and thus poor cell differentiation as shown in **Figure 5.65 (ii).** From these results, we conclude that expression

of genes related to early (Col-I, BSP) middle (ALP, ON) and late (OC) markers are up regulated and thus proved the superiority of fibrin coated scaffolds. Similar results were also reported with nanofibrous scaffolds for bone tissue regeneration [249] .

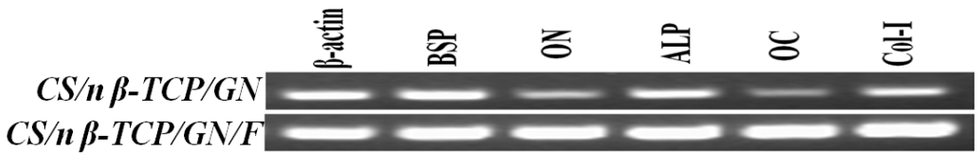

Figure 5.65 (i): ***Images of amplified cDNA products using specific osteogenic primers (BSP, ON, ALP, OC and Col-I) for hMSCs cultured on CS/nano β-TCP/GN and CS/nano β-TCP/GN/F scaffolds in osteogenic media for 21 days of incubation. Cell seeded on CS/nano/β-TCP/GN/F exhibited lower levels of osteogenic specific genes when compared to CS/nano β-TCP/GN scaffolds***

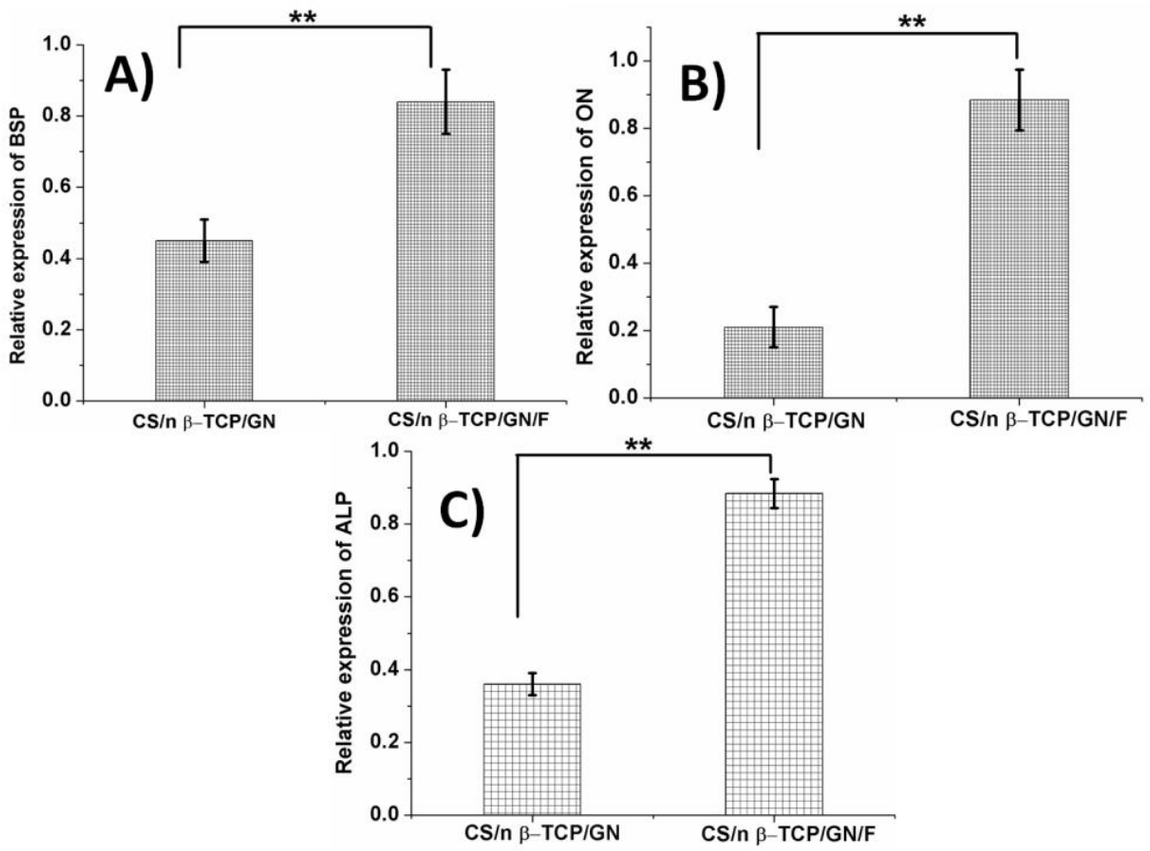

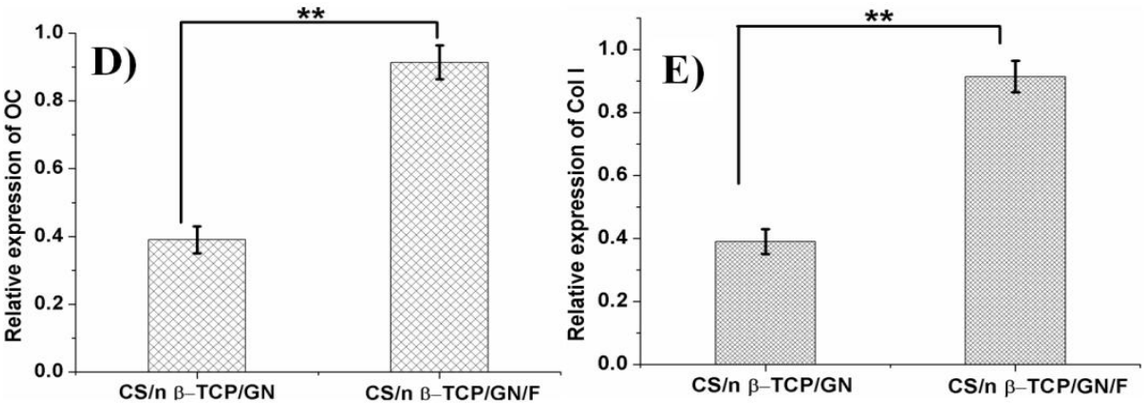

Figure 5.65 (ii): ***Relative Expression of BSP (a), ON (b), ALP (c), OC (d) and Col I (e) osteogenic markers on CS/nano β-TCP/GN and CS/nano β-TCP/GN/F. ** Represents a statistical difference at p < 0.05. The expression levels of all the genes selected in the study is higher on fibrin coated scaffolds when compared to uncoated scaffolds***

5.4.13 *In-vivo* biocompatibility

In-vivo biocompatibility of the most potential CS/nano β-TCP/GN/F scaffold was assessed by implanting it subcutaneously as shown in **Figure 5.66** (surgically created pouch) in both male and female mice for 7 and 28 days. Tissue responses after implantation of scaffolds are shown in **Figure 5.67 (i&ii).** The mice did not show any wound complications, no inflammatory and adverse tissue reactions throughout the experiment. Thus, scaffolds did not cause any health complications on the physiology of selected mice. After 7 and 28 days of implantation, mice were sacrificed. The host tissue reactions with implanted scaffolds were analyzed by H&E staining. On macroscopic observation, all the scaffolds are condensed in a thin fibro vascular tissue of mice. During initial days (7^{th} day), we observed the existence of few inflammatory cells and more number of fibroblasts were grown into the scaffold **[(Fig. 5.67 (i-a)].** However, at later time point (28^{th} day), the number of fibroblast infiltration into the scaffolds is high owing to the excellent porosity and interconnected porous architecture of the scaffold **[(Fig. 5.67 (i-b)].** Further, the morphology of scaffold was in pace with the neighbouring tissue **[Fig. 5.67 (i-b, ii-b)]** in both sexes as reported earlier with implantation of CS/alginate hybrid scaffolds used for bone tissue engineering applications [30]. Thus, the *in-vivo* biocompatibility of CS/nano β-TCP/GN/F composite scaffolds is proved using mice

model and thus the scaffolds support attachment, proliferation of cells without causing any adverse effects (infection, inflammation and cell death) in the transplanted mice.

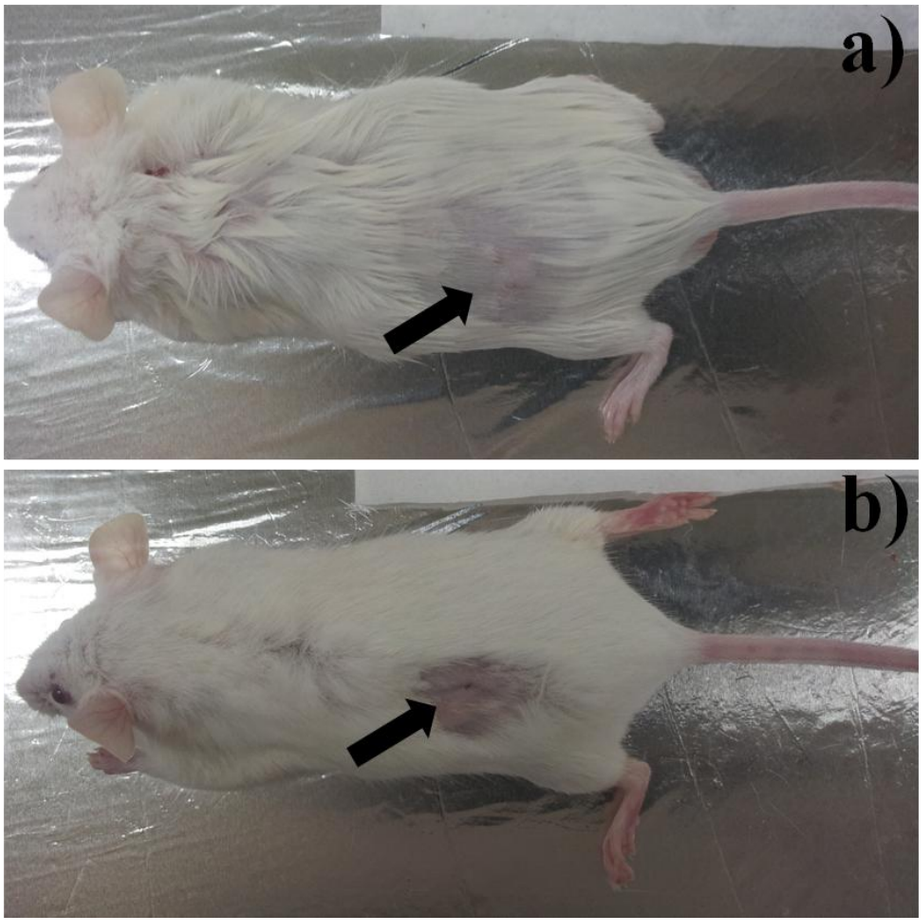

Figure 5.66: ***Implantation of CS/nano β-TCP/GN/F composite scaffolds in ICR mice strain for in-vivo biocompatibility study, (a) Male & (b) Female mice***

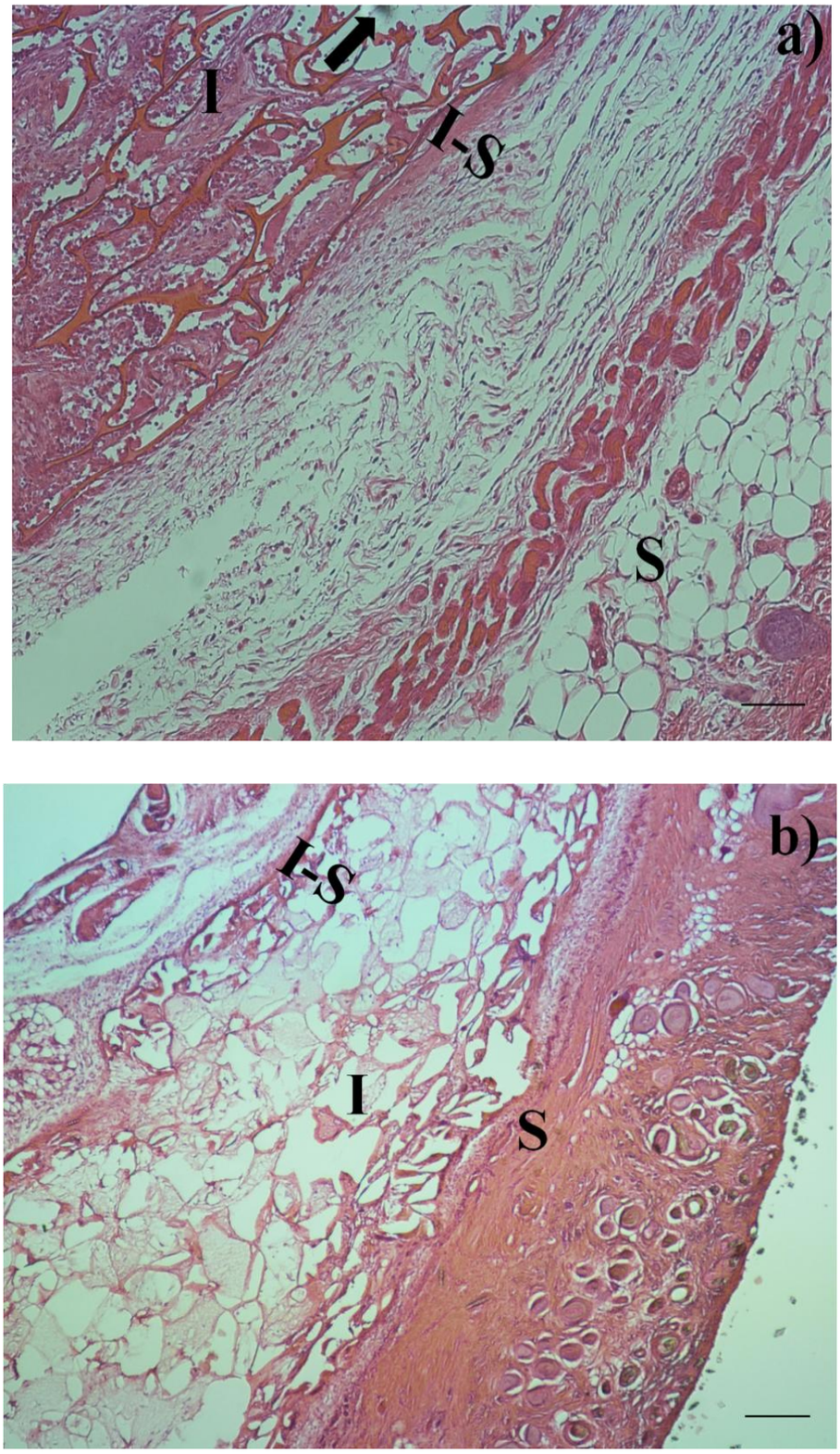

Figure 5.67 (i): ***Histological sections of subcutaneous skin of ICR mice (male) at the site of implanted CS/nano β-TCP/GN/F composite scaffolds after (a) 7 days & (b) 28 days. Bar indicates 200µm. I: Implanted scaffold site. S: Subcutaneous connective tissue and I-S: The meso-dermal site at the interface of scaffold and tissue during initial days (7th day), existence of few inflammatory cells is found and more number of fibroblasts was grown into the scaffold. However, at later time point (28th day), the number of fibroblast infiltration into the scaffolds is high***

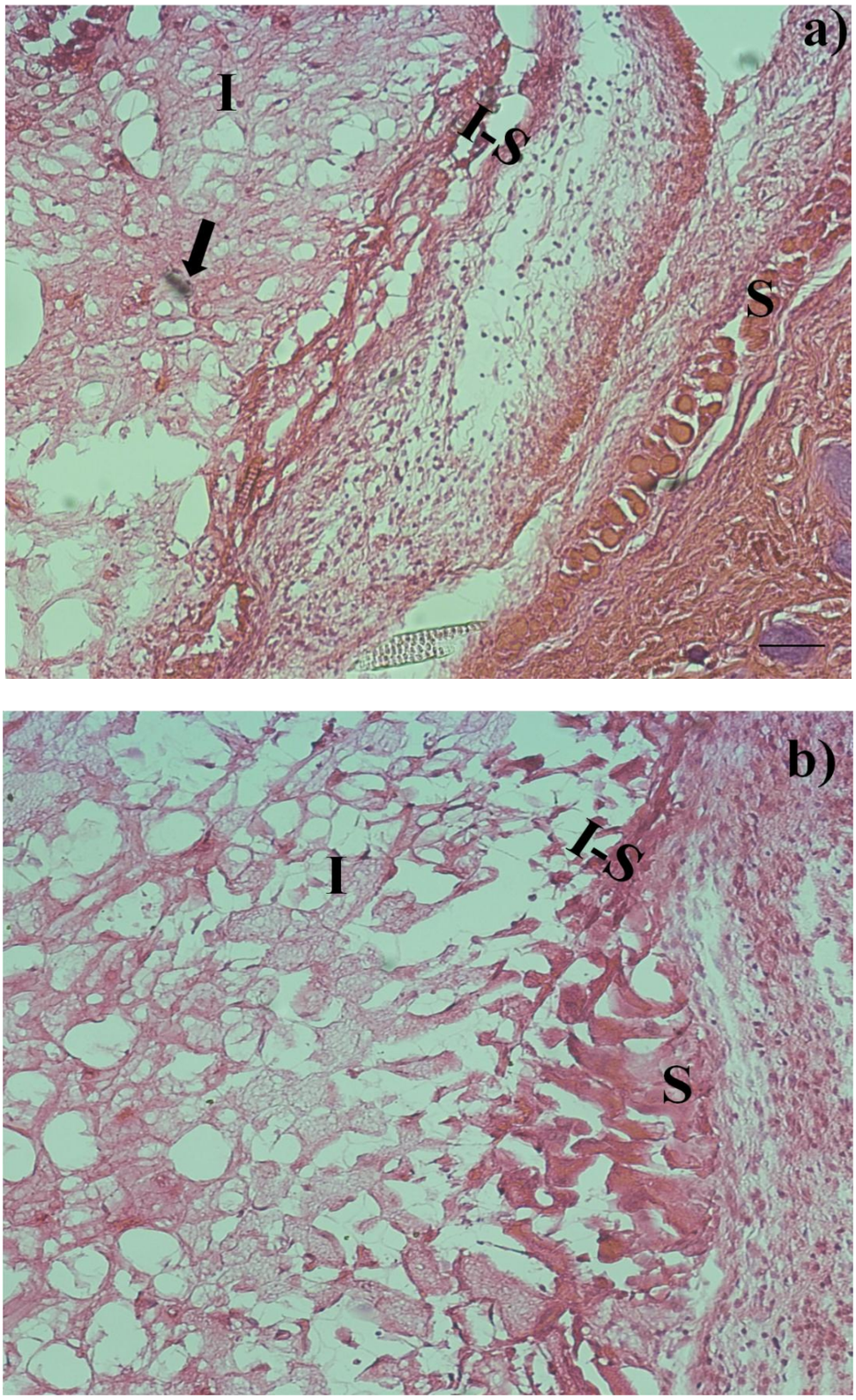

(ii): ***Histological section of subcutaneous skin of ICR mice (Female) at the site of implanted CS/nano β-TCP/GN/F composite scaffolds after (a) 7 days & (b) 28 days. Bar indicates 200µm. I: Implanted scaffold site. S: Subcutaneous connective tissue and I-S: The meso-dermal site at the interface of scaffold and tissue***

There is a very few report available in the literature for developing CS reinforced β-TCP composite scaffolds (4, 23, 55, 252-54). Most of these works are preliminary study with the main aim of improving the mechanical strength of CS scaffold by reinforcing with micro sized β-TCP as shown in **Table 5.4** To the best of our knowledge, the present work is the first report for developing CS composite scaffold using nano sized β-TCP. Further, no systematic work has been done so far to address the various lacuna of CS scaffold e.g. cell binding ability, degradation to make this potential biopolymer for use as artificial ECM for bone tissue regeneration except compressive strength and bioactivity. The novelty of our study includes the improvement of cell binding property (with surface modification by fibrin conjugation) biodegradation (by the development of cross-linked composite scaffold) along with the enhanced bioactivity and mechanical strength using nano β-TCP.

The developed CS/nano β-TCP has shown superior cell supportive property, bioactivity and compressive strength than the CS composite scaffold prepared by the widely used micro β-TCP study by us as well as by other researchers. Most importantly, the CS/nano β-TCP developed by us possess the highest compressive strength (2.67 MPa) among all the CS/β-TCP composite scaffolds reported so far even the compressive strength reported by Ruiran et al reference 10 as specified by the examiner. Besides, mechanical strength the developed scaffold has shown desired biocompatibility growth, proliferation and differentiation of hMSCs.

Furthermore, the genipin cross-linked CS/β-TCP and fibrin conjugated cross-linked scaffolds possess control degradation rate (8% of its initial weight for four weeks of incubation) and an improved compressive strength of 2.78 & 2.8MPa respectively.

Table 5.4: ***Comparison of results with the published data***

S.N	Scaffold	Type & Method	Mech.strength (MPa)	Cell study	Reference
1	CS/Gelatin/β-TCP (0.8µm)	3D Porous, Freeze drying	0.08-0.8	MTT	Yuji Yin,2003
2	CS/invert glass/β-TCP	3D Porous, Freeze drying	0.9-2.19	MTT, SEM	Zhang, 2001
3	CS/gelatin/β-TCP/PLA (<26µm)	3D Porous, Freeze drying	0.2-1.8	RT-PCR,SEM	Mohammadi,2004 ,
4	CS/β-TCP	3D Porous, Freeze gelation	0.2-1.75	MTT	Ruiran et.al, 2010
5	CS/β-TCP (82nm)	3D Porous, Freeze gelation	2.67 ± 0.21	MTT, Fluorescence	Siddiqui et.al, 2014
6	CS/β-TCP/Fibrin	3D Porous, Freeze gelation	2.71 ± 0.14	MTT, ALP, RT-PCR,	Siddiqui et.al, 2015
7	CS/β-TCP/Genipin	3D Porous, Freeze gelation	2.78 ± 0.14	MTT,ALP, Confocal	Under review: Siddiqui et.al,
8	CS/β-TCP/TPP	3D Porous, Freeze gelation	2.72 ± 0.11	MTT, ALP, Confocal, Ca content	-do-
9	CS/βTCP/Genipin/Fibrin	3D Porous, Freeze gelation	2.8±0.13	MTT, Osteogenic differentiation and *in-vivo*	Siddiqui et.al, Communicated

Chapter 6

Summary and conclusions

Bone tissue defects and diseases are increasing worldwide due to the shortage of organ donor. Allograft bone is used extensively in regeneration of large defects but its use is limited by immune rejection and the risk of disease transfer. To overcome these issues, bone tissue engineering has emerged as an alternative strategy to repair and/or replace diseased and/or damaged bone tissue through the development of biological substitutes that enable complete recovery of the tissue function. However, the development of 3D porous architecture from a suitable biopolymer or their composites with a desired set of properties is the key challenge of this technique. Among the various biopolymers explored in the last decade, chitosan is considered as one of the potential biomaterials because of its excellent hydrophilicity, biocompatibility and wound healing properties. However, chitosan has several limitations such as poor mechanical strength, lower bioactivity, fast degradation and low cell binding ability that limit its use in bone tissue engineering. Therefore, the present research has focussed on the development of novel chitosan based composite porous scaffold by addressing various limitations associated with chitosan to make it a potential biomaterial for bone tissue regeneration. The most interesting and encouraging results achieved through this research work are noted here-

Part I: In the first phase of research work, effort has been given to improve the mechanical strength and bioactivity of CS scaffold by reinforcing with bioactive β-TCP ceramic filler. Thus, pure CS and CS/β-TCP composite scaffolds using varying ratio of CS and β-TCP in micro and nano size were successfully prepared by freeze-gelation method. The scaffolds were characterized for morphology, pore size and porosity, compressive strength, swelling, structural, biodegradation and bioactivity property. Both pure CS and composite scaffolds exhibited interconnected open pore microstructure with a slight decrease in pore size and porosity obtained with composite scaffolds. The trend of pore size and porosity follows CS>nano>micro. The composite scaffolds still possess pore size and porosity suitable for bone tissue engineering application. The corresponding pore size and porosity values of CS/micro β-TCP scaffolds are 45-165 μm and 74.2 ± 5.2 to 80.7 ± 2.33% and that of CS/nano β-TCP scaffolds are 51-168 μm and 78.3 ± 2.9 to 84.6 ± 2.65 % respectively. Within the concentration limit < 50 wt %), the nano β-TCP were also found

to disperse more uniformly in the scaffold matrix compared to micro-β-TCP as evident from SEM micrographs. The compressive strength of CS scaffold was remarkably increased by the addition of both type of β-TCP. However, CS scaffold reinforced with nano β-TCP exhibited higher compressive strength, the optimum value being 2.67±0.21MPa obtained with the ratio of 60:40 CS:nano β-TCP as well as improved in vitro bioactivity than other composite matrices developed using different ratio and type of fillers. As expected, the degradation rate was slightly decreased by the addition of β-TCP and composite scaffold with nano β-TCP offers better degradation pattern.

The *in-vitro* cell culture study using UCB derived MSCs seeded on the composite matrices has confirmed the biocompatibility of the freeze-gelled composite scaffolds as assessed by the cell attachment and morphology (SEM), cell viability (MTT assay) and proliferation (Fluorescence microscopy, Alamar blue assay and DNA quantification). Among the composite scaffolds developed, CS/nano β-TCP scaffold (60:40) has shown superior cell supportive property achieving better cell attachment, cell proliferation and metabolic activity. Furthermore, higher mineralization (total calcium content) and ALP activity of MSCs proves the superior osteogenic potential of CS/nano β-TCP scaffold.

All these results suggest that the developed CS/β-TCP can be used as a base polymeric scaffold material for various bone tissue engineering application. However, the superior physico-chemical, mechanical and in vitro biological properties make CS/nano β-TCP most potential composite scaffold for bone tissue regeneration and hence used for further study.

Part II: In the previous section, CS/β-TCP composite scaffolds with improved mechanical and bioactive property were developed by freeze-gelation method and CS reinforced with nano β-TCP (CS/nano β-TCP) was found to the most potential. CS also lacks cell signalling molecules and hence offers less cellular affinity. So in this phase, effort has been given to investigate the effect of fibrin as a promising bioactive protein molecule having numerous cell binding RGD domains to improve cellular affinity of the CS/nano β-TCP scaffolds. Fibrin conjugated CS/nano β-TCP scaffold (CS/nano β-TCP/F) was prepared by cross-linking with

ethyl-3-(3-dimethylaminopropyl) carbodimide. The microstructure of the conjugated scaffold possess interconnected open pore and pore network with 49-151 μm pore size and 81.4±4.1% porosity suitable for bone tissue regeneration**.**

Further, the *in-vitro* cell culture study has shown an enhanced cell attachment (FE SEM), cell proliferation (Fluorescence microscopy, DNA quantification) and differentiation (ALP, total calcium content, alizarin red assay) on fibrin conjugated CS/nano β-TCP scaffold. The uniform cell distribution and cell infiltration throughout the scaffold pores were confirmed by confocal laser scanning microscopy (CLSM). Furthermore, higher expression of osteogenic specific genes such as Bone sialo protein (BSP), Osteonectin (ON), Alkaline Phosphatase (ALP), and Osteocalcin (OC) on fibrin conjugated scaffolds is observed compared to non-conjugated composite scaffolds.

Thus it has been concluded that the modification of composite scaffold with fibrin is beneficial for improving cellular affinity of the scaffold.

Part III: The rapid degradation of CS is another important aspect that needs to be addressed to achieve desired degradation rate compatible with the rate of neo tissue formation. Though a slight improvement in degradation rate (slow degradation) has been achieved in the first phase of research work by incorporating β-TCP, there is need of further controlling high degradation of scaffold to a desirable level. Keeping this aspect in view, an effort has been given in this part of thesis work for further reduction of degradation by the development of cross-linked composite scaffolds. The main aim was to develop genipin (GN) and sodium tripolyphosphate (TPP) cross-linked CS/nano β-TCP composite scaffolds with improved degradation characteristics along with other physico-chemical, mechanical and *in-vitro* biological property.

The cross-linked CS/nano β-TCP composite scaffolds were successfully developed using different concentrations of GN and TPP cross-linking agents. No significant change in scaffold architecture and morphology was observed due to cross-linking. Whereas the

degradation rate of the scaffold was significantly decreased by cross-linking and the optimal degradation rate was achieved with 0.1w/v% concentration of both GN and TPP. In comparison, GN cross-linked CS/nano β-TCP composite has shown lower degradation rate due to its strong cross-linking ability than TPP cross-linked scaffold. The corresponding degradation rates are 8% and 13% respectively. A slight increase in compressive strength is also achieved with cross-linked scaffolds; the maximum compressive strength is obtained at a concentration of 0.1 w/v% cross-linking agents. The corresponding compressive strength of GN and TPP cross-linked scaffolds is 2.78 ± 0.14 MPa and 2.72 ± 0.11 MPa respectively which is suitable for cancellous bone tissue regeneration.

Both GN and TPP cross-linked composite scaffolds were also evaluated for their performance in *in-vitro* cell culture study. The study has revealed enhanced cell supportive property of cross-linked scaffolds in terms of cell attachment (SEM), cellular metabolic activity (MTT assay) cell proliferation (DNA quantification), cytoskeletal organization (confocal laser scanning microscopy), total calcium content, and ALP activity. Furthermore, GN cross-linked scaffold has shown better performance than TPP cross-linked scaffold. Thus the developed CS/nano β-TCP/GN composite scaffold was selected for further study.

Part IV: As in part-II, fibrin has shown a positive impact on the cellular responses of the CS/nano β-TCP composite scaffolds. So, in this phase of work, attempt has been made to improve the cell binding ability of the most potential CS/nano β-TCP/GN composite scaffold by fibrin coating. The developed fibrin modified scaffold (CS/nano β-TCP/GN/F) possesses desired interconnected pores and pore network, porosity, hydrophilicity, and favourable biodegradation rate. The *in-vitro* cell culture study has confirmed enhanced cell adhesion property in terms of cell (hMSCs) attachment and spreading (FE-SEM study), cell proliferation (DNA quantification), cytoskeletal organization and cell infiltration (confocal microscopy) and cellular metabolic activity (MTT assay). Higher osteogenic differentiation potentiality of the fibrin coated composite scaffold has been proved by higher ALP activity, total calcium and GAG content and biomineralization ability of hMSCs seeded on the fibrin

coated scaffold than the uncoated one. The higher osteogenic differentiation of hMSCs is also evident from the semi quantitative RT-PCR study that revealed higher expression of osteogenic specific genes such as Bone sialo protein (BSP), Osteonectin (ON), Alkaline Phosphatase (ALP), Collagen I (Col 1) and Osteocalcin (OC) on the fibrin modified scaffolds as compared to uncoated scaffold. Finally, *in-vivo* biocompatibility of these scaffolds was proved by animal testing using mice model. All together, the fibrin coating has beneficial effect in enhancing various cellular responses of the composite scaffolds.

Overall, in this study a novel 3D porous composite scaffold has been developed from chitosan reinforced with CS/nano β-TCP as filler which can be used as a base polymeric scaffold for various bone tissue engineering applications. The property of the CS/nano β-TCP composite scaffolds was further improved by cross-linking with GN and fibrin coating thereby CS/nano β-TCP/GN and CS/nano β-TCP/GN/F scaffolds with favourable degradation, enhanced cellular responses and osteogenic differentiation were developed. It has been demonstrated in this dissertation work that the developed CS based composite scaffolds in particular CS/nano β-TCP/GN/F can serve as a potential artificial extra cellular scaffold matrix for various non load bearing bone tissue regeneration in future.

Suggested Future Work

The following research work are suggested for future study with the developed composite scaffolds-

i. Three dimensional scaffolds with appropriate design may be fabricated by adopting advanced scaffold fabrication technique like electrospinning, rapid protyping methods.
ii. Angiogenesis study can be performed to confirm the vascularisation aspect of the developed scaffold.
iii. Detail *in-vivo* animal study can be undertaken for assessing its suitability for possible future clinical application.

BIOGRAPHY

Nadeem Siddiqui is a PhD candidate in the Department of Biotechnology and Medical Engineering at National Institute of Technology Rourkela, India. He received his B.Tech (Biotechnology) in 2008 from C.M.R College of Engineering and Technology, JNTU Hyderabad, Telangana (India). He joined NIT Rourkela in the year of 2008 and completed his M.Tech (Biotechnology) in 2010. He started his Ph.D in NIT Rourkela in the year of 2010. His interests include biomaterials processing and application for bone and cartilage tissue engineering, nanotechnology and stem cell research for efficient and improved tissue regeneration.

Personal Details:

Father's Name	Mr. Late. Saleem Siddiqui
Mother's Name	Mrs. Siddiqua Begum
Date of Birth	15th August, 1985
Gender	Male
Nationality	Indian
Language Known	English, Hindi, Urdu, Telugu and Oriya
Permanent Address	C/O Waseem Siddiqui 5th Floor, Flat no: 515 Tirumala Alluri Nivas Apartments Malakpet, Hyderabad Telangana, India-500024
E.Mail:	nadeem.nitian.biotech@gmail.com

JOURNAL PUBLICATIONS

- **Published online: Nadeem Siddiqui**, Krishna Pramanik*, "Effects of micro and nano β-TCP fillers in freeze-gellled chitosan scaffold for bone tissue engineering". Journal of applied polymer science 13th may 2014, Inc. J.App. Polym. Sci. **2014,***131*,41025, [IF:(1.64)]
- **Published online: Nadeem Siddiqui**, Krishna Pramanik*, "Development of fibrin conjugated chitosan/nano β-TCP composite scaffolds with improved surface property for bone tissue regeneration". Journal of applied polymer science, Inc. J.App. Polym. Sci. **2015,** *132, DOI: 10.1002/app.41534*, [IF:1.64]
- **Under review: Nadeem Siddiqui**, Krishna Pramanik and Esmail Jabbari*,"Osteogenic Differentiation of Human Mesenchymal Stem Cells in Freeze-Gelled Chitosan/Nano beta Tricalcium Phosphate Porous Scaffolds Cross-linked with Genipin" communicated to Journal of Material science and Engg: C. [IF:3.0]
- **Communicated: Nadeem Siddiqui,** Bissoyi Akalabya Krishna Pramanik*, manuscript entitled "Enhanced cellular responses on fibrin coated GN cross-linked CS/nano β-TCP composite scaffolds", Journal of Biomedical Nanotechnology [IF:7.5]

Conference papers

- **Nadeem Siddiqui,** Krishna Pramanik*, "Development of cross-linked freeze-gellled chitosan based scaffolds for bone tissue regeneration" Indian Chitin and Chitosan society at Institute for Himalayan Bioresources Technolgy-2013 organized by IHBT Palampur, Himachal Pradesh, India, June -2013.
- **Nadeem Siddiqui,** Krishna Pramanik*, Role of Pluronics in blood vessel tissue engineering applications at International Conference on Tissue Engineering and Regenerative Medicine (ICTERM-2012), organized by NITRKL, India; Sept-2012.
- **Nadeem Siddiqui,** Krishna Pramanik*, "Development of freeze-gelled chitosan based scaffolds for bone tissue engineering" at NANOBIO-2012 organized by Amrita institute Kerala, India; Feb-2012.
- **Nadeem Siddiqui,** Krishna Pramanik*, "Chitosan as an ideal polymer for bone tissue engineering" Presented as a poster in National seminar entitled Tissue Engineering Prospects and Challenges (TEPC) organized by NIT Rourkela, India; Jan- 2011.

References

[1] V. C. Mow and R. Huiskers, *Basic orthopaedic biomechanics and mechano-biology*: Lippincott Williams & Wilkins, 2005.

[2] A. R. Costa-Pinto, *et al.*, "Scaffolds based bone tissue engineering: the role of chitosan," *Tissue Engineering Part B: Reviews*, vol. 17, pp. 331-347, 2011.

[3] A. M. Martins, *et al.*, "Responsive and in situ-forming chitosan scaffolds for bone tissue engineering applications: an overview of the last decade," *Journal of Materials Chemistry*, vol. 20, pp. 1638-1645, 2010.

[4] Y. Mohammadi, *et al.*, "Osteogenic Differentiation of Mesenchymal Stem Cells on Novel Three-Dimensional Poly (L-Lactic Acid)/Chitosan/Gelatin/Beta-Tricalcium Phosphate Hybrid Scaffolds," *Iranian Polymer Journal*, vol. 16, p. 57, 2007.

[5] M. I. Sabir, *et al.*, "A review on biodegradable polymeric materials for bone tissue engineering applications," *Journal of Materials Science*, vol. 44, pp. 5713-5724, 2009.

[6] L. Yunfeng, *et al.*, "Review on techniques of design and manufacturing for bone tissue engineering scaffold," in *Biomedical Engineering and Informatics, 2009. BMEI'09. 2nd International Conference on*, 2009, pp. 1-4.

[7] J. D. Stroncek and W. M. Reichert, "Overview of wound healing in different tissue types," *Indwelling Neural Implants: Strategies for contending with the in vivo environment*, 2008.

[8] H.I. Chang and Y. Wang, "Cell responses to surface and architecture of tissue engineering scaffolds," *Regenerative Medicine and Tissue Engineering—Cells and Biomaterials, InTech: Rijeka, Croatia*, pp. 569-588, 2011.

[9] J. Venkatesan and S.-K. Kim, "Chitosan composites for bone tissue engineering—An overview," *Marine drugs*, vol. 8, pp. 2252-2266, 2010.

[10] H. Ruiran, *et al.*, "Preparation of β-calcium phosphate/chitosan composite scaffolds and its effect on osteoblasts behaviour," *Journal of Functional Materials*, vol. 41, pp. 148-151, 2010.

[11] A. Di Martino, *et al.*, "Chitosan: a versatile biopolymer for orthopaedic tissue-engineering," *Biomaterials*, vol. 26, pp. 5983-5990, 2005.

[12] T. Jiang, *et al.*, "Fabrication of novel porous chitosan matrices as scaffolds for bone tissue engineering," DTIC Document2005.

[13] M. Yamamoto, *et al.*, "Controlled release by biodegradable hydrogels enhances the ectopic bone formation of bone morphogenetic protein," *Biomaterials*, vol. 24, pp. 4375-4383, 2003.

[14] N. Sultana and M. R. A. Kadir, "Study of in vitro degradation of biodegradable polymer based thin films and tissue engineering scaffolds," *African Journal of Biotechnology*, vol. 10, pp. 18709-18715, 2013.

[15] C. E. Orrego and J. S. Valencia, "Preparation and characterization of chitosan membranes by using a combined freeze gelation and mild crosslinking method," *Bioprocess and biosystems engineering*, vol. 32, pp. 197-206, 2009.

[16] F. Pati, *et al.*, "Osteoblastic cellular responses on ionically crosslinked chitosan-tripolyphosphate fibrous 3-D mesh scaffolds," *Journal of Biomedical Materials Research Part A*, vol. 101, pp. 2526-2537, 2013.

[17] N. Bhardwaj, *et al.*, "Freeze-gelled silk fibroin protein scaffolds for potential applications in soft tissue engineering," *International journal of biological macromolecules*, vol. 49, pp. 260-267, 2011.

[18] M. Okada and T. Furuzono, "Hydroxylapatite nanoparticles: fabrication methods and medical applications," *Science and Technology of Advanced Materials*, vol. 13, p. 064103, 2012.

[19] J. R. Porter, *et al.*, "Bone tissue engineering: a review in bone biomimetics and drug delivery strategies," *Biotechnology Progress*, vol. 25, pp. 1539-1560, 2009.

[20] A. Mol, *et al.*, "Fibrin as a cell carrier in cardiovascular tissue engineering applications," *Biomaterials*, vol. 26, pp. 3113-3121, 2005.

[21] T. Weigel, *et al.*, "Design and preparation of polymeric scaffolds for tissue engineering," 2006.

[22] S. J. Peter, *et al.*, "In vitro degradation of a poly (propylene fumarate)/β-tricalcium phosphate composite orthopaedic scaffold," *Tissue engineering*, vol. 3, pp. 207-215, 1997.

[23] Y. Zhang, *et al.*, "Calcium phosphate-chitosan composite scaffolds for bone tissue engineering," *Tissue engineering*, vol. 9, pp. 337-345, 2003.

[24] Y.M. Lee, *et al.*, "Tissue engineered bone formation using chitosan/tricalcium phosphate sponges," *Journal of Periodontology*, vol. 71, pp. 410-417, 2000.

[25] S. Jockenhoevel, *et al.*, "Fibrin gel–advantages of a new scaffold in cardiovascular tissue engineering," *European journal of cardio-thoracic surgery*, vol. 19, pp. 424-430, 2001.

[26] E. Gentleman, *et al.*, "Mechanical characterization of collagen fibers and scaffolds for tissue engineering," *Biomaterials*, vol. 24, pp. 3805-3813, 2003.

[27] S. Sahoo, *et al.*, "A bFGF-releasing silk/PLGA-based biohybrid scaffold for ligament/tendon tissue engineering using mesenchymal progenitor cells," *Biomaterials*, vol. 31, pp. 2990-2998, 2010.

[28] Y. Yang, *et al.*, "Enhancement of mechanical signals for tissue engineering bone," *Topics in Tissue Engineering*, vol. 2, pp. 1-21, 2005.

[29] T. Jiang, *et al.*, "Chitosan–poly (lactide-co-glycolide) microsphere-based scaffolds for bone tissue engineering: In vitro degradation and in vivo bone regeneration studies," *Acta Biomaterialia*, vol. 6, pp. 3457-3470, 2010.

[30] Z. Li, *et al.*, "Chitosan–alginate hybrid scaffolds for bone tissue engineering," *Biomaterials*, vol. 26, pp. 3919-3928, 2005.

[31] J. De Groot, *et al.*, "Use of porous polyurethanes for meniscal reconstruction and meniscal prostheses," *Biomaterials*, vol. 17, pp. 163-173, 1996.

[32] A. J. Salgado, *et al.*, "Bone tissue engineering: state of the art and future trends," *Macromolecular bioscience*, vol. 4, pp. 743-765, 2004.

[33] M. Barbosa, *et al.*, "Polysaccharides as scaffolds for bone regeneration," *Itbm-Rbm*, vol. 26, pp. 212-217, 2005.

[34] N. Bhardwaj and S. C. Kundu, "Electrospinning: a fascinating fiber fabrication technique," *Biotechnology advances*, vol. 28, pp. 325-347, 2010.

[35] M. E. Gomes, *et al.*, "Starch–poly (ε-caprolactone) and starch–poly (lactic acid) fibre-mesh scaffolds for bone tissue engineering applications: structure, mechanical properties and degradation behaviour," *Journal of Tissue Engineering and Regenerative Medicine*, vol. 2, pp. 243-252, 2008.

[36] G. Marino, *et al.*, "β-Tricalcium phosphate 3D scaffold promote alone osteogenic differentiation of human adipose stem cells: in vitro study," *Journal of Materials Science: Materials in Medicine*, vol. 21, pp. 353-363, 2010.

[37] R. Dorati, *et al.*, "Effect of porogen on the physico-chemical properties and degradation performance of PLGA scaffolds," *Polymer Degradation and Stability*, vol. 95, pp. 694-701, 2010.

[38] W. Thein-Han and R. Misra, "Biomimetic chitosan–nanohydroxyapatite composite scaffolds for bone tissue engineering," *Acta Biomaterialia*, vol. 5, pp. 1182-1197, 2009.

[39] M. Ngiam, *et al.*, "The fabrication of nano-hydroxyapatite on PLGA and PLGA/collagen nanofibrous composite scaffolds and their effects in osteoblastic behavior for bone tissue engineering," *Bone*, vol. 45, pp. 4-16, 2009.

[40] C. Li, *et al.*, "Bone morphogenetic protein-9 induces osteogenic differentiation of rat dental follicle stem cells in P38 and ERK1/2 MAPK dependent manner," *International journal of medical sciences*, vol. 9, pp. 862-871, 2011.

[41] B. Basu, *et al.*, *Advanced biomaterials: fundamentals, processing, and applications*: John Wiley & Sons, 2010.

[42] J. M. Dang and K. W. Leong, "Natural polymers for gene delivery and tissue engineering," *Advanced drug delivery reviews*, vol. 58, pp. 487-499, 2006.

[43] J. Venugopal, *et al.*, "Mineralization of osteoblasts with electrospun collagen/hydroxyapatite nanofibers," *Journal of Materials Science: Materials in Medicine*, vol. 19, pp. 2039-2046, 2008.

[44] R. Pallela, *et al.*, "Biophysicochemical evaluation of chitosan-hydroxyapatite-marine sponge collagen composite for bone tissue engineering," *Journal of Biomedical Materials Research Part A*, vol. 100, pp. 486-495, 2012.

[45] S. B. Lee, *et al.*, "Study of gelatin-containing artificial skin V: fabrication of gelatin scaffolds using a salt-leaching method," *Biomaterials*, vol. 26, pp. 1961-1968, 2005.

[46] Y. Zhang, *et al.*, "The osteogenic properties of CaP/silk composite scaffolds," *Biomaterials*, vol. 31, pp. 2848-2856, 2010.

[47] H. Ç. Arca and S. Senel, "Chitosan based systems for tissue engineering Part 1: Hard tissues," *FABAD J. Pharm. Sci*, vol. 33, pp. 35-49, 2008.

[48] X. X. Shao, *et al.*, "Evaluation of a hybrid scaffold/cell construct in repair of high-load-bearing osteochondral defects in rabbits," *Biomaterials*, vol. 27, pp. 1071-1080, 2006.

[49] Y.-C. Wu, *et al.*, "A comparative study of the physical and mechanical properties of three natural corals based on the criteria for bone–tissue engineering scaffolds," *Journal of Materials Science: Materials in Medicine*, vol. 20, pp. 1273-1280, 2009.

[50] H. Cao and N. Kuboyama, "A biodegradable porous composite scaffold of PGA/β-TCP for bone tissue engineering," *Bone*, vol. 46, pp. 386-395, 2010.

[51] X. Huang, *et al.*, "Peptide interfacial biomaterials improve endothelial cell adhesion and spreading on synthetic polyglycolic acid materials," *Annals of biomedical engineering*, vol. 38, pp. 1965-1976, 2010.

[52] H. Maachou, *et al.*, "Characterization and in vitro bioactivity of chitosan/hydroxyapatite composite membrane prepared by freeze-gelation method," *Trends Biomater Artif Organs*, vol. 22, pp. 15-24, 2008.

[53] Y. Yin, *et al.*, "Preparation and characterization of macroporous chitosan–gelatin/β-tricalcium phosphate composite scaffolds for bone tissue engineering," *Journal of Biomedical Materials Research Part A*, vol. 67, pp. 844-855, 2003.

[54] L. Zhao and J. Chang, "Preparation and characterization of macroporous chitosan/wollastonite composite scaffolds for tissue engineering," *Journal of Materials Science: Materials in Medicine*, vol. 15, pp. 625-629, 2004.

[55] M. Navarro, *et al.*, "Biomaterials in orthopaedics," *Journal of the Royal Society Interface*, vol. 5, pp. 1137-1158, 2008.

[56] J. Nakamatsu, *et al.*, "Processing and characterization of porous structures from chitosan and starch for tissue engineering scaffolds," *Biomacromolecules*, vol. 7, pp. 3345-3355, 2006.

[57] P. K. Dutta, *et al.*, "Chitin and chitosan: Chemistry, properties and applications," *Journal of Scientific and Industrial Research*, vol. 63, pp. 20-31, 2004.

[58] G. Chen, *et al.*, "Development of biodegradable porous scaffolds for tissue engineering," *Materials Science and Engineering: C*, vol. 17, pp. 63-69, 2001.

[59] Z. Ge, *et al.*, "Manufacture of degradable polymeric scaffolds for bone regeneration," *Biomedical Materials*, vol. 3, p. 022001, 2008.

[60] A. G. Mikos and J. S. Temenoff, "Formation of highly porous biodegradable scaffolds for tissue engineering," *Electronic Journal of Biotechnology*, vol. 3, pp. 23-24, 2000.

[61] J. J. Yoon, *et al.*, "Dexamethasone-releasing biodegradable polymer scaffolds fabricated by a gas-foaming/salt-leaching method," *Biomaterials*, vol. 24, pp. 2323-2329, 2003.

[62] Q. Hou, *et al.*, "Porous polymeric structures for tissue engineering prepared by a coagulation, compression moulding and salt leaching technique," *Biomaterials*, vol. 24, pp. 1937-1947, 2003.

[63] T. Weigel, *et al.*, "Design and preparation of polymeric scaffolds for tissue engineering," 2006.

[64] J. Li and A. F. Mak, "Transfer of collagen coating from porogen to scaffold: Collagen coating within poly (DL-lactic-co-glycolic acid) scaffold," *Composites Part B: Engineering*, vol. 38, pp. 317-323, 2007.

[65] M. T. Gokmen and F. E. Du Prez, "Porous polymer particles—A comprehensive guide to synthesis, characterization, functionalization and applications," *Progress in Polymer Science*, vol. 37, pp. 365-405, 2012.

[66] G. Chen, *et al.*, "Preparation of poly (L-lactic acid) and poly (DL-lactic-co-glycolic acid) foams by use of ice microparticulates," *Biomaterials*, vol. 22, pp. 2563-2567, 2001.

[67] A. Bottino, *et al.*, "The formation of microporous polyvinylidene difluoride membranes by phase separation," *Journal of membrane science*, vol. 57, pp. 1-20, 1991.

[68] C.Y. Hsieh, *et al.*, "Fabrication and release behavior of a novel freeze-gelled chitosan/γ-PGA scaffold as a carrier for rhBMP-2," *Dental Materials*, vol. 22, pp. 622-629, 2006.

[69] P. Van de Witte, *et al.*, "Phase separation processes in polymer solutions in relation to membrane formation," *Journal of membrane science*, vol. 117, pp. 1-31, 1996.

[70] Z. She, *et al.*, "Preparation and in vitro degradation of porous three-dimensional silk fibroin/chitosan scaffold," *Polymer Degradation and Stability*, vol. 93, pp. 1316-1322, 2008.

[71] T.-H. Young, *et al.*, "The formation mechanism of membranes prepared from the crystalline EVAL polymer–water (nonsolvent)–2-propanol (nonsolvent) system," *Journal of membrane science*, vol. 159, pp. 21-27, 1999.

[72] Q. Lv and Q. Feng, "Preparation of 3-D regenerated fibroin scaffolds with freeze drying method and freeze drying/foaming technique," *Journal of Materials Science: Materials in Medicine*, vol. 17, pp. 1349-1356, 2006.

[73] F. J. Hua, *et al.*, "Macroporous poly (L-lactide) scaffold 1. Preparation of a macroporous scaffold by liquid–liquid phase separation of a PLLA–dioxane–water system," *Journal of biomedical materials research*, vol. 63, pp. 161-167, 2002.

[74] N.-Y. Yuan, *et al.*, "Effects of the cooling mode on the structure and strength of porous scaffolds made of chitosan, alginate, and carboxymethyl cellulose by the freeze-gelation method," *Carbohydrate polymers*, vol. 78, pp. 349-356, 2009.

[75] L. Qian and H. Zhang, "Controlled freezing and freeze drying: a versatile route for porous and micro-/nano-structured materials," *Journal of chemical technology and biotechnology*, vol. 86, pp. 172-184, 2011.

[76] M.H. Ho, *et al.*, "Preparation of porous scaffolds by using freeze-extraction and freeze-gelation methods," *Biomaterials,* vol. 25, pp. 129-138, 2004.

[77] M. Statham, *et al.*, "Net-shape manufacture of low-cost ceramic shapes by freeze-gelation," *Journal of sol-gel science and technology,* vol. 13, pp. 171-175, 1998.

[78] C.Y. Hsieh, *et al.*, "Analysis of freeze-gelation and cross-linking processes for preparing porous chitosan scaffolds," *Carbohydrate polymers,* vol. 67, pp. 124-132, 2007.

[79] P.-H. Chen, *et al.*, "Novel chitosan–pectin composite membranes with enhanced strength, hydrophilicity and controllable disintegration," *Carbohydrate Polymers,* vol. 82, pp. 1236-1242, 2010.

[80] X. Zhu, *et al.*, "Electrospun fibrous mats with high porosity as potential scaffolds for skin tissue engineering," *Biomacromolecules,* vol. 9, pp. 1795-1801, 2008.

[81] G. Jin, *et al.*, "Stem cell differentiation to epidermal lineages on electrospun nanofibrous substrates for skin tissue engineering," *Acta biomaterialia,* vol. 7, pp. 3113-3122, 2011.

[82] A. Subramanian, *et al.*, "Preparation and evaluation of the electrospun chitosan/PEO fibers for potential applications in cartilage tissue engineering," *Journal of Biomaterials Science, Polymer Edition,* vol. 16, pp. 861-873, 2005.

[83] H. S. Yoo, *et al.*, "Surface-functionalized electrospun nanofibers for tissue engineering and drug delivery," *Advanced drug delivery reviews,* vol. 61, pp. 1033-1042, 2009.

[84] W. Cui, *et al.*, "Electrospun nanofibrous materials for tissue engineering and drug delivery," *Science and Technology of Advanced Materials,* vol. 11, p. 014108, 2010.

[85] C. Liu, *et al.*, "Novel 3D collagen scaffolds fabricated by indirect printing technique for tissue engineering," *Journal of Biomedical Materials Research Part B: Applied Biomaterials,* vol. 85, pp. 519-528, 2008.

[86] H. Seitz, *et al.*, "Three-dimensional printing of porous ceramic scaffolds for bone tissue engineering," *Journal of Biomedical Materials Research Part B: Applied Biomaterials,* vol. 74, pp. 782-788, 2005.

[87] D. Han, *et al.*, "Usage of Rapid Prototyping Technique in Customized Craniomaxillofacial Bone Tissue Engineering Scaffold," vol. 1, ed: InTech, 2011.

[88] L. Ciocca, *et al.*, "CAD/CAM and rapid prototyped scaffold construction for bone regenerative medicine and surgical transfer of virtual planning: a pilot study," *Computerized Medical Imaging and Graphics,* vol. 33, pp. 58-62, 2009.

[89] W. Sun and P. Lal, "Recent development on computer aided tissue engineering—a review," *Computer methods and programs in biomedicine,* vol. 67, pp. 85-103, 2002.

[90] A. J. Friedenstein, *et al.*, "Heterotopic transplants of bone marrow," *Transplantation,* vol. 6, pp. 230-247, 1968.

[91] E. Horwitz, *et al.*, "Clarification of the nomenclature for MSC: The International Society for Cellular Therapy position statement," *Cytotherapy,* vol. 7, pp. 393-395, 2005.

[92] A. Erices, *et al.*, "Mesenchymal progenitor cells in human umbilical cord blood," *British journal of haematology,* vol. 109, pp. 235-242, 2000.

[93] Y. J. Choi, *et al.*, "Determination of osteogenic or adipogenic lineages in muscle-derived stem cells (MDSCs) by a collagen-binding peptide (CBP) derived from bone sialoprotein (BSP)," *Biochemical and biophysical research communications,* vol. 419, pp. 326-332, 2012.

[94] M. V. Risbud and M. Sittinger, "Tissue engineering: advances in< i> in vitro</i> cartilage generation," *TRENDS in Biotechnology,* vol. 20, pp. 351-356, 2002.

[95] A. Wang, *et al.*, "Porous chitosan tubular scaffolds with knitted outer wall and controllable inner structure for nerve tissue engineering," *Journal of Biomedical Materials Research Part A*, vol. 79, pp. 36-46, 2006.

[96] Z.Q. Feng, *et al.*, "The effect of nanofibrous galactosylated chitosan scaffolds on the formation of rat primary hepatocyte aggregates and the maintenance of liver function," *Biomaterials*, vol. 30, pp. 2753-2763, 2009.

[97] F. Tortelli and R. Cancedda, "Three-dimensional cultures of osteogenic and chondrogenic cells: a tissue engineering approach to mimic bone and cartilage in vitro," *Eur Cell Mater*, vol. 17, pp. 1-14, 2009.

[98] O. F. Zouani, *et al.*, "Differentiation of pre-osteoblast cells on poly (ethylene terephthalate) grafted with RGD and/or BMPs mimetic peptides," *Biomaterials*, vol. 31, pp. 8245-8253, 2010.

[99] A. McLaren, "Ethical and social considerations of stem cell research," *Nature*, vol. 414, pp. 129-131, 2001.

[100] K. Tanner, "Bioactive composites for bone tissue engineering," *Proceedings of the Institution of Mechanical Engineers, Part H: Journal of Engineering in Medicine*, vol. 224, pp. 1359-1372, 2010.

[101] G. Han, *et al.*, "Osteogenic differentiation of bone marrow mesenchymal stem cells by adenovirus-mediated expression of leptin," *Regulatory peptides*, vol. 163, pp. 107-112, 2010.

[102] T. S. Karande, *et al.*, "Diffusion in musculoskeletal tissue engineering scaffolds: design issues related to porosity, permeability, architecture, and nutrient mixing," *Annals of biomedical engineering*, vol. 32, pp. 1728-1743, 2004.

[103] Y. Yamamoto, *et al.*, "Preparation of artificial skeletal muscle tissues by a magnetic force-based tissue engineering technique," *Journal of bioscience and bioengineering*, vol. 108, pp. 538-543, 2009.

[104] S. K. Nandi, *et al.*, "The repair of segmental bone defects with porous bioglass: an experimental study in goat," *Research in veterinary science*, vol. 86, pp. 162-173, 2009.

[105] A. I. Caplan, "Adult mesenchymal stem cells for tissue engineering versus regenerative medicine," *Journal of cellular physiology*, vol. 213, pp. 341-347, 2007.

[106] R. H. Lee, *et al.*, "Characterization and expression analysis of mesenchymal stem cells from human bone marrow and adipose tissue," *Cellular Physiology and Biochemistry*, vol. 14, pp. 311-324, 2004.

[107] M. Shin, *et al.*, "In vivo bone tissue engineering using mesenchymal stem cells on a novel electrospun nanofibrous scaffold," *Tissue Engineering*, vol. 10, pp. 33-41, 2004.

[108] W.-J. Li, *et al.*, "A three-dimensional nanofibrous scaffold for cartilage tissue engineering using human mesenchymal stem cells," *Biomaterials*, vol. 26, pp. 599-609, 2005.

[109] H. A. Awad, *et al.*, "Autologous mesenchymal stem cell-mediated repair of tendon," *Tissue Engineering*, vol. 5, pp. 267-277, 1999.

[110] H. Liu, *et al.*, "The interaction between a combined knitted silk scaffold and microporous silk sponge with human mesenchymal stem cells for ligament tissue engineering," *Biomaterials*, vol. 29, pp. 662-674, 2008.

[111] T. N. Vo, *et al.*, "Strategies for controlled delivery of growth factors and cells for bone regeneration," *Advanced drug delivery reviews*, vol. 64, pp. 1292-1309, 2012.

[112] J. Rossert and B. De Crombrugghe, "Type I collagen: structure, synthesis, and regulation," *Principles of bone biology*, vol. 2, pp. 189-210, 1996.

[113] D. E. Discher, *et al.*, "Growth factors, matrices, and forces combine and control stem cells," *Science*, vol. 324, pp. 1673-1677, 2009.

[114] J. E. Babensee, *et al.*, "Growth factor delivery for tissue engineering," *Pharmaceutical research*, vol. 17, pp. 497-504, 2000.

[115] M. Schmidt, *et al.*, "A review of the effects of insulin-like growth factor and platelet derived growth factor on *in-vivo* cartilage healing and repair," *Osteoarthritis and cartilage*, vol. 14, pp. 403-412, 2006.

[116] Y. Zhang, *et al.*, "A platelet-derived growth factor releasing chitosan/coral composite scaffold for periodontal tissue engineering," *Biomaterials*, vol. 28, pp. 1515-1522, 2007.

[117] P. Yilgor, *et al.*, "Effect of scaffold architecture and BMP-2/BMP-7 delivery on in vitro bone regeneration," *Journal of Materials Science: Materials in Medicine*, vol. 21, pp. 2999-3008, 2010.

[118] C. Kaps, *et al.*, "Bone morphogenetic proteins promote cartilage differentiation and protect engineered artificial cartilage from fibroblast invasion and destruction," *Arthritis & Rheumatism*, vol. 46, pp. 149-162, 2002.

[119] B. Chuenjitkuntaworn, *et al.*, "Polycaprolactone/hydroxyapatite composite scaffolds: preparation, characterization, and in vitro and in vivo biological responses of human primary bone cells," *Journal of Biomedical Materials Research Part A*, vol. 94, pp. 241-251, 2010.

[120] H. Zhou and J. Lee, "Nanoscale hydroxyapatite particles for bone tissue engineering," *Acta Biomaterialia*, vol. 7, pp. 2769-2781, 2011.

[121] Q. Fu, *et al.*, "Bioactive glass scaffolds for bone tissue engineering: state of the art and future perspectives," *Materials Science and Engineering: C*, vol. 31, pp. 1245-1256, 2011.

[122] L. McIntosh, *et al.*, "Impact of bone geometry on effective properties of bone scaffolds," *Acta Biomaterialia*, vol. 5, pp. 680-692, 2009.

[123] M. M. E. Gomes, "A bone tissue engineering strategy based on starch scaffolds and bone marrow cells cultured in a flow perfusion bioreactor," Universidade do Minho, 2004.

[124] T. W. Lin, *et al.*, "Biomechanics of tendon injury and repair," *Journal of biomechanics*, vol. 37, pp. 865-877, 2004.

[125] S. Sangadji and E. Schlangen, "Mimicking Bone Healing Process to Self Repair Concrete Structure Novel Approach Using Porous Network Concrete," *Procedia Engineering*, vol. 54, pp. 315-326, 2013.

[126] E. Margallo Balbás, "Optical techniques for the study of living tissue," 2010.

[127] A. Subramanian and H. Y. Lin, "Crosslinked chitosan: its physical properties and the effects of matrix stiffness on chondrocyte cell morphology and proliferation," *Journal of Biomedical Materials Research Part A*, vol. 75, pp. 742-753, 2005.

[128] T. Jiang, *et al.*, "In vitro evaluation of chitosan/poly (lactic acid-glycolic acid) sintered microsphere scaffolds for bone tissue engineering," *Biomaterials*, vol. 27, pp. 4894-4903, 2006.

[129] N.-C. Cheng, *et al.*, "Genipin-crosslinked cartilage-derived matrix as a scaffold for human adipose-derived stem cell chondrogenesis," *Tissue Engineering Part A*, vol. 19, pp. 484-496, 2012.

[130] G. Wang, *et al.*, "In vitro assessment of the differentiation potential of bone marrow-derived mesenchymal stem cells on genipin-chitosan conjugation scaffold with surface hydroxyapatite nanostructure for bone tissue engineering," *Tissue Engineering Part A*, vol. 17, pp. 1341-1349, 2011.

[131] Y. Yamada, *et al.*, "Bone regeneration following injection of mesenchymal stem cells and fibrin glue with a biodegradable scaffold," *Journal of Cranio-Maxillofacial Surgery*, vol. 31, pp. 27-33, 2003.

[132] M. Saccone and A. K. Jain, "Fracture healing in India: Available therapies, indications, and protocols," *Indian journal of orthopaedics,* vol. 43, p. 175, 2009.

[133] G. Gururaj, "Injuries in India: A national perspective," *Burden of disease in India. National Commission on Macroeconomics & Health. Ministry of Health & Family Welfare. Government of India, 2005a,* pp. 325-347, 2005.

[134] K. Whang, *et al.*, "Ectopic bone formation via rhBMP-2 delivery from porous bioabsorbable polymer scaffolds," *Journal of biomedical materials research,* vol. 42, pp. 491-499, 1998.

[135] J. E. Babensee, *et al.*, "Host response to tissue engineered devices," *Advanced drug delivery reviews,* vol. 33, pp. 111-139, 1998.

[136] M. B. Murphy, *et al.*, "Engineering a better way to heal broken bones," *Chemical engineering progress,* vol. 106, pp. 37-43, 2010.

[137] L. Y. Z. F. Z. Huiyong, "review on techniques of design and manufacturing for bone tissue engineering scaffold," *Biomedical Engineering,* 2009.

[138] K. Rezwan, *et al.*, "Biodegradable and bioactive porous polymer/inorganic composite scaffolds for bone tissue engineering," *Biomaterials,* vol. 27, pp. 3413-3431, 2006.

[139] X. Wang, *et al.*, "Silk nanospheres and microspheres from silk/pva blend films for drug delivery," *Biomaterials,* vol. 31, pp. 1025-1035, 2010.

[140] M. K. Sah and K. Pramanik, "Soluble-eggshell-membrane-protein-modified porous silk fibroin scaffolds with enhanced cell adhesion and proliferation properties," *Journal of Applied Polymer Science,* vol. 131, 2014.

[141] B. Stevens, *et al.*, "A review of materials, fabrication methods, and strategies used to enhance bone regeneration in engineered bone tissues," *Journal of Biomedical Materials Research Part B: Applied Biomaterials,* vol. 85, pp. 573-582, 2008.

[142] F. Pati, *et al.*, "Collagen Intermingled Chitosan-Tripolyphosphate Nano/Micro Fibrous Scaffolds for Tissue-Engineering Application," *Journal of Biomaterials Science, Polymer Edition,* vol. 23, pp. 1923-1938, 2012.

[143] B. C. Cho, *et al.*, "The role of hyaluronic acid, chitosan, and calcium sulfate and their combined effect on early bony consolidation in distraction osteogenesis of a canine model," *Journal of Craniofacial Surgery,* vol. 13, pp. 783-793, 2002.

[144] E.-J. Lee, *et al.*, "Membrane of hybrid chitosan–silica xerogel for guided bone regeneration," *Biomaterials,* vol. 30, pp. 743-750, 2009.

[145] M. E. Frohbergh, *et al.*, "Electrospun hydroxyapatite-containing chitosan nanofibers crosslinked with genipin for bone tissue engineering," *Biomaterials,* vol. 33, pp. 9167-9178, 2012.

[146] S. S. Silva, *et al.*, "Novel genipin-cross-linked chitosan/silk fibroin sponges for cartilage engineering strategies," *Biomacromolecules,* vol. 9, pp. 2764-2774, 2008.

[147] S.-S. Kim, *et al.*, "Poly (lactide-co-glycolide)/hydroxyapatite composite scaffolds for bone tissue engineering," *Biomaterials,* vol. 27, pp. 1399-1409, 2006.

[148] H. H. Xu and C. G. Simon Jr, "Fast setting calcium phosphate–chitosan scaffold: mechanical properties and biocompatibility," *Biomaterials,* vol. 26, pp. 1337-1348, 2005.

[149] P. Weimin, *et al.*, "Tendon-to-bone healing using an injectable calcium phosphate cement combined with bone xenograft/BMP composite," *Biomaterials,* vol. 34, pp. 9926-9936, 2013.

[150] S. Bose and S. Tarafder, "Calcium phosphate ceramic systems in growth factor and drug delivery for bone tissue engineering: a review," *Acta Biomaterialia,* vol. 8, pp. 1401-1421, 2012.

[151] Y. Liu, *et al.*, "Influence of calcium phosphate crystal assemblies on the proliferation and osteogenic gene expression of rat bone marrow stromal cells," *Biomaterials*, vol. 28, pp. 1393-1403, 2007.

[152] P. Wongwitwichot, *et al.*, "Comparison of TCP and TCP/HA hybrid scaffolds for osteoconductive activity," *The open biomedical engineering journal*, vol. 4, p. 279, 2010.

[153] L. Zhang and T. J. Webster, "Nanotechnology and nanomaterials: promises for improved tissue regeneration," *Nano Today*, vol. 4, pp. 66-80, 2009.

[154] A. Sendemir-Urkmez and R. D. Jamison, "The addition of biphasic calcium phosphate to porous chitosan scaffolds enhances bone tissue development in vitro," *Journal of Biomedical Materials Research Part A*, vol. 81, pp. 624-633, 2007.

[155] W.-B. Tsai, *et al.*, "Fabrication of UV-crosslinked chitosan scaffolds with conjugation of RGD peptides for bone tissue engineering," *Carbohydrate polymers*, vol. 85, pp. 129-137, 2011.

[156] Y.-Y. Wang, *et al.*, "Introducing RGD peptides on PHBV films through PEG-containing cross-linkers to improve the biocompatibility," *Biomacromolecules*, vol. 12, pp. 551-559, 2011.

[157] H. Zhou, *et al.*, "Enhanced bioactivity of bone morphogenetic protein-2 with low dose of 2 N, 6-sulfated chitosan in vitro andin vivo," *Biomaterials*, vol. 30, pp. 1715-1724, 2009.

[158] F. M. Shaikh, *et al.*, "Fibrin: a natural biodegradable scaffold in vascular tissue engineering," *Cells Tissues Organs*, vol. 188, pp. 333-346, 2008.

[159] L. He, *et al.*, "A comparative study of platelet-rich fibrin (PRF) and platelet-rich plasma (PRP) on the effect of proliferation and differentiation of rat osteoblasts in vitro," *Oral Surgery, Oral Medicine, Oral Pathology, Oral Radiology, and Endodontology*, vol. 108, pp. 707-713, 2009.

[160] R. J. Gray, *et al.*, "Percutaneous fibrin sheath stripping versus transcatheter urokinase infusion for malfunctioning wellpositioned tunneled central venous dialysis catheters: a prospective, randomized trial," *Journal of Vascular and Interventional Radiology*, vol. 11, pp. 1121-1129, 2000.

[161] S. S. Tholpady, *et al.*, "Repair of an Osseous Facial Critical-Size Defect Using Augmented Fibrin Sealant," *The Laryngoscope*, vol. 109, pp. 1585-1588, 1999.

[162] Q. Z. Chen, *et al.*, "45S5 Bioglass®derived glass–ceramic scaffolds for bone tissue engineering," *Biomaterials*, vol. 27, pp. 2414-2425, 2006.

[163] L. Luca, *et al.*, "Injectable rhBMP-2-loaded chitosan hydrogel composite: Osteoinduction at ectopic site and in segmental long bone defect," *Journal of Biomedical Materials Research Part A*, vol. 96, pp. 66-74, 2011.

[164] T. Majima, *et al.*, "Alginate and chitosan polyion complex hybrid fibers for scaffolds in ligament and tendon tissue engineering," *Journal of Orthopaedic Science*, vol. 10, pp. 302-307, 2005.

[165] Y. Lin, *et al.*, "Ectopic and in situ bone formation of adipose tissue-derived stromal cells in biphasic calcium phosphate nanocomposite," *Journal of Biomedical Materials Research Part A*, vol. 81, pp. 900-910, 2007.

[166] S. P. Tsai, *et al.*, "Preparation and cell compatibility evaluation of chitosan/collagen composite scaffolds using amino acids as crosslinking bridges," *Journal of applied polymer science*, vol. 105, pp. 1774-1785, 2007.

[167] D. L. Nettles, *et al.*, "Potential use of chitosan as a cell scaffold material for cartilage tissue engineering," *Tissue engineering*, vol. 8, pp. 1009-1016, 2002.

[168] P. Bagnaninchi, *et al.*, "Chitosan microchannel scaffolds for tendon tissue engineering characterized using optical coherence tomography," *Tissue engineering,* vol. 13, pp. 323-331, 2007.

[169] I. Adekogbe and A. Ghanem, "Fabrication and characterization of DTBP-crosslinked chitosan scaffolds for skin tissue engineering," *Biomaterials,* vol. 26, pp. 7241-7250, 2005.

[170] T. Funakoshi, *et al.*, "Novel chitosan-based hyaluronan hybrid polymer fibers as a scaffold in ligament tissue engineering," *Journal of Biomedical Materials Research Part A,* vol. 74, pp. 338-346, 2005.

[171] Y. Zhou, *et al.*, "Electrospun water-soluble carboxyethyl chitosan/poly (vinyl alcohol) nanofibrous membrane as potential wound dressing for skin regeneration," *Biomacromolecules,* vol. 9, pp. 349-354, 2007.

[172] K. Tuzlakoglu and R. Reis, "Formation of bone-like apatite layer on chitosan fiber mesh scaffolds by a biomimetic spraying process," *Journal of Materials Science: Materials in Medicine,* vol. 18, pp. 1279-1286, 2007.

[173] H. Wang, *et al.*, "Biocompatibility and osteogenesis of biomimetic nano-hydroxyapatite/polyamide composite scaffolds for bone tissue engineering," *Biomaterials,* vol. 28, pp. 3338-3348, 2007.

[174] J. L. Drury and D. J. Mooney, "Hydrogels for tissue engineering: scaffold design variables and applications," *Biomaterials,* vol. 24, pp. 4337-4351, 2003.

[175] E. B. Denkbaş, *et al.*, "Norfloxacin-loaded chitosan sponges as wound dressing material," *Journal of biomaterials applications,* vol. 18, pp. 291-303, 2004.

[176] Y.-J. Seol, *et al.*, "Chitosan sponges as tissue engineering scaffolds for bone formation," *Biotechnology letters,* vol. 26, pp. 1037-1041, 2004.

[177] M. Krampera, *et al.*, "Mesenchymal stem cells for bone, cartilage, tendon and skeletal muscle repair," *Bone,* vol. 39, pp. 678-683, 2006.

[178] P. Malafaya, *et al.*, "Chitosan particles agglomerated scaffolds for cartilage and osteochondral tissue engineering approaches with adipose tissue derived stem cells," *Journal of Materials Science: Materials in Medicine,* vol. 16, pp. 1077-1085, 2005.

[179] C.-T. Liao and M.H. Ho, "The fabrication of biomimetic chitosan scaffolds by using SBF treatment with different crosslinking agents," *Membranes,* vol. 1, pp. 3-12, 2010.

[180] L. Ma, *et al.*, "Collagen/chitosan porous scaffolds with improved biostability for skin tissue engineering," *Biomaterials,* vol. 24, pp. 4833-4841, 2003.

[181] A. C. Akman, *et al.*, "bFGF-loaded HA-chitosan: A promising scaffold for periodontal tissue engineering," *Journal of Biomedical Materials Research Part A,* vol. 92, pp. 953-962, 2010.

[182] J. Lu, *et al.*, "Role of interconnections in porous bioceramics on bone recolonization in vitro and in vivo," *Journal of Materials Science: Materials in Medicine,* vol. 10, pp. 111-120, 1999.

[183] P. J. VandeVord, *et al.*, "Evaluation of the biocompatibility of a chitosan scaffold in mice," *Journal of biomedical materials research,* vol. 59, pp. 585-590, 2002.

[184] Z. Zheng, *et al.*, "The behavior of MC3T3-E1 cells on chitosan/poly-L-lysine composite films: Effect of nanotopography, surface chemistry, and wettability," *Journal of Biomedical Materials Research Part A,* vol. 89, pp. 453-465, 2009.

[185] K.-A. Kwak, *et al.*, "Bio-functionalization of polycaprolactone infiltrated BCP scaffold with silicon and fibronectin enhances osteoblast activity *in-vitro*," *Applied Surface Science,* vol. 279, pp. 13-22, 2013.

[186] H. Jiankang, *et al.*, "Preparation of chitosan–gelatin hybrid scaffolds with well-organized microstructures for hepatic tissue engineering," *Acta Biomaterialia*, vol. 5, pp. 453-461, 2009.

[187] T. Masuko, *et al.*, "Chitosan–RGDSGGC conjugate as a scaffold material for musculoskeletal tissue engineering," *Biomaterials*, vol. 26, pp. 5339-5347, 2005.

[188] X. Shao and C. J. Hunter, "Developing an alginate/chitosan hybrid fiber scaffold for annulus fibrosus cells," *Journal of Biomedical Materials Research Part A*, vol. 82, pp. 701-710, 2007.

[189] L. Zhao, *et al.*, "Preparation and HL-7702 cell functionality of titania/chitosan composite scaffolds," *Journal of Materials Science: Materials in Medicine*, vol. 20, pp. 949-957, 2009.

[190] C.-m. Han, *et al.*, "Application of collagen-chitosan/fibrin glue asymmetric scaffolds in skin tissue engineering," *Journal of Zhejiang University SCIENCE B*, vol. 11, pp. 524-530, 2010.

[191] L. Bi, *et al.*, "Effects of different cross-linking conditions on the properties of genipin-cross-linked chitosan/collagen scaffolds for cartilage tissue engineering," *Journal of Materials Science: Materials in Medicine*, vol. 22, pp. 51-62, 2011.

[192] T. Gamboa-Martínez, *et al.*, "Fibrin coating on poly (L-lactide) scaffolds for tissue engineering," *Journal of Bioactive and Compatible Polymers*, vol. 26, pp. 464-477, 2011.

[193] C. Bhattacharya, *et al.*, "Development of span 80–tween 80 based fluid-filled organogels as a matrix for drug delivery," *Journal of pharmacy & bioallied sciences*, vol. 4, p. 155, 2012.

[194] H. Zhao, *et al.*, "Fabrication and properties of injectable β-tricalcium phosphate particles/fibrin gel composite scaffolds for bone tissue engineering," *Materials Science and Engineering: C*, vol. 29, pp. 836-842, 2009.

[195] T. Kokubo and H. Takadama, "How useful is SBF in predicting in vivo bone bioactivity?," *Biomaterials*, vol. 27, pp. 2907-2915, 2006.

[196] I. J. Fuss, *et al.*, "Isolation of whole mononuclear cells from peripheral blood and cord blood," *Current protocols in immunology*, pp. 7.1. 1-7.1. 8, 2009.

[197] A. Bissoyi and K. Pramanik, "Effects of Non-Toxic Cryoprotective Agents on the Viability of Cord Blood Derived MNCs," *CryoLetters*, vol. 34, pp. 453-465, 2013.

[198] N. Bhardwaj, *et al.*, "Potential of 3-D tissue constructs engineered from bovine chondrocytes/silk fibroin-chitosan for in vitro cartilage tissue engineering," *Biomaterials*, vol. 32, pp. 5773-5781, 2011.

[199] D. Singh, *et al.*, "Proliferation of myoblast skeletal cells on three-dimensional supermacroporous cryogels," *International journal of biological sciences*, vol. 6, p. 371, 2010.

[200] D. Singh, *et al.*, "Proliferation of myoblast skeletal cells on three-dimensional supermacroporous cryogels," *Int J Biol Sci*, vol. 6, pp. 371-381, 2010.

[201] W. Xu, *et al.*, "Material properties and osteogenic differentiation of marrow stromal cells on fiber-reinforced laminated hydrogel nanocomposites," *Acta Biomaterialia*, vol. 6, pp. 1992-2002, 2010.

[202] J. Qiu, *et al.*, "In vitro investigation on the biodegradability and biocompatibility of genipin cross-linked porcine acellular dermal matrix with intrinsic fluorescence," *ACS applied materials & interfaces*, vol. 5, pp. 344-350, 2012.

[203] C. A. Gregory, *et al.*, "An Alizarin red-based assay of mineralization by adherent cells in culture: comparison with cetylpyridinium chloride extraction," *Analytical biochemistry*, vol. 329, pp. 77-84, 2004.

[204] J. De Jong, *et al.*, "Dimethylmethylene blue-based spectrophotometry of glycosaminoglycans in untreated urine: a rapid screening procedure for mucopolysaccharidoses," *Clinical chemistry*, vol. 35, pp. 1472-1477, 1989.

[205] M. Marone, *et al.*, "Semiquantitative RT-PCR analysis to assess the expression levels of multiple transcripts from the same sample," *Biological procedures online*, vol. 3, pp. 19-25, 2001.

[206] J. Eyckmans and F. P. Luyten, "Species specificity of ectopic bone formation using periosteum-derived mesenchymal progenitor cells," *Tissue engineering*, vol. 12, pp. 2203-2213, 2006.

[207] S. Otsuru, *et al.*, "Bone marrow-derived osteoblast progenitor cells in circulating blood contribute to ectopic bone formation in mice," *Biochemical and biophysical research communications*, vol. 354, pp. 453-458, 2007.

[208] C. Trojani, *et al.*, "Ectopic bone formation using an injectable biphasic calcium phosphate/Si-HPMC hydrogel composite loaded with undifferentiated bone marrow stromal cells," *Biomaterials*, vol. 27, pp. 3256-3264, 2006.

[209] L. S. Nair and C. T. Laurencin, "Biodegradable polymers as biomaterials," *Progress in Polymer Science*, vol. 32, pp. 762-798, 2007.

[210] H. Orii, *et al.*, "Beta-tricalcium phosphate (beta-TCP) graft combined with bone marrow stromal cells (MSCs) for posterolateral spine fusion," *Journal of medical and dental sciences*, vol. 52, p. 51, 2005.

[211] M. Spataru, *et al.*, "rheology of tricalcium phosphate (β-TCP) suspensions," *Revue Roumaine de Chimie*, vol. 53, pp. 955-959, 2008.

[212] F. Causa, *et al.*, "Poly-ϵ-caprolactone/hydroxyapatite composites for bone regeneration: In vitro characterization and human osteoblast response," *Journal of Biomedical Materials Research Part A*, vol. 76, pp. 151-162, 2006.

[213] C. Chang, *et al.*, "Fabrication and properties of chitin/hydroxyapatite hybrid hydrogels as scaffold nano-materials," *Carbohydrate polymers*, vol. 91, pp. 7-13, 2013.

[214] J. S. Temenoff and A. G. Mikos, "Injectable biodegradable materials for orthopedic tissue engineering," *Biomaterials*, vol. 21, pp. 2405-2412, 2000.

[215] V. Karageorgiou and D. Kaplan, "Porosity of 3D biomaterial scaffolds and osteogenesis," *Biomaterials*, vol. 26, pp. 5474-5491, 2005.

[216] Y. Cao and B. Wang, "Biodegradation of silk biomaterials," *International journal of molecular sciences*, vol. 10, pp. 1514-1524, 2009.

[217] C. G. Havens, *et al.*, "Regulation of late G1/S phase transition and APCCdh1 by reactive oxygen species," *Molecular and cellular biology*, vol. 26, pp. 4701-4711, 2006.

[218] B. M. Chesnutt, *et al.*, "Design and characterization of a novel chitosan/nanocrystalline calcium phosphate composite scaffold for bone regeneration," *Journal of Biomedical Materials Research Part A*, vol. 88, pp. 491-502, 2009.

[219] S. Chatterjee, *et al.*, "Cryopreservation alters membrane sulfhydryl status of bull spermatozoa: protection by oxidized glutathione," *Molecular reproduction and development*, vol. 60, pp. 498-506, 2001.

[220] W.-J. Li, *et al.*, "Multilineage differentiation of human mesenchymal stem cells in a three-dimensional nanofibrous scaffold," *Biomaterials*, vol. 26, pp. 5158-5166, 2005.

[221] X. He, *et al.*, "Combined effect of osteopontin and BMP-2 derived peptides grafted to an adhesive hydrogel on osteogenic and vasculogenic differentiation of marrow stromal cells," *Langmuir*, vol. 28, pp. 5387-5397, 2012.

[222] C. Perka, *et al.*, "Segmental bone repair by tissue-engineered periosteal cell transplants with bioresorbable fleece and fibrin scaffolds in rabbits," *Biomaterials*, vol. 21, pp. 1145-1153, 2000.

[223] T. Gamboa-Martínez, *et al.*, "Fibrin coating on poly (L-lactide) scaffolds for tissue engineering," *Journal of Bioactive and Compatible Polymers*, p. 0883911511419834, 2011.

[224] M. Rafat, *et al.*, "PEG-stabilized carbodiimide crosslinked collagen–chitosan hydrogels for corneal tissue engineering," *Biomaterials*, vol. 29, pp. 3960-3972, 2008.

[225] S.-N. Park, *et al.*, "Characterization of porous collagen/hyaluronic acid scaffold modified by 1-ethyl-3-(3-dimethylaminopropyl) carbodiimide cross-linking," *Biomaterials*, vol. 23, pp. 1205-1212, 2002.

[226] S.-M. Lien, *et al.*, "Genipin-crosslinked gelatin scaffolds for articular cartilage tissue engineering with a novel crosslinking method," *Materials Science and Engineering: C*, vol. 28, pp. 36-43, 2008.

[227] K. Madhumathi, *et al.*, "Development of novel chitin/nanosilver composite scaffolds for wound dressing applications," *Journal of Materials Science: Materials in Medicine*, vol. 21, pp. 807-813, 2010.

[228] R. Deepachitra, *et al.*, "Osteo mineralization of fibrin-decorated graphene oxide," *Carbon*, vol. 56, pp. 64-76, 2013.

[229] R. Landers, *et al.*, "Rapid prototyping of scaffolds derived from thermoreversible hydrogels and tailored for applications in tissue engineering," *Biomaterials*, vol. 23, pp. 4437-4447, 2002.

[230] T. A. Ahmed, *et al.*, "Characterization and inhibition of fibrin hydrogel-degrading enzymes during development of tissue engineering scaffolds," *Tissue engineering*, vol. 13, pp. 1469-1477, 2007.

[231] M. Sarem, *et al.*, "How can genipin assist gelatin/carbohydrate chitosan scaffolds to act as replacements of load-bearing soft tissues?," *Carbohydrate polymers*, vol. 93, pp. 635-643, 2013.

[232] D. Le Nihouannen, *et al.*, "Micro-architecture of calcium phosphate granules and fibrin glue composites for bone tissue engineering," *Biomaterials*, vol. 27, pp. 2716-2722, 2006.

[233] S.-R. Son, *et al.*, "In vitro and in vivo evaluation of electrospun PCL/PMMA fibrous scaffolds for bone regeneration," *Science and Technology of Advanced Materials*, vol. 14, p. 015009, 2013.

[234] G. Diogo, *et al.*, "Manufacture of β-TCP/alginate scaffolds through a Fab@ home model for application in bone tissue engineering," *Biofabrication*, vol. 6, p. 025001, 2014.

[235] S.-W. Kang, *et al.*, "Surface modification with fibrin/hyaluronic acid hydrogel on solid-free form-based scaffolds followed by BMP-2 loading to enhance bone regeneration," *Bone*, vol. 48, pp. 298-306, 2011.

[236] Y. Liu, *et al.*, "Segmental bone regeneration using an rhBMP-2-loaded gelatin/nanohydroxyapatite/fibrin scaffold in a rabbit model," *Biomaterials*, vol. 30, pp. 6276-6285, 2009.

[237] Q. Liu, *et al.*, "A comparative study of proliferation and osteogenic differentiation of adipose-derived stem cells on akermanite and β-TCP ceramics," *Biomaterials*, vol. 29, pp. 4792-4799, 2008.

[238] H. W. Sung, *et al.*, "Crosslinking of biological tissues using genipin and/or carbodiimide," *Journal of Biomedical Materials Research Part A*, vol. 64, pp. 427-438, 2003.

[239] H. W. Sung, *et al.*, "Stability of a biological tissue fixed with a naturally occurring crosslinking agent (genipin)," *Journal of biomedical materials research*, vol. 55, pp. 538-546, 2001.

[240] F.-M. Hsieh, *et al.*, "Study of sodium tripolyphosphate-crosslinked chitosan beads entrapped with Pseudomonas putida for phenol degradation," *Process Biochemistry*, vol. 43, pp. 83-92, 2008.

[241] F. Pati, *et al.*, "Development of chitosan–tripolyphosphate fibers through pH dependent ionotropic gelation," *Carbohydrate research*, vol. 346, pp. 2582-2588, 2011.

[242] Y.-L. Si, *et al.*, "MSCs: biological characteristics, clinical applications and their outstanding concerns," *Ageing research reviews*, vol. 10, pp. 93-103, 2011.

[243] L. P. Yan, *et al.*, "Genipin-cross-linked collagen/chitosan biomimetic scaffolds for articular cartilage tissue engineering applications," *Journal of Biomedical Materials Research Part A*, vol. 95, pp. 465-475, 2010.

[244] B. Rai, *et al.*, "Differences betweenin vitro viability and differentiation and in vivo bone-forming efficacy of human mesenchymal stem cells cultured on PCL–TCP scaffolds," *Biomaterials*, vol. 31, pp. 7960-7970, 2010.

[245] R. L. Steward, *et al.*, "Mechanical stretch and shear flow induced reorganization and recruitment of fibronectin in fibroblasts," *Scientific reports*, vol. 1, 2011.

[246] X. He, *et al.*, "Effect of grafting RGD and BMP-2 protein-derived peptides to a hydrogel substrate on osteogenic differentiation of marrow stromal cells," *Langmuir*, vol. 24, pp. 12508-12516, 2008.

[247] P. de la Puente and D. Ludeña, "Cell culture in autologous fibrin scaffolds for applications in tissue engineering," *Experimental cell research*, 2013.

[248] K.-H. Choi, *et al.*, "The chondrogenic differentiation of mesenchymal stem cells on an extracellular matrix scaffold derived from porcine chondrocytes," *Biomaterials*, vol. 31, pp. 5355-5365, 2010.

[249] J. M. Grasman, *et al.*, "Crosslinking strategies facilitate tunable structural properties of fibrin microthreads," *Acta biomaterialia*, vol. 8, pp. 4020-4030, 2012.

[250] K. H. Gudmundasson, *et al.*, "An experimental investigation into the off-statae viscosity of MR Fluids," procedings of 12th International conference on Electro Rheological fluids and Magneto rheological suspensions, pp. 679-690, 2011.

[251] S. Moeinzadeh, *et.al.*, "Experimental and Computational Investigation of the Effect of Hydrophobicity on Aggregation and Osteoinductive Potential of BMP-2-Derived Peptide in a Hydrogel Matrix" . *Tissue Engineering Part A*, 2014.

[252] Zhang, *et.al*, "Three-dimensional macroporous calcium phosphate bioceramics with nested chitosan sponges for load-bearing bone implants." *Journal of biomedical materials research* Vol 61, pp. 1-8 2002.

[253] Y. Shu, *et al*. "Synthesis and sintering of nanocrystalline hydroxyapatite powders by gelatin-based precipitation method." *Ceramics international* Vol. 33. pp. 193-196, (2007).

[254] W.Christian, *et al.* "Hydrogel-β-TCP scaffolds and stem cells for tissue engineering bone." *Bone* Vol. 4, pp. 555-563, 2006.

[255] Lindahl, *et.al.* "Mechanical property of dried defatted spongy bone" Acta Orthopaedica stand. Vol 47 (1); pp. 11-19, 1976.